ON THE ROLE OF ENZYMATIC ACTIVITY OF AMMODYTOXIN AND ITS INTERACTION WITH SOME INTRACELLULAR PROTEINS IN THE PROCESS OF β-NEUROTOXICITY

Jernej Oberčkal

Doctoral Dissertation
Jožef Stefan International Postgraduate School
Ljubljana, Slovenia, March 2015

Evaluation Board:

Prof. Dr. Peter Maček, Chairman, Biotechnical Faculty, University of Ljubljana, Jamnikarjeva ulica 101, Ljubljana, Slovenia

Prof. Dr. Robert Frangež, Member, Veterinary Faculty, University of Ljubljana, Gerbičeva ulica 60, Ljubljana, Slovenia

Prof. Dr. Jože Pungerčar, Member, Jožef Stefan Institute, Jamova cesta 39, Ljubljana, Slovenia

MEDNARODNA PODIPLOMSKA ŠOLA JOŽEFA STEFANA
JOŽEF STEFAN INTERNATIONAL POSTGRADUATE SCHOOL



Jernej Oberčkal

ON THE ROLE OF ENZYMATIC ACTIVITY OF AMMODYTOXIN AND ITS INTERACTION WITH SOME INTRACELLULAR PROTEINS IN THE PROCESS OF β-NEUROTOXICITY

Doctoral Dissertation

O VLOGI ENCIMSKE AKTIVNOSTI AMODITOKSINA IN NJEGOVE VEZAVE NA NEKATERE ZNOTRAJCELIČNE PROTEINE V PROCESU β-NEVROTOKSIČNOSTI

Doktorska disertacija

Supervisor: Prof. Dr. Igor Križaj

Ljubljana, Slovenia, March 2015

Index

Abstract ..... **IX**

Povzetek ..... **XI**

Abbreviations ..... **XIII**

1 Introduction **1**
1.1 Phospholipases A_2 1
1.2 $sPLA_2$s 1
1.2.1 Enzymatic activity of $sPLA_2$ 2
1.2.1.1 Catalytic mechanism of $sPLA_2$ 2
1.2.1.2 $sPLA_2$s act at the surface of the lipid bilayer 3
1.2.2 Toxicity of $sPLA_2$ 4
1.3 Ammodytoxins from the venom of the nose-horned viper 4
1.4 Neurotoxic effects of Atx and homologous $sPLA_2$ 5
1.4.1 The importance of binding proteins in the process of β-neurotoxicity 7
1.4.1.1 Intracellular binding proteins for Atx 8
1.4.1.1.1 PDI 8
1.4.1.1.2 R25 9
1.4.1.1.3 Syt1 9
1.4.2 The role of enzymatic activity in β-neurotoxicity 10
1.4.3 Mechanism of action of β-neurotoxic $sPLA_2$ 11
1.5 Model systems 12
1.5.1 PC12 cell line 13

2 Aims and Hypotheses **15**

3 Materials and Methods **17**
3.1 Materials 17
3.1.1 Reagents 17
3.1.2 Antibodies 18
3.1.3 Proteins and DNA primers 19
3.1.4 $sPLA_2$s 19
3.1.5 Cell line and bacterial strains 19
3.1.6 Commonly used buffers and cell media 20
3.2 Methods 20
3.2.1 Analytical techniques of protein purity determination and protein characterization 20
3.2.1.1 Concentration of protein samples 20
3.2.1.2 Determination of protein concentration 20
3.2.1.2.1 Determination of total protein concentration 20

3.2.1.2.2 Determination of concentration of specific proteins in solution 21
3.2.1.3 Polyacrylamide gel electrophoresis in the presence of SDS (SDS-PAGE) 21
3.2.1.4 Western blotting 21
3.2.1.5 Mass spectrometry 21
3.2.2 *In vitro* affinity labelling of proteins 22
3.2.2.1 Extraction of membrane proteins 22
3.2.2.2 Affinity labelling of proteins with sulfo-SBED-AtxC 22
3.2.2.2.1 Preparation of sulfo-SBED-AtxC 22
3.2.2.2.2 Affinity labelling of proteins with sulfo-SBED-AtxC 22
3.2.2.3 Affinity labelling of proteins with ^{125}I-AtxC and DSS or paraformaldehyde 23
3.2.2.3.1 Cross-linking with disuccinimidyl suberate (DSS) 23
3.2.2.3.2 Cross-linking with paraformaldehyde 23
3.2.3 Working with the PC12 cell line 23
3.2.3.1 Cell culture 23
3.2.3.2 Freezing and revitalization of cells 24
3.2.4 Isolation of SVs 24
3.2.4.1 Isolation of SVs from porcine cerebral cortex 24
3.2.4.2 Isolation of SVs from PC12 cells 24
3.2.4.3 Isolation of Atx-binding proteins from SVs 25
3.2.5 Labelling of AtxC-binding proteins in live PC12 cells 26
3.2.5.1 Sulfo-SBED-AtxC labelling of AtxC-binding proteins in intact PC12 cells 26
3.2.5.1.1 Immunoprecipitation of Atx-binding proteins 27
3.2.6 Measuring PLA_2 activity with the PyPG method 27
3.2.6.1 Preparation of PyPG vesicles 27
3.2.6.2 Measuring phospholipase activity with a fluorescent microplate reader 27
3.2.7 Production of the enzymatically inactive mutant AtxA(D49S) 28
3.2.7.1 DNA sequence preparation 28
3.2.7.1.1 Preparation of the pJP4.1 plasmid for direct expression of AtxA 28
3.2.7.1.2 Site directed mutagenesis to produce the mutated gene for AtxA(D49S) 29
3.2.7.2 Expression in *E. coli* BL21(DE3) 29
3.2.7.3 Purification of inclusion bodies, S-sulfonation of Cys residues, refolding and purification of AtxA(D49S) 30
3.2.7.3.1 Purification of inclusion bodies and S-sulfonation of Cys residues. 30
3.2.7.3.2 Refolding of AtxA(D49S) 30
3.2.7.3.3 RP-HPLC 31
3.2.7.4 Labelling of AtxA and AtxA(D49S) with the fluorescent dye ^{546}Alexa-succinimide 31
3.2.7.4.1 Determining the concentration of ^{546}Alexa–AtxA(D49S) 32
3.2.8 Confocal microscopy 32
3.2.8.1 Coating of coverslips with poly-*L*-lysine 32
3.2.8.2 Slide preparation for confocal microscopy 32
3.2.8.2.1 Immunocytochemistry 32
3.2.8.2.2 Measuring co-localization of Alexa-Atx and Atx-binding proteins with confocal microscopy 33
3.2.9 Preparation of the three-dimensional models of complexes between $sPLA_2$s and PDI 33

4 Results 35

4.1 Atx's interaction with intracellular proteins 35
4.1.1 Atx-binding proteins in SVs 35
4.1.1.1 Isolation of SVs 35
4.1.1.2 Atx-binding proteins in SVs 36
4.1.1.3 Isolation of Atx-binding proteins from SV 37
4.1.2 Atx's interaction with Syt1, CcO and PDI 39
4.1.2.1 Syt1 and CcO are specific binding proteins of Atx 39
4.1.2.2 Atx's binding to CcO is Ca^{2+}-dependent 40
4.1.2.3 Syt1 has two binding sites for Atx 41
4.1.2.4 The binding of Atx at one site of Syt1 is Ca^{2+}-dependent 42
4.1.2.5 CaM blocks the binding of Atx to the cytosolic part of Syt1 43
4.1.2.6 Syt1 specifically interacts besides with Atx also with other $sPLA_2$s 44
4.1.2.7 Effect of Syt1 and CcO on Atx's phospholipase activity 45
4.1.2.8 AtxC interacts with Syt1, R25 and PDI also in live PC12 cells 46
4.1.2.9 The 3D model of Atx in complex with hPDI 47
4.1.2.10 Complexes between hPDI and Atx-like $sPLA_2$s 48
4.2 The role of enzymatic activity in the neurotoxic processes of Atx 50
4.2.1 Preparation of the enzymatically inactive mutant AtxA(D49S) 51
4.2.2 Characterization of AtxA(D49S) 52
4.2.3 AtxA(D49S) retained no measurable PLA_2 activity. 53
4.2.4 Preparation of the fluorescent probe of AtxA(D49S) 54
4.2.5 Immunofluorescence studies 58
4.2.5.1 The enzymatic activity of AtxA is not required for the entry of AtxA into PC12 cells but it facilitates the process. 58
4.2.5.1 AtxA or its enzymatically inactive mutant significantly co-localize with Syt1, CcO, PDI and 14-3-3p in PC12 cells. 61
4.2.5.2 AtxA(D49S) co-localizes with Syt1, CcO, PDI and 14-3-3p in PC12 cells to a lesser extent than the enzymatically active native AtxA 66

5 Discussion 69

6 Conclusions 79

7 Acknowledgements 81

8 References 83

Index of Figures 93

Appendices 101

Abstract

Ammodytoxins (Atxs) are presynaptically neurotoxic (β-neurotoxic) secreted phospholipases A_2 ($sPLA_2s$) from the venom of the nose-horned viper. The molecular mechanism of action of β-neurotoxins is not yet completely understood. It is clear, however, that the neurotoxic effects of these toxins are due to their enzymatic activity as well as their binding to specific receptors in target cells. The mechanisms and importance of several events in the action of β-neurotoxins still remain to be fully elucidated, among them the pathway of their translocation into the cell cytosol, their entry into mitochondria and what role the enzymatic activity of β-neurotoxins plays in these processes.

β-neurotoxins affect cycling of synaptic vesicles (SVs). These organelles were proposed as a possible point of entry of β-neurotoxins into target cells. Using two different Atx derivatives, we have shown the existence of several specific binding proteins in SVs, with molecular masses in the range from 25 to 72 kDa and 100 kDa to above 170 kDa. Several of these masses do not correspond to molecular masses of the so far indicated Atx-binding proteins and may represent novel Atx-binding proteins.

In neuronal tissues, several intracellular proteins have been previously indicated as potential receptors for Atx. These include synaptotagmin 1 (Syt1), cytochrome c oxidase (CcO) and protein disulfide isomerase (PDI). It was proposed that subunit 2 of CcO is the long-sought 25 kDa mitochondrial receptor of Atx, R25. Using competition assays, we have proven that Syt1 and several subunits of CcO, including the 25 kDa subunit 2, specifically bind Atx *in vitro*. The interaction between Atx and Syt1 was attenuated in the absence of Ca^{2+}. In conditions without Ca^{2+}, the complex between Atx and CcO did not form as observed also in the case of Atx and R25. Also due to this reason, we suggest that the CcO subunit 2 is R25. The binding of Atx to subunit 2 of CcO likely prevents the interaction between CcO and its native ligand cytochrome *c*. This would inhibit enzymatic activity of CcO, and lead to a reduction of ATP synthesis and loss of mitochondrial potential, the observed toxic effects of Atx on neuronal cells. We have shown that Atx specifically binds to Syt1 at two distinct sites, at the cytosolic side of Syt1 and the side, exposed to the lumen of the SV. The interaction of Atx with the cytosolic side of Syt1 was blocked with calmodulin, a cytosolic protein, which is known to bind to Atx and also Syt1. Syt1 likely represents a novel receptor for Atx on the plasma membrane. Its interaction with Atx may be relevant for internalization of the toxin into neuronal cells. Besides Atx, we have shown that also other toxic and mammalian $sPLA_2s$ bind Syt1, suggesting the role of this protein also in action of other $sPLA_2s$. Neither Syt1 nor CcO evidently affected the ability of Atx to hydrolyze phospholipids.

We have shown that Atx interacted with Syt1, PDI and a protein of 25 kDa, likely representing R25, also in the live PC12 cells soon after it was added into the cell growth medium. This suggests a physiological relevance of the observed interactions and confirms a fast internalization of the toxin into the SVs, endoplasmic reticulum (ER) and mitochondria of the nerve cells.

Using a protein docking algorithm we constructed three-dimensional models of complexes between human PDI and Atx or a few other structurally related $sPLA_2s$ and experimentally confirmed their accuracy. The models represent excellent tools to

rationally design $sPLA_2$ mutants to study their internalization and intracellular trafficking.

To assess the role of enzymatic activity in the neurotoxic processes of Atx, we prepared and characterized a recombinant variant of AtxA, AtxA(D49S), with a mutation in its catalytic site, rendering it enzymatically inactive. Using a fluorescent derivative of this mutant we found that the phospholipase activity of AtxA is not strictly required but facilitates the internalization of this molecule into the cytosol, ER, mitochondria and SVs of PC12 cells. Such result suggests the existence of more specific cell-internalization mechanisms for AtxA, some of which are independent of its enzymatic activity.

Povzetek

Amoditoksini (Atx) so presinaptično nevrotoksične (β-nevrotoksične) sekretorne fosfolipaze A_2 ($sPLA_2$) iz modrasovega strupa. Molekularni mehanizem njihovega delovanja še ni v celoti pojasnjen. Jasno pa je, da so nevrotoksični učinki pogojeni z encimsko aktivnostjo teh toksinov, kot tudi z njihovo interakcijo s specifičnimi receptorji v tarčnih celicah. Več točk v delovanju β-nevrotoksinov je potrebno še razjasniti. Najpomembnejše med njimi so mehanizem vstopa toksinov v celični citosol in mitohondrije ter vloga njihove encimske aktivnosti v teh procesih.

β-nevrotoksini vplivajo na kroženje sinaptičnih veziklov (SV). Te organele so predlagali kot možno točko vstopa β-nevrotoksinov v tarčne celice. Z uporabo dveh derivatov Atx smo odkrili obstoj več specifičnih vezavnih proteinov za Atx v SV. Molekulske mase teh proteinov so med 25 in 72 kDa ter med 100 in nad 170 kDa. Več označenih proteinov ima molekulske mase, ki ne odgovarjajo masam že odkritih receptorjev in lahko predstavljajo nove specifične vezavne proteine za Atx.

V nevronskih tkivih so odkrili več potencialnih receptorjev za Atx, med njimi sinaptotagmin 1 (Syt1), citokrom c-oksidazo (CcO) in protein-disulfid-izomerazo (PDI). Podenota 2 CcO naj bi predstavljala R25, mitohondrijski receptor za Atx z molekulsko maso 25 kDa, katerega identiteta je bila predmet dolgoletnih raziskav. Z uporabo homologne kompeticije smo dokazali, da Syt1 in več podenot CcO, med njimi tudi podenota 2 z molekulsko maso 25 kDa, specifično interagirajo z Atx *in vitro*. Odsotnost Ca^{2+} je delno inhibirala interakcijo Atx s Syt1. Pogoji brez Ca^{2+} so popolnoma preprečili nastanek kompleksa med Atx in CcO. Enako so opazili tudi pri interakciji Atx z R25, kar dodatno kaže na identiteto R25 kot podenote 2 CcO. Vezava Atx verjetno prepreči interakcijo podenote 2 CcO s citokromom *c*, kar bi lahko inhibiralo encimsko aktivnost CcO. To bi privedlo do padca mitohondrijskega potenciala in zmanjšanja sinteze ATP, učinkov, ki sta posledica toksičnega delovanja Atx na živčne celice. Pokazali smo, da se Atx veže na dve mesti na Syt1, eno na citosolni strani tega proteina in eno na strani, ki je usmerjena v lumen sinaptičnega vezikla. Vezavo Atx na citosolni del Syt1 je preprečila prisotnost kalmodulina, citosolnega proteina, ki veže Atx in tudi Syt1. Syt1 verjetno predstavlja nov receptor za Atx na plazemski membrani, ki bi lahko bil pomemben za internalizacijo toksina v nevronske celice. Zasledili smo, da se poleg Atx na Syt1 vežejo tudi nekatere druge toksične ali sesalske $sPLA_2$, kar nakazuje vlogo tega proteina v mehanizmu delovanja tudi teh $sPLA_2$. Očitnega učinka na encimsko aktivnost Atx nismo opazili niti v prisotnosti Syt1 niti CcO.

Pokazali smo, da se Atx kmalu po dodatku v rastno celično gojišče veže na Syt1, PDI in protein z molekulsko maso 25 kDa, ki verjetno predstavlja R25, tudi v živih celicah PC12. To nakazuje, da imajo opažene interakcije Atx tudi fiziološko vlogo in potrjuje hitro internalizacijo toksina v SV, endoplazemski retikel in mitohondrije nevronskih celic.

Z uporabo proteinskega modeliranja smo pripravili 3D-modele kompleksov človeške PDI z Atx in nekaterimi drugimi $sPLA_2$, ki so strukturno podobne Atx. Verodostojnost modelov smo eksperimentalno potrdili. Pripravljeni modeli kompleksov bodo koristno orodje za načrtovanje mutant $sPLA_2$ v raziskavi njihovega vstopa v celice in njihovega znotrajceličnega transporta.

Preverili smo tudi vlogo encimske aktivnosti Atx v toksičnosti te $sPLA_2$. Pripravili smo encimsko neaktivno mutanto AtxA, AtxA(D49S), z mutacijo v aktivnem mestu. Z uporabo fluorescenčnega derivata te rekombinantno pridobljene mutante in fluorescenčno označenega naravnega AtxA smo ugotovili, da encimska aktivnost ni nujno potrebna, ampak pripomore k vstopu te molekule v citosol, endoplazemski retikel, mitohondrije in SV celic PC12. Na podlagi omenjenih rezultatov predvidevamo, da Atx vstopa v živčne celice s pomočjo bolj specifičnih mehanizmov, med njimi tudi takšnih, ki so neodvisni od encimske aktivnosti Atx.

Abbreviations

°C	=	degree Celsius
^{125}I-AtxC	=	the radioactively labelled derivative of AtxC
14-3-3p	=	14-3-3 proteins
3D	=	three-dimensional
^{546}Alexa-Atx	=	fluorescent derivative of Atx
A_{215}	=	Absorbance at 215 nm
A_{260}	=	Absorbance at 260 nm
A_{280}	=	Absorbance at 280 nm
A_{342}	=	Absorbance at 342 nm
A_{600}	=	Absorbance at 600 nm
APS	=	ammonium persulfate
ATP	=	adenosine triphosphate
$AtnI_2$	=	ammodytin I_2
AtnL	=	ammodytin L
Atx	=	ammodytoxin
AtxA	=	ammodytoxin A
AtxA(D49S)	=	enzymatically inactive mutant of AtxA
AtxA WT	=	wild-type AtxA
AtxB	=	ammodytoxin B
AtxC	=	ammodytoxin C
BSA	=	bovine serum albumine
BoNT	=	botulinum neurotoxin
Ca^{2+}	=	calcium ions
CaM	=	calmodulin
CcO	=	cytochrome *c* oxidase
CNS	=	central nervous system
Da	=	dalton, a unit of molecular mass
dH_2O	=	distilled H_2O
ddH_2O	=	deionised and distilled H_2O
DMSO	=	dimethylsulfoxide
DNA	=	deoxyribonucleic acid
dNTP	=	deoxyribonucleoside triphosphates
DPBS	=	Dulbecco's phosphate buffered saline
DSS	=	disuccinimidyl suberate
DTT	=	dithiothreitol
ECL	=	enhanced chemiluminescence
EDTA	=	ethylenediaminetetraacetic acid
EGTA	=	ethylene glycol tetraacetic acid
ER	=	endoplasmic reticulum
F12K	=	cell growth medium
FBS	=	fetal bovine serum
g	=	acceleration of gravity
GIA	=	group IA $sPLA_2$

GIB	=	group IB $sPLA_2$
GII	=	group II $sPLA_2$
GIIA	=	group IIA $sPLA_2$
GV	=	group V $sPLA_2$
GX	=	group X $sPLA_2$
HADDOCK	=	high ambiguity-driven docking
HBSS	=	Hank's balanced salt solution
HCl	=	hydrochloric acid
hGIIA $sPLA_2$	=	human GIIA $sPLA_2$
hGV $sPLA_2$	=	human GV $sPLA_2$
hGX $sPLA_2$	=	human GX $sPLA_2$
hPDI	=	human PDI
HPLC	=	high performance liquid chromatography
HRP	=	horse-radish peroxidase
IBS	=	interfacial binding site of $sPLA_2$
IgG	=	immunoglobulin G
IPTG	=	isopropyl β-*D*-1-thiogalactopyranoside
kDa	=	kilodalton
LTB	=	label transfer buffer
M	=	molar
MS	=	mass spectrometry
ND	=	non-differentiated
NGFD	=	NGF-differentiated
NGF	=	nerve growth factor
NSC-34	=	mouse neuroblastoma spinal cord hybrid cell line
NTSB	=	2-nitro-5-thiosulfobenzoic acid
PC12	=	rat pheochromocytoma cell line
PCR	=	polymerase chain reaction
PDI	=	protein disulfide isomerase
PFA	=	paraformaldehyde
pGIB $sPLA_2$	=	porcine GIB $sPLA_2$
PMSF	=	phenylmethylsulfonyl fluoride
PLA_2s	=	phospholipases A_2
PVDF	=	polyvinylidene difluoride
PyPG	=	substrate for measuring PLA_2 activity
R25	=	mitochondrial membrane receptor for Atx
RP-HPLC	=	reverse phase HPLC
RPM	=	revolutions per min
SA-HRP	=	streptavidin conjugated with HRP
SDS	=	sodium dodecyl sulfate
SDS-PAGE	=	polyacrylamide gel electrophoresis in the presence of SDS
SNARE	=	soluble NSF attachment protein receptor
$sPLA_2$s	=	secreted PLA_2s
sulfo-SBED-AtxC	=	photo-active biotin-containing derivative of AtxC
SV	=	synaptic vesicles
Syt1	=	synaptotagmin 1
Syt2	=	synaptotagmin 2
TBS	=	tris buffered saline
TEMED	=	tetramethylethylenediamine
TFA	=	trifluoroacetic acid
Tris	=	tris(hydroxymethyl)aminomethane

TX-100	=	Triton X-100
UV	=	ultraviolet
W	=	Watt
yPDI	=	yeast PDI

1 Introduction

1.1 Phospholipases A_2

Phospholipases A_2 (PLA_2s) are enzymes that act on lipids in biological membranes. Specifically they catalyse hydrolysis of the *sn-2* ester bond in glycerophospholipids, yielding free fatty acids (typically unsaturated) and lysophospholipids (Figure 1) (Dennis, Cao, Hsu, Magrioti & Kokotos, 2011).

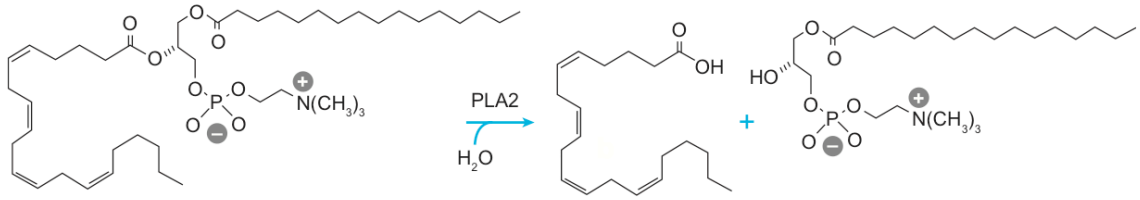

Figure 1: *Reaction catalyzed by PLA_2*. The figure shows hydrolysis of the *sn-2* ester bond of 1-palmitoyl-2-arachidonyl-phosphatidylcholine by PLA_2, yielding free arachidonic acid and 1-palmitoyl-lysophosphatidylcholine. The figure is taken from Lambeau & Gelb (2008).

In mammals, more than 30 enzymes, belonging to the PLA_2 superfamily were discovered (Murakami et al., 2011).

Based on their structure, localization, catalytic mechanism and molecular evolution, they are subdivided into several classes including secreted PLA_2s ($sPLA_2$s), Ca^{2+}-dependent cytosolic PLA_2s, Ca^{2+}-independent PLA_2s, platelet-activating factor acetylhydrolases, lysosomal PLA_2s and adipose-specific PLA_2 (Murakami et al., 2011).

Because of the diversity of pharmacological activities they exhibit, PLA_2s have been implicated in various physiological and pathological processes such as cell signalling, membrane remodelling, host defence, atherosclerosis, tumour progression and others (Lambeau & Gelb, 2008).

1.2 $sPLA_2$s

$sPLA_2$s are a class of mostly low-molecular mass PLA_2, ranging from 13–19 kDa. They are structurally conserved and disulphide rich, each containing 5–8 disulphide bridges, making them compact and stable in the extracellular environment. Their active site includes the His–Asp catalytic dyad. They contain a conserved Ca^{2+}-binding loop with a structurally-bound Ca^{2+} ion, required for their enzymatic activity.

$sPLA_2$s are divided into 12 groups (Murakami et al., 2011): groups (G) IB, IIA, IIC, IID, IIE, IIF, III, V, X, XIIA, XIIB and otoconin-90, an $sPLA_2$-like protein. GI, GII, GV and GX are structurally similar, whereas GIII and GXII are structurally more distinct from them (Singer et al., 2002; Lambeau & Gelb, 2008).

$sPLA_2$s contain an N-terminal signal peptide, which targets these enzymes for secretion into the extracellular space (Lambeau & Gelb, 2008). This signal peptide is

cleaved during the transfer of $sPLA_2$ into the lumen of the endoplasmic reticulum (ER).

$sPLA_2$s are secreted from a variety of cells and exhibit autocrine or paracrine action. They act on cellular phospholipid membranes and other phospholipids, and require micromolar to milimolar concentrations of Ca^{2+} for enzymatic activity. They exhibit a higher affinity for aggregated than for monomeric substrates. The majority of GII and GIB $sPLA_2$s show a preference for hydrolyzing membranes, consisted of negatively charged phospholipids like phosphatidylserine and phosphatidylglycerol. Unlike GII and GIB $sPLA_2$, GV and GX $sPLA_2$s efficiently hydrolyze also neutral phospholipid membranes. The efficiency of hydrolyzing phospholipids is mostly determined by the affinity of $sPLA_2$s for binding to the membrane.

Each $sPLA_2$ group exhibits distinct structural features. GIB $sPLA_2$ (GIB) has an insert of 5 additional amino acid residues in the middle of the molecule, called the pancreatic loop, and a GI-specific disulphide between Cys11 and Cys77. At the N-terminus, GIB $sPLA_2$ contains a propeptide of 8 amino acid residues, which is cleaved by trypsin to yield an active enzyme (Verheij, Slotboom & de Haas, 1981; Murakami et al, 2011). Its role is mostly the digestion of phospholipids. Among the GII $sPLA_2$s (GII), the GIIA $sPLA_2$ has been most thoroughly characterized. It is commonly referred to as the "inflammatory $sPLA_2$", due to its role in inflammatory diseases. GII $sPLA_2$s contain a C-terminal extension of 6 amino acid residues (Murakami et al, 2011). GV $sPLA_2$ (GV) contains no N-terminal propeptide or C-terminal extension. GX $sPLA_2$ (GX) has an N-terminal propeptide of 11 residues, which is cleaved to activate the $sPLA_2$ and a C-terminal extension. The GIII $sPLA_2$ (GIII) has unique N- and C-terminal domains in addition to the central $sPLA_2$ domain, which are thought to be removed *in vivo* (Murakami et al., 2005). GXII comprises two $sPLA_2$s, which are structurally very different from the other $sPLA_2$s, one of them being enzymatically inactive. They contain only the conserved Ca^{2+}-binding loop.

1.2.1 Enzymatic activity of $sPLA_2$

1.2.1.1 Catalytic mechanism of $sPLA_2$

The catalytic site in $sPLA_2$ is composed of His48, Asp49 and a Ca^{2+} ion, bound to oxygen atoms of Tyr28, Gly30, Gly32, Asp49 and two water molecules. Two different mechanisms of catalysis have been proposed, shown in Figure 2. According to Kuipers, van der Bergh, Verheij and de Haas (1990), the mechanism involves a water molecule bound to the Ca^{2+} ion in the active site. This water molecule acts as a nucleophile and attacks the carbonyl carbon of the substrate ester group. The proton of the water molecule is transferred to the imidazole nitrogen of His48 of the $sPLA_2$. The second mechanism was proposed by Jain & Berg (2006) and involves a second water molecule.

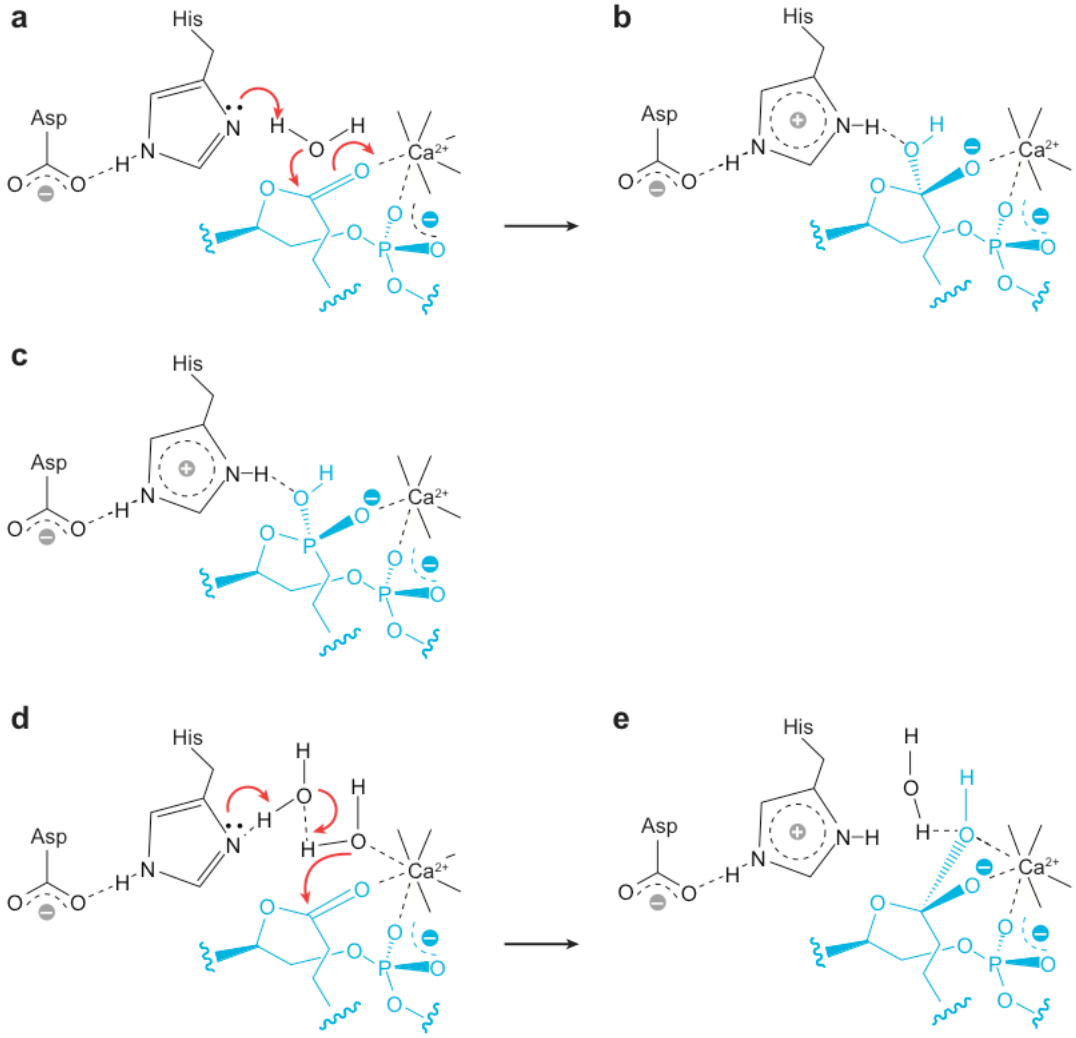

Figure 2: *The proposed mechanism of sPLA$_2$-catalyzed phospholipid hydrolysis.* (a) The first proposed mechanism of sPLA$_2$ catalytic action involves a water molecule that is hydrogen-bonded to the nitrogen atom in the imidazole ring of His48. The oxygen in the water molecule attacks the carbonyl carbon of the substrate. The proton is transferred from the water to the imidazole nitrogen. The carbonyl carbon of the substrate is bound to the Ca^{2+} ion. (b) A proposed tetrahedral intermediate resulting from the mechanism depicted in panel a. The Ca^{2+} ion stabilizes the oxyanion derived from the substrate carbonyl oxygen. (c) The phospholipid intermediate state analogue bound in the active site, as revealed by X-ray crystallography. The blue structure mimics the proposed intermediate in panel b. (d) Jain & Berg (2006) proposed a mechanism involving two water molecules. According to this scenario, the Ca^{2+}-coordinated water molecule acts as a nucleophile and the proton from this water molecule is transferred to another water molecule with concomitant proton transfer from this second water molecule to the imidazole nitrogen of His48. (e) The proposed tetrahedral intermediate resulting from the mechanism in (d). The substrate, substrate-derived intermediates and the phospholipid analogue are shown in blue. The figure is taken from Lambeau & Gelb (2008).

1.2.1.2 sPLA$_2$s act at the surface of the lipid bilayer

Naturally occurring phospholipids are water-insoluble molecules and form aggregates in water solutions. Since sPLA$_2$s are water-soluble proteins, they must adsorb to the phospholipid membrane interface to hydrolyze their substrate. Thus they act at the interface of the solid and liquid phases. They bind to phospholipid membranes *via* their interfacial binding site (IBS), which is distinct from their enzyme active site. By binding

to the membrane, the so called interfacial activation occurs, *i.e.* interfacial binding promotes binding of the substrate molecule to the active site and catalytic efficiency (Lambeau & Gelb, 2008).

1.2.2 Toxicity of $sPLA_2$

$sPLA_2$s represent the major toxic components of many animal venoms. From the ancestral role in digesting phospholipids and membrane homeostasis, some of them have evolved to exhibit a range of toxic activities, such as neurotoxic, myotoxic, anticoagulant, cardiotoxic or cytotoxic (Kini, 1997) and they are found in venoms of snakes, bees and scorpions.

Our research focuses on the group of $sPLA_2$s that act on neuromuscular junctions of vertebrate skeletal muscles, inhibiting the communication between the neuron and the muscle cell. These toxic $sPLA_2$s act on presynaptic neuronal cells and are called β-neurotoxins (β-ntxs).

Abundant sources of β-ntxs are venoms of Elapidae and Viperidae snakes. β-ntxs belong to the GI, GII and GIII $sPLA_2$s. They are monomers or form mostly non-covalent but also covalent complexes of two, three or five subunits, at least one of which is a $sPLA_2$. Up to 15 pharmacologically and enzymatically distinct $sPLA_2$s can be found in the venom of the same snake species (Valentin & Lambeau, 2000).

1.3 Ammodytoxins from the venom of the nose-horned viper

Ammodytoxins (Atxs) belong to the GIIA $sPLA_2$s of β-ntxs (Gubenšek & Križaj, 1997; Križaj, 2011). Three natural variants of Atx have been described, AtxA, AtxB and AtxC, in the venom of the nose-horned viper (*Vipera ammodytes ammodytes*). They contain 122 amino acid residues and have a molecular mass around 13.9 kDa. They differ in maximally 5 residues (Figure 3), but nonetheless exhibit very different toxicities. AtxA is the most toxic isoform, with an LD_{50} of 21 μg/kg in mice, and AtxB the least toxic. AtxC, exhibiting a 15-fold lower toxicity in mice than AtxA (Prijatelj-Žnidaršič & Pungerčar, 2012), differs from AtxA in only two residues (Thouin et al., 1982; Gubenšek & Križaj, 1997). Atxs are basic and hydrophobic, and tend to stick to surfaces. In comparison with AtxA, AtxC exhibits much less affinity to bind nonspecifically to plastic surfaces and is therefore preferentially used as a probe for studying biochemical properties of Atxs.

Also three homologues of Atx were isolated from *V. a. ammodytes* venom; ammodytin I_2 ($AtnI_2$), which is an active $sPLA_2$ but exerts no toxic effects (Križaj et al., 1992), a similar non-toxic $sPLA_2$, named $AtnI_1$, and the enzymatically inactive ammodytin L (AtnL), which is a potent myotoxin (Križaj, Bieber, Ritonja & Gubenšek, 1991; Rufini, Cesaroni, Balestro & Luly, 1996; Pungerčar et al., 1998).

Intoxication of humans with *V. a. ammodytes* venom causes blood clotting disorders, oedema, release of blood into the subcutaneous tissue and local lymph node inflammation. The neurotoxic effects have been reported in 16% of the victims and include ptosis, ophthalmoplegia, dysphagia, dysphonia, and neuromuscular weakness (Radonić et al., 1997; Lukšić, Bradarić & Prgomet, 2006).

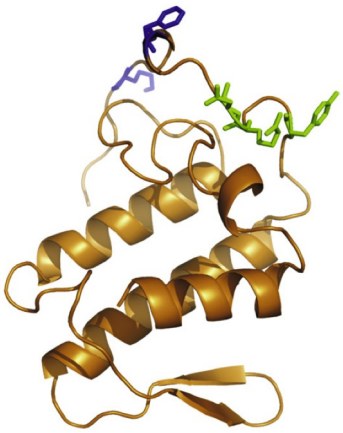

Figure 3: *Three-dimensional structure of ammodytoxin.* AtxA differs from AtxB in 3 amino acid residues (Y115H/R118M/N119Y, shown in green) and from AtxC in 2 residues (F124I/K128E, shown in blue). Figure is taken from Križaj (2011).

1.4 Neurotoxic effects of Atx and homologous sPLA$_2$

β-ntxs are usually injected into the periphery of prey organisms. These toxins cannot penetrate the blood-brain barrier, therefore the central nervous system (CNS) is usually not affected by their action. By a direct injection of β-ntxs into the brain, however, they have been proven highly toxic to CNS.

The target of Atx and similar β-ntxs is the peripheral nervous system, specifically cholinergic synapses of motoneurons. β-ntxs affect the presynaptic neuronal cell. They stop the release of acetylcholine from the motoneuron, thereby disrupting the neuromuscular communication. The prey usually dies as a result of respiratory muscle paralysis, whereas other tissues remain unaffected (Connoly et al., 1995, Prasarnpun, Walsh, Awad & Harris, 2005).

Despite structural and pharmacological differences between different β-ntxs, they exhibit a similar triphasic effect on the isolated neuromuscular junction (Pungerčar & Križaj, 2007) (Figure 4). First, shortly after the administration of the β-ntx, there is a transient loss of acetylcholine release that lasts for several min (phase 1). The second phase is characterized by a facilitation of neurotransmitter release, reaching its maximum in 10–20 min after the addition of the toxin. In the third phase a gradual irreversible inhibition of transmitter release is observed and the neuromuscular communication stops completely in 1–2 h.

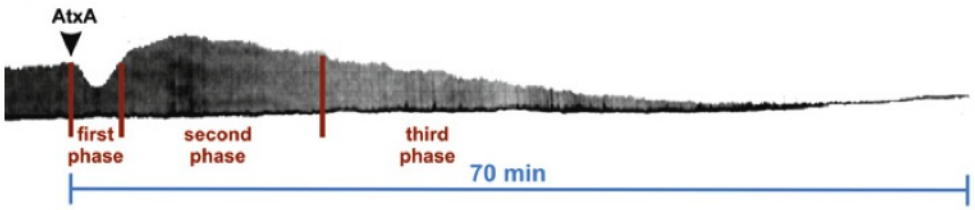

Figure 4: *The triphasic effect of Atx on the isolated neuromuscular preparation.* Indirectly stimulated isolated neuromuscular preparation exhibits the characteristic triphasic response due to the action of the β-ntx. The complete paralysis of the muscle occurs approximately 1 h after the exposure to Atx. Figure is taken from Križaj (2011).

No significant change in the amplitude of the miniature end plate potential was observed, meaning that the SVs do not fuse inside the nerve terminal prior to exocytosis. The acetylcholine transporter is not affected by the presence of β-ntxs. Phase one is dependent on temperature and is therefore not a consequence of just the binding of β-ntxs to their presynaptic receptor. β-ntxs do not require electrostimulation of the motor nerve to induce paralysis (Šribar, Oberčkal & Križaj, 2014).

Electron micrographs of neuromuscular junctions exposed to β-ntxs show characteristic morphological changes, as observed with β-bungarotoxin (Prasarnpun, Walsh & Harris, 2004). Synaptic vesicles (SV) decrease in number and omega-shaped invaginations, surrounded by an electron dense material (most likely clathrin), appear at the presynaptic plasma membrane. These invaginations could be due to the inability of SVs to endocytose after they fused with the membrane (Prasarnpun et al., 2004). Findings, obtained with AtxA-poisoned neuromuscular preparations, show a markedly lower reduction in SV and the absence of omega-shaped invaginations compared to the effect of β-bungarotoxin. Instead, Atx caused clustering of SVs in the cytosol and at release sites in nerve endings (Logonder, Križaj, Rowan & Harris, 2008b) (Figure 5).

As a result of the β-neurotoxic action, large vesicles appear in the cytosol and mitochondria lose their structural integrity. They become enlarged, rounded and the structure of cristae is compromised (Figure 5) (Lee, Tsai, Chen, Ritonja & Gubenšek, 1984; Montecucco & Rosetto, 2000; Rossetto, Morbiato, Caccin, Rigoni & Montecucco, 2006; Pungerčar & Križaj, 2007; Logonder et al., 2008b, Jenko Pražnikar et al, 2008).

Also, as a result of β-ntx poisoning, fragmentation of the F-actin cytoskeleton was observed (Neco, Rossetto, Gil, Montecucco & Gutierrez, 2003; Rigoni et al., 2004; Jenko Pražnikar et al., 2008), which was attributed to the activation of calpains due to the increase in Ca^{2+} concentration (Duregotti, Tedesco, Montecucco & Rigoni, 2013).

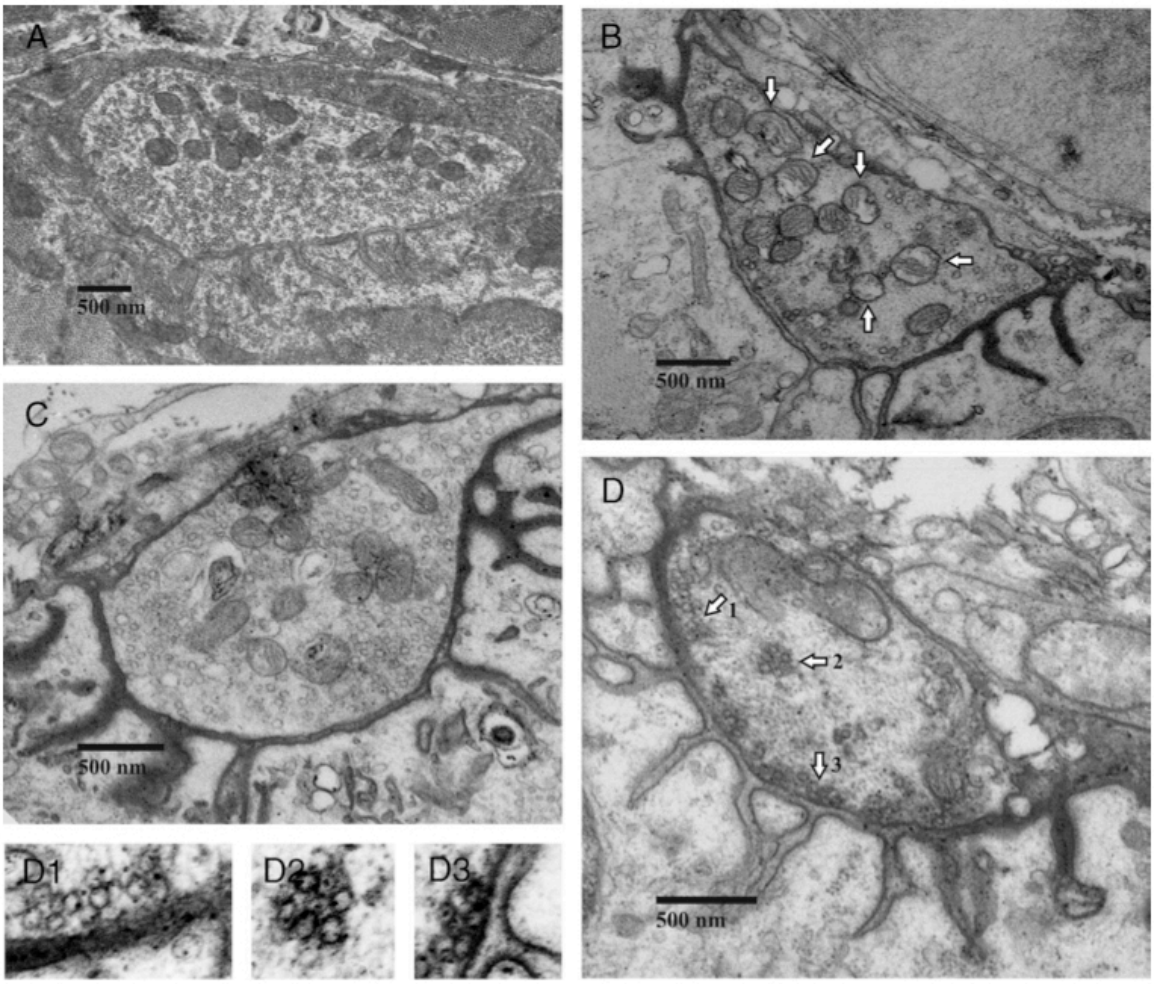

Figure 5: *Electron micrographs of motor endplates in a mouse soleus muscle fibre exposed to AtxA*. (A) The control muscle fibre without the added AtxA. (B–D) Muscle fibres exposed to AtxA. (B) The arrows point to damaged mitochondria in the motor neuron terminal. The depletion of SVs is evident (small circles in A that are largely absent in B). (D) SV clustering was observed within the cytosol and at release sites (indicated with arrows and numbers). Corresponding numbered areas of SV clustering are enlarged and shown in D1, D2 and D3. The figure was taken from Logonder et al. (2008b).

1.4.1 The importance of binding proteins in the process of β-neurotoxicity

The molecular basis of β-neurotoxicity has not yet been entirely elucidated. It has been debated extensively, whether β-ntxs act exclusively extracellularly or they enter target cells and if these processes are attributed to their enzymatic activity or binding to specific receptors. The enzymatic activities of β-ntxs on biologically relevant substrates do not correlate with their lethalities (Paoli et al., 2009), pointing to the importance of the ligand binding abilities of these toxins for their neurotoxic effect.

It is clear though that the enzymatic activity is not responsible alone for β-neurotoxicity.

Numerous β-ntx-binding proteins have been identified (Šribar & Križaj, 2011). So far, however, a presynaptic receptor, responsible for β-neurotoxicity, has not been identified. Most likely, several different β-neurotoxicity-related receptors exist at the presynaptic membrane (Šribar et al., 2014). The best candidate to date is the N-type receptor,

described by Lambeau et al. (1989). This receptor binds only neurotoxic $sPLA_2$s. The lethalities of β-ntxs correlate well with their affinities for the N-type receptor.

In the presynaptic membrane, only two binding proteins for β-ntxs have been identified so far. The voltage dependent K^+-channel binds only β-bungarotoxins (Scott et al., 1990). The other protein is the M-type receptor (Lambeau. Schmid-Alliana, Lazdunski & Barhanin, 1990). It was shown (Prijatelj, Vardjan, Rowan, Križaj & Pungerčar, 2006) that variants of AtxA with N-terminal extensions failed to interact with the M-type receptor, but still retained their neurotoxicity. This proved that this receptor is not (solely) responsible for the toxicity of Atx.

1.4.1.1 Intracellular binding proteins for Atx

It has been demonstrated several times that β-ntxs internalize into target cells, giving relevance to the discoveries of intracellular β-ntx-binding proteins.

In porcine cerebral cortex, one of the high-affinity binding proteins of Atx was identified as calmodulin (CaM) (Šribar et al., 2001). CaM is a Ca^{2+}-binding cytosolic protein, implicated in the regulation of many cellular processes. Besides Atx, it was shown to bind also other neurotoxic snake venom and non-toxic mammalian $sPLA_2$s (Šribar et al., 2001, Kovačič, Novinec, Petan & Križaj, 2010). *In vitro*, CaM was shown to stabilize Atx in reducing cytosol-like conditions and increase its enzymatic activity (Kovačič, Novinec, Petan, Baici & Križaj, 2009a; Kovačič et al., 2010) and could therefore act as an intracellular modulator of Atx's phospholipase activity.

Two other Atx-binding proteins, 14-3-3 protein (14-3-3p) γ and ε isoforms, were also discovered in the cytosol (Šribar et al., 2003a). 14-3-3ps are widespread and involved in several processes, including intracellular trafficking, signal transduction, cell cycle regulation and organization of the cytoskeleton (Šribar & Križaj, 2011). Interaction with 14-3-3ps was suggested to be responsible for Atx's inhibition of the cell cycle arrest in G2 phase in yeast cells (Petrovič et al., 2005). Besides Atx, 14-3-3ps were shown to bind also AtnL, β-bungarotoxin, taipoxin and bee venom $sPLA_2$ (Mattiazzi et al., 2012). 14-3-3ps have been detected associated with the synaptic junction and SV membranes (Martin, Rostas, Patel & Aitken, 1994) and could concentrate Atx at the active zones at the presynaptic membrane (Šribar et al., 2014). Once located there, Atx causes the inhibition of vesicle endocytosis. This process, shown in yeast with endogenously expressed Atx, is enzymatic activity-dependent and probably occurs through the interference of phospholipolysis products with the activity of the membrane curvature sensing protein amphiphysin (Mattiazzi et al., 2012).

Both, CaM and 14-3-3p proteins were shown to interact with Atx also in live neuronal cells (Jenko Pražnikar et al., 2008; Kovačič, 2009b), suggesting that they have physiological importance in β-neurotoxicity.

1.4.1.1.1 PDI

Šribar, Anderluh, Fox & Križaj (2005) identified protein disulfide isomerase (PDI) as one of the proteins, specifically eluted from the Atx-affinity chromatography of synaptosomal fraction of the porcine cerebral cortex. PDI is an oxido-reductase, located in the lumen of ER (Appenzeller-Herzog & Ellgaard, 2008), where it assists at oxidative folding of proteins and also acts as a molecular chaperone. The PDI family includes 19 enzymes, all of which have a thioredoxin-like domain with an active site of CXXC. These two Cys residues catalyze the formation of a disulphide bond in the substrate molecule. The PDI variant, identified as the Atx-binding protein, is comprised of domains a, b, b', x and a'. The catalytic thioredoxin-like domains a and a' are located at the N- and C-terminus of PDI, respectively, linked together by the domains b and b', which are enzymatically

inactive but play a role in protein interactions (Appenzeller-Herzog & Ellgaard, 2008).

PDI has been implicated in the retrograde trafficking of other toxins (Tsai, Ye & Rappaport, 2002; Lencer & Tsai, 2003; Lord, Roberts & Lencer, 2005; Wernick, Chinnapen, Cho & Lencer, 2010), and it was proposed by Šribar et al. (2005) to play a similar role in the case of Atx.

Besides PDI, also two binding proteins for taipoxin and crotoxin, TCBP-49 and crocalbin, respectively, were discovered in ER (Dodds, Schlimgen, Lu & Perin, 1995; Hseu, Yen, Tseng & Tzeng, 1997; Hseu, Yen & Tzeng, 1999).

Based on interaction site mapping, Kovačič (2009b) prepared a model of the complex between yeast PDI (yPDI) and Atx. In the model, Atx bound to two distinct sites on yPDI, at the b and b' domains and at the a' and c domains. The bb' binding site was proposed to have higher affinity for binding Atx than the a'c site. The bb' region of PDI also binds misfolded proteins and is implicated in actions of other toxins (Appenzeller-Herzog & Ellgaard, 2008), suggesting a similar role for PDI in the mechanism of action of Atx.

1.4.1.1.2 R25

R25 is an integral membrane Atx-binding protein, located in the mitochondria (Vučemilo, Čopič, Gubenšek & Križaj, 1998; Šribar et al., 2003b). This receptor seems to bind only Atx and its neurotoxic mutants but not other β-ntxs (Vučemilo et al., 1998), however, this observation is based on a heterologous competition with ^{125}I-AtxC binding to R25 and not by direct binding assays.

Kovačič (2009b) and our previous work (Oberčkal, 2010) indicated the identity of R25 most likely as subunit 2 of cytochrome c oxidase (CcO) (complex IV). CcO is located at the inner mitochondrial membrane. Subunit 2 is exposed to the intermembrane space (Yoshikawa, Muramoto, Shinzawa-Itoh & Mochizuki, 2012). Since CcO is the terminal oxidase of the respiratory chain, its interaction with Atx could explain the observed effects of Atx's action, namely mitochondrial uncoupling, the loss of structural integrity of cristae and the swelling of mitochondria (Pucer, 2008; Logonder et al., 2008b).

1.4.1.1.3 Syt1

One of the potential binding proteins for Atx was found to be synaptotagmin 1 (Syt1) (Kovačič, 2009b). This protein is localized in the membranes of SVs, where it acts as a Ca^{2+} sensor and triggers synchronous SV exocytosis (Koh & Bellen, 2003; Chapman, 2008). It interacts with SNARE proteins and plasma membrane. Syt1 comprises of two C2 subunits, C2a and C2b, exposed to the cytosol, which bind Ca^{2+} and are responsible for the tethering of the SVs to the plasma membrane at active sites in the presynaptic cell. The cytosolic subunits are connected *via* a transmembrane helix to a short domain in the lumen of SV.

Like PDI, Syt1 was also implicated in the actions of clostridial neurotoxins, specifically botulinum neurotoxins (BoNT). BoNT B and G isoforms have been shown to bind to the luminal part of Syt1 and Syt2 (Rummel, Karnath, Henke, Bigalke & Binz, 2004; Dong et al., 2003).

Due to the location in SVs, which are a known target of β-ntxs (Prasarnpun et al., 2004) and a proposed means of their internalization (Pungerčar & Križaj, 2007), Syt1 is a good candidate for the presynaptic receptor of these toxins. Additionally, its luminal part was shown to be exposed on the cell surface upon treatment of cells by β-ntxs (Rigoni et al., 2004).

1.4.2 The role of enzymatic activity in β-neurotoxicity

Experimental data indicate that phases 1 and 2 of β-ntxs' action on motoneurons do not depend on their enzymatic activity (Caratsch, Maranda, Miledi & Strong, 1981; Su & Chang, 1984, Prijatelj et al., 2006). However, Caccin, Rigoni, Bisceglie, Rossetto & Montecucco (2006) and Rigoni et al. (2005) have suggested the involvement of PLA_2 activity also in these two phases.

It is clear, however, that the third phase of β-ntxs' action is strictly dependent on the phospholipase activity of the β-ntxs. When a mouse hemidiaphragm preparation was incubated in the presence of enzymatically inactivated AtxA or a recombinant AtxA containing an N-terminal 5 amino acid residue fusion peptide (which rendered the molecule less than 0.1% active in comparison to the wild-type AtxA), the third phase of the Atx's neurotoxic effect (total paralysis of the hemidiaphragm) was not observed (Prijatelj et al., 2006; Logonder, 2008b). Instead, the intensity of the muscle twitching remained elevated throughout the experiment (7 h in the case of the enzymatically inactivated AtxA).

In another study, the myotoxic enzymatically inactive paralogue of Atx, AtnL, was mutated to become enzymatically active, which endowed it with β-neurotoxic activity (Petan, Križaj & Pungerčar, 2007).

Interestingly, the mixtures of fatty acids and lysophospholipids (the products of $sPLA_2$ activity) can themselves exert effects on neuromuscular junctions, similar to those induced by β-ntxs (Rigoni et al., 2005, 2007; Megighian, Rigoni, Caccin, Zordan & Montecucco, 2007; Caccin, Rossetto & Montecucco, 2009).

The enzymatic activity alone, however, cannot account for all the effects, exhibited by β-ntxs. This was proven in the study of Prasarnpun et al. (2004), who added β-bungarotoxin to a motoneuron, in which the endocytosis of SVs was blocked by previous addition of BoNT C. The authors found that the effects of β-bungarotoxin were very limited compared to an unpretreated motoneuron.

Rigoni et al. (2008) produced an acetylated variant of notexin with only 2.9% of enzymatic activity of the native toxin. This molecule did not significantly inhibit neurotransmission in a preparation of the mouse hemidiaphragm and also failed to open the mitochondrial permeability transition pores. The authors produced also other chemically modified variants of notexin expressing lower phospholipase activity as the native notexin. The extent of the loss of phospholipase activity of the notexin derivative correlated well with the extent of loss of its neurotoxicity and capability to open the permeability transition pores.

Recently, Simonato et al. (2014) produced an enzymatically inactive mutant of notexin and observed that the mutant still exerted neurotoxic effects on a neuromuscular preparation. It did not, however, open the mitochondrial permeability transition pores, in line with the results of Rigoni et al. (2008).

β-neurotoxic $sPLA_2$s preferentially bind to membranes enriched with anionic phospholipids (Radvanyi, Jordan, Russo-Marie & Bon, 1987; Petan, Križaj, Gelb & Pungerčar, 2005). These are mostly present in the cytosolic layer of cellular organelles and plasma membrane. This suggests that the enzymatic activity of β-ntxs is more important when the toxins are already inside their target cells.

For the complex nature of mechanism of β-neurotoxic action speaks also the existence of enzymatically active and structurally homologous, but not toxic, $sPLA_2$s. Thus $AtnI_2$ from the nose-horned viper venom is a more efficient enzyme than Atx, but possesses no β-neurotoxic activity. On the other hand, the enzymatically inactive AtnL is a potent myotoxin.

1.4.3 Mechanism of action of β-neurotoxic $sPLA_2$

Despite extensive research, the molecular mechanism of action of β-ntxs is still not completely understood. The main questions, remaining unanswered, concern the mechanism of entry of β-ntxs into the cytosol and mitochondria of target cells, intracellular phospholipase activity of β-ntxs and their protein binding.

Translocation of β-ntxs across the plasma membrane of certain cells has been demonstrated several times. Using a photo-reactive derivative of Atx, Jenko Pražnikar et al. (2008) and Kovačič (2009b) have shown that within minutes of addition to the cell medium, Atx translocated into NSC-34 and PC12 cells, where it interacted with CaM and 14-3-3p. Fluorescent or nanogold-labelled derivatives of Atx were found in SVs and mitochondria of NSC-34 cells (Jenko Pražnikar et al., 2008). Nanogold-AtxA was also found in mitochondria and vesicular structures in the cytosol of murine motor neurons (Logonder et al., 2009). Rigoni et al. (2008) showed that also fluorescently labelled notexin, β-bungarotoxin and taipoxin localize to mitochondria of rat cerebellar granular neurons and spinal cord motor neurons.

The mechanism of translocation of β-ntxs into nerve cells is still unknown. Several pathways are possible. One of them has been proposed to be *via* SVs as is the case of BoNT (Montecucco & Rosetto, 2000; Montecucco, Rossetto & Schiavo, 2004; Simpson, 2004; Pungerčar & Križaj, 2007). BoNTs block SV exocytosis by cleaving components of the SNARE complex (Montecucco et al., 2009). Studies with β-bungarotoxin on motor neurons have revealed that blocking SV exocytosis by BoNT C reduced the toxicity of β-bungarotoxin in motoneurons (Prasarnpun et al., 2004). Although the pathway may be the same, the mechanism for the translocation of β-ntxs from the SV lumen into the cytosol is unlikely to be the same as for BoNT. These toxins undergo structural changes, due to the acidification of SV lumen, which allow the metalloproteinase L chain of BoNT to be translocated across the SV membrane. In the case of β-neurotoxic $sPLA_2$s, such drastic structural changes are unlikely, because these proteins are rich in disulphides and are very compact molecules. In line with this, the inhibition of V-type ATP-ase, which acidifies the lumen of SVs, had no effect on toxic effects of β-ntxs (Simpson, Coffield & Bakry, 1994).

One potential pathway of β-ntx translocation into target cells has been proposed to be *via* retrograde transport from ER (Šribar et al., 2005), as is the case for cholera toxin, ricin and Shiga toxin (Sandvig & van Deurs, 2002; Spooner & Lord, 2012; Sandvig, Skotland, van Deurs & Klokk, 2013). In this scenario, PDI is ideally located to facilitate the trafficking of β-ntxs retrogradely from Golgi apparatus to ER, and from there across the ER membrane into the cytosol of the cell.

After the cell internalization, β-ntxs localize in certain cellular compartments, including SVs and mitochondria (Jenko Pražnikar et al., 2008; Rigoni et al., 2008) in cultured cells. In motor neurons, the nanogold-labelled AtxA was observed in vesicular structures in the cytosol and was associated with mitochondria (Logonder et al., 2009).

The current model of action of β-ntxs is presented in Figure 6. β-ntxs, localizing at the neuromuscular junction, bind to the presynaptic membrane and the different sets of β-neurotoxicity-related receptors at the presynaptic membrane. Associated with the axolemma, β-ntxs hydrolyze phospholipids in its external leaflet, producing fatty acids and lysophospholipids. These influence membrane curvature and promote SV exocytosis. Conductivity of some Ca^{2+} channels is increased, which further promotes the exocytosis of SVs. β-ntxs quickly translocate into the target cell, localizing in the cytosol and mitochondria, and utilizing probably multiple internalization pathways. In the cytosol, β-ntxs bind to CaM, 14-3-3p and, possibly, other cytosolic proteins, which might contribute to the β-neurotoxicity. CaM has been shown to stabilize β-ntxs and increase their

enzymatic activity. 14-3-3p might localize β-ntxs at the sites of SV endocytosis. The augmented phospholipase activity at specific sites inside the nerve ending is crucial for β-neurotoxicity. The hydrolysis of the inner layer of the plasma membrane causes the inhibition of SV endocytosis, due to the impairment of amphiphysin function (Mattiazzi et al., 2012). β-ntxs bind to specific sites in the mitochondria (R25 is a β-ntx receptor in mitochondria) and open the permeability transition pores. This results in the inhibition of ATP synthesis and loss of mitochondrial structural integrity. The phospholipolysis of cellular membranes causes the increase in cytosolic Ca^{2+} concentration, promoting the activity of cytosolic proteinases (calpains) and phospholipases, which leads to further degeneration of the nerve ending (Šribar et al., 2014).

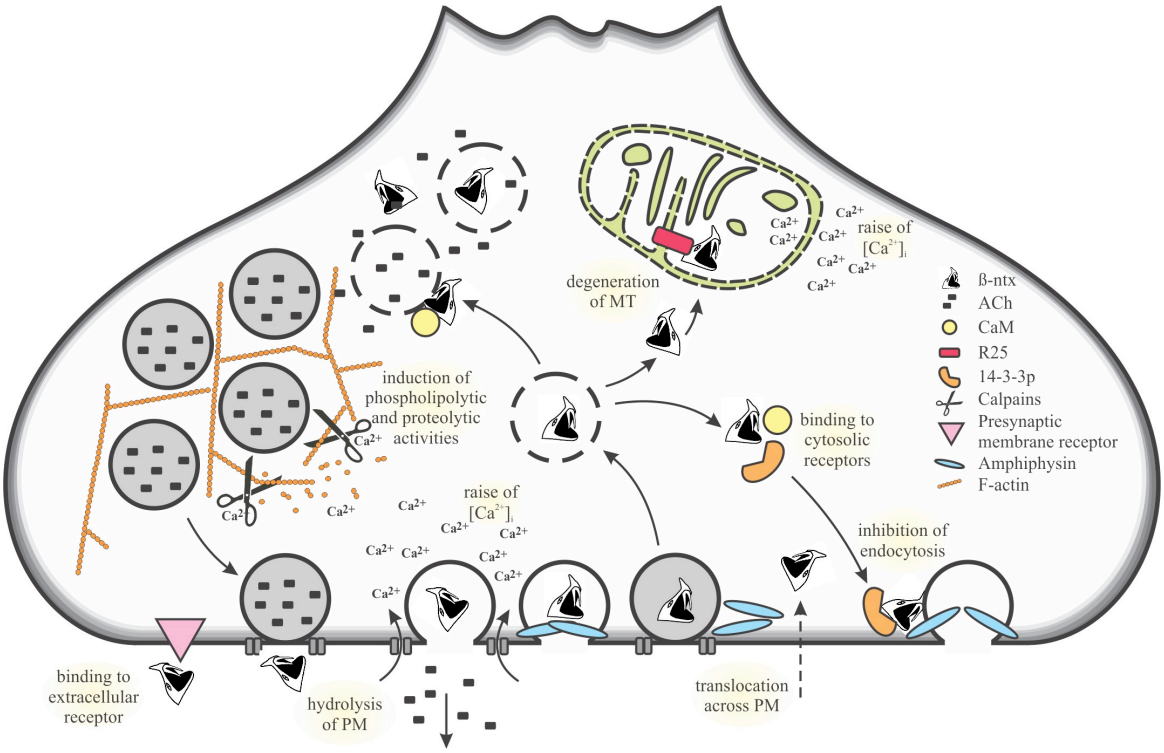

Figure 6: *Possible mode of action of β-ntxs.* The key events in the currently perceived model of β-neurotoxicity are indicated. Figure was taken from Kordiš & Križaj, 2015.

1.5 Model systems

β-ntxs act on the peripheral nervous system. The most appropriate system to study their effects is therefore an isolated neuromuscular preparation. But these preparations are very difficult to study in detail at the molecular level, therefore model systems are utilized for the study of β-neurotoxicity.

For biochemical analyses, brain preparations are often employed. Using these, a variety of β-ntx-binding proteins were discovered (reviewed in Šribar & Križaj, 2011).

For physiological studies, a number of cell lines that are affected by β-neurotoxins, have been used, among them also hippocampal, cortical and cerebellar granule neurons (CGN neurons). Besides the primary cultures of CNS neurons, also immortal cell lines such as the mouse neuroblastoma spinal cord hybrid line (NSC-34), which can be differentiated to motoneuron-like cells, and the rat pheochromocytoma cell line (PC12) are often used. The effects of β-neurotoxins on different model systems, however, may differ, and may also differ from the effects these toxins exert on their primary target – the neuromuscular junction. The results, obtained with model systems, must therefore be

interpreted with caution (Šribar et al., 2014).

1.5.1 PC12 cell line

The rat pheochromocytoma PC12 cells can be differentiated into neuron-like cells (NGFD PC12 cells) with nerve growth factor (NGF) (Green & Tischler, 1976). Non-differentiated PC12 cells (ND) are round, have a diameter of 6–14 μm and divide every 48–96 h. The cells adhere mildly to plastic surfaces and well to surfaces coated with poly-*L*-lysine or collagen.

The cells not only contain vesicles filled with epinephrine, norepinephrine and dopamine, but are also able to synthesize, store and release acetylcholine. They also express nicotinic and muscarinic acetylcholine receptors on their plasma membrane and may therefore serve as a model for studying cholinergic neurons (Fujita, Lazarovici & Guroff, 1989).

Upon addition of NGF, the cells enlarge and acquire the ability to form synapses. Neuronal processes (neurites and axons) start to grow from the main body of the cells. The differentiation causes a 10–20-fold rise in the number of Na^+-channels on the surface of the cells and results in the loss of the cells' ability to undergo mitosis (Hatanaka, 1981; Levi, Biocca, Cattaneo & Calissano, 1988).

Besides NGF, the cells are susceptible to other growth factors that also induce the growth of neuronal processes. The same effect has been observed in the treatment of PC12 cells with GV and GX $sPLA_2$s (Nakashima et al., 2003), and also with snake venom GI and GII $sPLA_2$s. In the case of the latter, the growth of the neurites was attributed to the enzymatic activity of $sPLA_2$s (Makarova, Osipov, Tsetlin & Utkin, 2006). A recent study observed an expression of the Atx-homologous GIIA $sPLA_2$ in PC12 cells, induced by NGF. The newly synthesized $sPLA_2$ was targeted to growing neurites (Nardicchi et al., 2014). GIIA was also found in the cytosol and mitochondria of ND PC12 cells and plasma membrane and neurites of NGFD cells (Macchioni et al., 2004; Ferrini et al., 2010). GIIA $sPLA_2$ was released from mitochondria of PC12 cells as a result of the lowering of mitochondrial potential (Macchioni et al., 2004).

Upon intoxication with AtxC, a release of cytochrome *c* was observed in PC12 cells, but the cells did not undergo apoptosis (Šribar, personal communication). A decrease in mitochondrial potential of the cells was observed by Pucer (2008) as a result of treatment with AtxC, whereas their metabolic activity was, interestingly, increased.

2 Aims and Hypotheses

The molecular mechanism of action of Atx and other β-ntxs is still not fully understood. Studies show that β-neurotoxicity is a sum of the phospholipase activity of these molecules as well as their binding to specific receptors in the nerve endings. SVs are a known target of β-neurotoxic action and as such could harbour as yet unidentified receptors for β-ntxs. The intracellular proteins PDI, Syt1 and CcO have been indicated as Atx-binding proteins *in vitro*. The principal aim of this study was to investigate the specificity and pathophysiological relevance of these interactions, and assess the existence of new receptors for β-ntxs in SVs.

The second part of our work was to investigate the role of phospholipase activity in the neurotoxic process of Atx. To this end, we prepared an enzymatically inactive mutant of AtxA, AtxA(D49S). Comparatively with AtxA we investigated then the internalization and localization of this mutant in the model neuronal cells, PC12 cells, as well as its co-localization with the intracellular binding proteins of Atx: Syt1, CcO, PDI and 14-3-3p.

We based our research on the following hypotheses:

1. The neurotoxic action of Atx depends on its internalization into the cytosol, SVs and mitochondria of the nerve cell and its intracellular phospholipase activity.

2. To enter neuronal cells, Atx utilizes its phospholipolytic activity as well as the interaction with specific receptor(s) in the presynaptic membrane.

3. One of the possible points of entry into the motor neuron is *via* SVs. We expect that specific Atx-binding proteins exist in these structures.

4. Possible pathway of internalization of Atx into cells is the retrograde transport, where its interaction with PDI may be important. We expect that Atx interacts with PDI also in living cells.

5. The neurotoxic action of Atx on motoneurons causes also mitochondrial damage and uncoupling of the respiratory chain, where the interaction of Atx with CcO may be crucial. We expect that CcO is a specific binding partner for Atx in mitochondria.

3 Materials and Methods

3.1 Materials

3.1.1 Reagents

Acetic acid (Applichem, Germany)
Acetonitrile (Sigma-Aldrich, USA; Merck, Germany)
Acrylamide (Sigma-Aldrich, USA)
Alexa Fluor 546, carboxylic acid, succinimide ester (Molecular Probes, USA)
Agar (Sigma-Aldrich, USA)
Agarose (Sigma-Aldrich, USA)
$AgNO_3$ (Fluka, Sigma-Aldrich, USA)
Amersham Hyperfilm ECL film, (GE Healthcare, UK)
APS (ammonium persulfate) (Serva, Germany)
Ampicillin (Sigma-Aldrich, USA)
Antifade reagent Prolong Gold (Molecular Probes, USA)
β-mercaptoethanol (Sigma-Aldrich, USA)
Bromophenol blue (Pharmacia, Sweden)
$CaCl_2$ x $2H_2O$ (Sigma-Aldrich, USA)
Casein hydrolysate (Sigma-Aldrich, USA)
Chloroform (Carlo Erba, Italy)
Citric acid (Serva, Germany)
Coomassie Brilliant Blue R350 (GE Healthcare, Sweden)
$CuSO_4$ x $5H_2O$ (Sigma-Aldrich, USA)
D-biotin (Pierce, USA)
Developer and replenisher for ECL and autoradiography films (Kodak, USA)
DMSO (dymethylsulfoxide) (Merck, Germany)
dNTP mix (1.25 mM each) (Promega, USA)
DSS (disuccinimidyl suberate) (Pierce, USA)
DTT (dithiothreitol) (Sigma-Aldrich, USA)
EDTA (ethylenediaminetetraacetic acid), disodium salt (Serva, Germany)
EGTA (ethylene glycol tetraacetic acid) (Sigma-Aldrich, USA)
Ethanol (Carlo Erba, Italy)
$FeSO_4$ (Fluka, Sigma-Aldrich, USA)
Fixer for ECL and autoradiography films (Kodak, USA)
Formaldehyde, 37% (w/v) (Merck, Germany)
Glycerol (Carlo Erba, Italy)
Glycine (Serva, Germany)
Glucose (Sigma-Aldrich, USA)
Glutathione, oxidized and reduced (Sigma-Aldrich, USA)
Guanidine hydrochloride (Gnd.HCl) (Sigma-Aldrich, USA)
HCl (hydrochloric acid), 37% (v/v) (Applichem, Germany)

Hepes (4-(2-hydroxyethyl)-1-piperazineethanesulfonic acid) (Serva, Germany)
Isopropanol (Merck, Germany)
KH_2PO_4 (Fluka, Sigma-Aldrich, USA)
Kodak Biomax autoradiography films (Kodak, USA)
Lactose (Sigma-Aldrich, USA)
Lumi-light Plus Western Blocking Substrate (Roche Applied Science, Germany)
Molecular mass marker, prestained (Fermentas, USA)
Molecular mass marker, unstained (Fermentas, USA)
Methanol (Merck, Germany)
$MgCl_2$ (Merck, Germany)
Na_2HPO_4 (Merck, Germany)
Na_2SO_3 (Sigma-Aldrich, USA)
NaCl (Applichem, Germany)
NaOH (Merck, Germany)
NH_4Cl (Sigma-Aldrich, USA)
Nitrocellulose membrane (Millipore, USA)
NTSB reagent, prepared by Dr. Vesna Brglez
PAGEr precast gels (12%T-G) (Lonza, Switzerland)
PCR grade water (Qiagen, Germany)
Penicillin and streptomycin (Gibco, USA)
PFA (paraformaldehyde) (Serva, Germany)
PMSF (phenylmethylsulfonyl fluoride) (Sigma-Aldrich, USA)
Poly-*L*-lysine (Sigma-Aldrich, USA)
Protease inhibitor cocktail, EDTA-free (Sigma-Aldrich, USA)
PVDF membrane (Millipore, USA)
PyPG (1-Hexadecanoyl-2-(1-Pyrenedecanoyl)-*sn*-Glycero-3-Phosphoglycerol) (Molecular Probes, USA)
Photographic film developer (Kodak, USA)
Rhodamine phalloidin (Life Technologies, USA)
SDS (sodium dodecyl sulfate) (Serva, Germany)
Sucrose (Fluka, Sigma-Aldrich, USA)
Sulfo-SBED (Pierce, USA)
SYBR Safe DNA gel stain (Invitrogen, USA)
Taurine (Sigma-Aldrich, USA)
Thiamine (Sigma-Aldrich, USA)
Toluene (Sigma-Aldrich, USA)
TEMED (Merck, Germany)
TFA (trifluoroacetic acid) (Applied Biosystems, USA)
Triethylamine (Pierce, USA)
Tris (tris(hydroxymethyl)aminomethane) (Serva, Germany)
Triton X-100 (Serva, Germany)
Tween-20 (Sigma-Aldrich, USA)
Western Blocking Reagent (Roche Applied Science, Germany)
Yeast extract (Sigma-Aldrich, USA)

3.1.2 Antibodies

Goat anti-mouse IgG, HRP-conjugated (Jackson ImmunoResearch, USA)
Goat anti-rabbit IgG, HRP-conjugated (Jackson ImmunoResearch, USA)
Goat anti-mouse IgG, labelled with Alexa Fluor 488 (Invitrogen, A11029, USA)
Goat anti-rabbit IgG, labelled with Alexa Fluor 488 (Invitrogen, A11070, USA)

Mouse anti-calmodulin (Calbiochem, 208696, Merck, Germany)
Mouse anti-cytochrome c oxidase subunit II antibodies (Molecular Probes, A6404, USA)
Rabbit anti-AtxA antibodies, prepared by Halassy et al. (2008)
Rabbit anti-protein disulfide isomerase antibodies (Stressgen, SPA-890, Canada)
Rabbit anti-14-3-3 proteins (Santa Cruz Biotechnology, Sc-629, USA)
Rabbit anti-synaptotagmin 1/2 (Signalway Antibody, 21293, USA)
Rabbit anti-synaptotagmin 1 (Signalway Antibody, 21292, USA)

3.1.3 Proteins and DNA primers

BSA (bovine serum albumine, fatty acid free) (Sigma-Aldrich, USA)
CaM (calmodulin) from porcine brain (Enzo Life Sciences)
CcO (cytochrome c oxidase) from bovine heart (Sigma-Aldrich, USA)
DNA ligase T4 and 10x ligation buffer (New England BioLabs, USA)
DNA polymerase *Pfu* and *Pfu* reaction buffer (Promega, USA)
Dnase I (Roche Applied Science, Germany)
Fish skin gelatin (Sigma-Aldrich, USA)
Human PDI 1A (protein disulfide isomerase) (Biorbyt, UK)
Human Syt1 (synaptotagmin 1) (Abnova, Taiwan)
Human Syt1, N-terminal peptide (ChinaPeptides, China)
^{125}I-AtxC (prepared by Dr. Jernej Šribar)
Monomeric avidin-agarose (Pierce, USA)
NGF (nerve growth factor) (Promega, USA)
Protein G-Sepharose (Pharmacia, Sweden)
Restriction endonuclease, FastDigest, *Nde*I (Thermo Scientific, USA)
Restriction endonuclease, FastDigest, *Hin*dIII (Thermo Scientific, USA)
Streptavidin, HRP-conjugated (Pierce, USA)
DNA primers (MWG Operon, Germany)

3.1.4 sPLA$_2$s

AtxA, AtxC, AtnL and AtnI$_2$ were isolated from *V. a. ammodytes* venom (Gubenšek, Ritonja, Zupan & Turk, 1980; Križaj et al., 1992).
β-bungarotoxin (from *Bungarus multicinctus*) (Sigma-Aldrich, USA)
Bee venom sPLA$_2$ (Roche Applied Science, USA)
Crotoxin (from *Crotalus durissus terrificus*), *Crotalus atrox* sPLA$_2$ and agkistrodotoxin (from *Agkistrodon blomhofii brevicaudus*) were a gift from Dr. Cassian Bon, Institut Pasteur, Paris, France.
Human GV and GX sPLA$_2$ were prepared by Dr. Lidija Kovačič, Dr. Vesna Brglez and Jernej Oberčkal as described (Kovačič et al., publication in preparation).
Human GIIA sPLA$_2$ was prepared by Franja Božič as described (Singer et al., 2002).
Notexin (from *Notechis scutatus scutatus*) was a gift from Dr. Sylvaine Gasparini, CEA, Saclay, France.
OS$_2$ (from *Oxyuranus s. scutellatus*) was a gift from Dr. Gerard Lambeau, Institut de Pharmacologie Moleculaire et Cellulaire, CNRS, Valbonne, France.

3.1.5 Cell line and bacterial strains

E. coli DH5α
E. coli BL21(DE3)
PC12 cell line (ATCC, CRL-1721, USA)

3.1.6 Commonly used buffers and cell media

LB medium: 10 g/l casein hydrolysate, 5 g/l yeast extract, 10 g/l NaCl, pH 7.0, 15 g/l agar (for solid medium)
LBA medium: 100 µg/ml ampicillin in LB
Autoinduction medium: 1.5% (v/v) glycerol, 0.05% (w/v) glucose, 0.2% (w/v) lactose, 0.01 mM $FeSO_4$, 2 mM $MgCl_2$, 0.01 mM $CaCl_2$, 0.05% (w/v) NH_4Cl, 0.05% (w/v) NaCl, 0.3% (w/v) KH_2PO_4, 0.6% (w/v) Na_2HPO_4, 0.01 mg/mL thiamine in LBA
F-12K cell medium (Gibco, USA)
Horse serum (Gibco, USA)
FBS (fetal bovine serum) (Gibco, USA)
complete F12K medium: 82.5% (v/v) F-12K medium, 15% (v/v) horse serum, 2.5% (v/v) FBS, 10 U/mL penicillin, 10 µg/mL streptomycin
DPBS (Dulbecco's phosphate buffered saline) (Gibco, USA)
HBSS (Hank's balanced salt solution) with Ca^{2+} and Mg^{2+} (Gibco, USA)
TBS (tris buffered saline): 50 mM Tris-HCl (pH 7.5), 150 mM NaCl
TBST: 0.1% (w/v) Tween-20 in TBS
LTB (label transfer buffer): 75 mM Hepes (pH 7.4), 150 mM NaCl
4x SDS loading buffer: 120 mM Tris-HCl (pH 6.8), 2.0% (w/v) SDS, 40% (v/v) glycerol, 50 mM EDTA, 4% (v/v) β-mercaptoethanol

3.2 Methods

3.2.1 Analytical techniques of protein purity determination and protein characterization

3.2.1.1 Concentration of protein samples

Some protein solutions (e.g. proteins isolated from SV) were too diluted for analysis or contained high concentrations of detergents and salts which would interfere with further analysis. To concentrate the proteins and remove unwanted solutes, we employed the method of Wessel & Flügge (1984). We dried the protein solutions using a vacuum concentrator (SpeedVac Plus SC110A, Savant, USA) and resuspended the pellets in 100 µL of ddH_2O. We added 400 µL of methanol and 100 µL of chloroform to the suspension and subjected it to vigorous vortexing. Then we added 300 µL of ddH_2O to separate the organic phase from the water phase and centrifuged the samples at 14,000 *g* for 2 min at room temperature. The proteins formed a precipitate at the interphase. The upper phase (water phase) was carefully removed and 300 µL of methanol added to the organic phase. The samples were mixed and centrifuged again at 14,000 *g* for 2 min. The supernatant was removed, and the pellet resuspended in 300 µL of 95% (v/v) methanol in ddH_2O. The samples were centrifuged at 14,000 *g* for 2 min, the supernatant carefully removed and the pellets dried in a vacuum concentrator. The dried samples were dissolved in the SDS-PAGE loading buffer, containing β-mercaptoethanol.

3.2.1.2 Determination of protein concentration

3.2.1.2.1 Determination of total protein concentration

0.02 mL or 0.05 mL of the sample was added to 0.98 mL or 0.95 mL 1 M NaOH, respectively, and the solutions incubated for 10 min at room temperature. The samples were then centrifuged for 5 min at 14,000 *g* at room temperature and then the absorbance

of the supernatants was measured at 260 nm and 280 nm (UV/VIS spectrophotometer Pharmacia Biotech Ultrospec 1000E, Amersham, USA). The concentration of the protein solutions was calculated with the following equation:

$$c(mg/mL) = 1.55 \times A_{280} - 0.76 \times A_{260} \quad (1)$$

3.2.1.2.2 Determination of concentration of specific proteins in solution

Concentration of protein solutions was determined by measuring absorbance at 280 nm using a Nanodrop 2000c spectrophotometer (Thermo Scientific, USA). The protein concentration was calculated using the molar extinction coefficient ε = 1.162 for AtxC and 1.159 for AtxA and AtxA(D49S). For other $sPLA_2$s the molar extinction coefficients were calculated with peptide properties calculator (http://www.basic.northwestern.edu/biotools/proteincalc.html).

3.2.1.3 Polyacrylamide gel electrophoresis in the presence of SDS (SDS-PAGE)

Samples were dissolved in the SDS-PAGE loading buffer, and heated at 95 °C for 5 min. Samples were then cooled and centrifuged at 14,000 *g* for 2 min, before being loaded onto the gel. We used a combination of a 4% (w/v) stacking polyacrylamide gel and a 10%, 12.5% or 15% (w/v) resolving polyacrylamide gel and 10–20 mA per 0.75 mm thick gel or 20–25 mA per 1.5 mm thick gel to separate the proteins (Laemmli, 1970). After the electrophoresis, the proteins were stained with Coomassie Brilliant Blue R350, silver nitrate or transferred to a membrane with western blotting.

3.2.1.4 Western blotting

The proteins, separated by SDS-PAGE, were electroblotted onto a PVDF or nitrocellulose membrane in a Tris-glycine/SDS/methanol buffer (Towbin, Staehelin & Gordon, 1979). The transfer was performed in a tank for 1.5 h at 200 mA. After the transfer, the membranes were blocked for 1 h at room temperature or overnight at 4 °C in a 1% solution (v/v) of western blocking reagent in TBS. For immunological detection of proteins, the blocked membranes were incubated in the presence of 1.3 μg/mL rabbit polyclonal anti-Syt1/2 antibodies or 0.3 μg/mL rabbit polyclonal anti-PDI antibodies for 1 h at room temperature. Afterwards, the membranes were washed twice for 15 min with TBST and then immersed in a 0.04 μg/mL solution of secondary goat anti-mouse or anti-rabbit antibodies, conjugated with horseradish peroxidase. All antibodies were diluted in a 0.5% solution of western blocking reagent in TBS.

For the detection of biotinylated proteins, after the blocking step, the membranes were incubated for 30 min at room temperature or overnight at 4 °C in the presence of 0.12 μg/mL streptavidin, conjugated with horseradish peroxidase (SA-HRP), in 0.5% western blocking reagent in TBS.

After secondary antibody or SA-HRP incubation, the membranes were washed 4 times for 10 to 15 min with TBST and then the blots developed using the Lumi-Light Plus ECL substrate, Kodak Biomax or Amersham Hyperfilm ECL films and Kodak developing solutions. All incubations and washing steps were performed with shaking.

3.2.1.5 Mass spectrometry

Mass spectrometry (MS) was used to identify new Atx-binding proteins in SVs or determine the purity and proper folding of recombinant proteins.

The identification of new Atx-binding proteins was performed by Dr. Marko Fonović from the Department of Biochemistry, Molecular and Structural Biology, Jožef Stefan

Institute, by using a MSD Trap XCT Ultra mass spectrometer (LC-MS-MS) with electrospray ionization (Agilent, USA).
The analyses of recombinant sPLA$_2$s were performed by Dr. Dušan Žigon from the Infrastructural Center for Mass Spectrometry, Jožef Stefan Institute, Ljubljana, on a Q-Tof Premier mass spectrometer with electrospray ionization (Micromass, UK).

3.2.2 *In vitro* affinity labelling of proteins

3.2.2.1 Extraction of membrane proteins

To the SV membrane suspension, an equal volume of a 2x extraction buffer was added (150 mM Hepes, pH 7.4, 300 mM NaCl, 5–6% (m/v TX-100). The membrane proteins were solubilized by shaking the samples for 1 h at 4 °C. The samples were then centrifuged for 1 h at 16,000 *g* and 4 °C and the supernatants analyzed further.

3.2.2.2 Affinity labelling of proteins with sulfo-SBED-AtxC

Sulfo-SBED is a trifunctional commercial reagent that contains biotin, an amine-reactive group and a photo-reactive phenyl-azide group. The amine-reactive group was used to covalently link the reagent to a primary amine of AtxC. The photo-reactive group of the sulfo-SBED reagent under the influence of UV radiation breaks apart and forms nitrenes, which react nonspecifically with nucleophiles. This nucleophilic group can be a part of AtxC or of a molecule which is in close proximity to sulfo-SBED-AtxC, like an Atx-receptor. Sulfo-SBED-AtxC can thus be used to covalently link to and tag Atx-binding proteins with biotin. The biotin-tagged protein complexes can then be isolated on an avidin-resin or detected on a western blot membrane with streptavidin, conjugated to horseradish peroxidase. Since sulfo-SBED contains a disulphide bond, the addition of a reducing agent like β-mercaptoethanol allows the dissociation of the covalently linked complex, in which the biotin moiety remains bound to the AtxC-binding protein.

3.2.2.2.1 Preparation of sulfo-SBED-AtxC

Sulfo-SBED AtxC was prepared according to the protocol developed by Kovačič, Šribar & Križaj (2007). 1 mg of sulfo-SBED was dissolved in 25 µL of DMSO directly before use. To a 1 mg/ml solution of AtxC in ddH_2O we added an equimolar amount of dissolved sulfo-SBED. The reaction mixture was then incubated for 30 min at room temperature. Excess sulfo-SBED was then removed by dialyzing the reaction mixture against 2 L of LTB buffer overnight at 4 °C with 2 changes of the dialysis buffer. The dialyzed sulfo-SBED-AtxC was aliquoted, protected from light and stored at –80 °C. The final concentration of sulfo-SBED-AtxC was determined spectrophotometrically (Nanodrop 2000c, Thermo Scientific, USA) and typically ranged from 100 to 130 µM. Due to the light sensitivity of sulfo-SBED, all procedures were performed in complete darkness. According to Kovačič et al. (2007), sulfo-SBED-AtxC had the same enzymatic activity, neurotoxic and immunological properties as the native AtxC.

3.2.2.2.2 Affinity labelling of proteins with sulfo-SBED-AtxC

Affinity labelling was performed in LTB with 2 mM $CaCl_2$ or 2 mM EGTA. Usually, 0.1% (w/v) detergent Triton X-100 was present in the reaction to prevent nonspecific interactions. To a suspension of extracted membrane proteins or recombinant proteins, where applicable, an equimolar concentration of sulfo-SBED-AtxC was added in complete darkness. The final concentration of sulfo-SBED-AtxC was 0.1–0.5 µM. The control samples contained a 100-fold excess of native AtxC over the labelled toxin. The samples were incubated at room temperature in complete darkness and shaken for 30 min.

Afterwards, the samples were exposed to UV light at 312 nm (five 15 W light bulbs) to induce the disintegration of the aryl-azide functionality and the covalent linking of sulfo-SBED-AtxC to its binding proteins. We added SDS-PAGE loading buffer to the samples, and analyzed them with SDS-PAGE, followed by western blotting, as described above. The labelled proteins were detected with streptavidin-HRP.

3.2.2.3 Affinity labelling of proteins with ^{125}I-AtxC and DSS or paraformaldehyde

^{125}I-AtxC was prepared by Dr. Jernej Šribar with chloramine-T following the protocol described by Križaj, Dolly & Gubenšek (1994). The functionality of ^{125}I-AtxC was tested by labelling CaM, a known binding protein for Atx, with DSS as described below.

To a suspension of extracted membrane proteins or recombinant proteins in LTB with 2 mM $CaCl_2$, ^{125}I-AtxC was added in the final concentration of 10 nM and the reaction mixture incubated at room temperature for 30 min to achieve equilibrium. 0.1% (w/v) Triton X-100 was present in the reaction to avoid nonspecific labelling. The control samples contained 100–200 molar excess of the unlabelled AtxC or other $sPLA_2$s over ^{125}I-AtxC. After the incubation the proteins were cross-linked and analyzed as described below.

3.2.2.3.1 Cross-linking with disuccinimidyl suberate (DSS)

After the incubation, DSS, dissolved in DMSO, was added to the samples in a final concentration of 100 μM. The samples were vigorously vortexed for 5 min and then the cross-linking reaction was stopped by the addition of SDS-PAGE loading buffer, containing Tris.

3.2.2.3.2 Cross-linking with paraformaldehyde

The complex of AtxC with Syt1 apparently cannot be cross-linked using DSS (our observation). We have therefore used paraformaldehyde as a cross-linker in a modified protocol of Klockenbusch & Kast (2010). Formaldehyde cross-links amino acids Lys, Cys and Trp at a distance of 2–3 Å (Nadeau & Carlson, 2007). The cross-linking is quenched by the addition of an excess of glycine or Tris, which contain primary amines.

To 62.5 μL solution of 40 nM Syt1 in LTB with 2 mM $CaCl_2$, already containing 10 nM ^{125}I-AtxC, 4% (w/v) formaldehyde in dH_2O was added to a final concentration of 0.252% (w/v). The reaction was mixed and incubated for 5 min at room temperature and then quenched with the addition of 16.5 μL 1.5M Tris-HCl, pH 6.8 and 26.7 μL 4x SDS-PAGE loading buffer, containing β-mercaptoethanol. The cross-linking with formaldehyde is reversible at temperatures over 65 °C (Klockenbusch & Kast, 2010), so the samples were incubated overnight at room temperature instead of 5 min at 95 °C to denature the proteins prior to SDS-PAGE analysis.

3.2.3 Working with the PC12 cell line

3.2.3.1 Cell culture

PC12 cells were grown at 37 °C and 5% (v/v) CO_2 in culture plates of 10 cm diameter or in tissue culture flasks with a growth surface of 150 cm^2 in complete F12K growth medium. To induce differentiation, NGF (100 ng/mL) was added to the growth medium. After 48 h, the cells were washed with DPBS, fresh NGF-containing growth medium was added and the cells grown for further 48 h. For confocal microscopy experiments, the cells were plated on poly-*L*-Lys coated coverslips.

3.2.3.2 Freezing and revitalization of cells

To freeze the cells, we washed them once with complete F12K medium, added fresh complete medium and dissociated them from the plate with gentle scraping. The suspension was then centrifuged for 8 min at 200 *g* and the pellet resuspended in 1 ml of a freshly prepared complete medium containing 5% (v/v) DMSO. The suspended cells were transferred to a cryo-tube and frozen in a "Mr. Frosty" device at –80 °C. After 24 h, the cells were transferred to a liquid nitrogen tank.

To revitalize the cells, cryo-tubes were quickly transferred from liquid nitrogen into a water bath of 37 °C and gently shaken. After thawing, the cells were transferred into 10 ml of freshly prepared complete F12K medium and centrifuged for 8 min at 200 *g*. The supernatant was removed, the pelleted cells resuspended in 10 mL of complete F12K medium and plated.

3.2.4 Isolation of SVs

3.2.4.1 Isolation of SVs from porcine cerebral cortex

SVs were isolated according to the Huttner method as described by Craige, Salazar & Faundez (2004). 35 g of porcine cerebral cortex was immersed in 100 mL buffer SB320 (5mM Hepes, pH 7.4, 320 mM sucrose, proteinase inhibitors) and homogenized with the Ultra-turrax homogenizer (IKA, Germany) on ice. Afterwards, the tissue was further disrupted with a teflon homogenizer (Potter-Elvehjem, USA). We added another 40 mL of SB320 to the homogenate and centrifuged the sample for 10 min at 1,000 *g* and 4 °C. To the supernatant we added SB320 to a total volume of 100 mL and centrifuged it for 15 min at 13,200 *g* and 4 °C. We carefully removed the supernatant and added SB320 to the pellet to a total volume 13 mL. Then we added 125 mL dH_2O to lower the sucrose concentration to 30 mM. We homogenized the suspension with a teflon homogenizer (Potter-Elvehjem, USA). We then added 1 mL 1 M Hepes, pH 7.4, and incubated it on ice for 30 min. We centrifuged the suspension for 20 min at 33,000 *g* and 4 °C. The supernatant was then transferred into a fresh centrifuge tube and centrifuged for 8 h at 120,000 *g* and 4 °C. We discarded the supernatant. To the pellet we added 5 mM Hepes, pH 7.4, 40 mM sucrose, 1x proteinase inhibitors to a final volume of 6 mL and homogenized the suspension with a glass homogenizer (Dounce Tight, Wheaton, USA). We added the suspension to two centrifuge tubes, 3 mL into each, on top of a discontinued sucrose gradient (19 mL 5 mM Hepes, pH 7.4, 50 mM sucrose on top of 16 mL 5 mM Hepes, pH 7.4, 800 mM sucrose) and centrifuged the samples for 5 h at 95,000 *g* and 4 °C. After the centrifugation we observed the SVs as a white haze 1/2 to 2/3 down from the top of the tubes. We carefully collected the suspension of SVs, flash frozen them in liquid N_2 and then stored them at –80 °C until use. Prior to freezing, an aliquot was taken to determine the total protein concentration as described in 3.2.1.2.1. Another aliquot was tested for the presence of Syt1/2 with SDS-PAGE and western blotting as described in 3.2.1.3. and 3.2.1.4.

All used buffers and gradient solutions were ice cold. All glassware and plastic, including centrifuge tubes and pipette tips that were in direct contact with the brain tissue, were coated with Sigmacote to lower the adsorption of SVs to surfaces.

3.2.4.2 Isolation of SVs from PC12 cells

About 2 x 10^8 ND or NGFD PC12 cells were grown in eight 150 mm flasks as described in 3.2.3.1. We dissociated the cells with gentle scraping and transferred them into a glass homogenizer (Dounce Tight, Wheaton, USA). We homogenized the cells and observed

the efficiency of homogenization with the use of a microscope. Then we proceeded with the SV isolation as described in 3.2.4.1. Where possible, the buffer volumes were adjusted according to the ratio of the mass of the PC12 cells and the cerebral cortex from 3.2.4.1. In the case of the ND cells the haze at the end of the isolation was not visible, so we collected SVs only from NGFD cells. The SVs were frozen in liquid N_2 and stored at –80 °C until use. In the same way as the brain SV preparation, total protein concentration was determined and an aliquot of PC12 SVs was probed for the presence of Syt1/2.

3.2.4.3 Isolation of Atx-binding proteins from SVs

Four 200 µL aliquots (A, B, C and D) of porcine cortex SVs were subjected to different treatments (Figure 7). From samples A and B the membrane proteins were extracted with the final concentration of 2.5 % (w/v) TX-100 in LTB as described in 3.2.2.1. The suspensions of extracted proteins in samples A and B were diluted with LTB to lower the concentration of TX-100 to 0.8 % (w/v). From a diluted sample A the biotinylated proteins were then removed from by binding to avidin. We achieved this by shaking the sample with 150 µL monomeric avidin beads for 1 h at 4 °C. Sample A was then centrifuged at 700 *g* for 1 min at room temperature to pellet the avidin beads with bound biotinylated material and the supernatant, now devoid of biotinylated proteins (the breakthrough fraction, A_{EX}), processed further as described below. The biotinylated proteins in diluted extracted sample B (B_{EX}) were directly processed further as described below. Samples C and D contained the still intact SV membranes and were not extracted (samples C_M and D_M).

Thus prepared samples A_{EX}, B_{EX} and D_M were incubated in the presence of 2 µM sulfo-SBED-AtxC and 10 mM $CaCl_2$ in LTB for 1 h at room temperature with shaking, protected from light. Sample C_M was the control sample and was incubated without the added sulfo-SBED-AtxC, but processed in the same way as others. After the incubation, all samples were exposed to UV light (five 15 W 312 nm UV lamps) for 5 min at a distance of 5 cm to trigger the cross-linking reaction. From samples C_M and D_M membrane proteins were extracted with 2.5% (w/v) TX-100 in LTB as described in 3.2.2.1. The extracted proteins of C_M (C_{EX}) and D_M (D_{EX}) were then diluted with LTB to lower the concentration of TX-100 to 0.8% (w/v). All samples (A_{EX}, B_{EX}, C_{EX} and D_{EX}) were then incubated with 150 µL monomeric avidin beads for 1 h at 4 °C with shaking. After the incubation, the beads were pelleted by centrifugation at 700 *g* for 1 min at room temperature. The supernatant was removed and the beads thoroughly washed with LTB, containing 0.1% (w/v) TX-100. The biotinylated proteins were eluted by incubating the avidin beads for 5 min with 200 µL 2 mM *D*-biotin in LTB, containing 0.1% (w/v) TX-100, and shaking at room temperature. The samples were centrifuged as before to pellet the beads and the supernatants (avidin eluates) collected. The elution of biotinylated proteins with free *D*-biotin was repeated 5 more times. In this manner, from each sample of A_{EX}, B_{EX}, C_{EX} and D_{EX}, six 200 µL fractions were collected and joined to yield the final samples of isolated SV biotinylated proteins A_{EL}, B_{EL}, C_{EL} and D_{EL}. These samples were then concentrated using a vacuum concentrator (SpeedVac, Savant, USA) to a volume of 100 µL and the proteins recovered as described in 3.2.1.1. The recovered proteins were dissolved in SDS-PAGE loading buffer, heated at 95 °C for 5 min and then analyzed on 12%T-G Lonza PAGEr gels with SDS-PAGE and silver staining or on 12.5% polyacrylamide gels with western blot and SA-HRP detection. Certain silver stained bands were excised and analyzed with MS as described in 3.2.1.5.

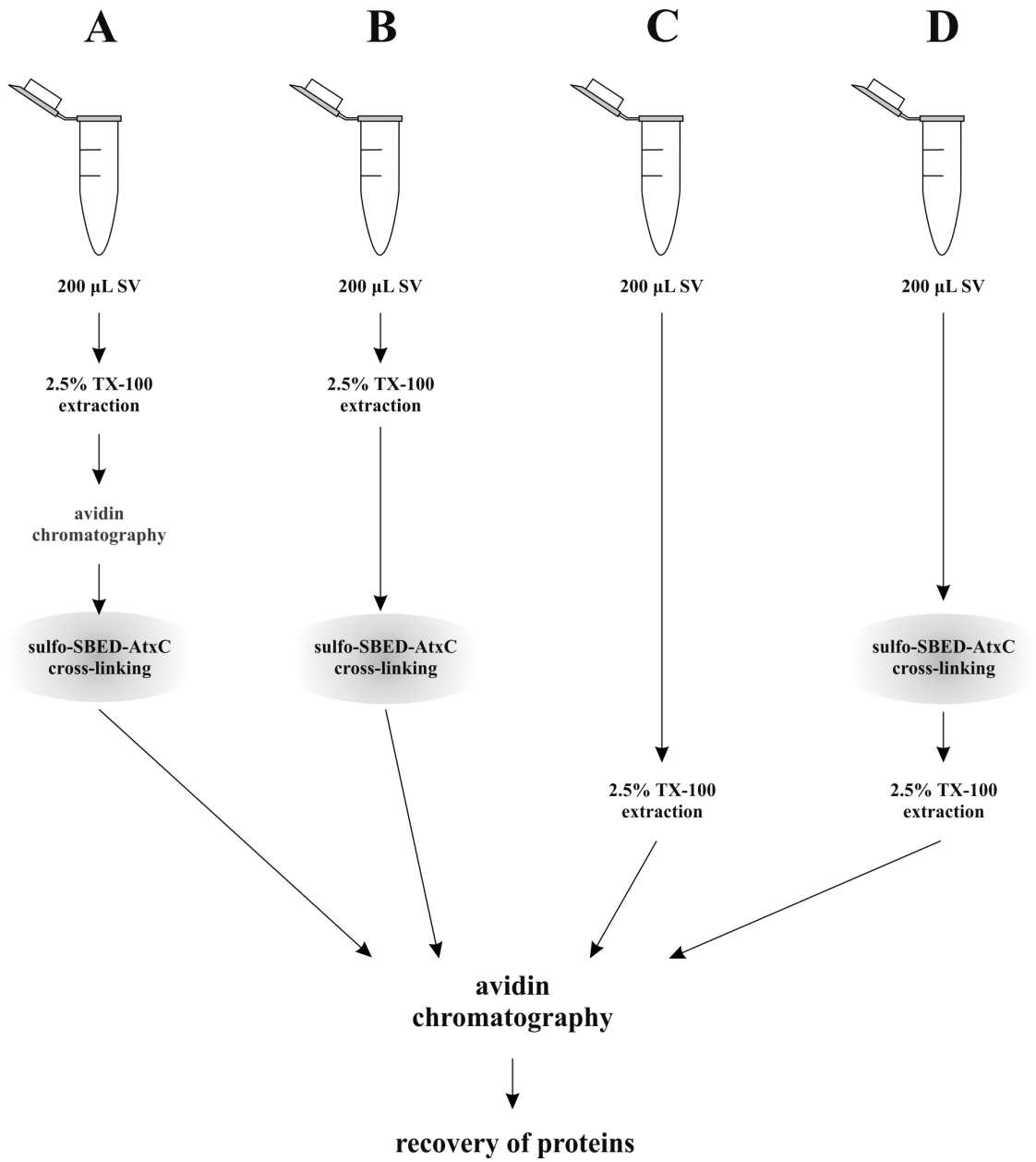

Figure 7: *Scheme of isolation of Atx-binding proteins from SVs.*

3.2.5 Labelling of AtxC-binding proteins in live PC12 cells

3.2.5.1 Sulfo-SBED-AtxC labelling of AtxC-binding proteins in intact PC12 cells

Intact PC12 cells (ND and NGFD), plated on 10 cm plates at 80–90 % confluence, were treated with sulfo-SBED-AtxC at a final concentration of 100 nM for 1, 2, 5, 15, 30 and 60 min in (HBSS) in the dark at 37 °C and 5 % (v/v) CO_2. In a control experiment, the cells were incubated without the added sulfo-SBED-AtxC for 5 min. Subsequently, the cells were cooled on ice, exposed for 5 min to five 15 W 312 nm UV lamps from a distance of 5 cm and washed twice with HBSS. The cells were then immersed in 1.8 mL 1.5 % (w/v) Triton X-100/HBSS for 15 min to extract the proteins. Experiments were performed in duplicate using cells of the same passage. The extracts were centrifuged for 45 min at 14,000 *g* and 4 °C. Supernatants were incubated with 375 µL monomeric avidin

agarose beads for 1 h at 4 °C. The beads were thoroughly washed with HBSS containing 0.1 % (w/v) Triton X-100 and biotin containing proteins then eluted with 2 mM *D*-biotin /0.1 % (w/v) Triton X-100/HBSS. Half of each eluted fraction was subjected to anti-Atx immunoprecipitation, as described below (3.2.3.3.1). The remainder of the fractions was concentrated using a vacuum concentrator (SpeedVac, Savant, USA) and the proteins recovered as described earlier (3.2.1.1.). The resulting pellets were dissolved in SDS-PAGE loading buffer and analyzed by SDS-PAGE on a 10% polyacrylamide gel. The gel was then stained with silver nitrate and a band corresponding to a protein of 85 kDa, which was present in control and sulfo-SBED-Atx labelled samples, quantified using ImageJ program (Schneider, Rasband & Eliceiri, 2012). This served as a means to standardise the loading of samples for subsequent western blot analysis. Positions of biotinylated Syt1 and PDI on the blots were determined immunologically as described in 3.2.1.4.

3.2.5.1.1 Immunoprecipitation of Atx-binding proteins

400 µL aliquots of the avidin-chromatography eluates were incubated with 100 µL protein G-Sepharose, carrying polyclonal antibodies against Anti-AtxA. The samples were incubated overnight at 4 °C. The beads were then extensively washed and the proteins eluted with the addition of the reducing SDS-PAGE loading buffer and heating at 95 °C for 5 min. The samples were analyzed by SDS-PAGE as described (3.2.1.3.). Afterwards, the proteins were western blotted onto a PVDF membrane and the biotinylated proteins visualized with SA-HRP as described in 3.2.1.4.

3.2.6 Measuring PLA_2 activity with the PyPG method

We measured the activity of AtxC and AtxA(D49S) with a modified method of Radvanyi et al. (1989). The method employs a fluorogenic phosphoglycerol analogue with a pyrene labelled acyl chain at the *sn-2* position (PyPG).

3.2.6.1 Preparation of PyPG vesicles

200 µL of a 1 mg/mL solution of PyPG in toluene : isopropanol (1 : 1) was dried in a vacuum concentrator and the pellet dissolved in absolute ethanol by vigorous vortexing. The mixture was centrifuged at 14,000 *g* for 2 min and the supernatant moved to a glass tube with a teflon stopper. The concentration of the phospholipids was determined by measuring absorbance at 342 nm (the molar extinction coefficient for PyPG is 40,000 M^{-1} cm^{-1}) and was typically 150–230 µM. The ethanol stock solution was stored at –20 °C. To prepare the working solution, the ethanol stock solution was vigorously vortexed, briefly treated with ultrasound and diluted into the HBSS buffer to a final phospholipid concentration of 1.4 µM.

3.2.6.2 Measuring phospholipase activity with a fluorescent microplate reader

The phospholipase activity of Atx was measured using a microplate reader (TECAN Infinite M1000, Tecan, Switzerland). To 200 µL of 0.06% (w/v) BSA in HBSS we added a desired amount of Atx. In the case of assessing the effect of the presence of CcO or Syt1 on Atx's phospholipase activity, the final concentration of AtxC was 0.30 nM. As a positive control in the measurement of the residual enzymatic activity of the mutant AtxA(D49S), the final concentration of AtxC was 0.23 nM. In this case, the final concentration of AtxA(D49S) was 23 nM. After the addition of the $sPLA_2$, we added 100 µL of 3x PyPG working solution (final concentration of PyPG was 0.47 µM) and immediately started measuring the fluorescence. The fluorofores were excited with laser

light at 342 nm and emission was measured at 395 nm. The control contained no $sPLA_2$. A third-order polynomial was fitted to the data with the program Graphpad Prism to calculate the initial rates of the phospholipase activity.

3.2.7 Production of the enzymatically inactive mutant AtxA(D49S)

3.2.7.1 DNA sequence preparation

3.2.7.1.1 Preparation of the pJP4.1 plasmid for direct expression of AtxA

The gene (nucleotide sequence) for AtxA in the plasmid pJP4.1 (prepared by Pungerčar, Križaj, Liang & Gubenšek, 1999) contains a propeptide sequence (MARIRARGSIEGR). The proteolytic removal of this peptide after expression of AtxA has been troublesome. To remove the propeptide sequence and prepare the plasmid for direct expression, the AtxA gene was amplified with PCR with the use of the following DNA primers:

Forward: 5'-agaaggagatatacatatgagcttgctcgaattc-3'
Back: 5'-agcttatcatcgataagcttttagcatttctctgac-3'

Primers were designed with the Agilent online tool (https://www.genomics.agilent.com/primerDesignProgram.jsp?_requestid=1289764).

The 25 µL PCR mix contained 2.5 µL 10x *Pfu* buffer, dNTPs at a final concentration of 200 µM each, both primers at a 500 nM final concentration, 150 ng pJP4.1 plasmid and 5 U *Pfu* DNA polymerase, and the rest was PCR grade H_2O. PCR was performed with a 2720 Thermal Cycler (Applied Biosystems, USA) with the following protocol:

Cycles	temperature [°C]	time [min]
1x	95	2
30x	95	1
	49	0.5
	72	3
1x	72	5

After the PCR, the DNA products were separated with agarose electrophoresis on a 1.5% (w/v) Sybr-safe stained agarose gel, the fragments of correct size excised and purified with the Qiagen gel-extraction kit (the Netherlands) according to the manufacturer's instructions.

Thus prepared DNA fragment, containing the AtxA gene with the start (ATG) codon, and separately a 2 µg aliquot of the pJP4.1 vector, were digested with the use of FastDigest enzymes *Nde*I and *Hin*dIII, following the manufacturer's instructions for 20 min at 37 °C.

After the digestion, the DNA was separated on a 1.5% (w/v) Sybr-safe stained agarose gel. The gel slices, representing the digested vector and PCR product, were excised and the DNA purified with the Qiagen gel-extraction kit according to the manufacturer's instructions.

The purified linearized pJP4.1 vector and the digested AtxA gene were ligated in a 10 µL ligation reaction, containing the following components: 85 ng AtxA gene, 20 ng linearized vector, 1 µL T4 DNA ligase and 1 µL of 10x T4 ligation buffer. The reaction was allowed to proceed for 3 h at room temperature, after which 1 µL was transformed

into competent *E. coli* DH5α. The bacteria were shaken overnight at 37 °C in 5 mL LBA medium, then the plasmid DNA was isolated with the Qiagen kit (the Netherlands), following manufacturer's instructions. The plasmid was sequenced to ensure the removal of the propeptide coding sequence and to check for potential errors in the DNA sequence.

3.2.7.1.2 Site directed mutagenesis to produce the mutated gene for AtxA(D49S)

To prepare the gene for AtxA(D49S), the codon for Asp49 (GAC) in the AtxA gene (in the prepared pJP4.1 plasmid for direct expression) was mutated to AGC, which is the optimal codon for Ser in *E. coli*. Site-directed mutagenesis was performed with the following DNA primers:

Sense: 5'-cgctgctgcttcgtgcatagctgctgttacgggaat-3'
Anti-sense: 5'-attcccgtaacagcagctatgcacgaagcagcagcg-3'

Primers were designed with the Agilent online tool the same as in 3.2.7.1.1.

The mutagenesis reaction contained 2.5 µL 10x *Pfu* buffer, 25 ng of the prepared direct expression pJP4.1 plasmid, 62.5 ng of each primer, 0.5 µL of a mix of dNTP, 19 µL PCR grade H_2O and 1.25 U *Pfu* DNA polymerase. The mutagenesis was performed using the PCR apparatus with the following protocol:

Cycles	temperature [°C]	time [min]
1x	95	2
12x	95	0.5
	55	1
	68	7
1x	68	5

After the mutagenesis, 1 µL of the mutagenesis reaction was transformed into competent *E. coli* DH5α. The bacteria were shaken overnight at 37 °C in 5 mL LBA medium, then the plasmid DNA was isolated with the Qiagen kit (the Netherlands), following manufacturer's instructions. Plasmid DNA was sequenced to assess the success of the mutagenesis.

3.2.7.2 Expression in *E. coli* BL21(DE3)

For expression, we used the autoinduction procedure, rather than the standard IPTG-induction. Auto-induction allows bacteria to grow until the primary source of carbon (glucose for *E. coli*) is depleted. Glucose indirectly influences the *lac* operon: at high levels of glucose, the transcription from the *lac* promoter is low (Inada, Kimata & Aiba, 1996; Hogema et al., 1998; Hogema, Arents, Bader & Postma, 1999). As glucose is depleted, bacteria change their metabolism and feed on an alternative source of carbon, such as glycerol and lactose, which are present in the autoinduction medium and begin pumping them into the cytosol. The presence of lactose (transformed into allolactose) induces the *lac* operon, which allows the production of the recombinant protein (Studier, 2005). This method of induction is slower than with IPTG and allows bacteria to reach greater concentrations in the expression mixture and this consequently leads to greater yields of recombinant protein than the standard IPTG-induction. In our case, the absorbance at 600 nm (A_{600}) at the end of expression was usually between 7 and 13, while with the IPTG method it was around 2.3–4. The auto-induction expression mixtures can in extreme cases reach an A_{600} of 27 (Studier, 2005).

We transformed the plasmid for AtxA(D49S) into competent *E. coli* BL21(DE3) cells

and grew them on an LBA agar plate. Next day, 1 colony was inoculated in 10 mL LBA medium and grown until A_{600} reached 0.7. The bacterial culture was then diluted 100-fold in the auto-induction medium. The cells were shaken at 230 RPM in 250 ml of the autoinduction medium in a 2 L shake flask for 2h at 37 °C and then overnight at 25 °C. The next day A_{600} of the expression mixture was measured once every hour until it remained constant. The typical A_{600} at the end of expression was between 8 and 12. Cells were then pelleted by centrifuging 25 min at 5,000 *g* and 4 °C. The pellets were frozen at –80 °C until use.

3.2.7.3 Purification of inclusion bodies, S-sulfonation of Cys residues, refolding and purification of AtxA(D49S)

3.2.7.3.1 Purification of inclusion bodies and S-sulfonation of Cys residues.

The bacterial pellets were resuspended for 10 min on ice in 30 mL 20 mM Tris-HCl, pH 7.5, 20 % (w/v) sucrose, 5 mM EDTA, 1 mM DTT and 1x concentration of protease inhibitors. The bacteria were then centrifuged for 10 min at 11,000 *g* and 4 °C. Cell lysis and digestion of DNA was achieved by resuspending the bacteria in 30 mL ice cold ddH_2O, 1 mM DTT, 10 mM $MgSO_4$, 0.03 mg/mL DnaseI, supplemented with protease inhibitors. The mixture was then centrifuged for 10 min at 11,000 *g* and 4 °C and the pellet resuspended in 30 mL ice cold PBS, 1 mM DTT, supplemented with protease inhibitors. The mixture was then sonicated (UP200S Ultrasonic processor, Hielscher, Germany) for 2 min with a 50 / 50 cycle at 80 % maximum amplitude and centrifuged 20 min at 14,000 *g* and 4 °C. The resulting pellet was washed twice with ice cold PBS, 25 % (w/v) sucrose, 1 % Triton X-100, supplemented with protease inhibitors, followed by centrifugation for 20 min at 14,000 *g* and 4 °C, which yielded the isolated inclusion bodies.

The isolated inclusion bodies were left overnight to dissolve in 50 mL 6 M Gnd.HCl, 0.3 M Na_2SO_3, pH 8.5. Then 3.75 mL NTSB reagent was added into the solution and mixed for 1 h at room temperature to sulfonate the Cys residues of Atx. Afterwards, 20 mL of 100 % acetic acid was added, followed by 950 mL ice cold ddH_2O and the protein was left to aggregate overnight at 4 °C. The next day, the protein was pelleted by centrifuging 15 min at 6,000 *g* and 4 °C and washed once with ddH_2O. The resulting pellet of the S-sulfonated AtxA(D49S) was dissolved in 50 mL 6 M Gnd.HCl, pH 8.3, and stored at –20 °C, where it was stable for at least 1.5 years. The purity and the quantity of the protein were assessed by SDS-PAGE as described in 3.2.1.3. The final concentration of AtxA(D49S) in 6 M Gdn.HCl was around 6 mg/mL as estimated from the Coomassie-stained SDS gel.

3.2.7.3.2 Refolding of AtxA(D49S)

The refolding of the S-sulfonated AtxA(D49S) was performed according to the protocol, developed by Dr. Lidija Kovačič (Kovačič et al., publication in preparation). About 30 mg of the denatured AtxA(D49S) in 6 M Gdn-HCl was diluted 10-fold in 50 ml of the refolding mixture, containing 75 mM Hepes (pH 7,5), 20 mM NaCl, 10 mM $CaCl_2$, 5 % (v/v) acetonitrile, 0.05 mM oxidized and 0.5 mM reduced glutathione and a chaperone. The refolding mixture was mixed with gentle aspiration and then incubated at room temperature for 24 h in the dark. Next day, the mixture was acidified to reach a pH of 3.5–4.0 by the addition of 3.5 ml of 15 % (v/v) acetic acid to cause the dissociation of the chaperone from AtxA(D49S). The mixture was then centrifuged for 20 min at 5,000 *g* and 4 °C and the supernatant filtered through a 0.2 μm filter. The filtrate was then separated with RP-HPLC.

3.2.7.3.3 RP-HPLC

RP-HPLC was used for the cleaning of refolded AtxA(D49S) and ^{546}Alexa-AtxA(D49S). The solvents used for separation were 0.1 % (v/v) TFA in ddH_2O (solvent A) and 90 % (v/v) acetonitrile, 0.1 % (v/v) TFA in ddH_2O (solvent B). The absorbance was monitored at 215 nm.

The filtered refolding mixture from 3.2.6.3.2. was loaded onto a Zorbax 300SB-C3 semi-preparative column (Agilent, USA), equilibrated in 5 % (v/v) solvent B in solvent A. The column was then washed for 25 min with 5 % (v/v) solvent B in solvent A at 2 mL/min and the sample eluted with the following protocol:

time [min]	solvent [% B in A]
0–3	5–20
3–38	20–55
38–43	55–100

The flow throughout the HPLC analysis was 2 mL/min.

The collected fractions were dried using a vacuum concentrator (SpeedVac, Savant, USA) and analyzed with SDS-PAGE and MS. The samples, containing the correctly folded mutant, as determined by MS, were subsequently subjected to another RP-HPLC step, utilizing a SymmetryShield RP18 analytical column (Waters, Ireland), equilibrated in 5 % (v/v) solvent B in solvent A. After the loading, the column was washed for 25 min with 5 % (v/v) solvent B in solvent A at 1 mL/min and the sample eluted at 1 mL/min with the following protocol:

time [min]	solvent [% B in A]
0–3	5–20
3–33	20–50
33–38	50–100

After the separation, the fractions were dried and characterized by SDS-PAGE, MS, checked for CaM-binding ability by heterologous competition with ^{125}I-AtxC and residual enzymatic activity as described earlier in the text.

Throughout the refolding and cleaning procedure, we ensured no contamination was made by enzymatically active sPLA$_2$s. The used HPLC columns were either brand new or rigorously cleaned before the application of the AtxA(D49S) samples.

3.2.7.4 Labelling of AtxA and AtxA(D49S) with the fluorescent dye ^{546}Alexa-succinimide

To prepare the fluorescent derivatives of AtxA or AtxA(D49S), the proteins were dissolved in DMSO (2 mg/mL final concentration) and Alexa Fluor 546 (Molecular Probes Alexa Fluor546 Protein Labelling Kit, Life Technologies, USA) was added to a final protein : dye molar ratio 1 : 1.5 in the presence of 100 mM triethylamine. After 1 h shaking in the dark at the room temperature, taurine was added at a 5 mM final concentration and the mixture incubated for further 30 min. The reaction products were separated by RP-HPLC using an Aquapore BU 300 column (30 mm × 4.6 mm) (PerkinElmer, USA) equilibrated with 5 % (v/v) of solvent B in solvent A. After application of the sample, the column was washed with 5 ml of 5 % (v/v) solvent B in solvent A and the bound proteins eluted at 1 mL/min with the following protocol:

time [min]	solvent [% B in A]
0–3	5–20
3–23	20–60
23–36	60–100

The absorbance was monitored at 215 nm. As selected by MS analysis, Alexa monoderivative of AtxA or AtxA(D49S) (^{546}Alexa–AtxA and ^{546}Alexa–AtxA(D49S), respectively) was further characterized regarding its ability to bind to CaM as described in 3.2.4.2. and 3.2.2.4., respectively.

^{546}Alexa–AtxA was prepared and characterized by Klemen Dolinar and Dr. Jernej Šribar (Dolinar, 2013). They found that the fluorescent derivative retained about 94% of the enzymatic activity of the native unmodified AtxA. Logonder (2008a) showed that ^{546}Alexa–AtxA, prepared in this manner was still neurotoxic, but required a 4 times longer period of time to arrest the twitching of the mouse hemidiaphragm than the unmodified AtxA, and had an LD_{50} of 750 μg/kg in mice.

3.2.7.4.1 Determining the concentration of ^{546}Alexa–AtxA(D49S)

The spectrophotometric determination of concentration of ^{546}Alexa–AtxA is not precise (Dolinar, 2013). To determine the concentration of the fluorescently labelled AtxA(D49S), we used instead densitometry of Coomassie R350-stained bands on an SDS gel. 0.1, 0.25, 0.5, 0.75 and 1 μg of AtxA were analyzed with SDS-PAGE as described earlier. On the same gel, a sample of ^{546}Alexa–AtxA(D49S) was analyzed. The same samples were analyzed in two replicas on separate SDS gels. After SDS-PAGE, the gels were stained with Coomassie R350, scanned and the bands quantified with ImageJ (Schneider et al., 2012). To the densitometry data of the known amounts of native AtxA on the gel a linear line was fitted with MS Excel. The slope of the line was used to calculate the amount of ^{546}Alexa–AtxA(D49S) on the gel. The calculated concentration of ^{546}Alexa–AtxA(D49S) in the initial sample was 16.6 μM and the result differed by only 2 % between both replicate experiments.

3.2.8 Confocal microscopy

3.2.8.1 Coating of coverslips with poly-*L*-lysine

Square coverslips (18 mm x 18 mm x 170 μm) were sterilized by immersion in absolute ethanol, dried and incubated for 1 h at room temperature in a sterile 0.01% (w/v) solution of poly–*L*–Lys. The solution was removed, stored and reused up to three times. The coverslips were then washed three times for 5 min with sterile ddH_2O, dried and stored at room temperature until use.

3.2.8.2 Slide preparation for confocal microscopy

3.2.8.2.1 Immunocytochemistry

PC12 cells on poly–*L*–Lys coated coverslips were incubated at 37 °C and 5 % (v/v) CO_2 in the presence of 100 nM ^{546}Alexa–AtxA or 100 nM ^{546}Alexa–AtxA(D49S) for 1, 2, 5, 15, 30, and 60 min. After the incubation, the cells were first washed 3 times with DPBS at room temperature and then fixed for 25 min in 4 % (w/v) paraformaldehyde in DPBS at room temperature. After fixation, the cells were washed 4 times (5 min each) with ice-cold DPBS and then incubated at room temperature in the blocking solution, containing 0.5 % (w/v) fish skin gelatin and 10 % (w/v) fetal bovine serum in DPBS for 20 min.

Coverslips were then immersed into primary antibody solution (anti–CcO diluted 1 : 200, anti–Syt1 diluted 1 : 300, anti–14-3-3p diluted 1 : 200 and anti–PDI diluted 1 : 300 in blocking solution). After 60 min incubation at room temperature, the cells were rinsed 5 times (5 min each) in DPBS and then incubated for 60 min at the room temperature in the secondary antibody solution (Alexa Fluor 488 Goat Anti–Rabbit or Alexa Fluor 488 Goat Anti–Mouse, diluted 1 : 2,000 in blocking solution), followed by washing 4 times (5 min each) in DPBS. Excess fluid was removed and the slides were mounted using ProLong Gold antifade reagent and left to cure. After 24 h at the room temperature in the dark, the edges of the coverslips were sealed with nail polish. The fixation, blocking and all washing steps were performed with gentle shaking and protected from light.

3.2.8.2.2 Measuring co-localization of Alexa-Atx and Atx-binding proteins with confocal microscopy

The prepared slides were analyzed on an inverted confocal laser scanning microscope (Axio Observer Z1 LSM 710, Carl Zeiss, Germany) with a Plan–Apochromat 63/1.40 oil objective. Fluorophores were excited sequentially using Ar (488 nm) and He–Ne (543 nm) lasers and the emitted light was collected through SP 545 and LP 545 filters. Stacks of fluorescent images were acquired and co-localization of the red and green signal was calculated with ImageJ (Schneider et al., 2012) and co-localization plugin JACoP (Bolte & Cordelières, 2006). The signal thresholds for the red and green channels were set at a value just above the highest signal of the control experiment without the added respective fluorescent probe. The thresholds were between 10 % and 20 % of the maximum signal intensity.

Co-localization was presented as Manders' coefficient – *i.e.* the ratio of the summed intensities of pixels from the green channel, for which the intensity in the red channel is above zero, to the total intensity in the green channel. Images of co-localization were displayed using the "Colocalization" tab in the Zen software (Zeiss).

3.2.9 Preparation of the three-dimensional models of complexes between $sPLA_2$s and PDI

The hPDI–$sPLA_2$ models were obtained based on the AtxA–yPDI model, prepared by Dr. Lidija Kovačič (2009b).

Crystal structures of human PDI (hPDI) (PDB ID 4el1, AtxA (PDB ID 3g8g), AtnL (PDB ID 3dih), porcine GIB (pGIB) $sPLA_2$ (ID 1pir), hGIIA $sPLA_2$ (ID 1pod), hGX $sPLA_2$ (ID 1le7) were obtained from the Protein Data Bank (PDB), whereas models of $AtnI_2$ and hGV $sPLA_2$ were constructed by Dr. Lidija Kovačič as described (Kovačič et al., 2010).

All water molecules and ions were removed from the three-dimensional (3D) structures. $sPLA_2$ structures were superimposed on the structure of Atx in the model of the Atx–yPDI complex. In the same way, the hPDI structure was superimposed on the yPDI structure in the bb' model of the Atx–yPDI complex. Thus obtained initial structures were uploaded onto the web server version of the high ambiguity-driven docking (HADDOCK) program (http://haddock.science.uu.nl/services/HADDOCK/haddock.php) (Karaca, Melquiond, de Vries, Kastritis & Bonvin, 2010). In the structures potential active residues (these are residues constituting the interaction area or being situated not more than 10 Å from it) were identified, semi-flexible segments were manually defined (each PDI domain represented one segment) while passive residues (these are residues that are not involved in the interaction) were defined automatically. Other parameters were set to default values. Then HADDOCK protocol was performed as described (Dominguez, Boelens & Bonvin, 2003; de Vries, van Dijk & Bonvin, 2010,

Karaca et al., 2010).

The best Atx–hPDI model was chosen according to the similarity of the interaction site with the Atx–yPDI model and the lowest non-bonded energy (*i.e.*, energy of interactions between atoms that are more than three bonds apart) criteria. Models of other $sPLA_2$–hPDI complexes were then evaluated by comparing them to the chosen Atx–hPDI model. The lowest energy $sPLA_2$–hPDI models that had a similar interaction site as Atx in the hPDI model were chosen. In all the cases, excepting hGX $sPLA_2$, the process of choosing the best $sPLA_2$–hPDI model was very straightforward, since the models with the same interaction site as Atx had the lowest non-bonded energy. For $AtnI_2$ and hGX $sPLA_2$ in the majority of models the respective $sPLA_2$ was offset significantly compared to Atx. Models in which hGX $sPLA_2$ exhibited the same interaction site as Atx in the Atx–hPDI complex had significantly higher non-bonded energy, therefore we chose the lowest energy model.

4 Results

4.1 Atx's interaction with intracellular proteins

4.1.1 Atx-binding proteins in SVs

4.1.1.1 Isolation of SVs

SVs are affected by β-neurotoxic action (Prasarnpun et al., 2004, Logonder et al., 2008b) and were proposed as one of the means of internalization of β-ntxs into target cells (Pungerčar & Križaj, 2007). In this role, SVs could harbour specific receptors for β-ntxs. In order to assess the existence of these, we isolated SVs from the porcine cerebral cortex and PC12 cells as described in 3.2.4.1 and 3.2.4.2. In the ND PC12 cells, we were unable to detect the haze, representing SV fraction, in the final step of SV purification. We were, however, succesful in isolating SVs from the NGFD PC12 cells. We measured the total protein concentration in both samples of isolated SVs as described in 3.2.1.2.1. In the brain SV preparation, the protein concentration was 1.6 mg/mL and in the PC12 SV preparation 0.24 mg/mL. Both samples were tested for the presence of the SV marker protein Syt1/2 with SDS-PAGE, followed by western blotting and immunodetection as described in 3.2.1.3 and 3.2.1.4 (Figure 8). In both preparations, we detected three bands, corresponding to Syt1/2. The high molecular mass protein represents the full length glycosylated Syt1/2, the intermediate mass protein probably the deglycosylated variant of the high molecular mass protein, while the low molecular mass protein probably corresponds to the cytosolic part of the Syt1/2, resulting from the proteolytic cleavage in the course of the isolation procedure.

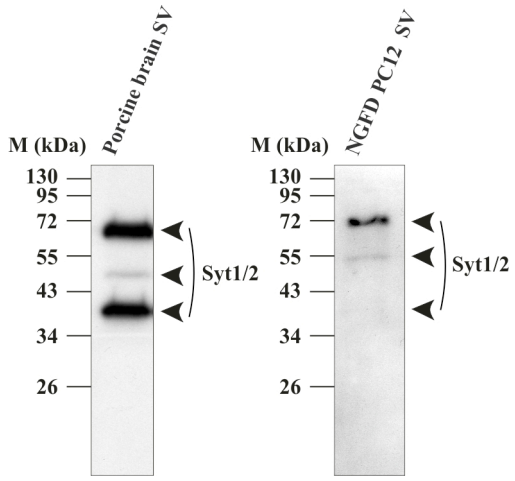

Figure 8: *Detection of Syt1/2 in isolated SV preparations from porcine cerebral cortex and NGFD PC12 cells.* Porcine brain SV and NGFD PC12 SV were dissolved and separated on a 12.5% (v/v) polyacrylamide gel by SDS-PAGE and probed for the presence of Syt1/2 by specific immunodetection following western blotting onto a PVDF membrane. Arrowheads indicate the anti-Syt1/2 polyclonal antibodies-reactive bands. In both preparations, three bands were detected, the upper representing the whole Syt1/2, the middle probably the deglycosylated Syt1/2 and the lower band the cytosolic part of Syt1/2 produced by proteolysis during the isolation.

4.1.1.2 Atx-binding proteins in SVs

Next, we probed the isolated SVs for the presence of Atx-binding proteins. We incubated the SVs or detergent-solubilized SV proteins with sulfo-SBED-AtxC in the presence or absence of Ca^{2+}. We also incubated the solubilized SV proteins with ^{125}I-AtxC in the presence of Ca^{2+}. Control samples contained a large excess of the native AtxC over the labelled one. Another control, in the case of cross-linking with sulfo-SBED-AtxC, contained no sulfo-SBED-AtxC to ensure that the detected bands were not due to proteins in SVs that intrinsically contain biotin. After the incubation, the Atx probes were covalently cross-linked with their binding proteins and analyzed as described in 3.2.2.2.2 and 3.2.2.3. Results are shown in Figure 9. In the samples, containing intact SV membranes, we were able to specifically cross-link several Atx-binding proteins in both preparations, brain and PC12 (Figure 9A and B). The apparent masses of Atx-binding proteins range from 26 to 72 kDa and also above 100 kDa. Atx-labelling of the majority of these proteins did not require Ca^{2+}. If labelling was performed on the porcine brain SV extracts, the number of detected specific interactions was much lower; in this case, sulfo-SBED-AtxC specifically interacted with only three proteins, 30 kDa, 50 kDa and 65 kDa protein (Figure 9C, left panel). In PC12 SV extracts, however, besides the proteins of 30, 50 and 65 kDa, sulfo-SBED-AtxC specifically labelled also a protein of 55 kDa and at least four proteins in the mass range between 80 kDa and more than 170 kDa (Figure 9C, right panel). In the latter case the cross-linking pattern was similar to that obtained on the SV membranes (Figure 9B). The ^{125}I-AtxC labelling was performed only on SV extracts. In this case only one SV component was strongly labelled in porcine brain as well as in PC12 SV sample (Figure 9D). The adduct migrated at about 26 kDa, therefore it was the result of covalent complexing between AtxC (14 kDa) and a SV component of about 12 kDa.

Using two affinity-labelling methods we confirmed the presence of specific binding proteins for Atx in porcine brain and PC12 SVs.

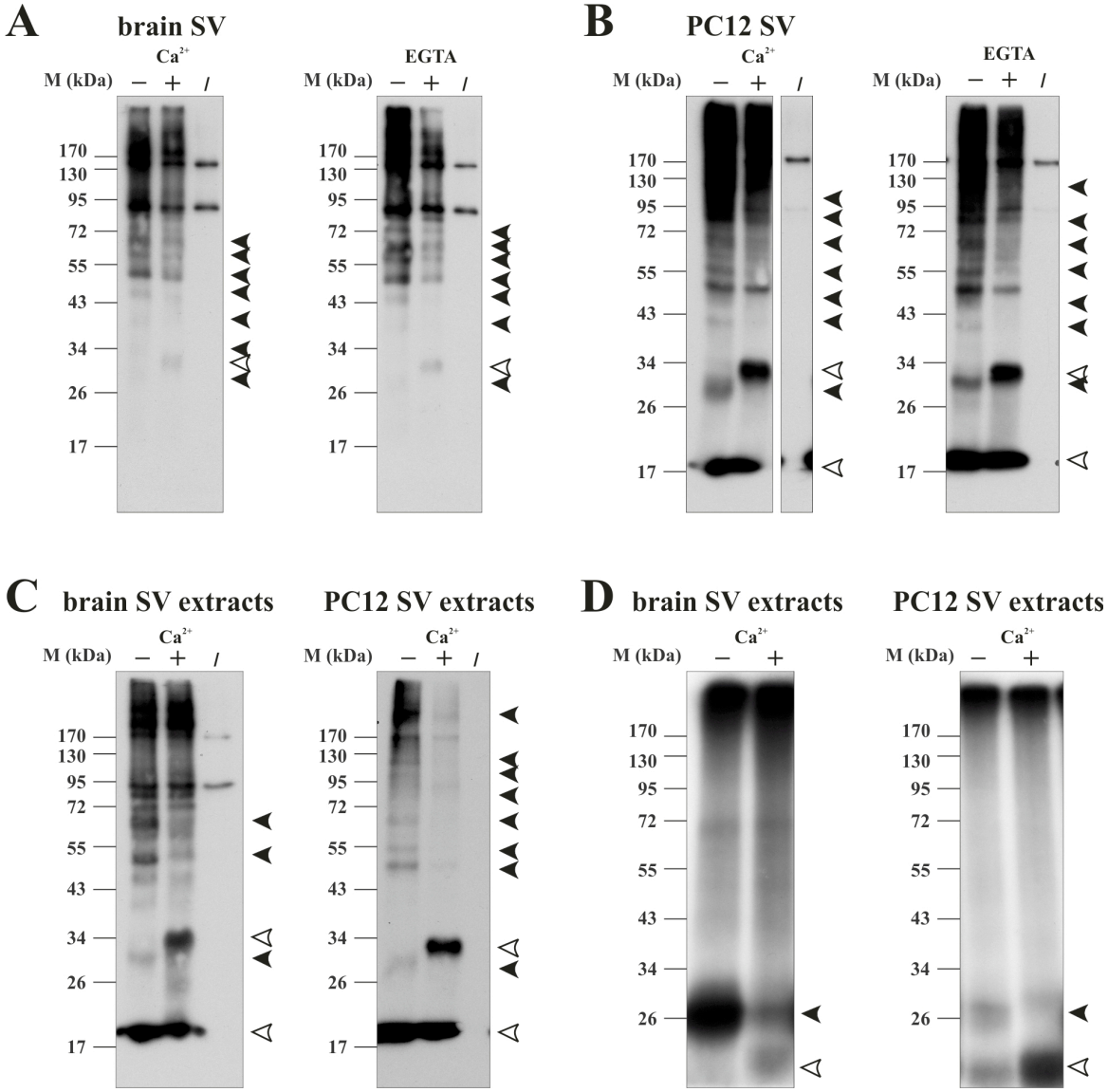

Figure 9: *Specific labelling of SV proteins with sulfo-SBED-AtxC and ^{125}I-AtxC.* Intact SV from porcine brain (A) or NGFD PC12 cells (B) or detergent-solubilized SV proteins from both sources (C) were incubated in the presence of the biotin-containing photo-reactive sulfo-SBED-AtxC in the presence of Ca^{2+} or EGTA. The control samples contained 100-fold molar excess of the native AtxC (+). Another control contained no sulfo-SBED-AtxC (/). After incubation, covalent cross-linking of Atx to its binding proteins was triggered by exposure to UV light. The biotin-containing proteins were detected by western blotting and strepatavidin-HRP detection. Black arrowheads indicate specific Atx-binding proteins. White arrowheads indicate sulfo-SBED-AtxC (B, C) and its dimer (A, B, C). (D) Detergent-solubilized SV proteins were incubated in the presence of the radioactive ^{125}I-AtxC and Ca^{2+}. The control samples (+) contained 200-fold molar excess of the native AtxC over ^{125}I-AtxC. ^{125}I-AtxC was covalently cross-linked to its binding proteins by the addition of DSS. Samples were analyzed by SDS-PAGE and autoradiography. The specific band is indicated with a black arrow and represents the covalent complex of ^{125}I-AtxC with its binding protein. White arrow indicates the dimer of ^{125}I-AtxC.

4.1.1.3 Isolation of Atx-binding proteins from SV

In an effort to identify the Atx-binding proteins in SV, we cross-linked proteins in porcine brain SVs with sulfo-SBED-AtxC, and isolated the biotin-containing Atx-binding proteins as described in 3.2.4.3. We performed four different isolation procedures, A, B, C and D. In samples A and B, the proteins were extracted before being processed further.

From sample A, the intrinsically biotinylated proteins were then removed with avidin-chromatography. Thus prepared extracted samples A and B, and the intact SV membranes in sample D were then incubated with sulfo-SBED-AtxC. Sample C, containing intact SV membranes, was the control sample, and was incubated without the added sulfo-SBED-AtxC. After the incubation, the photochemical cross-linking reaction was triggered with UV light, which bound Atx with its binding proteins into covalent complexes, which now contained biotin. All samples were then subjected to avidin-chromatography to isolate the biotin-containing proteins. The eluted fractions were named A_{EL}, B_{EL}, C_{EL} and D_{EL}. After recovery of proteins, the samples were analyzed using streptavidin detection (Figure 10A). On the same blot we analyzed also sulfo-SBED-AtxC-labelled extracts of SVs in the presence (Figure 10A, second lane on the blot) or absence (Figure 10A, first lane on the blot) of 100-fold molar excess of the native AtxC. This allowed us to distinguish the specific Atx-binding proteins in SVs from the sulfo-SBED-AtxC and its multimers. On the blot, four strong bands were detected in the samples A_{EL}, B_{EL} and D_{EL}, but not in the C_{EL} (control sample). The lightest band (at 15 kDa) probably represented sulfo-SBED-AtxC. The three heavyer bands in the samples A_{EL}, B_{EL} and D_{EL} (20 kDa, 28 kDa, 34 kDa) did not match neither position nor intensity of the bands corresponding to dimer or trimer of sulfo-SBED-AtxC, indicated in the control (+) (white arrowheads) in the second lane on the blot. These bands did, however, match the positions of specific Atx-binding proteins, observed in the first lane on the blot and therefore probably represent the same specific Atx-binding proteins, enriched by the isolation procedure. To identify these proteins, we separated the four samples with SDS-PAGE and stained the gel with silver nitrate (Figure 10B). Using this staining protocol, we visualized only two proteins, which were present in samples A and B, but absent in the sample C. The band at 14 kDa represented sulfo-SBED-AtxC. We excised the band at 25 kDa, along with several other bands from the gel and analyzed them with MS. The amounts of proteins in gel slices were, however, too low for reliable identification.

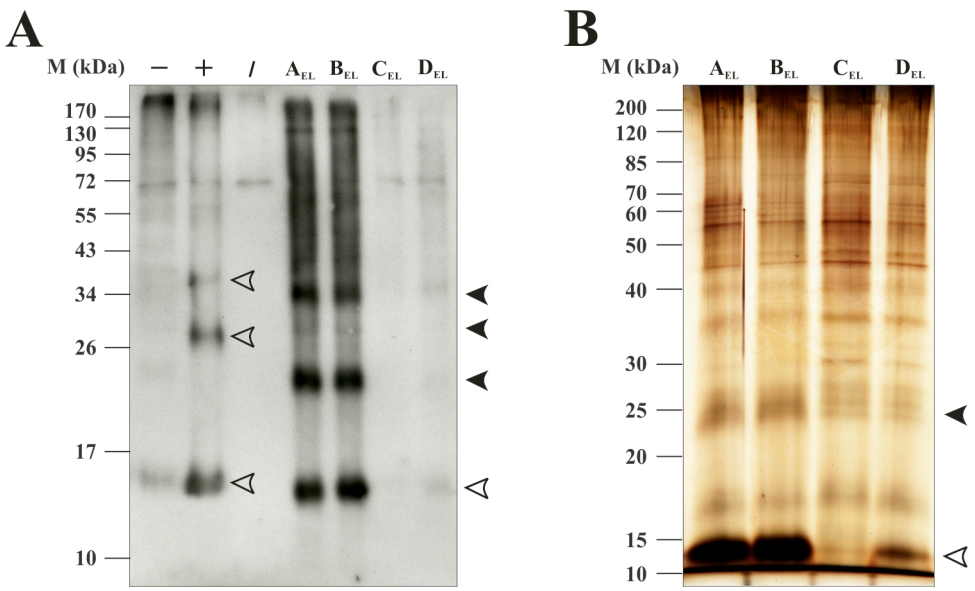

Figure 10: *Isolation of Atx-binding proteins from porcine brain SVs.* We isolated the Atx-binding proteins from SVs by cross-linking them first with sulfo-SBED-AtxC. In samples A and B, the proteins were extracted from SVs prior to cross-linking, while in samples C and D intact SV membranes were reacted with the AtxC photo-probe. From sample A we removed the intrinsically biotinylated proteins prior to addition of sulfo-SBED-AtxC. Sample C is a control with no sulfo-SBED-AtxC added. In samples C and D proteins were extracted after sulfo-SBED-AtxC labelling. All samples were then subjected to avidin-affinity chromatography to isolate the biotinylated proteins. The eluates A_{EL}, B_{EL}, C_{EL} and D_{EL} were then analyzed on SDS-PADE, blotted and detected with SA-HRP (A), or silver stained (B). As a control, on the same blot we also analyzed a sulfo-SBED-AtxC-labelled extract of SV proteins in the presence (+) or absence (–) of 100-fold molar excess of the native AtxC or the SV extract without the added sulfo-SBED-AtxC (/). Specific Atx-binding proteins are indicated with black arrowheads, and sulfo-SBED-AtxC and its multimeres with white arrowheads.

4.1.2 Atx's interaction with Syt1, CcO and PDI

4.1.2.1 Syt1 and CcO are specific binding proteins of Atx

Syt1 and subunit 2 of CcO have previously been identified as potential binding proteins of Atx (Kovačič, 2009b). In order to confirm these interactions as specific, we incubated recombinant human Syt1 and purified bovine heart CcO with sulfo-SBED-AtxC or ^{125}I-AtxC. Control samples contained a large excess of the native AtxC over the labelled one. Both, Syt1 and CcO have shown specific binding of AtxC as seen in Figure 11. With both methods of labelling, AtxC specifically labelled several subunits of CcO (Figure 11C and D), among them subunits 2 (26 kDa) and 4 (17 kDa), indicating that the interaction site for AtxC probably includes both subunits. We have thus confirmed the specific binding of AtxC to Syt1 and CcO *in vitro*.

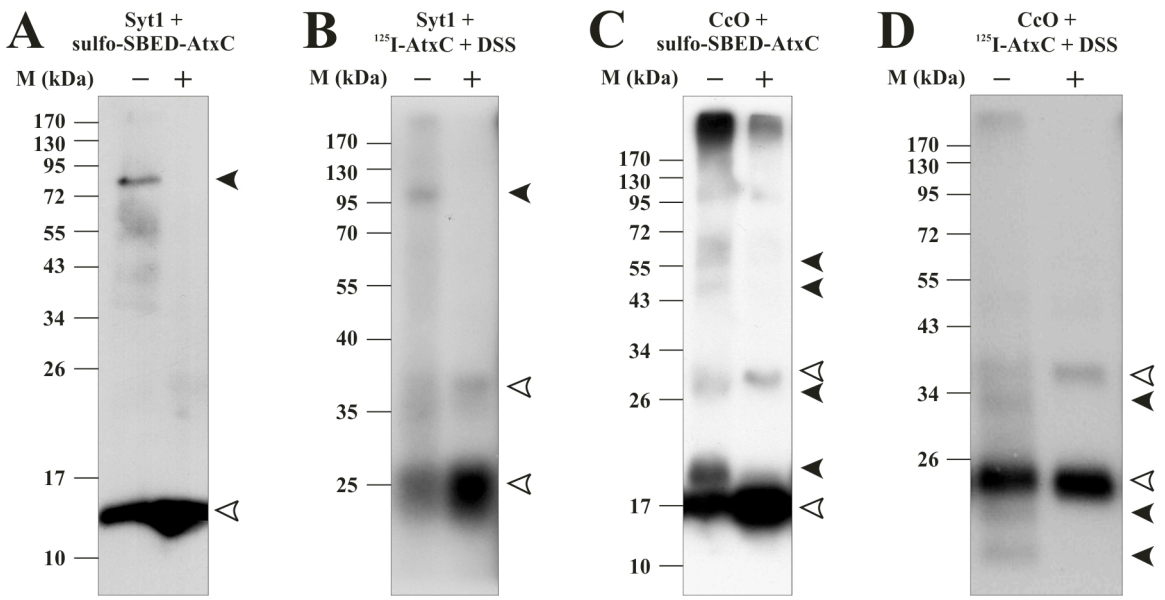

Figure 11: *Atx specifically binds to Syt1 and CcO.* Purified human Syt1 (A, B) and bovine heart CcO (C, D) were incubated in the presence of the biotin-containing photo-reactive sulfo-SBED-AtxC (A, C) or the radioactive ^{125}I-AtxC (B, D). The control samples contained 100-fold molar excess of the native AtxC (+). (A, C) After the incubation, the sulfo-SBED-AtxC samples were exposed to UV light to initiate the photo-chemical binding of AtxC to its binding protein, and analyzed with SDS-PAGE followed by western blotting. The presence of a reducing agent in the SDS-PAGE loading buffer caused the transfer of the biotin tag from sulfo-SBED-AtxC to the protein to which it was bound. We detected biotinylated Syt1 or subunits of CcO with SA-HRP on the blot. (B, D) ^{125}I-AtxC was covalently cross-linked to Syt1 or CcO using formaldehyde or DSS, respectively. Samples were analyzed by SDS-PAGE and autoradiography. Bands represent the covalent complexes of ^{125}I-AtxC and its binding proteins. Specific binding of AtxC to Syt1 and CcO is indicated with black arrowheads. Monomers and dimers of sulfo-SBED-AtxC or ^{125}I-AtxC are indicated with white arrowheads. Representative results of two independent assays are shown.

4.1.2.2 Atx's binding to CcO is Ca^{2+}-dependent

The binding of R25 to Atx has been shown to be Ca^{2+}-dependent (Vučemilo et al., 1998, Kovačič, 2009b). By performing the cross-linking of CcO and ^{125}I-AtxC in the presence of the Ca^{2+}-chelating agent EGTA we found that this divalent ion is necessary for the interaction between Atx and CcO (Figure 12). The same was the case for the Atx–R25 interaction (Vučemilo et al., 1998, Kovačič, 2009b), further indicating the identity of R25 as a part of the CcO complex.

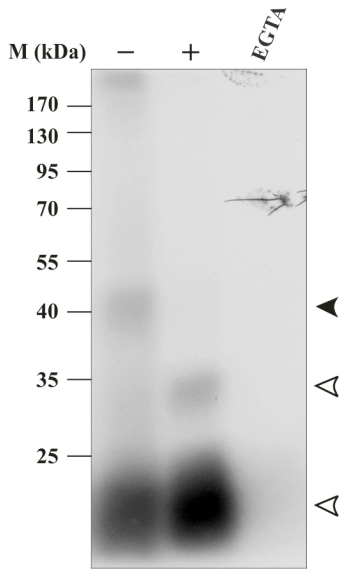

Figure 12: *Interaction of Atx with CcO is Ca^{2+}-dependent.* CcO was incubated with ^{125}I-AtxC and then the cross-linker DSS was added (–). The control sample contained also a 100-fold molar excess of the native AtxC (+). The third sample was the same as the first, just that instead of Ca^{2+} ions it contained EGTA. Samples were analyzed by SDS-PAGE and the gel autoradiographed. The results clearly show that ^{125}I-AtxC requires Ca^{2+} to complex with CcO (black arrow). Monomer and dimer of ^{125}I-AtxC are indicated with white arrowheads. A representative result of two independent assays is shown.

4.1.2.3 Syt1 has two binding sites for Atx

Syt1 is a transmembrane protein, with 2 cytosolic domains (C2a and C2b) and a short unstructured domain exposed to the lumen of the SV (Koh & Bellen, 2003). Therefore, several possible modes of binding Syt1 exist for Atx. For example, BoNT B and BoNT G have been shown to bind the luminal part of Syt1 (Dong et al., 2003; Rummel et al., 2004). This interaction is required for these toxins to exert their neurotoxic effect.

A similar role as in the neurotoxicity of BoNT might be expected for Syt1 also in the neurotoxicity of Atx. In order to investigate to which part of Syt1 Atx binds, we first tried to prevent Atx from binding to Syt1 by using antibodies, raised against the luminal or the cytosolic part of Syt1. Neither of the used antibodies inhibited the interaction between Atx and Syt1 (results not shown). Then we used a recombinant cytosolic part of Syt1 and also the 56 amino acid residues long luminal part of Syt1 to perform the homologous competition assay using sulfo-SBED-AtxC.

Figure 13A shows that sulfo-SBED-AtxC specifically labelled only the recombinant cytosolic part of Syt1, localizing the Atx binding site to this region of Syt1. We were not successful at directly cross-linking the luminal part of Syt1 at the equimolar concentration of both proteins (data not shown). However, the 100-fold molar excess of the luminal part of Syt1 was clearly able to attenuate, but not completely prevent, the full-length Syt1 labelling by sulfo-SBED-AtxC (Figure 13B). This indicated the presence of two binding sites for Atx on Syt1, one on the cytosolic part of the molecule and the other on its luminal side. In the cross-linking reaction with the 100-fold molar excess of the luminal part of Syt1 we also detected the band corresponding to labelling of the luminal part of Syt1 with sulfo-SBED-AtxC, further confirming our assumption of two binding sites for Atx on Syt1. This band appeared above the 10 kDa, higher than expected according to the molecular mass of 6 kDa for the luminal part of Syt1. It may be that Atx interacted with a dimer of the luminal Syt1.

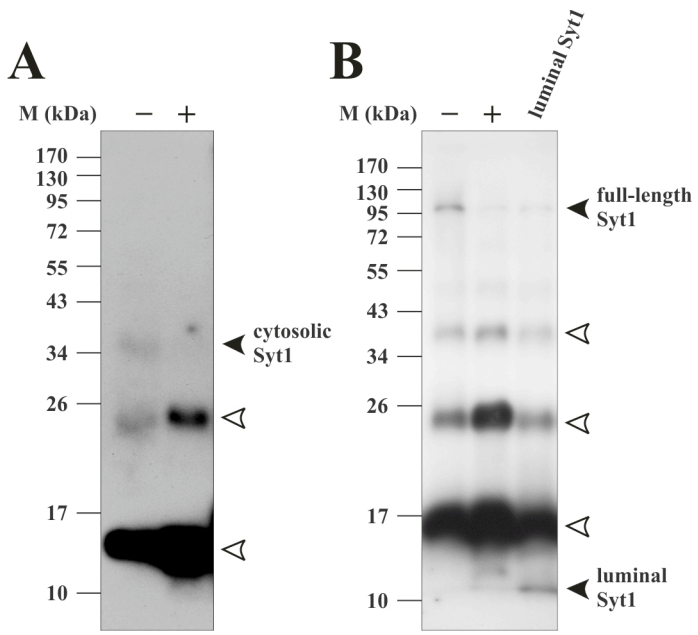

Figure 13: *Syt1 has two binding sites for Atx.* Recombinant cytosolic and the luminal part of Syt1 were probed for their ability to bind Atx. (A) The cytosolic part of Syt1 (500 nM final concentration) was incubated with sulfo-SBED-AtxC in the presence (+) or absence (–) of a large molar excess of the native AtxC. (B) In a similar assay the full-length Syt1 (100 nM final concentration) was incubated with sulfo-SBED-AtxC in the presence (+) or absence (–) of an excess of Atx over sulfo-SBED-AtxC or a 100-fold molar excess of the luminal part of Syt1 over the full-length Syt1. After UV-cross-linking the samples were analyzed with SDS-PAGE and western blot. The biotinylated Syt1 was detected using SA-HRP. (A) AtxC specifically interacted with the cytosolic part of Syt1, indicating the position of one binding site for Atx resides at this part of Syt (black arrowhead). (B) The interaction of AtxC with the full-length Syt1 was largely, but not completely, inhibited in the presence of an excess of the luminal Syt1 (upper black arrowhead). At these concentrations, also the luminal part of Syt1 was obviously cross-linked with sulfo-SBED-AtxC (black arrowhead at the bottom). Both these results indicate that Atx also interacts with the luminal part of Syt1. Atx therefore seems to bind to two discrete locations on Syt1. Monomer and multimers of biotinylated AtxC are indicated with white arrowheads. Representative results of two independent assays are shown.

4.1.2.4 The binding of Atx at one site of Syt1 is Ca^{2+}-dependent

When Syt1 was first indicated as a binding protein for Atx, it was suggested that their interaction is Ca^{2+}-dependent (Kovačič, 2009b). We further characterized the Atx-Syt1 interaction therefore, by investigating, whether it depends on the presence of Ca^{2+} ions or not. Our results show that the presence of EGTA inhibits the interaction between these two proteins to some extent (Figure 14), indicating that the binding of Atx to one of the binding sites on Syt1 is Ca^{2+}-dependent while to the other is not. Since Syt1's cytosolic domains bind Ca^{2+} (Koh & Bellen, 2003), we speculate that the cytosolic site is probably the one that requires Ca^{2+} to bind Atx.

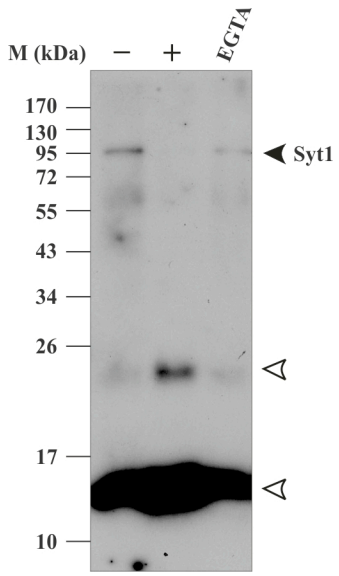

Figure 14: *The interaction of Atx with Syt1 is partially inhibited in the absence of* Ca^{2+}. Syt1 was labelled with sulfo-SBED-AtxC in the presence of Ca^{2+} and the presence (+) or absence (–) of a 100-fold molar excess of the unlabelled AtxC over the labelled. The third sample was the same as the first, except that instead of Ca^{2+} ions it contained EGTA. After the UV-cross-linking, the samples were analyzed by SDS-PAGE and western blotted onto a PVDF membrane. Biotinylated Syt1 was detected on the blot with SA-HRP. Monomer and dimer of biotinylated AtxC are indicated with white arrowheads. Representative result of three independent assays is shown.

4.1.2.5 CaM blocks the binding of Atx to the cytosolic part of Syt1

CaM, a known receptor for Atx, has been shown to bind to Syt1, too (Trifaro, Fournier & Novas, 1989). We investigated whether the addition of CaM (equimolar to Syt1) into the reaction mixture would inhibit the interaction between Atx and Syt1. Contrary to our expectations, the interaction of Atx with Syt1 was facilitated in the presence of CaM (Figure 15, lane four).

To investigate whether CaM and Atx simultaneously bind to the cytosolic part of Syt1 or CaM binds the cytosolic part, while Atx binds the luminal part, we performed the cross-linking with ^{125}I-AtxC in the presence of an excess of the luminal Syt1 over the full-length Syt1 and CaM (equimolar to Syt1). The addition of both, CaM and the 100-fold molar excess of luminal Syt1, almost completely inhibited the Atx-full length Syt1 interaction (Figure 15, lane five), suggesting that interaction of Atx with the cytosolic side of Syt1 was blocked by CaM and the other one by the luminal Syt1. It is unknown, however, if the interaction of Atx with the cytosolic part of Syt1 is prevented by the CaM–Syt1 or the CaM–Atx interaction.

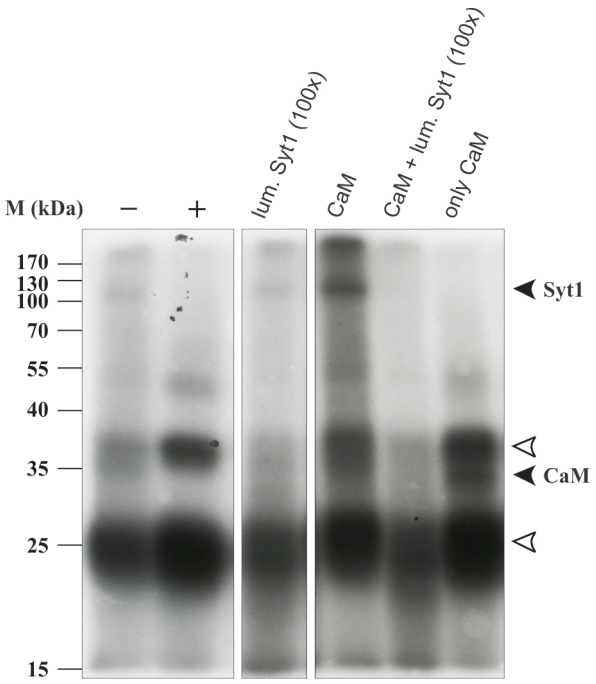

Figure 15: *Effect of the presence of CaM and the luminal Syt1 on the Atx–Syt1 complex formation.* Syt1 (40 nM) was incubated with ^{125}I-AtxC (10 nM) in the presence of a 100-fold molar excess of the luminal Syt1 over the full length Syt1, CaM, equimolar to the full-length Syt1, or CaM and the excess of the luminal Syt1. The control reaction (+) contained a large excess of unlabelled AtxC over ^{125}I-AtxC. Only CaM – the sample contained only CaM and ^{125}I-AtxC. After the incubation, the proteins in complex were cross-linked with paraformaldehyde and analyzed by SDS-PAGE, followed by autoradiography. Interestingly, the presence of CaM in the reaction increased cross-linking of Syt1 and ^{125}I-AtxC. The presence of both, luminal Syt1 and CaM, however, almost completely inhibited the formation of Atx–Syt1 complex, indicating that CaM inhibits the binding of Atx to the cytosolic part of Syt1. The bands, corresponding to complexes of Syt1 and CaM with ^{125}I-AtxC, are indicated with black arrowheads. White arrowheads indicate the dimer and trimer of ^{125}I-AtxC.

4.1.2.6 Syt1 specifically interacts besides with Atx also with other sPLA$_2$s

Different presynaptically neurotoxic sPLA$_2$s exert similar effects on target cells (Pungerčar & Križaj, 2007, Šribar et al., 2014). It is therefore reasonable to assume that some of them share the same cellular receptors, which may be also targeted by their mammalian sPLA$_2$ orthologues. Indeed, specificity for binding different sPLA$_2$ molecules, snake venom or mammalian, has been shown for almost all sPLA$_2$ receptors known to date (Šribar et al., 2014). In order to assess the potential role of Syt1 as a broader spectrum sPLA$_2$-receptor, we investigated if other sPLA$_2$s besides Atx also bind to Syt1. We performed a competitive binding experiment by incubating Syt1 in the presence or absence of an excess of different sPLA$_2$s. The results are shown in Figure 16. As we expected, AtxA, which is almost identical to AtxC, completely inhibited the interaction of Syt1 with AtxC. Interestingly, we found that the non-toxic homolog of AtxC, AtnI$_2$, inhibited the interaction between AtxC and Syt1 only to a certain extent. The myotoxic AtnL, on the other hand, inhibited the interaction between AtxC and Syt1 completely. Other neurotoxic sPLA$_2$s that inhibited this interaction well include crotoxin, agkistrodotoxin, bee venom sPLA$_2$, and to a lesser extent β-bungarotoxin and OS$_2$. Notexin and *crotalus atrox* sPLA$_2$ do not act as inhibitors. Interestingly, all tested mammalian sPLA$_2$s, GV, GX and GIIA sPLA$_2$, completely inhibited the Atx–Syt1 complex formation. Our results therefore suggest the involvement of Syt1 in the

mechanisms of action of also other toxic and mammalian $sPLA_2$s.

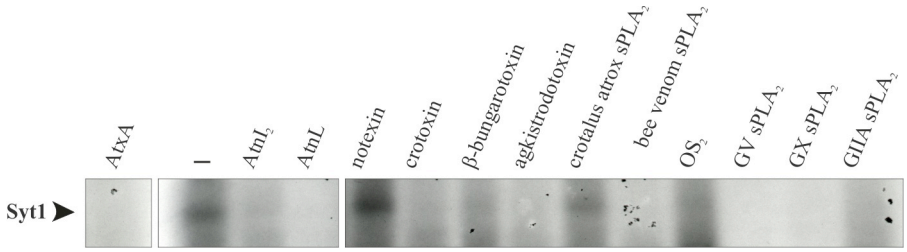

Figure 16: *Syt1 specifically interacts also with other $sPLA_2$s.* Syt1 was incubated with ^{125}I-AtxC in the absence (–) or the presence of a 100-fold molar excess of the indicated $sPLA_2$s. The interacting proteins were covalently cross-linked after the addition of formaldehyde. Then the samples were analyzed by SDS-PAGE and the gel autoradiographed. Results show that also some other $sPLA_2$s, neurotoxic or mammalian, specifically interact with Syt1.

4.1.2.7 Effect of Syt1 and CcO on Atx's phospholipase activity

To further assess the significance of the interactions of Atx with Syt1 and CcO, we examined their effect on AtxC's enzymatic activity using the PyPG method, as described in 3.2.6. In the case of Syt1 we detected no effect on the phospholipase activity of AtxC (Figure 17A).

The addition of CcO into the phospholipase activity assay largely increased the activity of AtxC (Figure 17B). However, we observed a similar increase in fluorescence when we performed the assay in the absence of CcO but in the presence of the same amount of the detergent lauryl maltoside, which is present in the sample of CcO (Figure 17B).

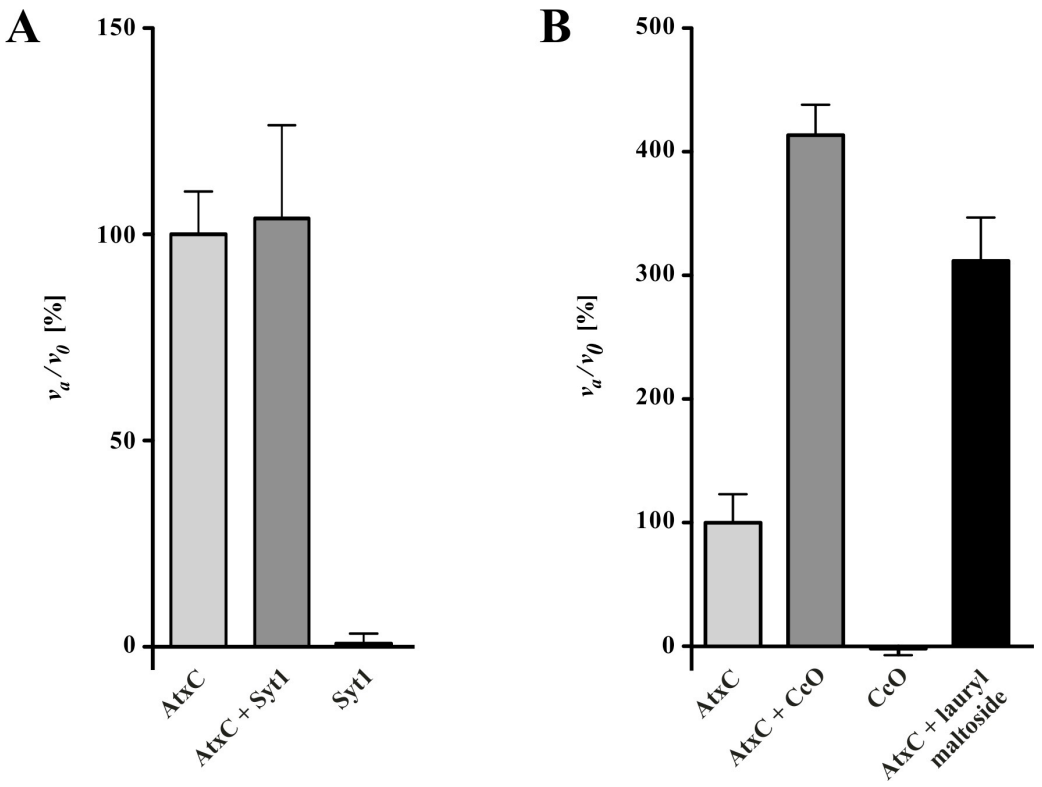

Figure 17: *Effect of the presence of Syt1 and CcO on Atx's phospholipase activity.* Syt1 (A) and CcO (B) were probed for the ability to modulate AtxC's enzymatic activity, as described in 3.2.6. Control samples contained no AtxC. Another control in the case of CcO contained AtxC and the detergent lauryl maltoside, but no CcO. Experimental data from two independent measurements were fitted with the 3rd order polynomial to calculate the initial velocity of the enzymatic reaction. The extent of modulation (v_a/v_0) is presented as the ratio between the initial velocity in the case of AtxC in the presence of Syt1 or CcO (v_a), and the initial velocity in the case of AtxC alone (v_0). Error bars represent standard deviation.

4.1.2.8 AtxC interacts with Syt1, R25 and PDI also in live PC12 cells

In order to assess the biological significance of interactions of Atx with CcO, PDI and Syt1, which were established *in vitro*, co-localization studies in PC12 cells were initiated. In preliminary studies, Atx was shown to significantly co-localize with CcO and PDI (Dolinar, 2013). We complemented and advanced these findings by showing a co-localization of Atx also with Syt1 in PC12 cells (presented in section 4.2.5.2).

Taking one step further, we wanted to assess, whether Atx actually interacts with these proteins inside living PC12 cells. To this end, we implemented an *in vivo* cross-linking assay (Jenko Pražnikar et al., 2008; Kovačič, 2009b) as described in 3.2.5.1. We incubated ND and NGFD PC12 cells in the presence of the photo-reactive biotin-containing sulfo-SBED-AtxC for 1, 2, 5, 15, 30 and 60 min. The control samples were incubated for 5 min without sulfo-SBED-AtxC. At the end of incubation, the cells were lysed and subjected to avidin-affinity purification step to isolate biotinylated protein complexes. The isolated proteins were analyzed by SDS-PAGE under reductive conditions, blotted onto a PVDF or nitrocellulose membrane and immunologically probed for the presence of Syt1, CcO subunit 2 and PDI. As shown in Figure 18 (panels A and B), after only 1 min, sulfo-SBED-AtxC reached and labelled Syt1 and PDI with biotin in living PC12 cells. Unlike with PDI, we were able to detect the interaction of Atx with Syt1 only in NGFD PC12 cells.

In the case of immunostaining using antibodies directed against CcO subunit 2, we

detected several bands at different molecular masses, casting doubt about the specificity of the antibodies used (results not shown). We have, however, performed an additional assay, in which after the avidin-chromatography step, the samples were subjected to immunoprecipitation with anti-Atx antibodies to isolate Atx-binding proteins (described in detail in 3.2.5.1.1). The samples were then analyzed by SDS-PAGE, followed by western blotting onto a PVDF membrane and testing for the presence of biotinylated proteins. In both, ND and NGFD PC12 cells, we detected a band at 25 kDa, which was absent in the control sample (Figure 18, panels C and D) and likely represents R25. This protein therefore specifically bound Atx also in living PC12 cells.

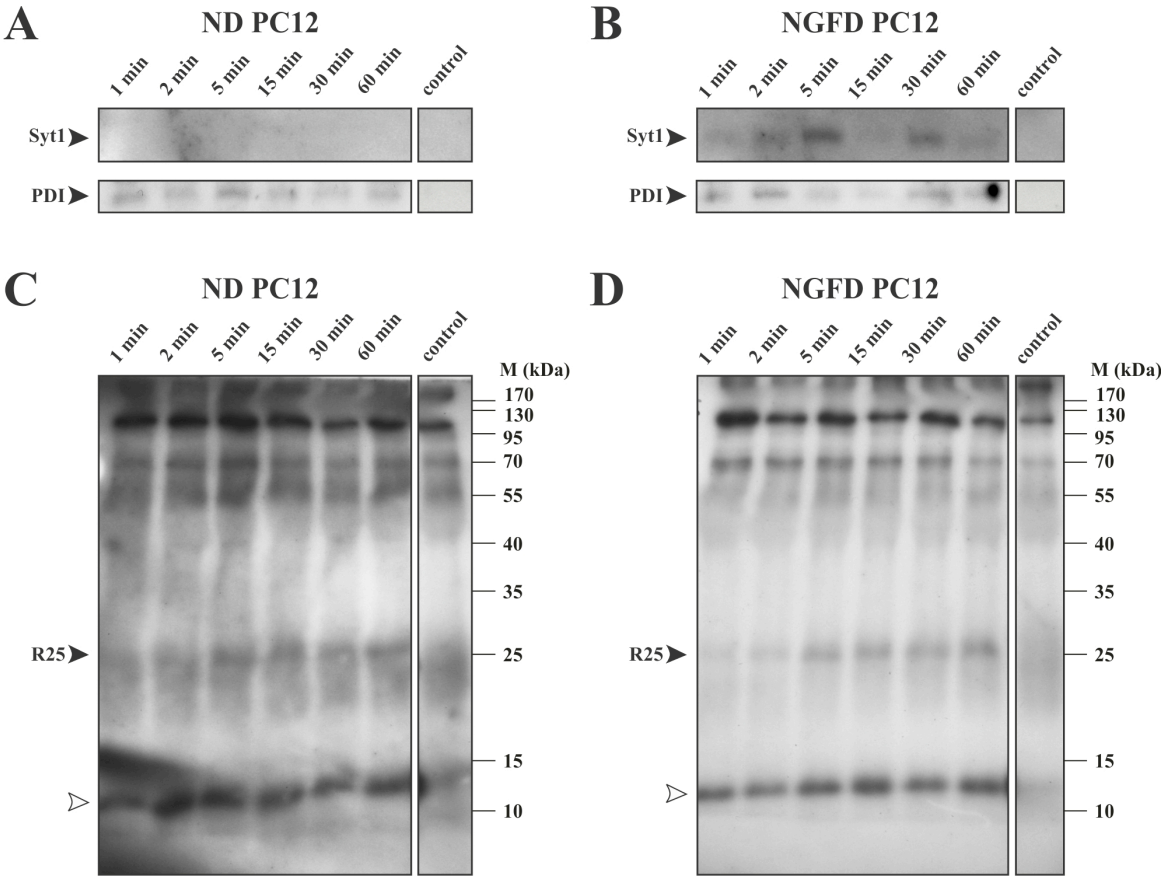

Figure 18: *Atx interacts with Syt1, PDI and R25 in intact PC12 cells.* ND and NGFD PC12 cells were incubated in the presence of sulfo-SBED-AtxC for indicated periods of time. The cells were then exposed to UV light to photo-chemically link AtxC-probe to its binding proteins. From cell lysates the biotinylated proteins were isolated on avidin-beads and (A, B) immunologically probed for the presence of Syt1 and PDI or (C) subjected to another affinity-based purification step, immunoprecipitation with anti-Atx antibodies, followed by detection of biotinylated proteins on the western blot. (A, B) PDI and Syt1 were immuno-detected in the samples but not in controls (no sulfo-SBED-AtxC added), indicating that Atx encountered these proteins also in living cells. (D) Using biotin-based detection, we visualized a band at 25 kDa, representing R25, suggesting that Atx interacts also with this protein in the living PC12 cells. Positions of sulfo-SBED-AtxC on blots are indicated by white arrowhead.

4.1.2.9 The 3D model of Atx in complex with hPDI

The interaction of Atx with PDI has been previously characterized in detail (Šribar et al., 2005; Kovačič, 2009b). Šribar et al. (2005) suggested that PDI may play a role at internalization of Atx *via* the retrograde protein transport pathway, a mechanism employed also by some bacterial toxins to invade cells, for example cholera toxin (Tsai et

al., 2002; Lencer et al., 2003; Lord et al., 2005). Our results show that Atx and PDI come in contact in living PC12 cells, suggesting physiological significance of their interaction.

In order to rationally design mutants for further study of the role of PDI in cell trafficking of Atx, the interaction between Atx and hPDI was structurally characterized. Based on the model of the interaction of Atx with yPDI (Kovačič, 2009b; Oberčkal et al., 2015) we prepared a model of the complex between Atx and hPDI, using protein docking with HADDOCK (described in 3.2.9).

The 3D structure of hPDI was superimposed on the structure of yPDI in the model of its complex with Atx (Kovačič, 2009b; Oberčkal et al., 2015). The HADDOCK procedure was then implemented to obtain the energetically most favourable model of the complex, shown in Figure 19A. In the model, Atx binds *via* its IBS to the surface of the b and b' domains of hPDI, remote from PDI catalytic site and in a similar way as misfolded proteins and cholera toxin (Tian et al., 2006; Forster et al., 2009; Taylor et al., 2011a and 2011b). As indicated in Figure 19B, Atx binds to hPDI with the basic residues K69, R72, K74, K86 and R188, polar N17 and N119 and hydrophobic L3, L19 and F24.

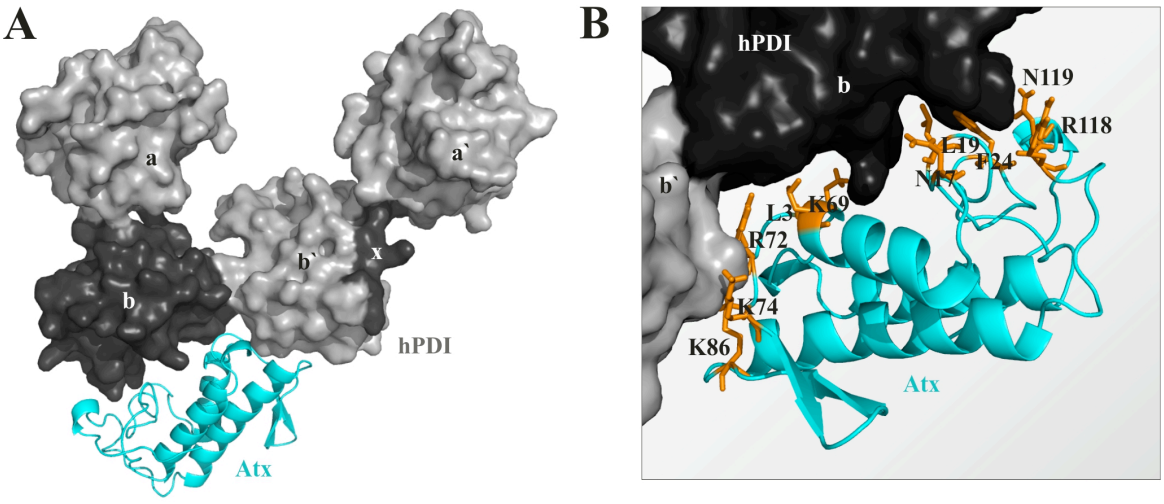

Figure 19: *The 3D model of the interaction between Atx and hPDI.* To obtain the model of the Atx–hPDI complex, the structure of hPDI was superimposed on the structure of yPDI in the model of its complex with Atx. Then, the energetically most favourable model was generated by protein docking with HADDOCK. Docking resulted in a model (A), where Atx (shown in cartoon mode) binds *via* its IBS site to the surface of b and b' domains of hPDI (shown in space-filling mode). PDI domains are indicated. (B) A detailed view of the Atx–hPDI interaction site. The amino acid residues of Atx (cartoon mode) that interact with PDI (space-fill mode) are shown in stick mode and are numbered. The b and b' domains of PDI are indicated. The images were displayed with PyMOL.

4.1.2.10 Complexes between hPDI and Atx-like sPLA$_2$s

Toxins often take advantage of their similarity with endogenous molecules to exert their effects on target cells. Besides the neurotoxic sPLA$_2$s, several mammalian sPLA$_2$s, for example GIB, GIIA, GV and GX sPLA$_2$, are structurally highly similar to Atx. GIB, GIIA and GV sPLA$_2$ have been detected inside cells (Fayard, Tessier, Pageaux, Lagarde & Laugier, 1998; Macchioni et al., 2004; Nardicchi, Macchioni, Ferrini & Goracci, 2007; Kim et al., 2002, Birts, Barton & Wilton, 2008), while GX sPLA$_2$ was not. Pathway of the cellular internalization of sPLA$_2$s has not been established yet. In order to consider the possible involvement of PDI in the cell trafficking of mammalian sPLA$_2$s, we inspected *in silico* whether the latter are able to form complexes with PDI in a similar way as Atx or

not. We did the same for the myotoxic and non-toxic homologs of Atx, AtnL and $AtnI_2$, respectively. The 3D structure of each of these molecules was superimposed on the structure of Atx in its complex with PDI. HADDOCK was then used to generate the energetically most favourable models, shown in Figure 20 (panels A and B). Besides some differences in relative orientation between respective $sPLA_2$s in complexes, the studied $sPLA_2$s form very similar complexes with hPDI as Atx. This is reflected in the average backbone root-mean-square deviation (RMSD) values calculated for Atx and for each of the substituting $sPLA_2$s in the complex with PDI. These values were calculated by Dr. Lidija Kovačič and were 9 and 1 Å, for $AtnI_2$ and AtnL, respectively, and 3, 7, 4 and 12 Å for GIB, GIIA, GV and GX $sPLA_2$, respectively. The orientation of all these $sPLA_2$s in the complex with hPDI is similar to the orientation of Atx. All of them bind hPDI with their IBS. Differently from the other $sPLA_2$ molecules, $AtnI_2$ and GIIA $sPLA_2$ are rotated in the complex by 30° in their IBS plane. Consistent with their RMSD values, $AtnI_2$ and GX $sPLA_2$ are offset from the Atx-interaction site in their complexes with hPDI, so that they cover only about half of the Atx's binding surface on PDI. Figure 20 shows the superposition of AtnL, $AtnI_2$, GIB, GIIA, GV and GX $sPLA_2$ on the Atx-hPDI model (Figure 20, panels A and B). Different position of $AtnI_2$ and GX $sPLA_2$ in the complex with hPDI comparing to that of Atx is clearly visible in Figure 20B.

Figure 20C shows the electrostatic and hydrophobic energy of $sPLA_2$–hPDI interactions, calculated by HADDOCK. The interaction of all $sPLA_2$s with hPDI is predominantly electrostatic. All tested $sPLA_2$s exhibit similar strength of electrostatic and hydrophobic interactions with PDI as Atx.

To validate our model, we experimentally tested the ability of AtnL, $AtnI_2$, GV and GX $sPLA_2$ to bind hPDI. From the model, we expected that AtnL and GV $sPLA_2$ will block the Atx–hPDI formation more effectively than $AtnI_2$ and GX $sPLA_2$. The first two namely interact with hPDI in the same manner than Atx while the latter two in a slightly different way. The results of the competition experiment confirmed our model-based prediction (Figure 20D), confirming the relevance of the model.

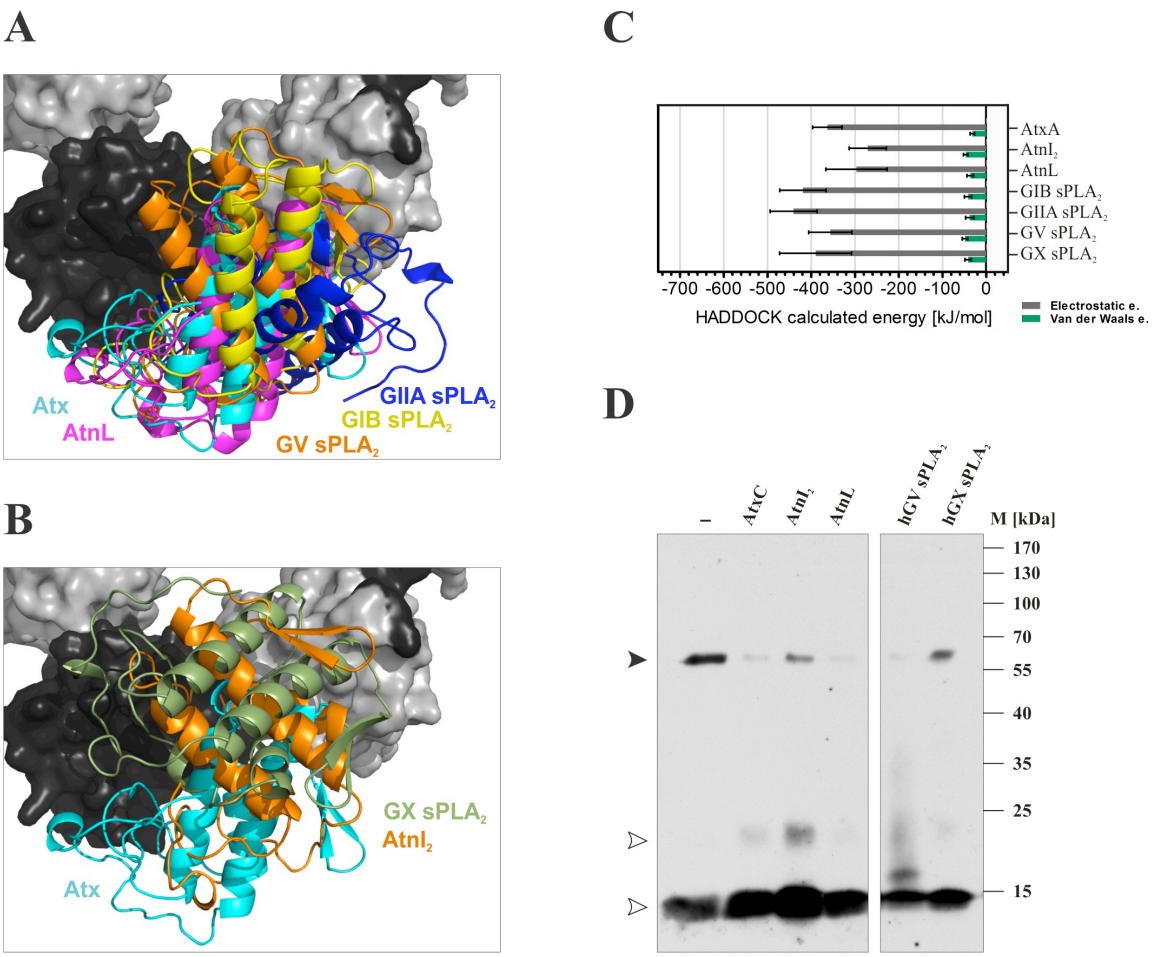

Figure 20: *3D models of complexes between sPLA$_2$s and hPDI.* By substitution of Atx in the model of Atx–hPDI complex with AtnL, AtnI$_2$, GIB, GIIA, GV or GX sPLA$_2$, and HADDOCK molecular docking, complexes of these sPLA$_2$s with hPDI were modelled. AtnL, GV, GIB and GIIA sPLA$_2$ interact with the same area on hPDI as Atx (A), while AtnI$_2$ and GX sPLA$_2$ interact with only part of this area (B). (C) Interactions of these sPLA$_2$s with hPDI are mostly electrostatic. The strength of their interactions is similar as in the case of Atx. (D) Heterologous competition of sulfo-SBED-AtxC binding to hPDI by AtnI$_2$, AtnL, GV and GX sPLA$_2$s confirms validity of proposed sPLA$_2$–hPDI 3D models. Human PDI was incubated with sulfo-SBED-AtxC in the dark in the presence of 26 to 100-fold molar excess of AtxC, AtnI$_2$, AtnL, hGV or hGX sPLA$_2$ over the sulfo-SBED-AtxC. The photo cross-linking reaction was triggered by irradiation at 312 nm. SDS-PAGE analysis under reducing conditions was followed by western blotting of the samples on the nitrocellulose membrane and biotin-specific detection. Black arrowhead indicates the biotinylated hPDI. White arrowheads indicate positions of biotinylated monomeric and dimeric AtxC.

4.2 The role of enzymatic activity in the neurotoxic processes of Atx

In order to assess the role of enzymatic activity in the neurotoxic processes of Atx, an enzymatically inactive variant of AtxA was produced. One way to obtain an enzymatically inactive variant of an enzyme is site-directed mutagenesis of its catalytic site. In the case of Atx, this means substitution of one of the catalytic site amino acids residues, His48 (H48) or Asp49 (D49). All attempts to produce correctly folded AtxA with a mutated H48 failed (Dolinar, 2013; Petan, personal communication), probably due to the essence of interactions of this residue with other residues during the folding of the

toxin. For these reasons we decided to use the option to mutate D49. Since the enzymatically inactive native structural homolog of Atx, AtnL, has the mutation of D49S, we decided to try to substitute Asp49 in AtxA with Ser and produce the mutant AtxA(D49S).

4.2.1 Preparation of the enzymatically inactive mutant AtxA(D49S)

The standard protocol for expressing sPLA$_2$s involves the expression of the protein with an N-terminal propeptide, which is subsequently cleaved by the addition of a protease (Pungerčar et al., 1999; Petan et al., 2005). This ensures the absence of Met from the N-terminal, which dramatically decrease the enzymatic activity of an sPLA$_2$ (Jemel et al., 2011), and is usually added to proteins expressed in *E. coli*. We faced, however, problems with controling proteolysis, the result of which was not only removal of the propeptide but also unwanted fragmentation of the sPLA$_2$ molecule. Therefore, we decided to produce AtxA(D49S) by direct expression without an N-terminal propeptide. During direct expression using the standard protocol, the N-terminal Met is usually cleaved off in about 2/3 of the expressed protein by the bacterial aminopeptidase. The remaining Met-variant of the recombinant protein is very difficult to remove by separation. We therefore employed methods of expression, refolding and purification of AtxA(D49S), which differed from the standard methods.

The propeptide sequence of the gene for AtxA was removed from the plasmid pJP4.1 and thus prepared for direct expression. Then the codon for Asp49 was changed into a codon for Ser by site-directed mutagenesis. The gene was sequenced to check the success of the mutagenesis and the plasmid was transformed into an *E. coli* expression strain. For the expression, we used an auto-induction method, rather than the standard IPTG-induction. This method of induction is slower than that where IPTG is used and allows bacteria to reach higher concentrations, consequently leading to higher yields of recombinant protein. In our case, the A_{600} at the end of expression was usually between 7 and 13, while that with the IPTG method was around 2.3–4.

sPLA$_2$s, expressed in bacteria, usually cannot fold correctly as they need to form disulphide bonds. The sPLA$_2$s are usually synthesized in the bacterial cytoplasm in a form of insoluble inclusion bodies. These allow easy isolation of the recombinant protein, usually already in quite pure form. The insoluble protein is then dissolved in a concentrated denaturant, the disulphides are reduced and the thiol groups S-sulfonated. The denatured, S-sulfonated protein is then allowed to refold in the presence of a reducing and an oxidizing agent in an appropriate ratio. We utilized a novel refolding approach, where the addition of a chaperone drives the refolding reaction to the formation of the correctly folded sPLA$_2$ (Kovačič et al., publication in preparation). In this way, we were able to substantially increase the yield of properly refolded sPLA$_2$s with simultaneous decrease in the time of refolding procedure. As well, the number of steps required for the purification of the protein lowered. In the case of recombinant production of AtxA(D49S), the best yield was achieved by a 1 : 10 dilution (5 ml into 50 ml) of the S-sulfonated mutant in 6 M Gdn.HCl into the refolding mixture followed by an overnight refolding at the room temperature. The highest purity of the properly folded AtxA(D49S) was achieved by two sequential RP-HPLC analyses. Experimental details are described in 3.2.7.3.

Figure 21 shows a chromatogram of the final purification of AtxA(D49S) on a C18 RP-HPLC column. The peak containing the mutant was well-resolved and had the same retention time as the native AtxA (indicated with an arrowhead in Figure 21). The collected sample was dried and characterized. The final amount of AtxA(D49S), as determined by measuring protein concentration (3.2.1.2.2), was around 150 µg, which

corresponds to 0.5–1.5 % of the initial denatured protein, added into the refolding reaction.

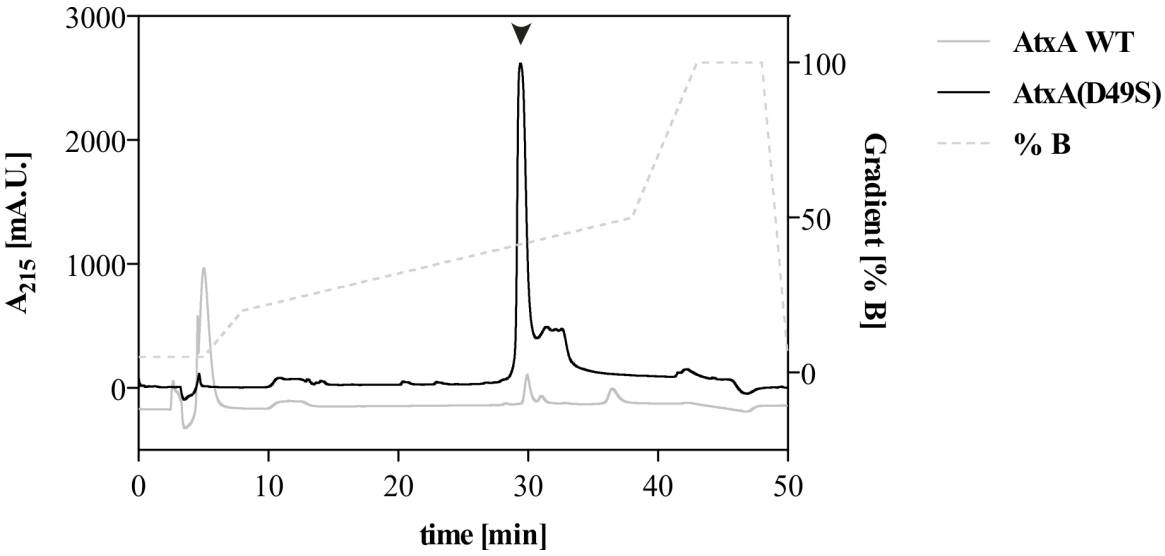

Figure 21: *Purification of AtxA(D49S by RP-HPLC.* The last purification step of the AtxA(D49S) mutant was on the analytical C18 RP-HPLC column, as described in 3.2.7.3.3. AtxA(D49S) (black line) eluted at the same retention time (indicated with the arrowhead) as the wild-type AtxA (AtxA WT, grey solid line), indicating the correct folding of the mutant.

4.2.2 Characterization of AtxA(D49S)

The purity of the AtxA(D49S) sample was checked by SDS-PAGE (Figure 22A) and MS (Figure 22B). As we demonstrated, the sample was more than 95% pure and suitable for further use.

According to the mass spectrum (Figure 22B), the molecular mass of our product (13747 Da) was identical to the theoretical molecular mass of AtxA(D49S), confirming the formation of all 7 disulphide bonds in the molecule. Taking this into account, it is practically imposible that AtxA(D49S) would be incorrectly folded. Importantly, also the variant of AtxA(D49S) with Met on the N-terminal was not detected by MS.

To further ascertain whether AtxA(D49S) was correctly folded or not, we performed a competitive inhibition assay of ^{125}I-AtxC binding to CaM in the presence or absence of an excess of AtxA(D49S). CaM is a target of Atx (Šribar et al., 2001) with a large surface area of interaction with Atx (Kovačič et al., 2010). The ability to bind to CaM can therefore additionaly affirm correct tertiary structure of the AtxA(D49S) that we prepared. We cross-linked ^{125}I-AtxC with CaM in the presence of a 100-fold, 10-fold or 1-fold molar excess of the native AtxC or AtxA(D49S) to check a difference in affinity between the native AtxC and the mutant for CaM. The results in Figure 22C show that AtxA(D49S) inhibited the binding of ^{125}I-AtxC and CaM, once again proving the correct folding of the mutant. As the native AtxC, also the 100-fold molar excess of the mutant over ^{125}I-AtxC completely blocked the AtxC-CaM complex formation. At the 10-fold molar excess, AtxC was a slightly more efficient competitor of ^{125}I-AtxC than the mutant.

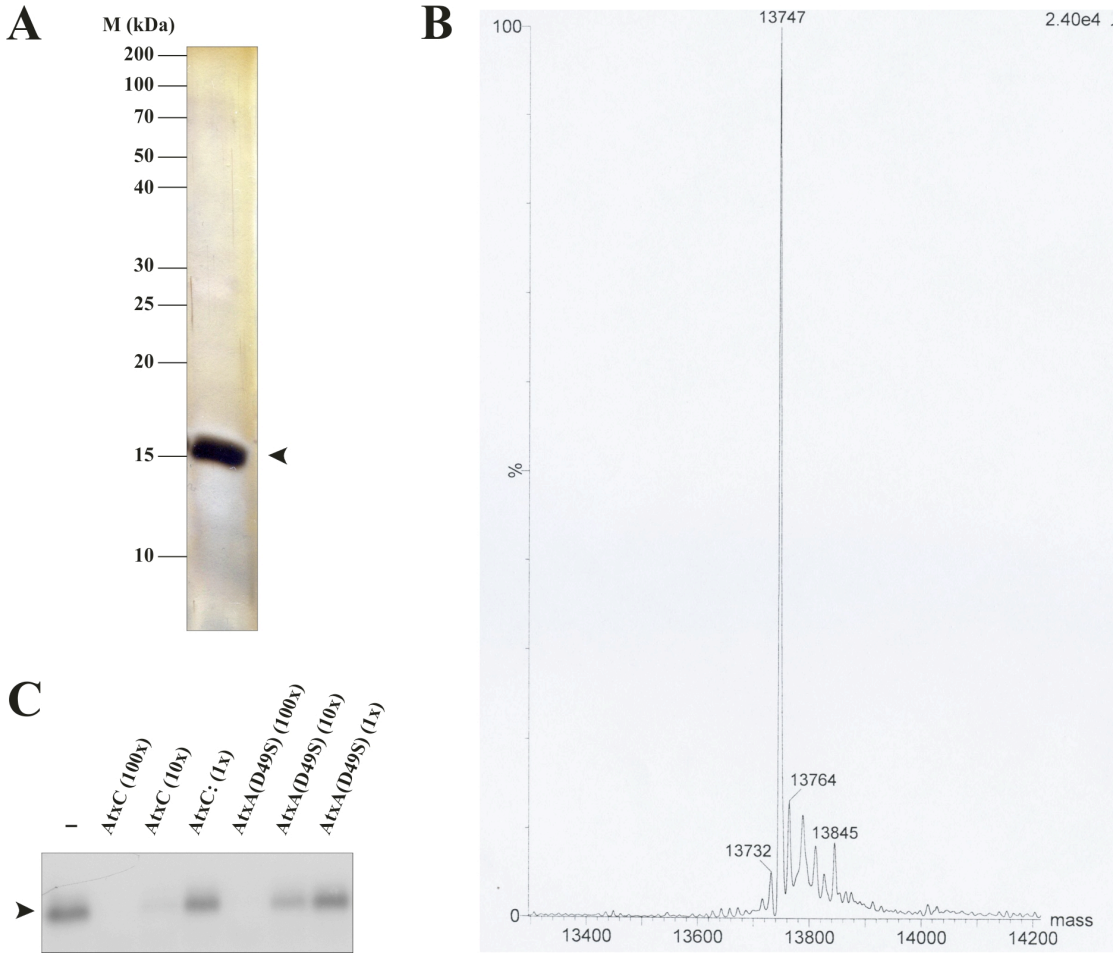

Figure 22: *AtxA(D49S) was pure and correctly folded.* The purity of the refolded mutant was assayed by SDS-PAGE, followed by silver staining (A) and by MS (B). (A) The arrowhead shows the position of AtxA(D49S). (B) The molecular mass of the product was 13747 Da, identical to the theoretical mass of AtxA(D49S). This indicates that all 14 Cys were connected to form 7 disulphide bonds. The recombinant product, containing Met on its N-terminus, was undetectable at 13895 Da. (C) CaM was cross-linked with ^{125}I-AtxC in the absence (–) or the presence of indicated excess amounts of native AtxC or AtxA(D49S). Samples were analyzed by SDS-PAGE and the gel autoradiographed. Results indicate that the mutant binds CaM with a similar affinity as AtxC, additionally indicating the correct folding of the mutant.

4.2.3 AtxA(D49S) retained no measurable PLA_2 activity.

The pure AtxA(D49S) mutant was examined for residual phospholipase A_2 activity as described in 3.2.6. The mutant was assayed at a 100-fold higher concentration (23 nM) than the native AtxC (0.23 nM). The 3rd order polynomial was fitted to the experimental data (Figure 23A) to calculate the linear coefficients, corresponding to the initial velocity of the enzymatic reaction. The initial velocity obtained in the case of AtxA(D49S) was similar to the one obtained in the blank runs, containing no $sPLA_2$ (Figure 23B). This indicates that the potential residual phospholipase activity of AtxA(D49S) was under the detection limit of our test. This qualified the mutant as a suitable tool to investigate the role of enzymatic activity in the neurotoxic action of Atx.

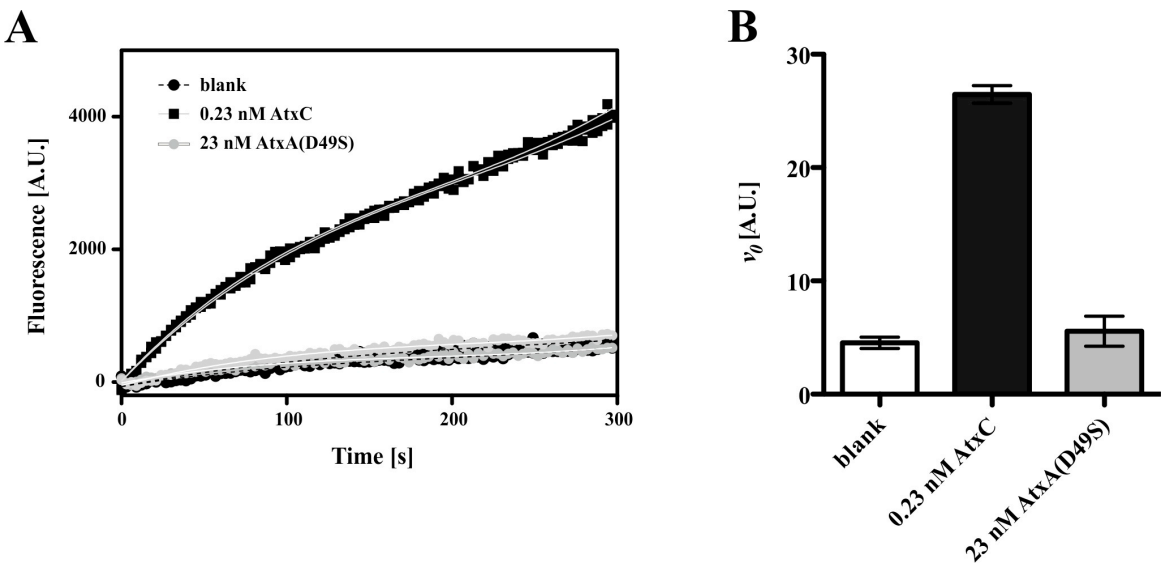

Figure 23: *Phospholipase activity of AtxA(D49S) is below the detection limit.* (A) The AtxA(D49S) mutant was probed for its enzymatic activity with the PyPG method (3.2.6) at a 100-fold higher concentration as the native AtxC. Experimental data were fitted with the 3rd order polynomial to calculate the initial velocity of the enzymatic reaction. (B) Initial enzyme reaction velocity of AtxA(D49S) (v_0) from two independent measurements was compared with the initial velocity of the native AtxC at a 100 times lower concentration or the blank without an $sPLA_2$. The mutant did not exhibit any measurable phospholipase activity. Error bars represent standard deviation.

4.2.4 Preparation of the fluorescent probe of AtxA(D49S)

In order to assay the effect of Atx's enzymatic activity on the localization of the toxin in neuronal cells, we prepared a fluorescently labelled probe of enzymatically inactive mutant AtxA(D49S). We labelled the mutant with an amine-reactive ^{546}Alexa dye, as described in 3.2.7.4. After the conjugation reaction, the fluorescent derivative was purified by RP-HPLC using a C4 column. The sample separated in 3 distinct peaks (Figure 24). The fractions, designated from Alexa-DS2 to Alexa-DS8, were collected, dried and characterized by MS and SDS-PAGE, followed by detection using a fluorescence gel scanner and Coomassie staining.

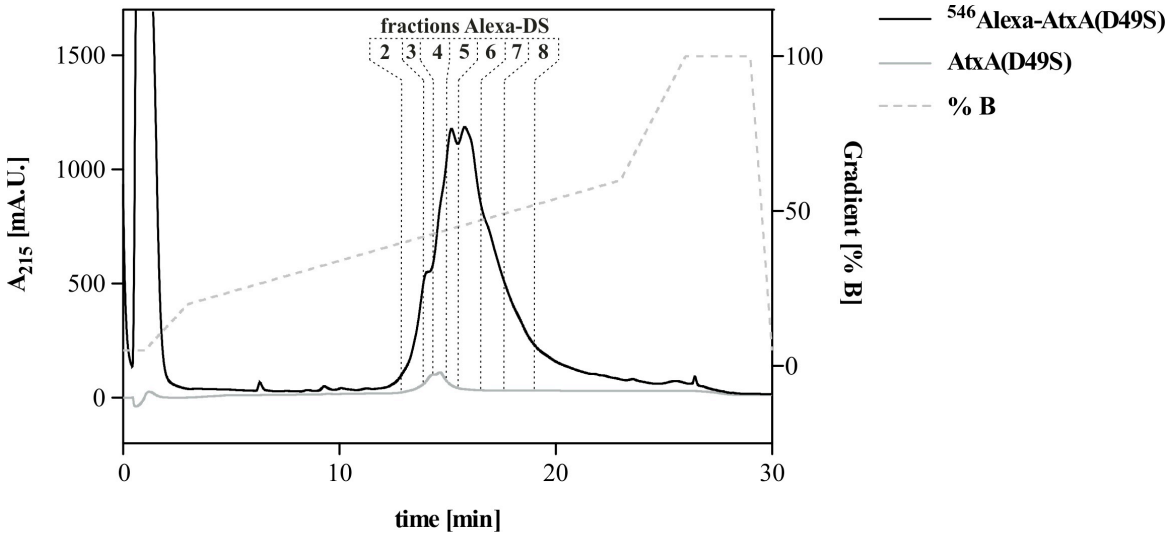

Figure 24: *RP-HPLC purification of ^{546}Alexa-AtxA(D49S).* After the conjugation reaction, ^{546}Alexa-AtxA(D49S) was purified on a C4 RP-HPLC column, as described in 3.2.7.4. Collected fractions of AtxA(D49S) (black line) Alexa-DS2 – Alexa-DS8 are indicated. As a standard, the non-labelled AtxA(D49S) was also analyzed (grey solid line).

MS revealed that the fraction Alexa-DS5 from the RP-HPLC purification contained the ^{546}Alexa-AtxA(D49S) monoderivative (Figure 25A). The experimental molecular mass of the labelled toxin was 7 Da higher than it should be theoretically (13747 Da + 942 Da for the Alexa dye = 14689 Da). Another peak was present in the sample, with additional mass shift of +16 Da (total shift of +23 Da compared to the theoretical mass) (Figure 25A). This peak probably resulted from the oxidation of one of the two Met at the N-terminal part of AtxA. Fraction Alexa-DS3 contained unlabelled toxin, fraction Alexa-DS4 a mixture of the unlabelled toxin and the monoderivative, whereas fraction Alexa-DS6 contained also the doubly labelled toxin.

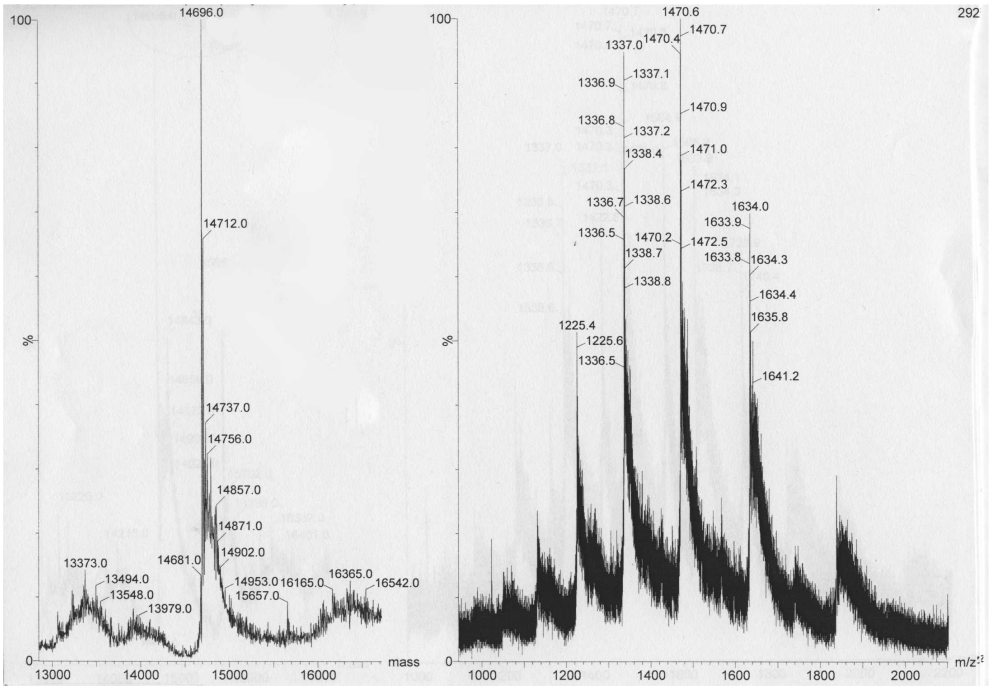

Figure 25: *Mass spectrum of ^{546}Alexa-AtxA(D49S).* After labelling AtxA(D49S) with ^{546}Alexa, the reaction mixture was purified by RP-HPLC and fractions analyzed by MS. The MS spectra revealed two main products in the fraction Alexa-DS5. The main one corresponded to the ^{546}Alexa-AtxA(D49S) monoderivative, the molecular mass of which was 7 Da higher than the theoretical (14689 Da). The mass of the minor product was 14712 Da and probably represented the form with one of the two Met, present in ^{546}Alexa-AtxA(D49S), oxidized.

Visualization of the labelled fractions on the gel fluorescence scanner (Figure 26, left panel) revealed that the RP-HPLC fractions (also the fraction Alexa-DS5) still contained some free Alexa dye. However, since after 120 min of incubation of PC12 cells in the presence of 500 nM free ^{546}Alexa dye no cellular staining with ^{546}Alexa was observed (Dolinar, 2013), we assumed that the presence of a small amount of ^{546}Alexa in our sample should not affect our cell studies. The dimer and trimer of ^{546}Alexa-AtxA(D49S) were also observed on the SDS-PAGE gel, indicating that the structure of the toxin was not altered by the labelling in a way to prevent multimerisation. Staining of the same gel with Coomassie blue did not reveal the presence of any other proteins in the sample than ^{546}Alexa-AtxA(D49S) (Figure 26, right panel).

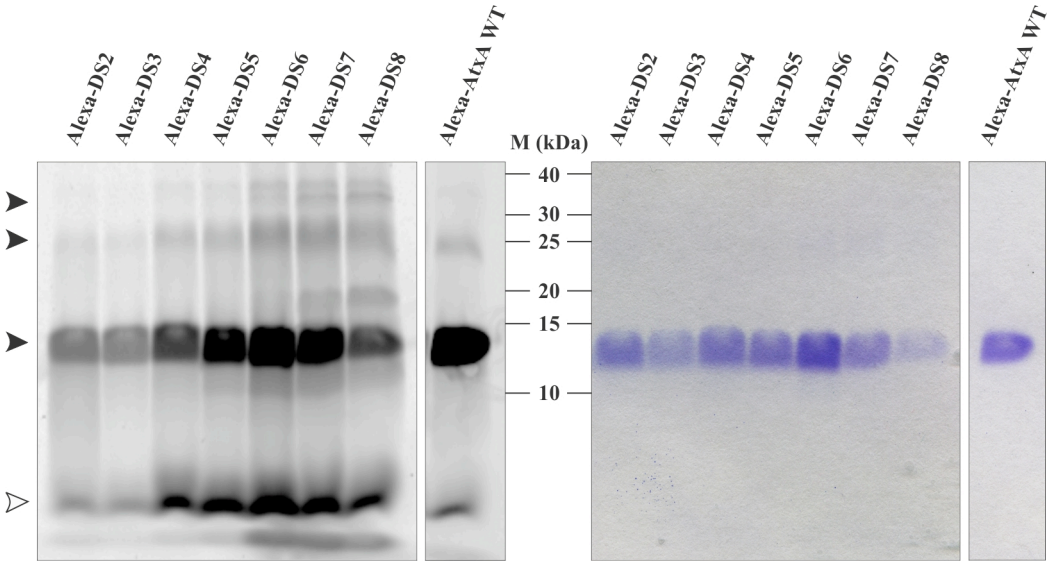

Figure 26: *Analysis of ^{546}Alexa-AtxA(D49S) fractions from the RP-HPLC.* After labelling AtxA(D49S) with ^{546}Alexa, the reaction mixture was purified by RP-HPLC and the fractions analyzed by SDS-PAGE. In the right-most lane on the gel, Alexa-labelled native AtxA was analyzed. The gel was visualized using fluorescence scanner (left picture) and Coomassie blue staining (right picture). As evident from the left picture, fraction Alexa-DS5, which contained the ^{546}Alexa-AtxA(D49S) monoderivative (the lowest black arrowhead), still contained some free ^{546}Alexa dye (white arrowhead). Also some dimer and trimer of ^{546}Alexa-AtxA(D49S) are visible (upper two black arrowheads). Coomassie blue staining (right picture) did not reveal the presence of other proteins than ^{546}Alexa-AtxA(D49S).

The Alexa-labelled AtxA(D49S) mutant was assayed for its ability to bind CaM. The labelling was performed in the presence of 10- or 100-fold molar excess of the respective $sPLA_2$, to check also a change in the affinity for CaM of respective Alexa-derivative. As revealed in Figure 27, all Alexa-derivatives of AtxA(D49S) (RP-HPLC fractions Alexa-DS3 to 5) efficiently prevented labelling of CaM by ^{125}I-AtxC at 100-fold molar excess over the ^{125}I-AtxC. At a 10-fold molar excess of respective competitor over ^{125}I-AtxC, however, all of the AtxA(D49S) Alexa-derivatives inhibited ^{125}I-AtxC–CaM complex formation with a lower potency than the native AtxC.

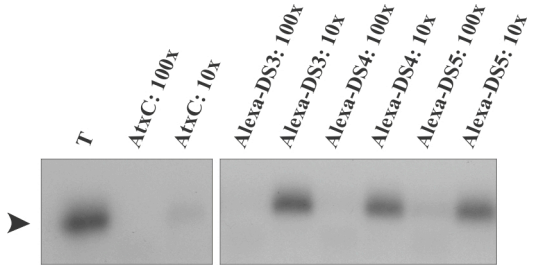

Figure 27: *The ability of ^{546}Alexa-AtxA(D49S) to bind to CaM.* CaM was incubated with ^{125}I-AtxC in the absence (T) or in the presence of 10- and 100-fold molar excess of AtxC, and the RP-HPLC fractions of ^{546}Alexa-labelled AtxA(D49S): Alexa-DS3, Alexa-DS4 and Alexa-DS5. The proteins were covalently cross-linked by the addition of cross-linker DSS and analyzed by SDS-PAGE followed by autoradiography of the gel. All Alexa-derivatives of AtxA(D49S) (fractions Alexa-DS3 to 5) were able to inhibit the binding of ^{125}I-AtxC to CaM but with lower potency than the native AtxC.

4.2.5 Immunofluorescence studies

It has been demonstrated several times that Atx enters neuronal cells (Jenko Pražnikar et al., 2008; Logonder et al., 2009; Kovačič, 2009b). Upon entry into the cell, also a substantial co-localization with the intracellular proteins CcO, PDI and 14-33p has been demonstrated (Dolinar, 2013).

In order to check what role Atx's phospholipolytic activity plays in these processes, we incubated ND and NGFD PC12 cells in the presence of ^{546}Alexa-AtxA(D49S), which was demonstrated to have no enzymatic activity (4.2.3), and in parallel with ^{546}Alexa-AtxA for different periods of time. After fixation, cells were immunocytochemically stained for Syt1, CcO, PDI or 14-3-3p and inspected under confocal microscope as described in 3.2.8.2.

4.2.5.1 The enzymatic activity of AtxA is not required for the entry of AtxA into PC12 cells but it facilitates the process.

The red signal in Figure 28 shows the entry and localization of the fluorescently, ^{546}Alexa-labelled AtxA or its enzymatically inactive mutant AtxA(D49S) into the PC12 cells.

In ND PC12 cells (Figure 28, panels A and B), the signal of both molecules was visible within cells already after 1 min of incubation. It appeared in the form of small circular dots, localizing predominantly near the plasma membrane. In both cases, the signal was punctate, indicating clustering at specific sites or vesicular localization. Already after 1 min, the punctate signal of both, AtxA and the AtxA(D49S), was also found inside the cytoplasm of several cells, not just at the plasma membrane. This indicated that AtxA does not need to be enzymatically active to enter PC12 cells. With further incubation, the number of red dots, as well as their intensity and size, were increasing. The quantity and intensity of the signal of the native toxin, however, was increasing more rapidly than that of the enzymatically inactive mutant. Namely, in ND PC12 cells, the signal for the native AtxA became more pronounced already after 5 min of the incubation, but the signal for AtxA(D49S) only after 15 min, indicating the different abilities of both variants of AtxA to localize in the vesicular structures. Also, the signal for the enzymatically inactive mutant was less intense and the circular structures appeared smaller after 15 min of incubation when compared to the native AtxA. In the case of the native toxin, the larger red dots became visible after already 15 min of incubation. In the case of the mutant AtxA, they appeared small also after 30 min of incubation and a higher number of the larger dots appeared only after 60 min of the incubation. Even then, they were not so abundant as the small dots, and as in the case of the native toxin.

In NGFD PC12 cells (Figure 28, panels C and D) the signal for both fluorescent proteins appeared not just in the soma, but also in or on the neurites. In the case of both Alexa probes the signal appeared in the form of discrete circular dots. Signals were visible already after 1 min of the incubation. The difference in quantity and intensity of the fluorescent signal between the enzymatically active and inactive variants of AtxA was less pronounced in NGFD PC12 cells than in the ND PC12 cells. In the case of both molecules, signals were becoming stronger with the time of incubation. The signal for the native AtxA became more apparent after 5 min of incubation, and the signal for AtxA(D49S) after 15 min. The larger red dots in the case of both probes appeared more frequently in the soma of the cells than in the neurites. After 30 min of incubation, the difference in the intensity and distribution of signals for both probes was less pronounced in NGFD than in ND PC12 cells. Therefore, the enzymatic activity seems to be less important for internalization of AtxA into NGFD PC12 cells than to ND PC12 cells.

Besides the intensity and quantity of the signal, we observed no other difference in the signals produced by the fluorescently-labelled native or the mutant AtxA. They appeared localized at same sites in the cells. Red fluorescence signal has never been detected inside the nuclei of the cells.

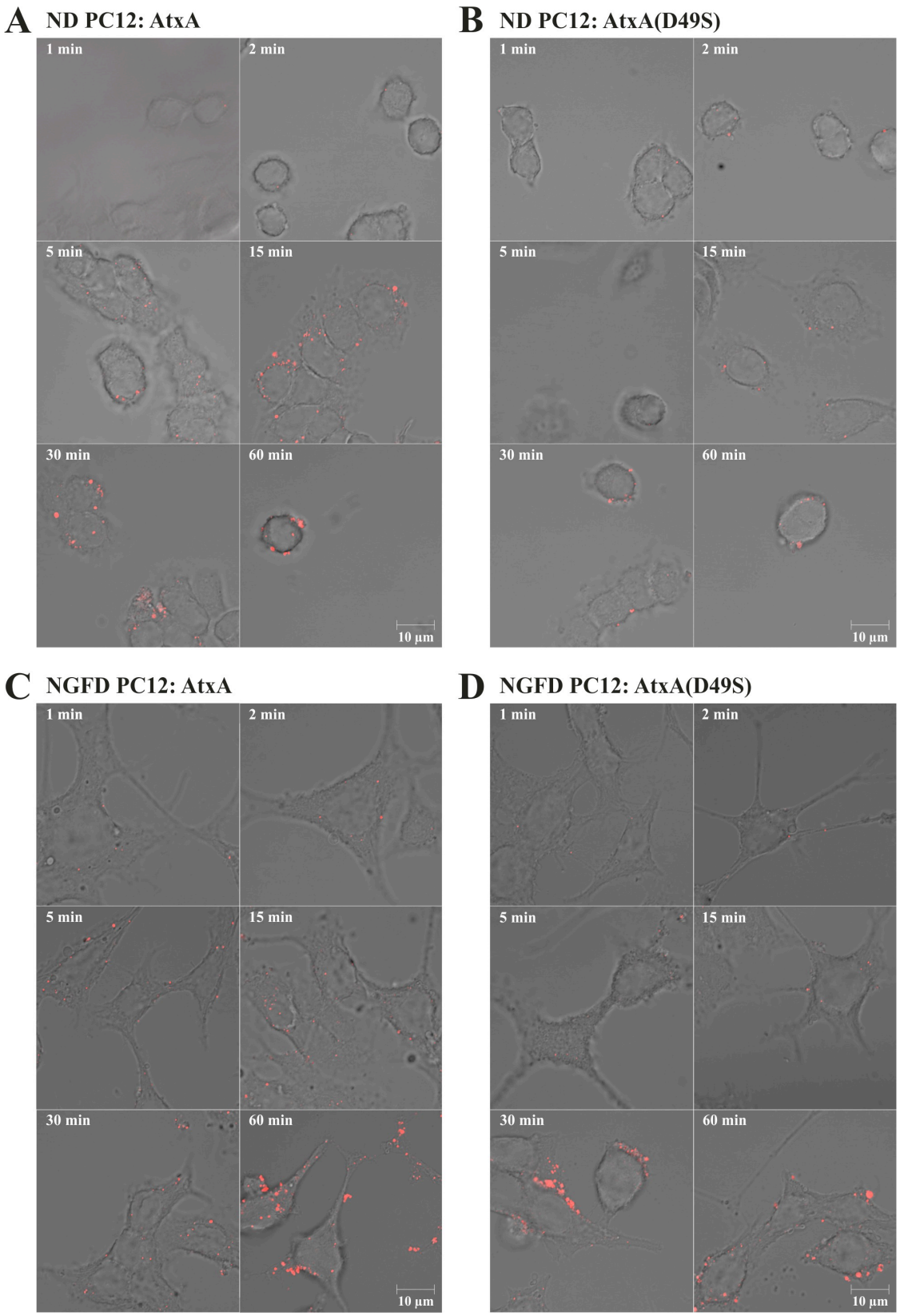

Figure 28: *Internalization and localization of ^{546}Alexa-AtxA and ^{546}Alexa-AtxA(D49S) in PC12 cells.* ND and NGFD PC12 cells were incubated in the presence of 100 nM ^{546}Alexa-AtxA or ^{546}Alexa-AtxA(D49S), the enzymatically inactive mutant. Cells were washed and fixed and the cover glasses prepared as described in 3.2.8.2.1. The images show the transmitted light and the red signal of both variants of ^{546}Alexa-Atx. The images were obtained with the Carl Zeiss LSM 710 confocal microscope at 63x magnification and displayed with the ZEN software. Scale bars represent 10 µm. For experimental details, refer to the section 3.2.8.2.2.

4.2.5.1 AtxA or its enzymatically inactive mutant significantly co-localize with Syt1, CcO, PDI and 14-3-3p in PC12 cells.

The immunocytochemical labelling of proteins was successful in all cases. After visual inspection of the slides, Z-stacks were obtained and threshold values for the green and red channel set above the signal from the control experiment performed without the primary antibodies or from the control experiment performed without the ^{546}Alexa-labelled probes, respectively. The images were displayed with the use of the "co-localization" tab in the ZEN software.

Figure 29 shows the co-localization of the red fluorescence signal of ^{546}Alexa-AtxA (Figure 29, left panels) and ^{546}Alexa-AtxA(D49S) (Figure 29, right panels) and the green fluorescence signal of the ^{488}Alexa-secondary antibodies used to indirectly label Syt1 (Figure 29, panels A and B), CcO (Figure 29, panels C and D), PDI (Figure 29, panels E and F) and 14-3-3p (Figure 29, panels G and H). The sites of co-localization of red and green fluorescence signal were displayed as white areas and are indicated with arrows. To avoid redundancy, only incubation times of 1, 15, 30 and 60 min are shown in Figure 29.

AtxA and its enzymatically inactive mutant co-localized with all tested proteins already after 1 min of incubation. The extent of co-localization between both variants of AtxA was, however, different and in line with our observations of the different abilities of both variants to enter the PC12 cells (Figure 28).

The native AtxA and AtxA(D49S) exhibit significantly different ability to co-localize with Syt1 in ND PC12 cells (Figure 29A), but less so in NGFD PC12 cells (Figure 29B). Once detected inside the cell, however, we observed no difference in the ability of the two toxin variants to co-localize with Syt1. After 1 min of incubation, the co-localization appeared to be predominantly located at the periphery (inside cells, but not distributed throughtout the cytoplasm) of the ND and NGFD PC12 cells. After 15 min, the co-localization of the native AtxA and Syt1 was distributed more evenly throughout the cytoplasm of the ND and NGFD PC12 cells. After 30 min the same was true also for AtxA(D49S) in NGFD PC12 cells. In ND PC12 cells, however, the majority of the co-localization between AtxA(D49S) and Syt1 remained at the periphery of the cells, even after 60 min of incubation. In NGFD PC12 cells the co-localization of both AtxA-probes and Syt1 was more pronounced in the soma of the cells but was visible also in neurites.

The same distribution of the co-localization was observed for AtxA or AtxA(D49S) and CcO (Figure 29, panels C and D), with the exception that, unlike in ND cells, in NGFD PC12 cells the signal was already seen throughout the cytoplasm after 1 min of incubation of the cells with both AtxA probes. Similarly, as with Syt1 in ND cells, the co-localization of CcO and AtxA(D49S) was much less pronounced than the co-localization of CcO and the native AtxA. The co-localizations with CcO in NGFD PC12 cells were similar for both AtxA probes as in the case of Syt1. The co-localization was mostly seen in the soma of NGFD PC12 cells and rarely in the neurites.

In the case of PDI (Figure 29, panels E and F), there was less difference between the co-localization of both AtxA-probes in ND PC12 cells than in the case of Syt1 or CcO. The co-localization seems to persist at the periphery of the ND PC12 cells in the case of AtxA and AtxA(D49S). In NGFD PC12 cells, the co-localization between PDI and AtxA or AtxA(D49S) was distributed in the cytoplasm after 15 min of incubation. Besides in the soma of NGFD cells, the co-localization was clearly visible also in the neurites.

14-3-3p signal (Figure 29, panels G and H) co-localized with signal for either AtxA or AtxA(D49S) similarly in both, ND and NGFD, PC12 cells. In ND cells, the co-localization remained peripheral in the case of both AtxA-probes even after 60 min. In NGFD PC12 cells, the co-localization with 14-3-3p was observed in the cytoplasm for AtxA or AtxA(D49S) after 15 min. Almost no 14-3-3p immuno-staining was observed in

neurites, therefore also no co-localization with the two AtxA probes.

A **ND PC12: Syt1: AtxA**

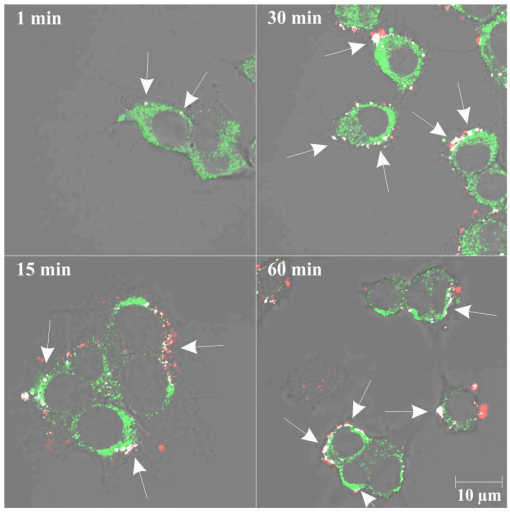

ND PC12: Syt1: AtxA(D49S)

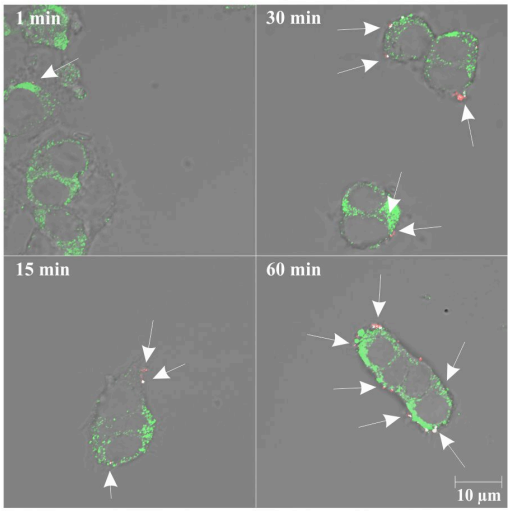

B **NGFD PC12: Syt1: AtxA**

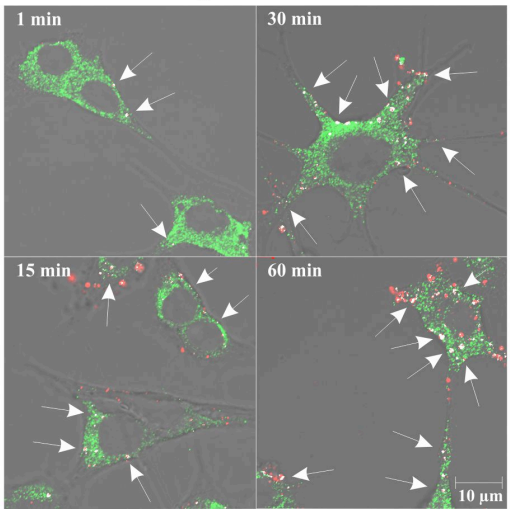

NGFD PC12: Syt1: AtxA(D49S)

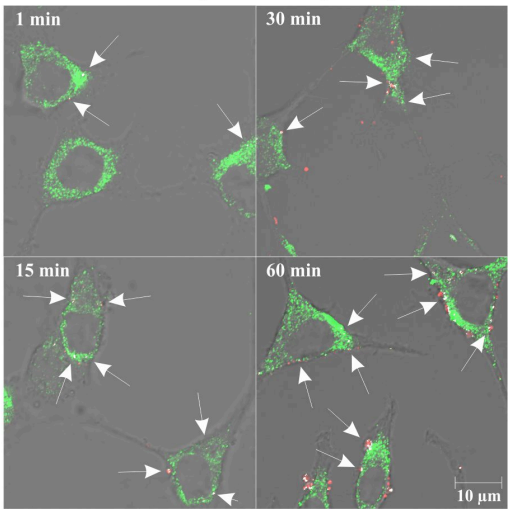

C **ND PC12: CcO: AtxA**

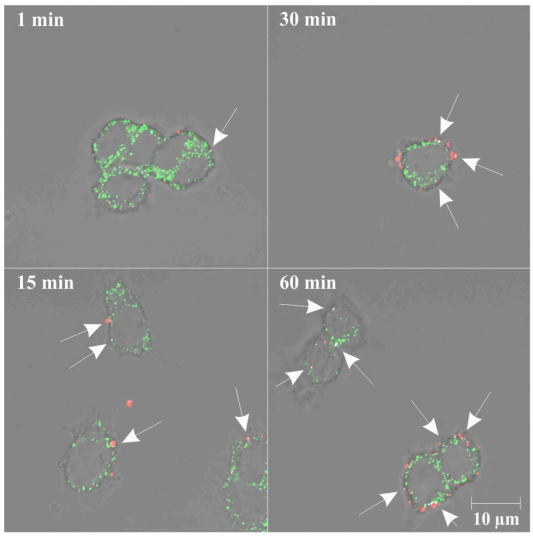

ND PC12: CcO: AtxA(D49S)

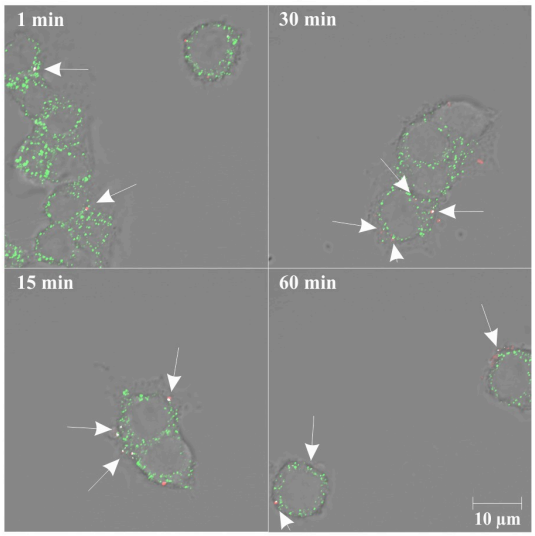

D **NGFD PC12: CcO: AtxA**

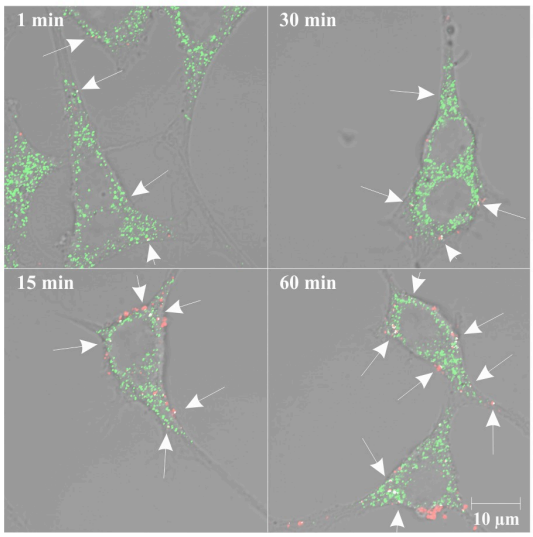

NGFD PC12: CcO: AtxA(D49S)

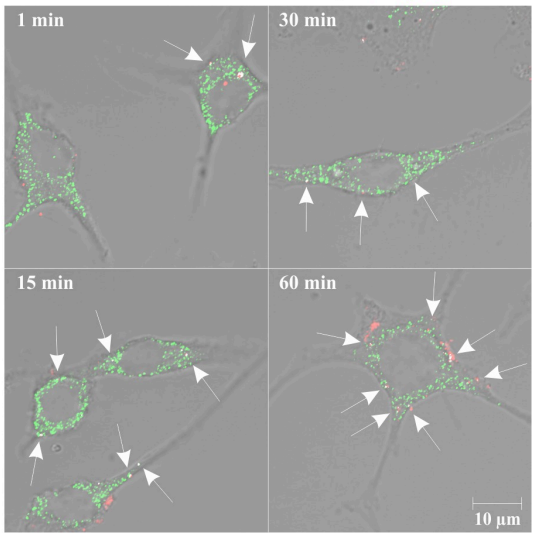

E **ND PC12: PDI: AtxA**

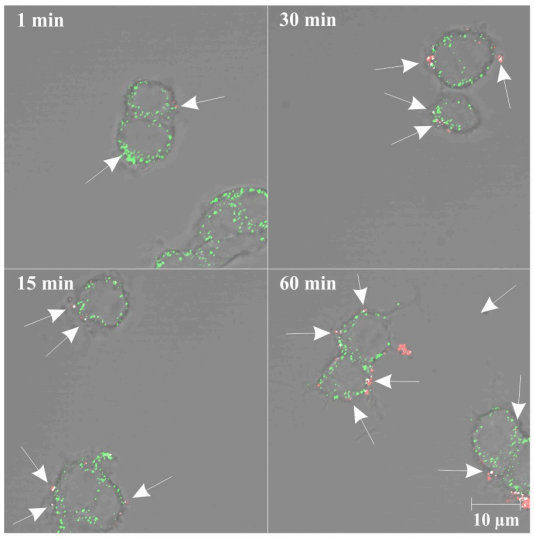

ND PC12: PDI: AtxA(D49S)

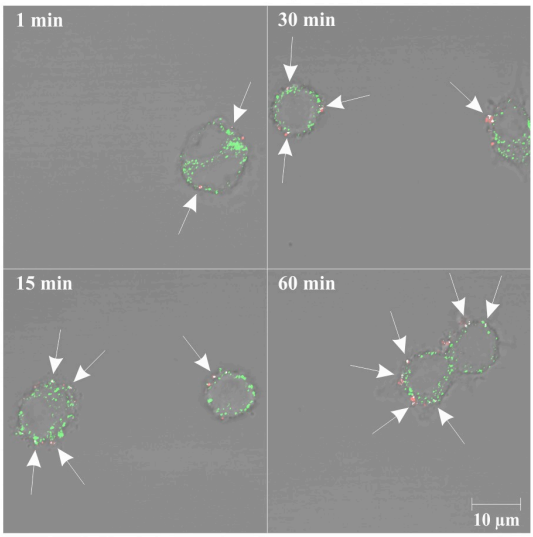

F **NGFD PC12: PDI: AtxA**

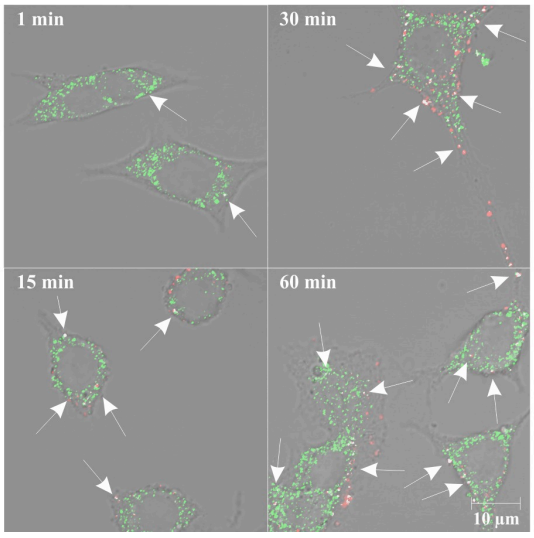

NGFD PC12: PDI: AtxA(D49S)

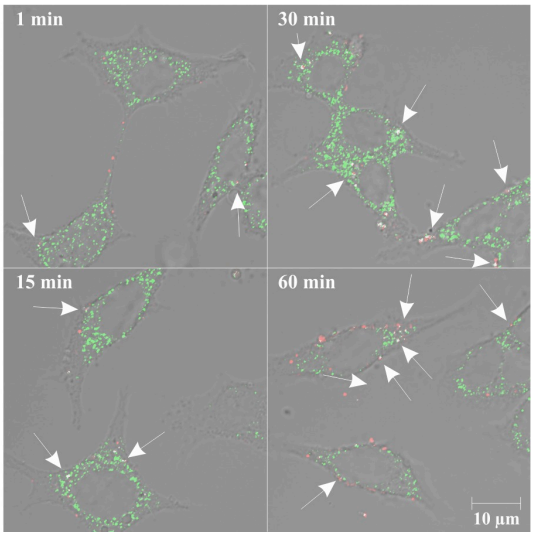

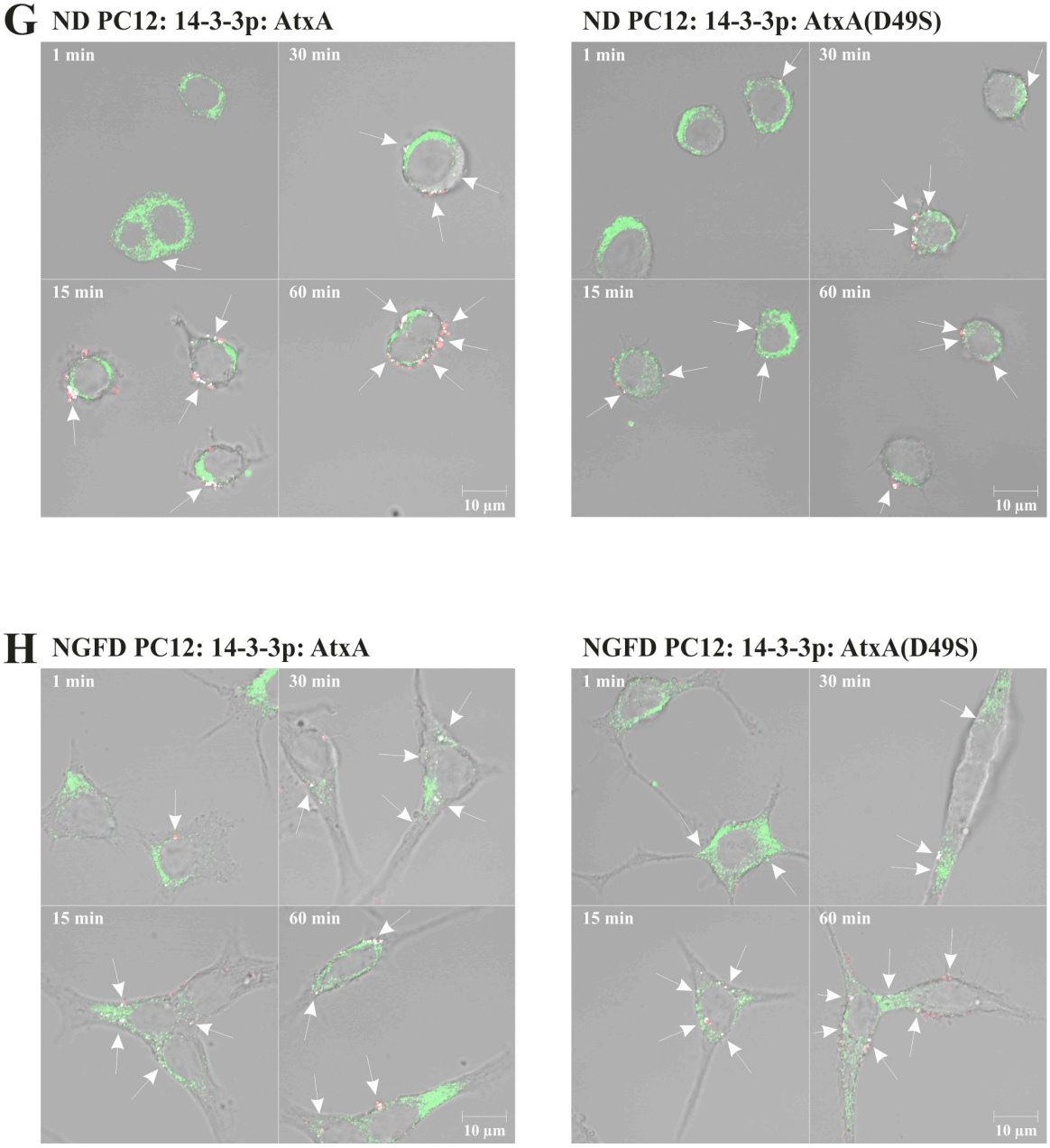

Figure 29: *Co-localization of ^{546}Alexa-AtxA and ^{546}Alexa-AtxA(D49S) with Syt1, CcO, PDI and 14-3-3p in PC12 cells.* ND and NGFD PC12 cells were incubated in the presence of 100 nM ^{546}Alexa-AtxA or ^{546}Alexa-AtxA(D49S) for the indicated time periods. After fixation, the cells were immunologically stained for Syt1 (A, B), CcO subunit 2 (C, D), PDI (E, F) or 14-3-3p (G, H). The cover glasses were mounted and slides analyzed with fluorescence microscopy, using a Carl Zeiss LSM 710 confocal microscope. Images were obtained at 63x magnification. The red signal represents ^{546}Alexa-AtxA or its enzymatically inactive variant. The green signal represents immunologically detected cellular proteins, Syt1 (A, B), CcO subunit 2 (C, D), PDI (E, F) or 14-3-3p, respectively. Sites of co-localization of the red and green signal are displayed in white and indicated by arrows. Scale bars represent 10 µm. Experimental details can be found in section 3.2.8.2.

4.2.5.2 AtxA(D49S) co-localizes with Syt1, CcO, PDI and 14-3-3p in PC12 cells to a lesser extent than the enzymatically active native AtxA

Next, we processed the confocal microscopy images acquired at co-localization studies with ImageJ with the plugin JACoP, which calculates the extent of co-localization as

described in 3.2.8.2.2. This allowed us to quantitatively assess, how the extent of co-localization changes with the time of incubation. 2 to 3 Z-stacks of confocal images (each Z-stack containing several cells) from each slide were inspected visually. If necessary, parts of images were cropped to ensure that only the images of most relevant cells were processed further. As relevant we designated the cells or cell groups in which:

1. The extent of the red signal was representative for the slide. Both variants of ^{546}Alexa-AtxA exhibited an ability to associate with some PC12 cells to a much greater extent than the rest. These cells otherwise appeared normal, but they could have been damaged prior to treatment with Atx, so we excluded them from the analyses.

2. The red signal was distributed evenly around a cell or a group of cells. This indicated that a cell or a cell group, during the treatment with an ^{546}Alexa probe, was not a part of a larger cluster of cells. The multiple washing steps in the processing of the slides after the treatment with Atx could wash away such clusters. This might have exposed individual cells, still sticking to the cover glass, which were not in contact with an ^{546}Alexa-probe. The analysis of such cells would give false negative results.

The Z-stacks were then processed with ImageJ with the plugin JACoP to calculate the Manders' coefficients, which define the extent of co-localization. In all Z-stacks, all confocal planes, except those closest the cover glass or those including artefacts, were used. We calculated Manders' coefficients for the green channel, *i.e.* the ratio of the summed intensities of pixels from the green channel (^{488}Alexa-tagged secondary antibodies), for which the intensity in the red channel (^{546}Alexa-AtxA or ^{546}Alexa-AtxA(D49S)) is above zero, to the total intensity in the green channel. We assumed that the quantity of the antibody-labelled protein is the same in every cell. The results are shown in Figure 30.

Figure 30A shows Manders' coefficients for Syt1 plotted over the time of incubation with ^{546}Alexa-AtxA or ^{546}Alexa-AtxA(D49S). The extent of co-localization of the enzymatically inactive mutant with Syt1 is significantly lower than that of the native AtxA, as was apparent already from visual inspection of the confocal microscope images. This difference is much more apparent in ND than NGFD PC12 cells, suggesting different modes of cellular trafficking of AtxA molecules in the two types of cells. The extent of co-localization of AtxA(D49S) and Syt1 is much lower in ND cells than NGFD PC12 cells. In the case of the native AtxA, however, there is no significant difference between co-localizations in ND and NGFD PC12 cells. Interestingly the co-localization curves for AtxA and AtxA(D49S) with Syt1 also have different trends, similarly in ND and NGFD PC12 cells. The change of the extent of co-localization between Syt1 and the native AtxA is logarithmic, rising quickly at short incubation times and settling at the longer times, whereas the change in the case of AtxA(D49S) rises more constantly with the incubation time.

In the case of co-localization with CcO (Figure 30B), once again a significant difference was observed between the enzymatically active and inactive variants of AtxA in ND PC12 cells. Such difference almost disappeared in NGFD PC12 cells. After 60 min of incubation with NGFD PC12 cells, AtxA(D49S) exhibited even higher extent of co-localization with CcO than AtxA. Unlike in the case of co-localization with Syt1, in the case of CcO the trends of the co-localization curves for the same probe varied between ND and NGFD PC12 cells. For ^{546}Alexa-AtxA and ^{546}Alexa-AtxA(D49S), in ND cells, the co-localization changes with time in a logarithmic manner while in the NGFD cells in more linear fashion. The significant deviation from a linear curve at 30 min in the case of NGFD cells is likely due to a smaller number of cells imaged, nevertheless, as such drop after 30 min of incubation was already observed before (Dolinar, 2013), there may be also some other explanation.

Analysing the co-localization with PDI (Figure 30C), we also noticed the difference between ^{546}Alexa-AtxA and ^{546}Alexa-AtxA(D49S). The enzymatically inactive mutant of AtxA exhibited a lower extent of co-localization with PDI than AtxA. Again, this result was more pronounced in ND PC12 cells, but to a lesser extent than in the case of Syt1 and CcO. For both ^{546}Alexa probes, the extent of co-localization in ND cells was larger than in NGFD PC12 cells. The extent of co-localization in the case of both AtxA variants and in both types of PC12 cells reached its maximum after 30 min of incubation. After that it started even to decline in all cases but in ND cells with the ^{546}Alexa-AtxA(D49S), where it was still increasing, but only slightly.

Trends of the extent of co-localization between ^{546}Alexa-AtxA or ^{546}Alexa-AtxA(D49S) and 14-3-3p were more linear than with the other proteins tested (Figure 30D). As in other cases, the extent of co-localization with the enzymatically inactive mutant of AtxA was lower than with AtxA. The spike at 15 min in the case of native AtxA in ND cells is probably due to a stronger staining of 14-3-3p on this particular slide, which obviously influenced quantification of the co-localization and should be regarded as an outlier.

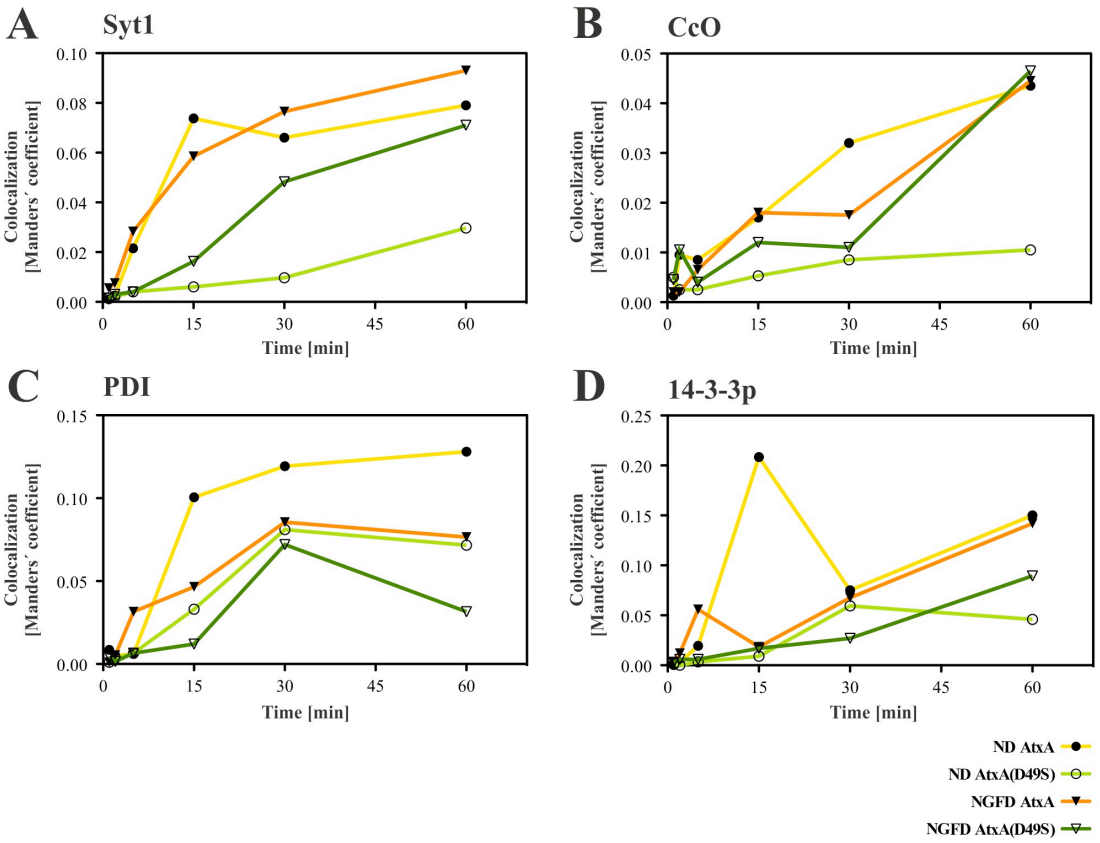

Figure 30: *Extent of co-localization of ^{546}Alexa-AtxA or ^{546}Alexa-AtxA(D49S) with intracellular proteins over time.* The Z-stacks of confocal microscopy images of co-localization of either ^{546}Alexa-AtxA or ^{546}Alexa-AtxA(D49S) with Syt1 (A), CcO (B), PDI (C) or 14-3-3p (D) were processed with ImageJ with the co-localization plugin JaCOP. The extent of co-localization was expressed in terms of Manders' coefficient and plotted as a function of incubation time of PC12 cells with ^{546}Alexa-labelled protein. In all cases, except for CcO in NGFD PC12 cells, the enzymatically inactive mutant of AtxA co-localized with the assayed intracellular proteins to a lesser extent than AtxA.

5 Discussion

The molecular mechanism of β-neurotoxicity is not entirely known. Studies show that the process involves the interaction of β-ntxs with specific receptors on the presynaptic membrane and also inside the target cell, as well as their hydrolytic activity of the cellular phospholipids.

As part of the neurotoxic effect of β-ntxs, SV endocytosis is blocked and the SVs are reduced in number. This effect is the principal reason of synaptic transmission blockade in the case of GIA $sPLA_2$ β-ntxs, β-bungarotoxin and notexin (Šribar et al., 2014). In the case of Atx, the number of SVs in the mouse hemidiaphragm was reduced, compared to the control, by only 13.6% (Logonder et al., 2008b). Nevertheles, SVs obviously represent a target for both groups of β-ntxs. The endocytosis of SVs may also serve to internalize β-ntxs into their target cells (Pungerčar & Križaj, 2007). If this is the case, β-ntxs would need to specifically bind to a SV-specific receptor, either proteinaceous or carbohydrate/lipid in nature, to anchor in the endocyting SV. To investigate whether SVs harbour protein receptors that bind Atx, we have isolated these organelles from the porcine cerebral cortex and the NGFD PC12 cells. We were unable to isolate SVs from ND PC12 cells, probably because the number of SVs in these cells is too low (Green & Tischler, 1976). By cross-linking with sulfo-SBED-AtxC we have shown the existence of several specific Atx-binding proteins in SVs from both sources (Figures 9 and 10). By cross-linking detergent extracts of SVs with ^{125}I-AtxC and DSS, we only observed one strong specific band (Figure 9D), at about 25 kDa, which would correspond to a protein of 12 kDa in the complex with the 13.7 kDa AtxC. Despite the difference in molecular masses, this band could be CaM (molecular mass of CaM is 17 kDa). The covalent complex of Atx with CaM migrates at around 30 kDa on an SDS gel, above the Atx dimer, which is between 26 and 28 kDa. We see that this band in SV is above the 28 kDa Atx dimer, even though, according to the molecular mass markers, it is at about 25 kDa. The lower amount of detected proteins with cross-linking with the ^{125}I-AtxC and DSS versus sulfo-SBED-AtxC can be explained by the fact that DSS covalently reacts with only primary amines, whereas the photo-reactive group of sulfo-SBED is less specific and links also other nucleophiles (Kovačič et al., 2007). The other reason for fewer specific binding partners detected with the radioactive Atx probe is that, in this assay, the concentration of Atx was 50-fold lower than in the sulfo-SBED-linking assay, which results in fewer collisions between Atx and its binding proteins, decreasing the quantity of successfull cross-linking events.

In the samples of Atx-binding proteins isolated from porcine brain SVs three strong bands of 20 kDa, 28 kDa and 34 kDa were detected (Figure 10). However, none of these molecular masses match the masses of known Atx-binding proteins, so these proteins might represent as yet unknown receptors for Atx. The protein, cross-linked with ^{125}I-AtxC and DSS, seen in Figure 9D, whether CaM or not, was not detected in the samples of isolated SV proteins. This could be due to the fact that CaM requires special conditions to be succesfully electroblotted onto a membrane (Hincke, 1988). If it is not CaM, the novel SV-binding protein of 12 kDa could be hidden by the band for sulfo-SBED-AtxC on the blot, due to similar molecular masses. Due to the low amount of proteins in samples, we were unable to identify the new Atx-binding proteins, isolated from SVs.

The existence of β-ntx-binding proteins in SV was also shown with taipoxin and paradoxin: these toxins were shown to block the interaction between synaptobrevin and synaptophysin, which was not dependent on the phospholipase activity of the toxins (Treppmann, Brunk, Afube, Richter & Ahnert-Hilger, 2011). Both proteins, synaptobrevin with a molecular mass of 18 kDa and synaptophysin with a molecular mass of 38 kDa, could be among the isolated specific Atx-binding proteins in the isolates from SV.

The search for a β-neurotoxic receptor has thus far been unsuccessful. After 25 years of research, the most likely candidate is still the N-type $sPLA_2$ receptor (Lambeau, Barhanin, Schweitz, Qar & Lazdunski, 1989) that was shown to bind only neurotoxic $sPLA_2$s (reviewed in Šribar et al., 2014). Several binding proteins for β-ntxs have, however, been identified but their role in β-neurotoxic processes needs to be investigated further. One such protein is Syt1, a SV-residing protein, which acts as the Ca^{2+} sensor and is responsible for synchronous release of neurotransmitters by triggering SV exocytosis (Chapman, 2008). Due to its localization in SVs, Syt1 could play a role in the internalization of Atx (Kovačič, 2009b). In this work, we have shown a specific interaction of Atx with purified Syt1 with two different methods of cross-linking (Figure 11A), thus validating it as a binding protein for Atx. We have observed the existence of two binding sites for Atx on Syt1. Kovačič (2009b) reported that Atx probably binds to the cytosolic part of Syt1. In line with this, we have shown specific interaction of Atx with the cytosolic portion of Syt1 (Figure 13). An excess of the luminal part of Syt1 inhibited the Atx–full length Syt1 complex, therefore, also the luminal part of Syt1 specifically binds Atx (Figure 13). If Atx binds the cytosolic part of Syt1 *in vivo*, this interaction might prevent Syt1 binding to the SNARE assembly or the plasma membrane. The effect of Atx on these interactions of Syt1 should be tested.

When Syt1 was first indicated as an Atx-binding protein, it was eluted from an Atx-affinity chromatography column by the addition of EGTA (Kovačič, 2009b). This suggested that the interaction is dependent on the presence of Ca^{2+} ions. Both, Atx and Syt (cytosolic domains) bind Ca^{2+}, so the necessity for Ca^{2+} ions for their interaction is to be expected. Our results show that the absence of Ca^{2+} only partially inhibited the interaction of Atx with Syt1 (Figure 14). This means that either one binding site for Atx is dependent on Ca^{2+} and the other is not or that Ca^{2+} facilitates but is not essential for the Atx–Syt1 interaction. In the latter case, Atx could interact with Syt1 inside the nerve terminal also outside active zones or prior to the activation of voltage-gated Ca^{2+} channels, when the intracellular Ca^{2+} concentration is still low (Pang & Südhof, 2010).

CaM, the known binding protein of Atx and similar $sPLA_2$s (Šribar et al., 2001; Kovačič et al., 2009a and 2010), has been shown to bind to synaptobrevin (Quetglas, Leveque, Miquelis, Sato & Seagar, 2000) and has been suggested to be one of the Ca^{2+} sensors that trigger the formation of the SNARE complex (Quetglas et al., 2000 and 2002; De Haro, Quetglas, Iborra, Leveque & Seagar, 2003; De Haro et al., 2004), leading to exocytosis. Since CaM has been also shown to bind Syt1 (Trifaro et al., 1989), this interaction could be important for the toxicity of Atx. We have observed that the addition of CaM at the same concentration as Syt1 into the cross-linking reaction facilitated the interaction of Atx with Syt1 (Figure 15). The addition of both CaM and the excess of luminal Syt1 almost completely inhibited the interaction. This indicates that the interaction of Atx with Syt1 was blocked at one site by the luminal Syt1 and at the other site by CaM. Since CaM is apparently located near the SNARE proteins (Quetglas et al., 2000) the interaction of Atx with the cytosolic part of Syt1 could be prevented by CaM also *in vivo*. This casts doubt on the relevance of the cytosolic binding site for Atx on Syt1. Because of the complexity of the system, *i.e.*, all proteins bind to each other, the interpretation of the competitive inhibition experiment results is not straightforward. We

cannot deduce whether CaM's ability to inhibit the Syt1-Atx complex is due to CaM's binding to Syt1 or to Atx or both. A possibility for a ternary complex of Atx–Syt1–CaM exists but we were unable to detect its presence.

We have shown that AtnL, crotoxin, agkistrodotoxin, bee venom $sPLA_2$, and to a lesser extent $AtnI_2$, β-bungarotoxin and OS_2 are able to inhibit the interaction of Atx with Syt1. In addition to this, all three tested mammalian $sPLA_2$s, GV, GX and GIIA $sPLA_2$, completely inhibited the interaction (Figure 16). These results implicate Syt1 also in the actions of these $sPLA_2$s. In the mechanism of action of β-bungarotoxin and notexin, GIA $sPLA_2$ β-ntxs, the main cause of neuromuscular blockade is depletion of SVs (Šribar et al., 2014). Our results show that both β-bungarotoxin and notexin failed to fully inhibit the interaction of Atx with Syt1 and are therefore unlikely bind to Syt1. At least in the case of these two β-ntxs, the depletion of SVs is therefore probably not a consequence of their interaction with Syt1.

Due to the similarity of molecular masses, Syt1 could be one of the N-type receptor proteins. This receptor consists of membrane proteins of 18–24, 36–51 and 85 kDa (Lambeau et al., 1989). Among other $sPLA_2$s, the N-type receptor has been shown to Ca^{2+}-dependently bind OS_2, crotoxin, bee venom $sPLA_2$, notexin and Atx with decreasing affinity, but not human GIIA $sPLA_2$ (Lambeau et al., 1989; Lambeau & Lazdunski, 1999; Valentin & Lambeau, 2000; Šribar & Križaj, 2011). Comparing this to the ability of Syt1 to bind GIIA $sPLA_2$, but not OS_2 or notexin, we conclude that Syt1 is probably not one of the N-type receptor proteins. Atx- and crotoxin-binding proteins of similar molecular masss as the N-type receptor and Syt1 were discovered in bovine synaptic membranes and in the *Torpedo marmorata* electric organ (Križaj, Rowan & Gubenšek, 1995; Križaj et al., 1997). These proteins have also shown different specificities for neurotoxic $sPLA_2$s as Syt1. Since we have shown the existence of two binding sites on Syt1 for Atx, however, the competitive binding assays are not conclusive and the interactions of other $sPLA_2$s with Syt1 should be assayed by a direct labelling method. Also, the different $sPLA_2$-binding specificities of human Syt1 and receptors from bovine and *Torpedo* tissue could be due to interspecies heterogeneity of binding proteins.

Another one of the *in vitro* identified Atx-binding proteins is R25, which is a high affinity mitochondrial membrane receptor for Atx (Vučemilo et al., 1998; Čopič, Vučemilo, Gubenšek & Križaj, 1999; Šribar, 2003b). The binding affinity of AtxA and its mutants for R25 shows some correlation with their respective neurotoxicities (Ivanovski et al., 2004). All AtxA mutants with high toxicity have also shown a high affinity for R25. But the high affinity for R25 is not sufficient for neurotoxicity. This suggests that the interaction with R25 may be important in later stages of the neurotoxicity, after the internalization of the toxin (reviewed in Pungerčar & Križaj, 2007). Kovačič (2009b) has identified R25 as the subunit 2 of CcO. This protein is the terminal oxidase in the mitochondrial respiratory chain and the physiological role of CcO subunit 2 is the binding of cytochrome *c* (Sampson & Alleyne, 2001).

With both affinity-labelling methods, we have shown the specific binding of Atx to purified CcO, thus confirming this protein as a specific binding protein of Atx. Interestingly, in both affinity-labelling assays, AtxC specifically labelled several subunits of CcO. The most intensively labelled band using sulfo-SBED-AtxC labelling migrated around 17 kDa on the SDS-PAGE gel (Figure 11C), and probably corresponds to subunit 4 of CcO (with a molecular mass of 17.2 kDa). This suggested that more sulfo-SBED-AtxC reacted with subunit 4 than with subunit 2 of CcO. CcO is a multi-protein complex, consisting of 13 peptide chains (Yoshikawa et al., 2012). It is possible that ^{125}I-AtxC and sulfo-SBED-AtxC bind to one subunit, *e.g.*, subunit 2, but the cross-linker then covalently links AtxC to another subunit, *e.g.*, subunit 4, which may harbour nucleophilic group more readily accessible for reacting with cross-linker than the binding site-containing

subunit. Subunits 2 and 4 are in contact in the CcO complex (Yoshikawa et al., 2012), which corroborates this theory. In line with this, it has been observed (Šribar, personal communication) that as the Triton X-100 extracts of mitochondria from porcine cerebral cortex were subjected to repeated freeze-thaw cycles, R25 was increasingly less successfully linked with ^{125}I-AtxC and DSS, but at the same time the band at about 17 kDa, thought to be CaM, was increasingly more intense. This was speculated then that CaM may represent a part of R25 and is released from this complex by freezing and thawing. CaM and subunit 4 of CcO differ by less than 0.5 kDa. The products of their cross-linking with ^{125}I-AtxC and DSS would both migrate at around 31 kDa and the difference between these two bands would be impossible to distinguish. Therefore, in the adduct of about 31 kDa, ^{125}I-AtxC could be linked to either CaM and/or CcO subunit 4. Since R25 is likely subunit 2 of CcO, CaM is probably released from some other (multi)protein or membrane complex due to freezing and thawing. Since freezing and thawing can disrupt the structure of a protein, especially if this is a detergent-solubilized multi-subunit membrane protein, this might explain the decreasing ability of ^{125}I-AtxC to bind and cross-link CcO subunit 2. The detergent used to solubilize the mitochondrial membrane proteins was Triton X-100. This detergent has been shown to inhibit the activity of CcO 100-fold (Mahapatro & Robinson, 1990), suggesting that it has an effect on the enzyme's native quaternary structure, which would also explain the decreasing labelling of R25. The strong labelling of CcO subunit 4 suggests that the bands which were thought to be CaM in several other protein preparations, including the mitochondrial fraction of porcine or murine cerebral cortex and in the CcO isolated from the porcine cerebral cortex (Kovačič, 2009b; Oberčkal, 2010), might actually represent (at least in part) CcO subunit 4.

Atx and cytochrome *c* are both basic and very similar in size, cytochrome *c* being 13 kDa and Atx 13.7 kDa. Atx could bind to the same site on CcO as cytochrome *c*. Since the interaction of cytochrome *c* with CcO is transient and exhibits very low affinity (K_D in the 10 μM range) (Salamon & Tollin, 1996), Atx could efficiently block their interaction and inhibit enzymatic activity of CcO. Possible effect of Atx binding to subunit 2 of CcO is therefore displacement of cytochrome *c* from the complex with CcO. This would inhibit CcO's proton pumping action, diminishing the electrochemical gradient across the mitochondrial inner membrane, which drives the production of ATP (Erecinska & Wilson, 1982). This would lead to loss of the electrochemical gradient across the mitochondrial inner membrane and loss of ATP synthesis, and would explain the loss of mitochondrial potential and mitochondrial structural integrity observed after Atx treatment (Pucer, 2008; Logonder et al., 2008b). Due to the complexity of the measurement of CcO activity, where the buffer must contain potassium phosphate, but the binding of Atx to CcO requires Ca^{2+}, we were unable to investigate the effect of Atx on CcO enzymatic activity. The addition of Ca^{2+} ions into the buffer would cause the precipitation of the insoluble salt $Ca_3(PO_4)_2$. It would be hard to show the inhibition of the Atx–CcO interaction by an excess of cytochrome *c*, due to the low affinity of the latter for CcO. In addition to CcO, also complexes I and III of the mitochondrial respiratory chain have been indicated as potential Atx-binding proteins (Kovačič, 2009b; Oberčkal, 2010). Together with CcO these proteins form the 1700 kDa mitochondrial supercomplex $I_1III_2IV_1$ (Althoff, Mills, Popot & Kühlbrandt, 2011). Interaction of Atx with these proteins would also disrupt the eletrochemical gradient in mitochondria, leading to the observed loss of ATP synthesis, due to Atx's action.

In order to assess the pathophysiological relevance of the interactions of Atx with Syt1 and CcO, we first assayed their effect on Atx's phospholipolytic activity. Since Atx is an active $sPLA_2$, binding to other proteins can affect its enzymatic activity. Several proteins have been shown to inhibit or augment Atx's enzyme activity (reviewed in Šribar &

Križaj, 2011). The binding of Syt1 to Atx did not affect its phospholipase activity, at least not at the conditions of our standard assay (Figure 17A). We do not know the orientation of the Atx molecule binding to Syt1, however, the lack of the negative effect of binding on Atx's enzymatic activity suggests that Atx's IBS is not obstructed in the complex with Syt1 in the case of the both binding sites detected. In the case of CcO, the effect on Atx's enzymatic activity was unclear, due to the presence of the detergent lauryl maltoside in the CcO sample. We have namely observed an augmentation of Atx's enzyme activity solely by addition of the detergent (Figure 17B).

The affinity between Atx and Syt1, CcO or PDI has been demonstrated *in vitro*. All three proteins are located at such positions in the cells that they could play roles in the action of Atx and related sPLA$_2$s. Dolinar (2013) found that Atx significantly co-localized with CcO and PDI in PC12 cells. The co-localization of Atx with Syt1 has also been shown in NSC-34 cells (Jenko Pražnikar et al., 2008). In our work we have observed a substantial co-localization of Atx with Syt1 also in the PC12 cells. To further substantiate the role of Syt1, CcO and PDI in β-neurotoxicity, we incubated PC12 cells with sulfo-SBED-AtxC and after the incubation triggered the photo-cross-linking of the toxin probe with cellular proteins in its close proximity. We observed that Atx was able to reach and react with Syt1 and PDI in the cells already after 1 min of incubation (Figure 18, panels A and B). This is in agreement with the rapid labelling of cytosolic CaM and 14-3-3p that was previously reported (Jenko Pražnikar et al, 2008; Kovačič, 2009b). We have also observed a rapid labelling of a cellular protein of about 25 kDa that likely corresponds to R25 in PC12 cells (Figure18, panels C and D). We have indications that R25 is subunit 2 of CcO, which would suggest that after only 1 min Atx reached the mitochondria of PC12 cells. We were able to detect Syt1 only in the NGFD PC12 cell samples, but not in the samples of ND cells. This indicates that NGFD but not the ND cells have the machinery required to bring Atx and Syt1 in contact. We have shown in this work that, besides with CaM and 14-3-3p (Jenko-Pražnikar et al., 2008; Kovačič, 2009b), Atx interacted also with Syt1, PDI and likely CcO in the living PC12 cells. Our results suggest a very rapid internalization of Atx into these cells and its intracellular targeting and localization to SVs, ER and mitochondria.

The internalization of Atx and similar β-ntxs into neuronal cells has been demonstrated several times (Petrovič et al., 2004; Rigoni et al., 2008; Jenko Pražnikar et al., 2008; Kovačič, 2009b; Logonder et al., 2009). Multiple pathways for internalization of β-ntxs probably exist (Šribar et al., 2014). Jenko Pražnikar et al. (2008) have observed a partial co-localization of Atx with Syt1 in NSC-34 cells and as we report in this work, we also observed a substantial co-localization of Atx with Syt1 in ND and NGFD PC12 cells (Figure 29, panels A and B; Figure 28A). The luminal part of Syt1 has been shown to be exposed on the surfaces of cells in primary CNS cultures due to action of β-ntxs (Rigoni et al., 2004) and was therefore available for interacting with β-ntxs from the extracellular space. We have shown that the luminal part of Syt1 binds Atx. Syt1 might therefore represent a novel cell surface receptor for Atx and similar sPLA$_2$s. The interaction with Syt1 has been implicated also in the internalization of BoNT B and BoNT G into motor nerve terminals (Dong et al., 2003; Rummel et al., 2004). Atx is unlikely to cross the SV membrane by the same mechanism as these bacterial neurotoxins (Pungerčar & Križaj, 2007.). But being a potent phospholipase, Atx could hydrolyze the inner membrane of the SV and thus gain entry into cell cytosol. The depletion of the SVs is thus explained by the Atx's hydrolytic action (Jenko Pražnikar et al., 2008; Logonder et al., 2009). Since we have observed no effect on Atx's phospholipase activity in the presence of Syt1, Atx could hydrolyze the membrane while in complex with Syt1. The interaction with Syt1 could also keep Atx anchored and prevent it from dissociating from the membrane. Besides Syt1, we have shown the existence of also other specific binding proteins for Atx

in SVs. Based on the co-localization of Syt1 and Atx in PC12 cells, we can conclude that one of the internalization pathways of Atx goes likely *via* SVs, where the interaction of Atx with Syt1 may play a crucial role. Syt1 displayed specific binding of also other, snake venom and mammalian $sPLA_2$s, suggesting that also these proteins might utilize the SV endocytotic pathway to enter the motor nerve cells.

Another potential pathway of internalization of Atx is *via* the retrograde protein transport, assisted by PDI in the lumen of the ER, as suggested by Šribar et al. (2005). Besides PDI, the binding proteins of also two other β-ntxs, taipoxin and crotoxin (TCBP-49 and crocalbin, respectively), are proteins from the lumen of the ER (Dodds et al., 1995; Hseu et al., 1997 and 1999). Ultrastructural evidence suggests that motoneuron axons do not contain rough ER or the components of Golgi apparatus (Tsukita & Ishikawa, 1976 and 1979). Nevertheless, a vesicular localization of PDI and several other ER components, involved in protein synthesis and transport, has been detected in motoneuron axons (Merianda et al., 2009). In our work we have also observed the PDI immunoreactivity in neuronal processes of PC12 cells (Figure 29F), additionally suggesting that also in motoneuron terminals, PDI finds itself in position to come across Atx. In order to design mutants for studying of the role of PDI in Atx cellular trafficking, we prepared the model of the complex between hPDI and Atx, based on the model of the Atx and yPDI (Kovačič, 2009b). Molecular docking procedure resulted in a structure where the position of Atx in the complex with hPDI is substantially different from its position in the complex with yPDI. Nevertheless, as with yPDI, Atx interacts with hPDI *via* its IBS, contacting hPDI with the same amino acid residues (except for R77) as yPDI (Figure 19B) (Kovačič, 2009b). The binding to PDI *via* Atx's IBS should obstruct the binding of Atx to phospholipid membranes, inhibiting its phospholipase activity. However, no influence on the enzymatic activity of Atx has been detected in the presence of hPDI, probably due to the almost 10,000-fold higher affinity of the $sPLA_2$ molecule for PG membranes than for hPDI (Kovačič, 2009b). The pathway of the $sPLA_2$ cellular internalization has not yet been established. To consider the possible involvement of hPDI in the cell trafficking of also other $sPLA_2$s, we first prepared models of their interactions with hPDI. Besides some differences in relative orientation between respective $sPLA_2$s in complexes, all tested $sPLA_2$s form very similar complexes with hPDI as Atx (Figure 20, panels A, B and C). The interaction of Atx and other tested $sPLA_2$s with hPDI is predominantly electrostatic, which is in line with the observation that the interaction of hPDI with Atx was abolished at pH 5.0 (Šribar et al., 2005). The interaction area with hPDI is the same in the case of Atx and the mammalian GIB, GIIA and GV $sPLA_2$s, which have been detected inside cells, while that of the non-toxic $AtnI_2$ or GX $sPLA_2$, which have not so far been observed inside cells, differs from the interaction area of Atx with hPDI. The models were validated in a heterologous competition experiment. In line with our predictions, we found that AtnL and GV $sPLA_2$ inhibited the interaction of Atx with hPDI much more effectively than $AtnI_2$ and GX $sPLA_2$ (Figure 20D). Our modelling approach thus gives relevant models of complexes between mammalian $sPLA_2$s and hPDI. Models of the complex between hPDI and Atx or the Atx-structurally related mammalian $sPLA_2$s thus provide us with a structural understanding of how these proteins associate. This offers the possibility of facilitating the study of the role of hPDI in the $sPLA_2$ cell internalization process using targeted mutagenesis. Altogether, the results presented here strongly support the proposal that PDI, an oxido-reductase from the lumen of ER, is involved in the retrograde cell transport of Atx and structurally related toxic or mammalian $sPLA_2$s.

Besides the two above mentioned, probably also other routes of β-ntx internalization exist. Several β-ntxs have been observed localized at the mitochondria (Rigoni et al., 2008). Logonder et al. (2009) have demonstrated that nanogold-labelled AtxA associated

with mitochondria. Upon close inspection of their electron micrographs, Atx seems to be located in the mitochondrial intermembrane space. Dolinar (2013) and also we in this work have demonstrated an extensive co-localization of Atx and CcO in PC12 cells (Figure 29, panels C and D; Figure 30B). However, based on co-localization data alone, we could not claim whether Atx bound just to the outer membrane of mitochondria or actually enter this organelle. CcO subunit 2 is the mitochondrial inner membrane protein accessible from the solution in the space between mitochondrial outer and inner membranes. Atx would therefore need to cross only the outer membrane of mitochondria to interact with the subunit 2 of CcO. Our cross-linking results in PC12 cells (Figure 18, panels C and D) suggest that Atx binds to R25 in these cells and therefore likely enters the intermembrane space of mitochondria. Since mitochondria are the obvious target of β-ntxs, these organelles themselves might facilitate entry of β-ntxs into the cell. Boudreau et al. (2014) have shown that mitochondria could enter and exit platelet cells and that they are a substrate for the GIIA $sPLA_2$, a mammalian homologue of Atx. If also neuronal cells are able to release and take up mitochondria, β-ntxs could bind to mitochondria outside the cell and then stowaway inside this organelle, as it is internalized into the neuron again. GIIA $sPLA_2$ has been found also within the mitochondria, associated with mitoplasts (Macchioni et al., 2004), indicating its localization in the intermembrane space. Since GIIA $sPLA_2$ is structurally homologous to GIIA β-ntxs, among them Atx, these could use the same mode of internalization into mitochondria as GIIA $sPLA_2$.

The role of PLA_2 enzymatic activity in β-neurotoxicity has been much debated and is largely not understood yet. It is known, however, that it is not solely responsible for the observed neurotoxic effects of β-ntxs, since their lethalities do not correlate with their respective enzymatic activities (reviewed in Pungerčar & Križaj, 2007; reviewed in Šribar et al., 2014). A likely interplay then exists between the enzymatic activity and binding to specific receptors on the presynaptic membrane, as well as inside the target cells, for the β-ntxs to exert the full range of their effects.

The role of phospholipase activity in the first two phases of the typical triphasic muscle twitching effect of β-ntxs on isolated neuro-muscular preparation *ex vivo* is not completely clear (reviewed in Pungerčar & Križaj, 2007). It has been shown, however, that phospholipase activity is necessary for the third phase (the irreversible blockade of the indirectly elicited muscle twitching or neurotransmitter release) to take place (Prijatelj et al., 2006; Logonder, 2008a). A recent study by Simonato et al. (2014), using an enzymatically inactive mutant of the GIA $sPLA_2$ notexin, has shown that the inactive $sPLA_2$ still inhibited neuromuscular communication in the mouse phrenic nerve–hemidiaphragm preparation, albeit this effect was slower than in the case of the wild-type, enzymatically active notexin. They have also shown that the enzymatically inactive notexin failed to open the mitochondrial permeability pore in isolated mitochondria. Jenko Pražnikar et al. (2008) have also demonstrated that replacing Ca^{2+} with Sr^{2+} during the incubation with Atx almost completely abolished the toxin's entry into NSC-34 cells, suggesting that the $sPLA_2$ activity, requiring Ca^{2+}, is also required for the toxin's internalization. However, since a lot of protein–protein interactions of $sPLA_2$s are Ca^{2+}-dependent (reviewed in Šribar & Križaj, 2011), it could also mean that a Ca^{2+}-dependent interaction with some receptor is responsible for the internalization.

To investigate the role of phospholipase activity in the neurotoxic processes of Atx, we prepared AtxA with a mutation in its active site, rendering it enzymatically inactive. We used novel methods of expression, refolding and cleaning of AtxA(D49S), which shortened the time and decreased the number of steps necessary to produce the pure, correctly folded protein. The mutant also did not possess Met residue at its N-terminal due to the production in *E. coli*, which may render the purification very difficult (Jemel et al., 2011).

We compared the ability of AtxA(D49S), the enzymatically inactive mutant, and the wild-type AtxA to internalize into PC12 cells and to co-localize with the known protein targets of Atx, Syt1, CcO, PDI and 14-3-3p. In line with observations of our colleagues (Jenko Pražnikar et al., 2008; Logonder, 2008a; Dolinar, 2013) we have observed a punctate signal for AtxA inside the cells, indicating a vesicular localization or clustering at specific sites (Figure 28, panels A and C). Comparing our findings with the findings of Jenko Pražnikar et al. (2008) in NSC-43 cells, we concluded that AtxA entered PC12 cells slower than NSC-34 cells. Although scarce at these low incubation times, the signal for Atx was observed inside PC12 cells already after 1 min of incubation. Such rapid internalization of Atx is in line with the observations that after 30 min of mouse hemidiaphragm exposure to the β-ntxs, these became inaccessible to neutralizing antibodies, but not to Sr^{2+}, which can enter cells (Simpson, Lautenslager, Kaiser & Middlebrook, 1993). It is also in line with the effects of β-bungarotoxin on the rat hemidiaphragm that were similar if the toxin was left in the bath or was removed after 10 min of exposure of the cells (Prasarnpun et al., 2004). We observed a punctate signal also for the AtxA(D49S) fluorescent derivative inside the PC12 cells after only 1 min of incubation (Figure 28, panels B and D). This means that at least one of the pathways of Atx internalization is independent on the toxin's enzymatic activity in the used cellular model. This enzymatic activity-independent internalization is in line with the results of Neco et al. (2003), who observed that taipoxin entry into bovine chromaffin cells was not dependent on Ca^{2+}.

The quick entrance of the enzymatically inactive AtxA(D49S) into the cells suggests that Atx's enzymatic activity is more important after its translocation into the cell than before. Petrovič et al. (2005) have demonstrated that Atx retained a significant fraction of its enzymatic activity in a reducing environment of the cytosol, despite the fact that it contains 7 disulphide bonds. Kovačič (2009a) has shown that the binding of Atx to the cytosolic CaM and 14-3-3p protected Atx from reduction in the cytosol-like environment and even restored the activity of a partially reduced Atx to the initial level. These findings suggested that β-ntxs could be enzymatically active also in the nerve cell cytosol, pointing to the potential importance of the intracellular enzymatic activity of these toxins. To the possibility of the intracellular activity of Atx points also the fact that Atx and structurally-related $sPLA_2$s have higher affinity for the negatively charged phospholipids that are also predominately found on the intracellular leaflets of biological membranes (Radvanyi et al., 1987; Petan et al., 2005).

After short incubation times of PC12 cells with Atx, there was a low amount of Atx present in or on the cells than after longer incubations. The shorter incubation times are therefore subject to larger errors regarding calculation of co-localization extent. Errors might result also from the fact that some cells were internalizing the toxin more extensively than the others and that some cells were parts of larger clusters of cells during Atx-treatment and were not in contact with Atx. At short incubation times, with low amounts of Atx, these cells were harder to be distinguished from the cells, relevant to our experiment, which might lead to errors.

We observed that AtxA(D49S) co-localized with all the inspected proteins, Syt1, CcO, PDI and 14-3-3p, to a lesser extent than AtxA (Figure 30). Especially with Syt1 and CcO, this effect was much more pronounced in ND than in NGFD PC12 cells. Enzymatic activity therefore seems to be important for AtxA to reach Syt1 and CcO in ND PC12 cells, whereas in NGFD cells, which are more similar to actual target cells of Atx, there seem to exist specific mechanisms to facilitate Atx entry into the cell, regardless of its enzymatic activity. From this we conclude that ND cells are deficient in at least one Atx-internalizing pathway compared to NGFD cells. Due to the lower amount of SVs in ND comparing to NGFD PC12 cells (Green & Tischler, 1976), this points to the SV-

internalization pathway. It also strengthens the suggestion that more than one mechanism of translocation of Atx into the cell exist. In the case of Syt1, the lower extent of co-localization with the enzymatically inactive mutant of AtxA could mean that Atx did not come close to Syt1 in ND PC12 cells *via* entering SVs, as their lumen is exposed to the extracellular environment. Because in this case the enzymatically inactive mutant of AtxA would be able to reach Syt1 from outside the cell as easily as the native AtxA, since it would not need to cross any membrane. This might be due to the fact that in ND cells there are fewer SVs than in NGFD PC12 cells (Greene & Tischler, 1976) and the lumen of SV is less frequently exposed to the extracellular space in ND than in NGFD PC12 cells. The fact that the active Atx still co-localizes with Syt1 in ND PC12 cells means that Atx enters the ND PC12 cells by some other pathway, which includes membrane hydrolysis, and is then targeted to the SVs, probably to their cytosolic side. Since we failed to detect the direct interaction of sulfo-SBED-AtxC with Syt1 in ND PC12 cells (Figure 18A), this indicates that the co-localization in ND PC12 cells may be just due to the similar localization of Syt1 and Atx, that is, at the SV. In NGFD cells, however, the smaller difference in the extent of co-localization with Syt1 suggests that both AtxA and AtxA(D49S) localize near Syt1 *via* the same, phospholipase activity-independent, mechanism.

Logonder et al. (2008b) observed only a 13.6% percent loss of SVs in the endings of the AtxA-intoxicated murine motoneurons and Jenko Pražnikar et al. (2008) observed a loss of synaptophysin and Syt1 in NSC-34 cells. In PC12 cells we observed no visually detectable loss of the Syt1 signal as a result of treatment with either AtxA variant (Figure 29, panels A and B). This suggests that AtxA does not cause depletion of SVs in PC12 cells. In CNS neurons, the signal for synaptophysin also was not attenuated (Rigoni et al., 2004 and 2005), so the depletion of SVs due to action of β-ntxs might be specific to motor neurons.

In the case of Atx's co-localization with PDI and 14-3-3p (Figure 29, panels E–H), the difference between the enzymatically inactive and active AtxA is smaller, but it is still more pronounced in ND than in NGFD cells. Enzymatic activity therefore does not seem to be as important as in the case of Syt1 and CcO to reach these proteins and the compartments they reside, the lumen of ER and the cytosol, respectively. With PDI, interestingly, a higher co-localization was observed in ND PC12 cells than in NGFD cells, suggesting that the proposed retrograde pathway of Atx cell internalization is more pronounced in ND PC12 cells. In the case of PDI, after 30 min of incubation of Atxs with the cells, the co-localization reached the maximum. This indicates saturation or an equilibrium state. In the latter case, this may indicate that the interaction between Atx and PDI is transient and that the equilibrium between Atx coming into the lumen of ER and Atx leaving this compartment through the ER membrane into the cytosol is rapidly established. In favour of transient nature of the interaction between Atx and PDI is the apparent dissociation constant of the interaction between these two proteins which is only 1.27 ± 0.05 μM as determined by surface plasmon resonance (Šribar et al., 2005).

Based on all co-localization experiments, we suggest that the enzymatic activity facilitates Atx's entry into the cells and its trafficking to SVs, mitochondria and the ER, but is not absolutely required for these events to take place.

Logonder (2008a) observed that by treating the neuromuscular preparation with the enzymatically inactive derivative of AtxA, there was no characteristic third phase in the muscle response to the indirectly evoked twitching in the presence of β-ntxs. The neuromuscular communication was not blocked. Since we have seen that the enzymatically inactive mutant of AtxA entered PC12 cells and co-localized with mitochondria, the third phase might be due to Atx's intracellular enzymatic activity, causing SV depletion and uncoupling of mitochondria (Pucer, 2008; Logonder et al.,

2009). Simpson et al. (1993) have shown that substituting Ca^{2+} for Sr^{2+} in the bath with the neuromuscular preparation inhibited the neurotoxicity of β-ntxs, if Sr^{2+} was administered up to 30 min after the addition of the β-ntx. Since β-ntxs internalize by that time (Prasarnpun et al., 2004), this also suggests that enzymatic activity is required for neurotoxicity after the internalization of β-ntxs. Rigoni et al. (2008) have shown that the extent of inactivation of enzymatic activity of notexin corresponded to its lethality and Simonato et al. (2014) observed that enzymatic activity was required for notexin to open the permeability transition pore in isolated mitochondria. Since we have now demonstrated that Atx can enter cells and co-localize with mitochondria irrespective of its enzymatic activity, this suggests that the opening of the permeability transition pore is due to hydrolysis of the mitochondrial membrane by a β-ntx and not by hydrolysing the external side of the plasma membrane. This is corroborated with the fact that mitochondria have been shown as a good substrate for $sPLA_2$s (Boudreau et al., 2014).

Based on our results we propose a slightly updated model of the neurotoxicity of Atx: Atx binds to the presynaptic membrane, on receptors located there. These include also protein(s) located in the SV membrane, for example Syt1. Associated with the axolemma or anchored *via* luminal region of Syt1 to recycling SVs, Atx hydrolyses the phospholipids in the membrane's external leaflet, producing fatty acids and lysophospholipids. Accumulating products of hydrolysis affect the membrane curvature and promote SV exocytosis. Conductivity of some Ca^{2+} channels is increased (Prasarnpun et al., 2004), which further promotes the exocytosis of SV. Atx quickly internalizes into the nerve ending utilizing multiple pathways, including the recycling SVs. At least some of the Atx-internalization pathways are independent of its enzymatic activity. The interaction with PDI concentrates Atx in the lumen of ER (Oberčkal et al., 2015), from where it is translocated further into the cell cytosol. Atx might enter the cytosol of the nerve cell also by hydrolysing the SV membrane. In the cytosol, Atx binds to proteins involved in SV endo- and exocytosis, CaM, 14-3-3ps and the cytosolic part of Syt1, and possibly to some other cytosolic proteins. CaM stabilizes Atx and increases its enzymatic activity (Kovačič et al., 2009a and 2010). 14-3-3ps presumably localize Atx at the sites of SV endocytosis (Mattiazzi et al., 2012). The augmented phospholipase activity at specific sites inside the nerve ending is crucial for β-neurotoxicity. The hydrolysis of the inner layer of the plasma membrane causes the inhibition of SV endocytosis, due to the impairment of amphiphysin function (Mattiazzi et al., 2012). Atx localizes at the mitochondria. It then translocates into their intermembrane space in a phospholipase activity-independent process. Atx binds to CcO and possibly to other specific sites inside the mitochondria. The hydrolysis of mitochondrial membranes induces opening of the permeability transition pores (Rigoni et al., 2008, Simonato et al., 2014). Along with Atx's interaction with mitochondrial proteins this results in the loss of mitochondrial potential, inhibition of ATP synthesis and loss of mitochondrial structural integrity (Pucer, 2008, Logonder et al., 2009). The extended phospholipolysis of cellular membranes causes the increase in cytosolic Ca^{2+} concentration, leading to the activation of cytosolic proteinases (Duregotti et al., 2013). The latter disrupt the integrity of the F-actin cytoskeleton (Jenko Pražnikar et al., 2008), resulting in further degeneration of the nerve ending.

6 Conclusions

1. Binding of Atx to the 25 kDa CcO subunit 2 is specific and Ca^{2+}-dependent, suggesting that R25 is the CcO subunit 2. The interaction of Atx with CcO subunit 2 may prevent the transient interaction between CcO and cytochrome *c*, inhibit the activity of CcO and dissipate the mitochondrial membrane potential, which would lead to the arrest of ATP synthesis, all the effects observed upon Atx intoxication of neuronal cells.

2. Syt1 is a specific Atx-binding protein that possesses two binding sites for Atx, one at its cytosolic and the other at its luminal side. The binding of Atx to Syt1 partially depends on Ca^{2+}, suggesting that the binding to one of the binding sites requires Ca^{2+} while to the other does not. The presence of CaM and the luminal segment of Syt1 completely inhibited labelling of the full length Syt1 with sulfo-SBED-AtxC, suggesting that CaM and Atx either compete for the cytosolic binding site on Syt1 or that CaM and Syt1 compete for the same binding site on Atx. In either case, CaM is able to hinder *in vitro* the interaction between Atx and the cytosolic part of Syt1. The luminal part of Syt1 likely represents a novel receptor for Atx on the external side of the presynaptic membrane.

3. In addition to Atx, also AtnL, crotoxin, agkistrodotoxin, bee venom $sPLA_2$, mammalian GV, GX and GIIA $sPLA_2$s and to a lesser extent $AtnI_2$, β-bungarotoxin, OS_2, bind Syt1, which is not the case with notexin and *Crotalus atrox* $sPLA_2$. This suggests that Syt1 takes part in the pathophysiological action of the former $sPLA_2$s, but not the latter two.

4. Atx directly interacts with Syt1, PDI and likely R25 (putatitvely representing subunit 2 of CcO) also in the living PC12 cells. This additionally points to the relevance of these interactions in the neurotoxicity of Atx. Interactions of Atx with Syt1 and PDI are likely important for the internalization of Atx into neuronal cells.

5. The 3D models of complexes between $sPLA_2$s, structurally related to Atx, and hPDI, as well as the heterologous competition assays suggest a role of PDI in the intracellular trafficking of also these $sPLA_2$s.

6. Based on the significant co-localization of AtxA with Syt1, CcO, PDI and 14-3-3p in ND and NGFD PC12 cells we conclude that this toxin upon internalization localizes in SVs, mitochondria, lumen of the ER and the cytosol of these cells, respectively.

7. Based on the immunofluorescence studies with the enzymatically inactive mutant AtxA(D49S), we conclude that the enzymatic activity of AtxA facilitates but is not absolutely required for the internalization of AtxA into the PC12 cells and its co-localization with Syt1, CcO, PDI and 14-3-3p. The dependence of the co-localization of AtxA with CcO and Syt1 on AtxA's enzymatic activity was far more pronounced in ND cells than NGFD cells. This indicates that the enzymatic activity is more important for the

internalization and intracellular trafficking of Atx to SVs and mitochondria in ND cells than in NGFD PC12 cells. It seems that in NGFD PC12 cells specific pathway(s) for the internalization and intracellular trafficking of Atx exists that does not depend on Atx's enzymatic activity.

7 Acknowledgements

I sincerely thank my supervisor Professor Igor Križaj for his mentorship, guidance, advice and patience, as well as critical reading and correction of all written texts, including this one.

I sincerely thank also my co-supervisors, Dr. Jernej Šribar and Dr. Lidija Kovačič, for broadening my horizons, teaching me science, in either the methodological or the mental sense, and selflessly providing help at any and all times during my stay at the Jožef Stefan Institute. I am very grateful to them also for critical reading and help with the preparation of this thesis.

For reviewing and evaluating my thesis I would like to thank Professor Peter Maček, Professor Jože Pungerčar and Professor Robert Frangež.

I am very grateful to Dr. Toni Petan for his advices and many discussions regarding the production of recombinant Atxs.

I am grateful to Dr. Adrijana Leonardi for N-terminal sequencing of proteins and to Dr. Dušan Žigon and Dr. Marko Fonović for mass spectrometry analyses of proteins.

I am grateful to Dr. Petra Prijatelj Žnidaršič for teaching me the basics of recombinant DNA technology.

I also thank all the colleagues from the Department of Molecular and Biomedical Sciences for the coffee-break discussions and making our lab a pleasant environment. I especially thank Dr. Vesna Brglez for many fruitful and fruitless discussions, which aided my research and shortened the late night sessions in the lab, as well as her emotional support in trying circumstances.

Thanks also go to the Slovenian Research Agency for financing my research and education.

I dedicate the thesis to my parents, Viljenka and Bojan, who have stood behind me and supported me, regardless the cost.

8 References

Althoff, T., Mills, D. J., Popot, J. L., & Kühlbrandt, W. (2011). Arrangement of electron transport chain components in bovine mitochondrial supercomplex I1III2IV1. *The EMBO Journal*, 30(22), 4652–4664.

Appenzeller-Herzog, C., & Ellgaard, L. (2008). The human PDI family: versatility packed into a single fold. *Biochimica et Biophysica Acta*, 1783(4), 535–548.

Birts, C. N., Barton, C. H., & Wilton, D. C. (2008). A catalytically independent physiological function for human acute phase protein group IIA phospholipase A_2: cellular uptake facilitates cell debris removal. *The Journal of Biological Chemistry*, 283(8), 5034–5045.

Bolte, S. & Cordelières, F. P. (2006). A guided tour into subcellular colocalization analysis in light microscopy. *Journal of Microscopy*, 224(3), 213–232.

Boudreau, L. H., Duchez, A., Cloutier, N., Soulet, D., Martin., N, Bollinger, J., ... Boilard, E. (2014). Platelets release mitochondria serving as substrate for bactericidal group IIA-secreted phospholipase A_2 to promote inflammation. *Blood*, 124(14), 2173–2183.

Caccin, P., Rigoni, M., Bisceglie, A., Rossetto, O., & Montecucco, C. (2006). Reversible skeletal neuromuscular paralysis induced by different lysophospholipids. *FEBS Letters*. 580(27), 6317–6321.

Caccin, P., Rossetto, O., & Montecucco, C. (2009). Neurotoxicity of inverted-cone shaped lipids. *Neurotoxicology* 30(2), 174–181.

Caratsch, C. G., Maranda, B., Miledi, R., & Strong, P. N. (1981). A further study of the phospholipase-independent action of β-bungarotoxin at frog end-plates. *The Journal of Physiology*, 319, 179–191.

Chapman, E. R., (2008). How does synaptotagmin trigger neurotransmitter release? *Annual Review of Biochemistry*, 77, 615–641.

Connolly, S., Trevett, A. J., Nwokolo, N. C., Lalloo, D. G., Naraqi, S., Mantle, D., ... Warrell, D. A. (1995). Neuromuscular effects of Papuan Taipan snake venom. *Annals of Neurolology*, 38(6), 916–920.

Craige, B., Salazar, G., & Faundez, V. (2004). Isolation of synaptic vesicles. In J. S. Bonifacino et al. (Eds.), *Current Protocols in Cell Biology*, unit 3.12, doi:10.1002/0471143030.cb0312s25.

Čopič, A., Vučemilo, N., Gubenšek, F., & Križaj, I. (1999). Identification and purification of a novel receptor for secretory phospholipase A_2 in porcine cerebral cortex. *The Journal of Biological Chemistry*, 274(37), 26315–26320.

De Haro, L., Ferracci, G., Opi, S., Iborra, C., Quetglas, S., Miquelis, R., ... Seagar, M., (2004). Ca^{2+}/calmodulin transfers the membraneproximal lipid-binding domain of the v-SNARE synaptobrevin from cis to trans bilayers. *Proceedings of the National Academy of Sciences USA*, 101(6), 1578–1583.

De Haro, L., Quetglas, S., Iborra, C., Leveque, C., & Seagar, M. (2003). Calmodulin-dependent regulation of a lipid binding domain in the v-SNARE synaptobrevin and its role in vesicular fusion. *Biology of the Cell*, 95(7), 459–464.

Dennis E.A., Cao J., Hsu, Y., Magrioti, V., & Kokotos, G (2011). Phospholipase A_2 enzymes: physical structure, biological function, disease implication, chemical inhibition, and therapeutic intervention. *Chemical Reviews*, 111(10), 6130–6185.

de Vries, S. J., van Dijk, M., & Bonvin, A. M. J. J. (2010). The HADDOCK web server for data-driven biomolecular docking. *Nature Protocols*, 5(5), 883–897.

Dodds, D., Schlimgen, A. K., Lu, S. Y., & Perin, M. S. (1995). Novel reticular calcium binding protein is purified on taipoxin columns. *Journal of Neurochemistry*, 64(5), 2339–2344.

Dolinar, K. (2013). *Synthesis of a fluorescently labelled derivative of ammodytoxin A and its use in immunofluorescence studies on the PC12 cell line.* Bachelor thesis. Ljubljana, Slovenija: Faculty of Chemistry and Chemical Technology, University of Ljubljana.

Dominguez, C., Boelens, R., & Bonvin, A. M. J. J. (2003). HADDOCK: A protein-protein docking approach based on biochemical or biophysical information. *Journal of the American Chemical Society*, 125(7), 1731–1737.

Dong, M., Richards, D. A., Goodnough, M. C., Tepp, W. H., Johnson, E. A., & Chapman, E. R. (2003). Synaptotagmins I and II mediate entry of botulinum neurotoxin B into cells. *The Journal of Cell Biology*, 162(7), 1293–1303.

Duregotti, E., Tedesco, E., Montecucco, C., & Rigoni, M., (2013). Calpains participate in nerve terminal degeneration induced by spider and snake presynaptic neurotoxins. *Toxicon*, 64, 20–28.

Erecińska, M., & Wilson, D. F. (1982). Regulation of cellular energy metabolism. *The Journal of Membrane Biology*, 70(1), 1–14.

Fayard, J. M., Tessier, C., Pageaux, J. F., Lagarde, M., & Laugier, C. (1998). Nuclear location of PLA_2-I in proliferative cells. *Journal of Cell Science*, 111(7), 985–994.

Ferrini, M., Nardicchi, V., Mannucci, R., Arcuri, C., Nicoletti, I., Donato, R., & Goracci, G. (2010). Effect of NGF on the subcellular localization of group IIA secretory phospholipase A_2 (GIIA) in PC12 cells: role in neuritogenesis. *Neurochemical Research*, 35(12), 2168–2174.

Forster, M. L., Mahn, J. J., & Tsai, B. (2009). Generating an unfoldase from thioredoxin-like domains. *The Journal of Biological Chemistry*, 284(19), 13045–13056.

Fujita, K., Lazarovici, P. & Guroff, G. (1989). Regulation of the differentiation of PC12 pheochromocytoma cells. *Environmental Health Perspectives*, 80, 127–142.

Greene, L. A., & Tischler, A. S. (1976). Establishment of a noradrenergic clonal line of rat adrenal pheochromocytoma cells which respond to nerve growth factor. *Proceedings of the National Academy of Sciences USA*, 73(7), 2424–2428.

Gubenšek, F., & Križaj I. (1997). Ammodytoxins (*Vipera ammodytes ammodytes*). In R. Rappuoli & C. Montecucco (Eds.), *Guidebook to protein toxins and their use in cell biology* (pp. 224–226). New York, NY: Oxford University Press.

Gubenšek, F., Ritonja, A., Zupan, J., & Turk, V. (1980). Basic proteins of *Vipera ammodytes* venom – studies of structure and function. *Periodicum Biologorum*, 82, 443–447.

Hatanaka, H. (1981). Nerve growth factor-mediated stimulation of tyrosine hydroxylase activity in a clonal rat pheochromocytoma cell line. *Brain Research*, 222(2), 225–233.

Hincke, M. T. (1988). Conditions for improved adsorption of calmodulin to nitrocellulose: detection by 45Ca binding. *Electrophoresis*, 9(7), 303–306.

Hogema, B. M., Arents, J. C., Bader, R., Eijkemans, K., Inada, T., Aiba, H., & Postma, P. W. (1998). Inducer exclusion by glucose 6-phosphate in *Escherichia Coli*. *Molecular Microbiology*, 28(4), 755–765.

Hogema, B. M., Arents, J. C., Bader, R., & Postma, P. W. (1999). Autoregulation of lactose uptake through the LacY permease by enzyme IIA_{glc} of the PTS in *Escherichia Coli* K-12. *Molecular Microbiology*, 31(6),1825–1833.

Hseu, M. J, Yen, C. Y, Tseng, C. C, & Tzeng, M. C. (1997). Purification and partial amino acid sequence of a novel protein of the reticulocalbin family. *Biochemical and Biophysical Research Communications,* 239(1), 18–22.

Hseu, M. J., Yen, C. Y., & Tzeng, M. C. (1999). Crocalbin: a new calcium-binding protein that is also a binding protein for crotoxin, a neurotoxic phospholipase A_2. *FEBS Letters*, 445(2–3), 440–444.

Inada, T., Kimata, K., & Aiba, H. (1996). Mechanism responsible for glucose-lactose diauxie in *Escherichia Coli*: Challenge to the cAMP model. *Genes to Cells*, 1(3), 293–301.

Ivanovski, G., Petan, T., Križaj, I., Gelb, M. H., Gubenšek, F., & Pungerčar, J. (2004). Basic amino acid residues in the beta-structure region contribute, but not critically, to presynaptic neurotoxicity of ammodytoxin A. *Biochimica et Biophysica Acta*, 1702(2), 217–225.

Jain, M. K, & Berg, O. G. (2006). Coupling of the i-face and the active site of phospholipase A_2 for interfacial activation. *Current Opinion in Chemical Biology*, 10(5), 473–479.

Jemel, I., Ii, H., Oslund, R. C., Payré, C., Dabert-Gay, A., Douguet, D., ... Lambeau, G. (2011). Group X secreted phospholipase A_2 proenzyme is matured by a furin-like proprotein convertase and releases arachidonic acid inside of human HEK293 cells. *The Journal of Biological Chemistry*, 286(42), 36509–36521.

Jenko Pražnikar, Z., Kovačič, L., Rowan, E. G., Romih, R., Rusmini P, Poletti A, ... Pungerčar, J. (2008). A presynaptically toxic secreted phospholipase A_2 is internalized into motoneuron-like cells where it is rapidly translocated into the cytosol. *Biochimica et Biophysica Acta*,1783(6), 1129–1139.

Karaca, E., Melquiond, A. S. J., de Vries, S. J., Kastritis, P. L., & Bonvin, A. M. J. J. (2010). Building macromolecular assemblies by information-driven docking: introducing the HADDOCK multibody docking server. *Molecular & Cellular Proteomics*, 9(8), 1784–1794.

Kim, Y. J., Kim, K. P., Han, S. K., Munoz, N. M., Zhu, X., Sano, H., ... Cho, W. (2002). Group V phospholipase A_2 induces leukotriene biosynthesis in human neutrophils through the activation of group IVA phospholipase A_2. *The Journal of Biological Chemistry*, 277(39), 36479–36488.

Kini, R. M., (1997). *Venom phospholipase A2 enzymes: structure, function and mechanism.* Chichester, NY: John Wiley & Sons.

Klockenbusch, C., & Kast, J. (2010). Optimization of formaldehyde cross-linking for protein interaction analysis of non-tagged integrin β1. *Journal of Biomedicine and Biotechnology*, 2010(5), 1–13.

Koh, T. W., & Bellen, H. J. (2003). Synaptotagmin I, a Ca^{2+} sensor for neurotransmitter release. *Trends in Neurosciences*, 26(8), 413–422.

Kordiš, D., & Križaj, I. (2015). Secreted phospholipases A_2 with β-neurotoxic activity. In P. Gopalakrishnakone (Ed.), *Handbook on Toxinology*. New York, NY: Springer, in

press.

Kovačič, L. (2009b). *Characterization of ammodytoxin's interaction to its binding proteins to explain their role in the process of neurotoxicity.* Doctoral dissertation. Ljubljana, Slovenija: Faculty of Medicine, University of Ljubljana.

Kovačič, L., Novinec, M., Petan, T., Baici, A., & Križaj, I. (2009a). Calmodulin is a nonessential activator of secretory phospholipase A_2. *Biochemistry* 48(47), 11319–11328.

Kovačič, L., Novinec, M., Petan, T., & Križaj, I. (2010). Structural basis of the significant calmodulin-induced increase in the enzymatic activity of secreted phospholipases A_2. *Protein Engineering, Design & Selection*, 23(6), 479–487.

Kovačič, L., Šribar, J., & Križaj, I., (2007). A new photoprobe for studying biological activities of secreted phospholipases A_2. *Bioorganic Chemistry*, 35(4), 295–305.

Križaj, I. (2011). Ammodytoxin: a window into understanding presynaptic toxicity of secreted phospholipases A_2 and more. *Toxicon*, 58(3), 219–229.

Križaj, I., Bieber, A. L., Ritonja, A. & Gubenšek, F. (1991). The primary structure of ammodytin L, a myotoxic phospholipase A_2 homologue from *Vipera ammodytes* venom. *European Journal of Biochemistry*, 202(3), 1165–1168.

Križaj, I., Dolly, J. O. & Gubenšek, F. (1994). Identification of the neuronal acceptor in bovine cortex for ammodytoxin C, a presynaptically neurotoxic phospholipase A_2. *Biochemistry*, 33(46), 13938–13945.

Križaj, I., Faure, G., Gubenšek, F. & Bon, C. (1997). Neurotoxic phospholipases A_2 ammodytoxin and crotoxin bind to distinct high-affinity protein acceptors in *Torpedo marmorata* electric organ. *Biochemistry*, 36(10), 2779–2787.

Križaj, I., Liang, N. S., Pungerčar, J., Štrukelj, B., Ritonja, A. & Gubenšek, F. (1992). Amino acid and cDNA sequences of a neutral phospholipase A_2 from the long-nosed viper (*Vipera ammodytes ammodytes*) venom. *European Journal of Biochemistry*. 204(3), 1057–1062.

Križaj, I., Rowan, E. G. & Gubenšek, F. (1995). Ammodytoxin A acceptor in bovine brain synaptic membranes. *Toxicon*, 33(4), 437–449.

Kuipers, O. P., van der Bergh, C. J., Verheij, H. M., & de Haas, G. H. (1990). Probing the mechanism of pancreatic phospholipase A_2 with the aid of recombinant DNA techniques. *Advances in Experimental Medicine and Biology*, 279, 65–84.

Laemmli, U. K. (1970). Cleavage of structural proteins during the assembly of the head of bacteriophage T4. *Nature*, 227(5259), 680–685.

Lambeau, G., Barhanin, J., Schweitz, H., Qar, J., & Lazdunski, M., (1989). Identification and properties of very high affinity brain membrane-binding sites for a neurotoxic phospholipase from the taipan venom. *The Journal of Biological Chemistry*, 264(19), 11503–11510.

Lambeau, G. & Gelb, M. H. (2008). Biochemistry and physiology of mammalian secreted phospholipases A_2. *Annual Review of Biochemistry*, 77, 495–520.

Lambeau, G., & Lazdunski, M. (1999). Receptors for a growing family of secreted phospholipases A_2. *Trends in Pharmacological Sciences*, 20(4), 162–170.

Lambeau. G., Schmid-Alliana, A., Lazdunski, M., & Barhanin, J., (1990). Identification and purification of a very high affinity binding protein for toxic phospholipases A_2 in skeletal muscle. *The Journal of Biological Chemistry*, 265(16), 9526–9532.

Lee, C. Y., Tsai, M. C., Chen, Y. M., Ritonja, A. & Gubenšek, F. (1984). Mode of

neuromuscular blocking action of toxic phospholipases A_2 from *Vipera ammodytes* venom. *Archives Internationales de Pharmacodynamie et de Therapie*. 268(2), 313–324.

Lencer, W. I., & Tsai, B. (2003). The intracellular voyage of cholera toxin: going retro. *Trends in Biochemical Sciences*, 28(12), 639–645.

Levi, A., Biocca, S., Cattaneo, A. & Calissano, P. (1988). The mode of action of nerve growth factor in PC12 cells. *Molecular Neurobiology*, 2(3), 201–226.

Logonder, U. (2008a). *Interaction of a neurotoxic phospholipase A_2 with the presynaptic membrane*. Doctoral dissertation. Ljubljana, Slovenija: Faculty of Medicine, University of Ljubljana.

Logonder, U., Jenko-Pražnikar, Z., Scott-Davey, T., Pungerčar, J., Križaj, I., & Harris, J. B. (2009). Ultrastructural evidence for the uptake of a neurotoxic snake venom phospholipase A_2 into mammalian motor nerve terminals. *Experimental Neurology*, 219(2), 591–594.

Logonder, U., Križaj, I., Rowan, E. G., & Harris, J. B. (2008b). Neurotoxicity of ammodytoxin a in the envenoming bites of Vipera ammodytes ammodytes. *Journal of Neuropathology & Experimental Neurology*, 67(10), 1011–1019.

Lord, J. M., Roberts, L. M., & Lencer, W. I. (2005). Entry of protein toxins into mammalian cells by crossing the endoplasmic reticulum membrane: co-opting basic mechanisms of endoplasmic reticulum-associated degradation. *Current Topics in Microbiology and Immunology*, 300, 149–168.

Lukšić, B., Bradarić, N., & Prgomet, S., (2006). Venomous snakebites in southern Croatia. *Collegium Antropologicum*, 30(1), 191–197.

Macchioni, L., Corazzi, L., Nardicchi, V., Mannucci, R., Arcuri, C., Porcellati, S., ... Goracci, G. (2004). Rat brain cortex mitochondria release group II secretory phospholipase A_2 under reduced membrane potential. *The Journal of Biological Chemistry*, 279(36), 37860–37869.

Mahapatro, S. N., & Robinson, N. C. (1990). Effect of changing the detergent bound to bovine cytochrome c oxidase upon its individual electron-transfer steps. *Biochemistry*, 29(3), 764–770.

Makarova, Y. V., Osipov, A. V., Tsetlin, V. I. & Utkin, Y. N. (2006). Influence of phospholipases A_2 from snake venoms on survival and neurite outgrowth in pheochromocytoma cell line PC12. *Biochemistry (Moscow)*, 71(6), 678–684.

Martin, H., Rostas, J., Patel, Y., & Aitken, A., (1994). Subcellular localisation of 14-3-3 isoforms in rat brain using specific antibodies. *Journal of Neurochemistry*. 63(6), 2259–2265.

Mattiazzi, M., Sun, Y., Wolinski, H., Bavdek, A., Petan, T., Anderluh, ... Petrovič, U. (2012). A neurotoxic phospholipase A_2 impairs yeast amphiphysin activity and reduces endocytosis. *PLoS One*, 7(7), e40931, doi:10.1371/journal.pone.0040931.

Megighian, A., Rigoni, M., Caccin, P., Zordan, M. A., & Montecucco, C. (2007). A lysolecithin/fatty acid mixture promotes and then blocks neurotransmitter release at the Drosophila melanogaster larval neuromuscular junction. *Neuroscience Letters*, 416(1), 6–11.

Merianda, T. T., Lin, A. C., Lam, J. S. Y., Vuppalanchi, D., Willis, D. E., Karin, N., ... Twiss, J. L. (2009). A functional equivalent of endoplasmic reticulum and Golgi in axons for secretion of locally synthesized proteins. *Molecular and Cellular Neurosciences*, 40(2), 128–142.

Montecucco, C., & Rossetto, O. (2000). How do presynaptic PLA_2 neurotoxins block nerve terminals? *Trends in Biochemical Sciences*, 25(6), 266–270.

Montecucco, C., Rossetto, O., Caccin, P., Rigoni, M., Carli, L., Morbiato, L., ... Paoli, M. (2009). Different mechanisms of inhibition of nerve terminals by botulinum and snake presynaptic neurotoxins. *Toxicon*, 54(5), 561–564.

Montecucco, C., Rossetto, O. & Schiavo, G. (2004). Presynaptic receptor arrays for clostridial neurotoxins. *Trends in Microbiology*, 12(10), 442–446.

Murakami, M., Masuda, S., Shimbara, S., Ishikawa, Y., Ishii, T., & Kudo, I. (2005). Cellular distribution, post-translational modification, and tumorigenic potential of human group III secreted phospholipase A_2. *The Journal of Biological Chemistry*, 280(26), 24987–24998.

Murakami, M., Taketomi, Y., Miki, Y., Sato, H., Hirabayashi, T., & Yamamoto, K. (2011). Recent progress in phospholipase A_2 research: from cells to animals to humans. *Progress in Lipid Research*, 50(2), 152–192.

Nadeau, O. W., & Carlson, G. M. (2007). Protein interactions captured by chemical cross-linking: one-step cross-linking with formaldehyde. *Cold Spring Harbor Protocols*, 2007, doi:10.1101/pdb.prot4634.

Nakashima, S., Ikeno, Y., Yokoyama, T., Kuwana, M, Bolchi, A., Ottonello, S., ... Arioka, M. (2003). Secretory phospholipases A_2 induce neurite outgrowth in PC12 cells. *The Biochemical Journal*, 376(3), 655–666.

Nardicchi, V., Ferrini, M., Pilolli, F., Angeli, E. B., Persichetti, E., Beccari, T., ... Goracci, G. (2014). NGF induces the expression of group IIA secretory phospholipase A_2 in PC12 cells: the newly synthesized enzyme is addressed to growing neurites. *Molecular Neurobiology*, 50(1), 15–25.

Nardicchi, V., Macchioni, L., Ferrini, M., & Goracci, G. (2007). The presence of a secretory phospholipase A_2 in the nuclei of neuronal and glial cells of rat brain cortex. *Biochimica et Biophysica Acta*, 1771(11), 1345–1352.

Neco, P., Rossetto, O., Gil, A., Montecucco, C., & Gutierrez, L. M., (2003). Taipoxin induces F-actin fragmentation and enhances release of catecholamines in bovine chromaffin cells. *Journal of Neurochemistry*, 85(2), 329–337.

Oberčkal, J. (2010). *Identification of ammodytoxin C-binding proteins in mammalian neuronal cells.* Bachelor thesis. Ljubljana, Slovenija: Faculty of Chemistry and Chemical Technology, University of Ljubljana.

Oberčkal, J., Kovačič, L., Šribar, J., Leonardi, A., Dolinar, K. Pucer Janež, A., & Križaj, I. (2015). On the role of protein disulfide isomerase in the retrograde cell transport of secreted phospholipases A_2. *PLoS One*, 10(3), e0120692, doi: 10.1371/journal.pone. 0120692.

Pang, Z. P., & Südhof, T. C. (2010). Cell biology of Ca^{2+}-triggered exocytosis. *Current Opinion in Cell Biology*, 22(4), 496–505.

Paoli, M., Rigoni, M., Koster, G., Rossetto, O., Montecucco, C., & Postle, A. D. (2009). Mass spectrometry analysis of the phospholipase A_2 activity of snake pre-synaptic neurotoxins in cultured neurons. *Journal of Neurochemistry*, 111(3), 737–744.

Petan, T., Križaj, I., Gelb, M. H., & Pungerčar, J. (2005). Ammodytoxins, potent presynaptic neurotoxins, are also highly efficient phospholipase A_2 enzymes. *Biochemistry*, 44(37), 12535–12545.

Petan, T., Križaj, I., & Pungerčar, J. (2007). Restoration of enzymatic activity in a Ser-49 phospholipase A_2 homologue decreases its Ca^{2+}-independent membrane-damaging

activity and increases its toxicity. *Biochemistry*, 46(44), 12795–12809.

Petrovič, U., Šribar, J., Matis, M., Anderluh, G., Peter-Katalinić, J., Križaj, I., & Gubenšek, F. (2005). Ammodytoxin, a secretory phospholipase A_2, inhibits G_2 cell cycle arrest in yeast *Saccharomyces cerevisiae*. *The Biochemical Journal*, 391(2), 383–388.

Petrovič, U., Šribar, J., Pariš, A., Rupnik, M., Kržan, M., Vardjan, N., ... Križaj, I. (2004). Ammodytoxin, a neurotoxic secreted phospholipase A_2, can act in the cytosol of the nerve cell. *Biochemical and Biophysical Research Communications*, 324(3), 981–985.

Prasarnpun, S., Walsh, J., Awad, S. S. & Harris, J. B. (2005). Envenoming bites by kraits: the biological basis of treatment-resistant neuromuscular paralysis. *Brain*, 128(12), 2987–2996.

Prasarnpun, S., Walsh, J., & Harris, J. B. (2004). Beta-bungarotoxin-induced depletion of synaptic vesicles at the mammalian neuromuscular junction. *Neuropharmacology*, 47(2), 304–14.

Prijatelj, P., Vardjan, N., Rowan, E. G., Križaj, I. & Pungerčar, J. (2006). Binding to the high-affinity M-type receptor for secreted phospholipases A_2 is not obligatory for the presynaptic neurotoxicity of ammodytoxin A. *Biochimie*, 88(10), 1425–1433.

Prijatelj-Žnidaršič, P., & Pungerčar, J. (2012). A recent evaluation of the lethal potencies of ammodytoxins. *Toxicon*, 59(6), 642–643.

Pucer, A. (2008). *The effect of ammodytoxin, the secreted phospholipase A_2 from the venom of the long-nosed viper, on the mitochondria of the model cell line PC12*. Bachelor thesis. Ljubljana, Slovenija: Faculty of Chemistry and Chemical Technology, University of Ljubljana.

Pungerčar, J., & Križaj, I. (2007). Understanding the molecular mechanism underlying the presynaptic toxicity of secreted phospholipases A_2. *Toxicon* 50(7), 871–892.

Pungercar, J., Križaj, I., Liang, N. S., & Gubenšek, F. (1999). An aromatic, but not a basic, residue is involved in the toxicity of group-II phospholipase A_2 neurotoxins. *The Biochemical Journal*, 341(1), 139–145.

Pungerčar, J., Vučemilo, N., Faure, G., Bon, C., Verheij, H. M., Gubenšek, F., & Križaj, I. (1998). Ammodytin L, an inactive phospholipase A_2 homologue with myotoxicity in mice, binds to the presynaptic acceptor of the beta-neurotoxic ammodytoxin C in *Torpedo*: an indication for a phospholipase A_2 activity-independent mechanism of action of beta-neurotoxins in fish? *Biochemical and Biophysical Research Communications*, 244(2), 514–518.

Quetglas, S., Iborra, C., Sasakawa, N., de Haro, L., Kumakura, K., Sato, K., ... Seagar, M., (2002). Calmodulin and lipid binding to synaptobrevin regulates calcium-dependent exocytosis. *The EMBO Journal*, 21(15), 3970–3979.

Quetglas, S., Leveque, C., Miquelis, R., Sato, K., & Seagar, M., (2000): Ca^{2+}-dependent regulation of synaptic SNARE complex assembly via a calmodulin- and phospholipid-binding domain of synaptobrevin. *Proceedings of the National Academy of Sciences USA*, 97(17), 9695–9700.

Radonić, V., Budimir, D., Bradarić, N., Lukšić, B., Sapunar, D., & Vilović, K. (1997). Envenomation by the horned viper (*Vipera ammodytes L.*). *Military Medicine*, 162(3), 179–182.

Radvanyi, F., Jordan, L., Russo-Marie, F., & Bon, C. (1989). A sensitive and continuous fluorometric assay for phospholipase A_2 using pyrene-labelled phospholipids in the presence of serum albumin. *Analytical Biochemistry*, 177(1), 103–109.

Rigoni, M., Caccin, P., Gschmeissner, S., Koster, G., Postle, A.D., Rossetto, O., ... Montecucco, C. (2005). Equivalent effects of snake PLA_2 neurotoxins and lysophospholipid-fatty acid mixtures. *Science*, 310(5754), 1678–1680.

Rigoni, M., Paoli, M., Milanesi, E., Caccin, P., Rasola, A., Bernardi, P., & Montecucco, C. (2008). Snake phospholipase A_2 neurotoxins enter neurons, bind specifically to mitochondria, and open their transition pores. *The Journal of Biological Chemistry*, 283(49), 34013–34020.

Rigoni, M., Pizzo, P., Schiavo, G., Weston, A.E., Zatti, G., Caccin, P., ... Montecucco, C. (2007). Calcium influx and mitochondrial alterations at synapses exposed to snake neurotoxins or their phospholipid hydrolysis products. *The Journal of Biological Chemistry*, 282(15), 11238–11245.

Rigoni, M., Schiavo, G., Weston, A. E., Caccin, P., Allegrini, F., Pennuto, M., ... Rossetto, O. (2004). Snake presynaptic neurotoxins with phospholipase A_2 activity induce punctate swellings of neurites and exocytosis of synaptic vesicles. *Journal of Cell Science*, 117(16), 3561–3570.

Rossetto, O., Morbiato, L., Caccin, P., Rigoni, M. & Montecucco, C. (2006). Presynaptic enzymatic neurotoxins. *Journal of Neurochemistry*, 97(6), 1534–1545.

Rufini, S., Cesaroni, M. P., Balestro, N., & Luly, P. (1996). Proliferative effect of ammodytin L from the venom of *Vipera ammodytes* on 208F rat fibroblasts in culture. *The Biochemical Journal*, 320(2), 467–472.

Rummel, A., Karnath, T., Henke, T., Bigalke, H., & Binz, T. (2004). Synaptotagmins I and II act as nerve cell receptors for botulinum neurotoxin G. *The Journal of Biological Chemistry*, 279(29), 30865–30870.

Salamon, Z., & Tollin, G. (1996). Surface plasmon resonance studies of complex formation between cytochrome c and bovine cytochrome c oxidase incorporated into a supported planar lipid bilayer. II. Binding of cytochrome c to oxidase-containing cardiolipin/phosphatidylcholine membranes. *Biophysical Journal*, 71(2), 858–867.

Sampson, V., & Alleyne, T. (2001). Cytochrome *c*/cytochrome c oxidase interaction. Direct structural evidence for conformational changes during enzyme turnover. *European Journal of Biochemistry / FEBS*, 268(24), 6534–6544.

Sandvig, K., Skotland, T., van Deurs, B., & Klokk, T. I. (2013). Retrograde transport of protein toxins through the Golgi apparatus. *Histochemistry and Cell Biology*, 140(3), 317–326.

Sandvig, K., & van Deurs, B. (2002). Transport of protein toxins into cells: pathways used by ricin, cholera toxin and Shiga toxin. *FEBS Letters*, 529(1), 49–53.

Schneider, C. A., Rasband, W. S., & Eliceiri, K. W. (2012). NIH Image to ImageJ: 25 years of image analysis. *Nature Methods*, 9(7), 671–675.

Scott, V. E. S., Parcej, D. N., Keen, J. N., Findlay, J. B. C., & Dolly, J. O. (1990). Alpha-dendrotoxin acceptor from bovine brain is a K+ channel protein. Evidence from the N-terminal sequence of its larger subunit. *The Journal of Biological Chemistry*, 265(33), 20094–20097.

Simonato, M., Morbiato, L., Zorzi, V., Caccin, P., Fernández, J., Massimino, M. L., ... Tonello, F. (2014). Production in *Escherichia coli*, folding, purification and characterization of notexin with wild type sequence and with N-terminal and catalytic site mutations. *Toxicon*, 88, 11–20.

Simpson, L. L. (2004) Identification of the major steps in botulinum toxin action. *Annual Review of Pharmacology and Toxicology*, 44, 167–193.

Simpson, L. L., Coffield, J. A., & Bakry, N. (1994). Inhibition of vacuolar adenosine triphosphatase antagonizes the effects of clostridial neurotoxins but not phospholipase A_2 neurotoxins. *The Journal of Pharmacology and Experimental Therapeutics*, 269(1), 256–262.

Simpson, L. L., Lautenslager, G. T., Kaiser, I. I., & Middlebrook, J.L. (1993). Identification of the site at which phospholipase A_2 neurotoxins localize to produce their neuromuscular blocking effects. *Toxicon*, 31(1), 13–26.

Singer, A. G., Ghomashchi, F., Le Calvez, C., Bollinger, J., Bezzine, S., Rouault, M., ... Gelb, M. H. (2002). Interfacial kinetic and binding properties of the complete set of human and mouse groups I, II, V, X, and XII secreted phospholipases A_2. *The Journal of Biological Chemistry*, 277(50), 48535–48549.

Spooner, R. A., & Lord, J. M. (2012). How ricin and Shiga toxin reach the cytosol of target cells: retrotranslocation from the endoplasmic reticulum. *Current Topics in Microbiology and Immunology*, 357, 19–40.

Studier, W. S. (2005). Protein production by auto-induction in high density shaking cultures. *Protein Expression and Purification*, 41(1), 207–234.

Su, M. J., & Chang, C. C. (1984). Presynaptic effects of snake venom toxins which have phospholipase A_2 activity (beta-bungarotoxin, taipoxin, crotoxin). *Toxicon*, 22(4), 631–640.

Šribar, J., Anderluh, G., Fox, J. W., & Križaj, I. (2005). Protein disulphide isomerase binds ammodytoxin strongly: possible implications for toxin trafficking. *Biochemical and Biophysical Research Communications*, 329(2), 733–737.

Šribar, J., Čopič, A., Pariš, A., Sherman, N. E., Gubenšek, F., Fox, J. W., & Križaj, I. (2001). A high affinity acceptor for phospholipase A_2 with neurotoxic activity is a calmodulin. *The Journal of Biological Chemistry*, 276(16), 12493–12496.

Šribar, J., Čopič, A., Poljšak-Prijatelj, M., Kuret, J., Logonder, U., Gubenšek, F., & Križaj, I. (2003b): R25 is an intracellular membrane receptor for a snake venom secretory phospholipase A_2. *FEBS Letters*, 552, 309-314.

Šribar, J., & Križaj, I. (2011). Secreted phospholipases A_2 – not just enzymes. *Acta Chimica Slovenica*, 58(4), 678–688.

Šribar, J., Oberčkal, J., & Križaj, I. (2014). Understanding the molecular mechanism underlying the presynaptic toxicity of secreted phospholipases A_2: an update. *Toxicon*, 89, 9–16.

Šribar, J., Sherman, N. E., Prijatelj, P., Faure, G., Gubenšek, F., Fox, J. W., ... Križaj, I. (2003a). The neurotoxic phospholipase A_2 associates, trough a non-phosphorylated binding motif, with 14-3-3 protein γ and ε isoforms. *Biochemical and Biophysical Research Communications,* 302(4), 691–696.

Taylor, M., Banerjee, T., Navarro-Garcia, F., Huerta, J., Massey, S., Burlingame, M., ... Teter, K. (2011a). A therapeutic chemical chaperone inhibits cholera intoxication and unfolding/translocation of the cholera toxin A1 subunit. *PLoS One*, 6(4), e18825, doi:10.1371/journal.pone.0018825.

Taylor, M., Banerjee, T., Ray, S., Tatulian, S. A., & Teter, K. (2011b). Protein-disulfide isomerase displaces the cholera toxin A1 subunit from the holotoxin without unfolding the A1 subunit. *The Journal of Biological Chemistry*, 286(25), 22090–22100.

Thouin, L. G., Ritonja, A., Gubenšek, F. & Russell, F. E. (1982). Neuromuscular and lethal effects of phospholipase A from *Vipera ammodytes* venom. *Toxicon*, 20(6), 1051–1058.

Tian, G., Xiang, S., Noiva, R., Lennarz, W. J., & Schindelin, H. (2006). The crystal structure of yeast protein disulfide isomerase suggests cooperativity between its active sites. *Cell*, 124(1), 61–73.

Towbin, H., Staehelin, T. & Gordon, J. (1979). Electrophoretic transfer of proteins from polyacrylamide gels to nitrocellulose sheets: procedure and some applications. *Proceedings of the National Academy of Sciences USA*, 76(9), 4350–4354.

Treppmann, F., Brunk, I., Afube, T., Richter, K., & Ahnert-Hilger, G. (2011). Neurotoxic phospholipases directly affect synaptic vesicle function. *Journal of Neurochemistry*, 117(4), 757–764.

Trifaró, J. M., Fournier, S., & Novas, M. L. (1989). The p65 protein is a calmodulin-binding protein present in several types of secretory vesicles. *Neuroscience*, 29(1), 1–8.

Tsai, B., Ye, Y., & Rapoport, T. A. (2002). Retro-translocation of proteins from the endoplasmic reticulum into the cytosol. *Nature Reviews. Molecular Cell Biology*, 3(4), 246–255.

Tsukita, S., & Ishikawa, H. (1976). Three-dimensional distribution of smooth endoplasmic reticulum in myelinated axons. *Journal of Electron Microscopy (Tokyo),* 25(3), 141–149.

Tsukita, S., & Ishikawa, H. (1979). Morphological evidence for the involvement of the smooth endoplasmic reticulum in axonal transport. *Brain Research*, 174 (2), 315–318.

Valentin, E., & Lambeau, G. (2000). Increasing molecular diversity of secreted phospholipases A_2 and their receptors and binding proteins. *Biochimica et Biophysica Acta*, 1488(1–2), 59–70.

Verheij, H. M., Slotboom, A. J., & de Haas, G. H. (1981). Structure and function of phospholipase A_2. *Reviews of Physiology, Biochemistry and Pharmacology*, 91, 91–203.

Vučemilo, N., Čopič, A., Gubenšek, F., & Križaj, I. (1998). Identification of a new high-affinity binding protein for neurotoxic phospholipases A_2. *Biochemical and Biophysical Research Communications*, 251(1), 209–212.

Wernick, N. L. B., Chinnapen, D. J., Cho, J. A., & Lencer, W. I. (2010). Cholera toxin: an intracellular journey into the cytosol by way of the endoplasmic reticulum. *Toxins*, 2(3), 310–325.

Wessel, D., & Flügge, U. I. (1984). A method for the quantitative recovery of protein in dilute solution in the presence of detergents and lipids. *Analytical Biochemistry*, 138(1), 141–143.

Yoshikawa, S., Muramoto, K., Shinzawa-Itoh, K., & Mochizuki, M. (2012). Structural studies on bovine heart cytochrome c oxidase. *Biochimica et Biophysica Acta*, 1817(4), 579–589.

Index of Figures

Figure 1: *Reaction catalyzed by PLA_2*. The figure shows hydrolysis of the *sn-2* ester bond of 1-palmitoyl-2-arachidonyl-phosphatidylcholine by PLA_2, yielding free arachidonic acid and 1-palmitoyl-lysophosphatidylcholine. The figure is taken from Lambeau & Gelb (2008). 1

Figure 2: *The proposed mechanism of $sPLA_2$-catalyzed phospholipid hydrolysis.* (a) The first proposed mechanism of $sPLA_2$ catalytic action involves a water molecule that is hydrogen-bonded to the nitrogen atom in the imidazole ring of His48. The oxygen in the water molecule attacks the carbonyl carbon of the substrate. The proton is transferred from the water to the imidazole nitrogen. The carbonyl carbon of the substrate is bound to the Ca^{2+} ion. (b) A proposed tetrahedral intermediate resulting from the mechanism depicted in panel a. The Ca^{2+} ion stabilizes the oxyanion derived from the substrate carbonyl oxygen. (c) The phospholipid intermediate state analogue bound in the active site, as revealed by X-ray crystallography. The blue structure mimics the proposed intermediate in panel b. (d) Jain & Berg (2006) proposed a mechanism involving two water molecules. According to this scenario, the Ca^{2+}-coordinated water molecule acts as a nucleophile and the proton from this water molecule is transferred to another water molecule with concomitant proton transfer from this second water molecule to the imidazole nitrogen of His48. (e) The proposed tetrahedral intermediate resulting from the mechanism in (d). The substrate, substrate-derived intermediates and the phospholipid analogue are shown in blue. The figure is taken from Lambeau & Gelb (2008). 3

Figure 3: *Three-dimensional structure of ammodytoxin.* AtxA differs from AtxB in 3 amino acid residues (Y115H/R118M/N119Y, shown in green) and from AtxC in 2 residues (F124I/K128E, shown in blue). Figure is taken from Križaj (2011). 5

Figure 4: *The triphasic effect of Atx on the isolated neuromuscular preparation.* Indirectly stimulated isolated neuromuscular preparation exhibits the characteristic triphasic response due to the action of the β-ntx. The complete paralysis of the muscle occurs approximately 1 h after the exposure to Atx. Figure is taken from Križaj (2011)..... 5

Figure 5: *Electron micrographs of motor endplates in a mouse soleus muscle fibre exposed to AtxA*. (A) The control muscle fibre without the added AtxA. (B–D) Muscle fibres exposed to AtxA. (B) The arrows point to damaged mitochondria in the motor neuron terminal. The depletion of SVs is evident (small circles in A that are largely absent in B). (D) SV clustering was observed within the cytosol and at release sites (indicated with arrows and numbers). Corresponding numbered areas of SV clustering are enlarged and shown in D1, D2 and D3. The figure was taken from Logonder et al. (2008b). 7

Figure 6: *Possible mode of action of β-ntxs.* The key events in the currently perceived model of β-neurotoxicity are indicated. Figure was taken from Kordiš & Križaj, 2015. 12

Figure 7: *Scheme of isolation of Atx-binding proteins from SVs.* 26

Figure 8: *Detection of Syt1/2 in isolated SV preparations from porcine cerebral cortex and NGFD PC12 cells.* Porcine brain SV and NGFD PC12 SV were dissolved and separated on a 12.5% (v/v) polyacrylamide gel by SDS-PAGE and probed for the presence of Syt1/2 by specific immunodetection following western blotting onto a PVDF membrane. Arrowheads indicate the anti-Syt1/2 polyclonal antibodies-reactive bands. In both preparations, three bands were detected, the upper representing the whole Syt1/2, the middle probably the deglycosylated Syt1/2 and the lower band the cytosolic part of Syt1/2 produced by proteolysis during the isolation. 36

Figure 9: *Specific labelling of SV proteins with sulfo-SBED-AtxC and ^{125}I-AtxC.* Intact SV from porcine brain (A) or NGFD PC12 cells (B) or detergent-solubilized SV proteins from both sources (C) were incubated in the presence of the biotin-containing photo-reactive sulfo-SBED-AtxC in the presence of Ca^{2+} or EGTA. The control samples contained 100-fold molar excess of the native AtxC (+). Another control contained no sulfo-SBED-AtxC (/). After incubation, covalent cross-linking of Atx to its binding proteins was triggered by exposure to UV light. The biotin-containing proteins were detected by western blotting and strepatavidin-HRP detection. Black arrowheads indicate specific Atx-binding proteins. White arrowheads indicate sulfo-SBED-AtxC (B, C) and its dimer (A, B, C). (D) Detergent-solubilized SV proteins were incubated in the presence of the radioactive ^{125}I-AtxC and Ca^{2+}. The control samples (+) contained 200-fold molar excess of the native AtxC over ^{125}I-AtxC. ^{125}I-AtxC was covalently cross-linked to its binding proteins by the addition of DSS. Samples were analyzed by SDS-PAGE and autoradiography. The specific band is indicated with a black arrow and represents the covalent complex of ^{125}I-AtxC with its binding protein. White arrow indicates the dimer of ^{125}I-AtxC. 37

Figure 10: *Isolation of Atx-binding proteins from porcine brain SVs.* We isolated the Atx-binding proteins from SVs by cross-linking them first with sulfo-SBED-AtxC. In samples A and B, the proteins were extracted from SVs prior to cross-linking, while in samples C and D intact SV membranes were reacted with the AtxC photo-probe. From sample A we removed the intrinsically biotinylated proteins prior to addition of sulfo-SBED-AtxC. Sample C is a control with no sulfo-SBED-AtxC added. In samples C and D proteins were extracted after sulfo-SBED-AtxC labelling. All samples were then subjected to avidin-affinity chromatography to isolate the biotinylated proteins. The eluates A_{EL}, B_{EL}, C_{EL} and D_{EL} were then analyzed on SDS-PADE, blotted and detected with SA-HRP (A), or silver stained (B). As a control, on the same blot we also analyzed a sulfo-SBED-AtxC-labelled extract of SV proteins in the presence (+) or absence (–) of 100-fold molar excess of the native AtxC or the SV extract without the added sulfo-SBED-AtxC (/). Specific Atx-binding proteins are indicated with black arrowheads, and sulfo-SBED-AtxC and its multimeres with white arrowheads. 39

Figure 11: *Atx specifically binds to Syt1 and CcO.* Purified human Syt1 (A, B) and bovine heart CcO (C, D) were incubated in the presence of the biotin-containing photo-reactive sulfo-SBED-AtxC (A, C) or the radioactive ^{125}I-AtxC (B, D). The control samples contained 100-fold molar excess of the native AtxC (+). (A, C) After the incubation, the sulfo-SBED-AtxC samples were exposed to UV light to initiate the photo-chemical binding of AtxC to its binding protein, and analyzed with SDS-PAGE followed by western blotting. The presence of a reducing agent in the SDS-PAGE loading buffer caused the transfer of the biotin tag from sulfo-SBED-AtxC to the protein to which it was bound. We detected biotinylated Syt1 or subunits of CcO with SA-HRP on the blot. (B, D) ^{125}I-AtxC was covalently cross-linked to Syt1 or CcO using formaldehyde or DSS, respectively. Samples were analyzed by SDS-PAGE and autoradiography. Bands represent the covalent complexes of ^{125}I-AtxC and its binding proteins. Specific binding of AtxC to Syt1 and CcO is indicated with black arrowheads. Monomers and dimers of sulfo-SBED-AtxC or ^{125}I-AtxC are indicated with white arrowheads. Representative results of two independent assays are shown. 40

Figure 12: *Interaction of Atx with CcO is Ca^{2+}-dependent.* CcO was incubated with ^{125}I-AtxC and then the cross-linker DSS was added (–). The control sample contained also a 100-fold molar excess of the native AtxC (+). The third sample was the same as the first, just that instead of Ca^{2+} ions it contained EGTA. Samples were analyzed by SDS-PAGE and the gel autoradiographed. The results clearly show that ^{125}I-AtxC requires Ca^{2+} to complex with CcO (black arrow). Monomer and dimer of ^{125}I-AtxC are indicated with white arrowheads. A representative result of two independent assays is shown. 41

Figure 13: *Syt1 has two binding sites for Atx.* Recombinant cytosolic and the luminal part of Syt1 were probed for their ability to bind Atx. (A) The cytosolic part of Syt1 (500 nM final concentration) was incubated with sulfo-SBED-AtxC in the presence (+) or absence (–) of a large molar excess of the native AtxC. (B) In a similar assay the full-length Syt1 (100 nM final concentration) was incubated with sulfo-SBED-AtxC in the presence (+) or absence (–) of an excess of Atx over sulfo-SBED-AtxC or a 100-fold molar excess of the luminal part of Syt1 over the full-length Syt1. After UV-cross-linking the samples were analyzed with SDS-PAGE and western blot. The biotinylated Syt1 was detected using SA-HRP. (A) AtxC specifically interacted with the cytosolic part of Syt1, indicating the position of one binding site for Atx resides at this part of Syt (black arrowhead). (B) The interaction of AtxC with the full-length Syt1 was largely, but not completely, inhibited in the presence of an excess of the luminal Syt1 (upper black arrowhead). At these concentrations, also the luminal part of Syt1 was obviously cross-linked with sulfo-SBED-AtxC (black arrowhead at the bottom). Both these results indicate that Atx also interacts with the luminal part of Syt1. Atx therefore seems to bind to two discrete locations on Syt1. Monomer and multimers of biotinylated AtxC are indicated with white arrowheads. Representative results of two independent assays are shown. 42

Figure 14: *The interaction of Atx with Syt1 is partially inhibited in the absence of Ca^{2+}.* Syt1 was labelled with sulfo-SBED-AtxC in the presence of Ca^{2+} and the presence (+) or absence (–) of a 100-fold molar excess of the unlabelled AtxC over the labelled. The third sample was the same as the first, except that instead of Ca^{2+} ions it contained EGTA. After the UV-cross-linking, the samples were analyzed by SDS-PAGE and western blotted onto a PVDF membrane. Biotinylated Syt1 was detected on the blot with SA-HRP. Monomer and dimer of biotinylated AtxC are indicated with white arrowheads. Representative result of three independent assays is shown. 43

Figure 15: *Effect of the presence of CaM and the luminal Syt1 on the Atx–Syt1 complex formation.* Syt1 (40 nM) was incubated with ^{125}I-AtxC (10 nM) in the presence of a 100-fold molar excess of the luminal Syt1 over the full length Syt1, CaM, equimolar to the full-length Syt1, or CaM and the excess of the luminal Syt1. The control reaction (+) contained a large excess of unlabelled AtxC over ^{125}I-AtxC. Only CaM – the sample contained only CaM and ^{125}I-AtxC. After the incubation, the proteins in complex were cross-linked with paraformaldehyde and analyzed by SDS-PAGE, followed by autoradiography. Interestingly, the presence of CaM in the reaction increased cross-linking of Syt1 and ^{125}I-AtxC. The presence of both, luminal Syt1 and CaM, however, almost completely inhibited the formation of Atx–Syt1 complex, indicating that CaM inhibits the binding of Atx to the cytosolic part of Syt1. The bands, corresponding to complexes of Syt1 and CaM with ^{125}I-AtxC, are indicated with black arrowheads. White arrowheads indicate the dimer and trimer of ^{125}I-AtxC. 44

Figure 16: *Syt1 specifically interacts also with other sPLA$_2$s.* Syt1 was incubated with ^{125}I-AtxC in the absence (–) or the presence of a 100-fold molar excess of the indicated sPLA$_2$s. The interacting proteins were covalently cross-linked after the addition of formaldehyde. Then the samples were analyzed by SDS-PAGE and the gel autoradiographed. Results show that also some other sPLA$_2$s, neurotoxic or mammalian, specifically interact with Syt1. 45

Figure 17: *Effect of the presence of Syt1 and CcO on Atx's phospholipase activity.* Syt1 (A) and CcO (B) were probed for the ability to modulate AtxC's enzymatic activity, as described in 3.2.6. Control samples contained no AtxC. Another control in the case of CcO contained AtxC and the detergent lauryl maltoside, but no CcO. Experimental data from two independent measurements were fitted with the 3rd order polynomial to calculate the initial velocity of the enzymatic reaction. The extent of modulation (v_a/v_0) is presented as the ratio between the initial velocity in the case of AtxC in the presence of Syt1 or CcO (v_a), and the initial velocity in the case of AtxC alone (v_0). Error bars represent standard deviation. 46

Figure 18: *Atx interacts with Syt1, PDI and R25 in intact PC12 cells.* ND and NGFD PC12 cells were incubated in the presence of sulfo-SBED-AtxC for indicated periods of time. The cells were then exposed to UV light to photo-chemically link AtxC-probe to its binding proteins. From cell lysates the biotinylated proteins were isolated on avidin-beads and (A, B) immunologically probed for the presence of Syt1 and PDI or (C) subjected to another affinity-based purification step, immunoprecipitation with anti-Atx antibodies, followed by detection of biotinylated proteins on the western blot. (A, B) PDI and Syt1 were immuno-detected in the samples but not in controls (no sulfo-SBED-AtxC added), indicating that Atx encountered these proteins also in living cells. (D) Using biotin-based detection, we visualized a band at 25 kDa, representing R25, suggesting that Atx interacts also with this protein in the living PC12 cells. Positions of sulfo-SBED-AtxC on blots are indicated by white arrowhead. 47

Figure 19: *The 3D model of the interaction between Atx and hPDI.* To obtain the model of the Atx–hPDI complex, the structure of hPDI was superimposed on the structure of yPDI in the model of its complex with Atx. Then, the energetically most favourable model was generated by protein docking with HADDOCK. Docking resulted in a model (A), where Atx (shown in cartoon mode) binds *via* its IBS site to the surface of b and b' domains of hPDI (shown in space-filling mode). PDI domains are indicated. (B) A detailed view of the Atx–hPDI interaction site. The amino acid residues of Atx (cartoon mode) that interact with PDI (space-fill mode) are shown in stick mode and are numbered. The b and b' domains of PDI are indicated. The images were displayed with PyMOL. 48

Figure 20: *3D models of complexes between $sPLA_2$s and hPDI.* By substitution of Atx in the model of Atx–hPDI complex with AtnL, $AtnI_2$, GIB, GIIA, GV or GX $sPLA_2$, and HADDOCK molecular docking, complexes of these $sPLA_2$s with hPDI were modelled. AtnL, GV, GIB and GIIA $sPLA_2$ interact with the same area on hPDI as Atx (A), while $AtnI_2$ and GX $sPLA_2$ interact with only part of this area (B). (C) Interactions of these $sPLA_2$s with hPDI are mostly electrostatic. The strength of their interactions is similar as in the case of Atx. (D) Heterologous competition of sulfo-SBED-AtxC binding to hPDI by $AtnI_2$, AtnL, GV and GX $sPLA_2$s confirms validity of proposed $sPLA_2$–hPDI 3D models. Human PDI was incubated with sulfo-SBED-AtxC in the dark in the presence of 26 to 100-fold molar excess of AtxC, $AtnI_2$, AtnL, hGV or hGX $sPLA_2$ over the sulfo-SBED-AtxC. The photo cross-linking reaction was triggered by irradiation at 312 nm. SDS-PAGE analysis under reducing conditions was followed by western blotting of the samples on the nitrocellulose membrane and biotin-specific detection. Black arrowhead indicates the biotinylated hPDI. White arrowheads indicate positions of biotinylated monomeric and dimeric AtxC. 50

Figure 21: *Purification of AtxA(D49S by RP-HPLC.* The last purification step of the AtxA(D49S) mutant was on the analytical C18 RP-HPLC column, as described in 3.2.7.3.3. AtxA(D49S) (black line) eluted at the same retention time (indicated with the arrowhead) as the wild-type AtxA (AtxA WT, grey solid line), indicating the correct folding of the mutant. 52

Figure 22: *AtxA(D49S) was pure and correctly folded.* The purity of the refolded mutant was assayed by SDS-PAGE, followed by silver staining (A) and by MS (B). (A) The arrowhead shows the position of AtxA(D49S). (B) The molecular mass of the product was 13747 Da, identical to the theoretical mass of AtxA(D49S). This indicates that all 14 Cys were connected to form 7 disulphide bonds. The recombinant product, containing Met on its N-terminus, was undetectable at 13895 Da. (C) CaM was cross-linked with ^{125}I-AtxC in the absence (–) or the presence of indicated excess amounts of native AtxC or AtxA(D49S). Samples were analyzed by SDS-PAGE and the gel autoradiographed. Results indicate that the mutant binds CaM with a similar affinity as AtxC, additionally indicating the correct folding of the mutant. 53

Figure 23: *Phospholipase activity of AtxA(D49S) is below the detection limit.* (A) The AtxA(D49S) mutant was probed for its enzymatic activity with the PyPG method (3.2.6) at a 100-fold higher concentration as the native AtxC. Experimental data were fitted with the 3rd order polynomial to calculate the initial velocity of the enzymatic reaction. (B) Initial enzyme reaction velocity of AtxA(D49S) (v_0) from two independent measurements was compared with the initial velocity of the native AtxC at a 100 times lower concentration or the blank without an sPLA$_2$. The mutant did not exhibit any measurable phospholipase activity. Error bars represent standard deviation. 54

Figure 24: *RP-HPLC purification of ^{546}Alexa-AtxA(D49S).* After the conjugation reaction, ^{546}Alexa-AtxA(D49S) was purified on a C4 RP-HPLC column, as described in 3.2.7.4. Collected fractions of AtxA(D49S) (black line) Alexa-DS2 – Alexa-DS8 are indicated. As a standard, the non-labelled AtxA(D49S) was also analyzed (grey solid line). 55

Figure 25: *Mass spectrum of ^{546}Alexa-AtxA(D49S).* After labelling AtxA(D49S) with ^{546}Alexa, the reaction mixture was purified by RP-HPLC and fractions analyzed by MS. The MS spectra revealed two main products in the fraction Alexa-DS5. The main one corresponded to the ^{546}Alexa-AtxA(D49S) monoderivative, the molecular mass of which was 7 Da higher than the theoretical (14689 Da). The mass of the minor product was 14712 Da and probably represented the form with one of the two Met, present in ^{546}Alexa-AtxA(D49S), oxidized. 56

Figure 26: *Analysis of ^{546}Alexa-AtxA(D49S) fractions from the RP-HPLC.* After labelling AtxA(D49S) with ^{546}Alexa, the reaction mixture was purified by RP-HPLC and the fractions analyzed by SDS-PAGE. In the right-most lane on the gel, Alexa-labelled native AtxA was analyzed. The gel was visualized using fluorescence scanner (left picture) and Coomassie blue staining (right picture). As evident from the left picture, fraction Alexa-DS5, which contained the ^{546}Alexa-AtxA(D49S) monoderivative (the lowest black arrowhead), still contained some free ^{546}Alexa dye (white arrowhead). Also some dimer and trimer of ^{546}Alexa-AtxA(D49S) are visible (upper two black arrowheads). Coomassie blue staining (right picture) did not reveal the presence of other proteins than ^{546}Alexa-AtxA(D49S). 57

Figure 27: *The ability of ^{546}Alexa-AtxA(D49S) to bind to CaM.* CaM was incubated with ^{125}I-AtxC in the absence (T) or in the presence of 10- and 100-fold molar excess of AtxC, and the RP-HPLC fractions of ^{546}Alexa-labelled AtxA(D49S): Alexa-DS3, Alexa-DS4 and Alexa-DS5. The proteins were covalently cross-linked by the addition of cross-linker DSS and analyzed by SDS-PAGE followed by autoradiography of the gel. All Alexa-derivatives of AtxA(D49S) (fractions Alexa-DS3 to 5) were able to inhibit the binding of ^{125}I-AtxC to CaM but with lower potency than the native AtxC. 57

Figure 28: *Internalization and localization of ^{546}Alexa-AtxA and ^{546}Alexa-AtxA(D49S) in PC12 cells.* ND and NGFD PC12 cells were incubated in the presence of 100 nM ^{546}Alexa-AtxA or ^{546}Alexa-AtxA(D49S), the enzymatically inactive mutant. Cells were washed and fixed and the cover glasses prepared as described in 3.2.8.2.1. The images show the transmitted light and the red signal of both variants of ^{546}Alexa-Atx. The images were obtained with the Carl Zeiss LSM 710 confocal microscope at 63x magnification and displayed with the ZEN software. Scale bars represent 10 µm. For experimental details, refer to the section 3.2.8.2.2. 60

Figure 29: *Co-localization of ^{546}Alexa-AtxA and ^{546}Alexa-AtxA(D49S) with Syt1, CcO, PDI and 14-3-3p in PC12 cells.* ND and NGFD PC12 cells were incubated in the presence of 100 nM ^{546}Alexa-AtxA or ^{546}Alexa-AtxA(D49S) for the indicated time periods. After fixation, the cells were immunologically stained for Syt1 (A, B), CcO subunit 2 (C, D), PDI (E, F) or 14-3-3p (G, H). The cover glasses were mounted and slides analyzed with fluorescence microscopy, using a Carl Zeiss LSM 710 confocal microscope. Images were obtained at 63x magnification. The red signal represents ^{546}Alexa-AtxA or its enzymatically inactive variant. The green signal represents immunologically detected cellular proteins, Syt1 (A, B), CcO subunit 2 (C, D), PDI (E, F) or 14-3-3p, respectively. Sites of co-localization of the red and green signal are displayed in white and indicated by arrows. Scale bars represent 10 µm. Experimental details can be found in section 3.2.8.2. 66

Figure 30: *Extent of co-localization of ^{546}Alexa-AtxA or ^{546}Alexa-AtxA(D49S) with intracellular proteins over time.* The Z-stacks of confocal microscopy images of co-localization of either ^{546}Alexa-AtxA or ^{546}Alexa-AtxA(D49S) with Syt1 (A), CcO (B), PDI (C) or 14-3-3p (D) were processed with ImageJ with the co-localization plugin JaCOP. The extent of co-localization was expressed in terms of Manders' coefficient and plotted as a function of incubation time of PC12 cells with ^{546}Alexa-labelled protein. In all cases, except for CcO in NGFD PC12 cells, the enzymatically inactive mutant of AtxA co-localized with the assayed intracellular proteins to a lesser extent than AtxA. 68

Appendices

Oberčkal, J., Kovačič, L., Šribar, J., Leonardi, A., Dolinar, K., Pucer Janež, A., & Križaj, I. (2015). On the role of protein disulfide isomerase in the retrograde cell transport of secreted phospholipases A_2. *PLoS One*, 10(3), e0120692, doi: 10.1371/journal.pone. 0120692.

Šribar, J., Oberčkal, J., & Križaj, I. (2014). Understanding the molecular mechanism underlying the presynaptic toxicity of secreted phospholipases A(2): an update. *Toxicon*, 89, 9–16.

PLOS ONE

RESEARCH ARTICLE

On the Role of Protein Disulfide Isomerase in the Retrograde Cell Transport of Secreted Phospholipases A_2

Jernej Oberčkal[1☯], Lidija Kovačič[1☯], Jernej Šribar[1☯], Adrijana Leonardi[1], Klemen Dolinar[1], Anja Pucer Janež[1], Igor Križaj[1,2]*

1 Department of Molecular and Biomedical Sciences, Jožef Stefan Institute, Ljubljana, Slovenia,
2 Department of Chemistry and Biochemistry, Faculty of Chemistry and Chemical Technology, University of Ljubljana, Ljubljana, Slovenia

☯ These authors contributed equally to this work.
* igor.krizaj@ijs.si

CrossMark
click for updates

OPEN ACCESS

Citation: Oberčkal J, Kovačič L, Šribar J, Leonardi A, Dolinar K, Pucer Janež A, et al. (2015) On the Role of Protein Disulfide Isomerase in the Retrograde Cell Transport of Secreted Phospholipases A_2. PLoS ONE 10(3): e0120692. doi:10.1371/journal.pone.0120692

Academic Editor: Bruno Lomonte, Universidad de Costa Rica, COSTA RICA

Received: November 21, 2014

Accepted: January 25, 2015

Published: March 12, 2015

Copyright: © 2015 Oberčkal et al. This is an open access article distributed under the terms of the Creative Commons Attribution License, which permits unrestricted use, distribution, and reproduction in any medium, provided the original author and source are credited.

Data Availability Statement: All relevant data are within the paper and its Supporting Information files.

Funding: This work was supported by grants P1-0207 (to IK) and Z1-4071 (to LK) from the Slovenian Research Agency (http://www.arrs.gov.si/sl/). The funder had no role in study design, data collection and analysis, decision to publish, or preparation of the manuscript.

Competing Interests: The authors have declared that no competing interests exist.

Abstract

Following the finding that ammodytoxin (Atx), a neurotoxic secreted phospholipase A_2 ($sPLA_2$) in snake venom, binds specifically to protein disulfide isomerase (PDI) *in vitro* we show that these proteins also interact in living rat PC12 cells that are able to internalize this group IIA (GIIA) $sPLA_2$. Atx and PDI co-localize in both differentiated and non-differentiated PC12 cells, as shown by fluorescence microscopy. Based on a model of the complex between Atx and yeast PDI (yPDI), a three-dimensional model of the complex between Atx and human PDI (hPDI) was constructed. The Atx binding site on hPDI is situated between domains b and b'. Atx interacts hPDI with an extensive area on its interfacial binding surface. The mammalian GIB, GIIA, GV and GX $sPLA_2$s have the same fold as Atx. The first three $sPLA_2$s have been detected intracellularly but not the last one. The models of their complexes with hPDI were constructed by replacement of Atx with the respective mammalian $sPLA_2$ in the Atx—hPDI complex and molecular docking of the structures. According to the generated models, mammalian GIB, GIIA and GV $sPLA_2$s form complexes with hPDI very similar to that with Atx. The contact area between GX $sPLA_2$ and hPDI is however different from that of the other $sPLA_2$s. Heterologous competition of Atx binding to hPDI with GV and GX $sPLA_2$s confirmed the model-based expectation that GV $sPLA_2$ was a more effective inhibitor than GX $sPLA_2$, thus validating our model. The results suggest a role of hPDI in the (patho)physiology of some snake venom and mammalian $sPLA_2$s by assisting the retrograde transport of these molecules from the cell surface. The $sPLA_2$–hPDI model constitutes a valuable tool to facilitate further insights into this process and into the (patho) physiology of $sPLA_2$s in relation to their action intracellularly.

Introduction

Secreted phospholipases A_2 ($sPLA_2$s, EC 3.1.1.4) form an assemblage of enzymes secreted by cells that hydrolyse glycerophospholipids to *sn*-2 lysoglycerophospholipids and fatty acids [1]. The fundamental role of these molecules in physiology is reflected in the fact that they have been described from viruses to mammals. Based on their structural characteristics they are classified into eleven groups [2]. In humans there are ten enzymatically active $sPLA_2$s known, GIB, GIIA, GIIC-F, GIII, GV, GX and GXIIA, and two $sPLA_2$s apparently without enzymatic activity, GXIIB and otoconin-90/95. Expression patterns of these molecules in mammalian tissues differ, so their functions appear to be non-redundant [3]. Either by enzymatic activity or by binding to soluble or membrane receptors [4] these molecules are implicated in many physiological and pathological settings, such as innate immunity, asthma, atherosclerosis, inflammatory diseases, Alzheimer's disease, neuritogenesis, neurotransmitter release and various forms of cancer [5–8]. Despite intensive research on $sPLA_2$ pathophysiology, the mechanisms of action of most of the known $sPLA_2$-associated phenomena are not well understood. It is still widely supposed that $sPLA_2$s act exclusively extracellularly. However, growing evidence concerning the localization of some types of $sPLA_2$s inside various cells suggests that they also induce certain cellular processes from inside cells. In compartments other than those leading imported proteins to degradation or *de novo* synthesized proteins to secretion, three mammalian $sPLA_2$s have been detected, GIB, GIIA and GV $sPLA_2$. GIB $sPLA_2$ was found in the nucleus of UIII cells, a stromal cell line derived from normal rat uterus, GIIA in the mitochondria and GV $sPLA_2$ in the nucleus and cytoplasm of U251 astrocytoma, PC12 and P388D1 macrophage-like cells [9–12].

Snake venoms are a rich source of GI and GII $sPLA_2$s. These are closely related structurally to mammalian $sPLA_2$s and thus very useful for studying the function of the latter. Ammodytoxin (Atx), the GIIA $sPLA_2$ from the nose-horned viper (*Vipera a. ammodytes*) is among the most thoroughly studied snake venom $sPLA_2$s. This molecule is neurotoxic, acting at the presynaptic side of the neuro-muscular synapse [13]. It is internalized into the cytosol, synaptic vesicles and mitochondria of the motoneuron-like NSC34 cells [14], and into the mammalian motor nerve terminal, where it becomes associated with mitochondria and cytoplasmic vesicles [15]. Specific pathways must exist by which Atx crosses the plasma membrane to enter the cytosol and mitochondria of nerve cells and which are likely to share at least some common characteristics with pathways that mammalian orthologues are using. It is important to answer the question as to how Atx crosses cellular membranes, not only in describing the molecular mechanism of its neurotoxicity but also in shedding more light on the pathophysiological function of some homologous mammalian $sPLA_2$s.

Several years ago we demonstrated that Atx binds strongly *in vitro* to protein disulfide isomerase (PDI) [16]. PDI is an oxido-reductase, located in the lumen of the endoplasmic reticulum (ER) [17]. We proposed then that it could be implicated in the retrograde trafficking of this toxin in a similar way as revealed in the case of some other protein toxins [18–22]. Besides assisting Atx to move retrogradely from Golgi apparatus to ER, PDI can also help Atx to translocate across the ER membrane. Transport between Golgi apparatus and ER is mediated by cycling of the KDEL receptor. KDEL, or a similar sequence, is located specifically at the C-termini of the ER-resident proteins and prevents them from escaping from the ER lumen. While cholera toxin possesses this signal sequence intrinsically, in its A-subunit, Atx does not but may take advantage of the signal sequence of PDI if complexed with PDI *in vivo*, in the lumen of the ER. The results reported here strongly support the hypothesis that PDI partakes at the retrograde cellular transport of Atx and the related mammalian $sPLA_2$s. The $sPLA_2$–

hPDI model that we present provides a structural insight into the interaction between these proteins thus enabling a targeted study of the $sPLA_2$ cell internalization process.

Materials and Methods

Materials

Two isoforms of Atx, AtxA and AtxC, having very similar biological activity [13], were used in our experiments. They were purified from *Vaa* venom as described previously [23]. Sulfo-SBED reagent (sulfosuccinimidyl-2-[6-(biotinamido)-2-(*p*-azidobenzamido)-hexanoamido] ethyl-1,3′-dithio propionate), streptavidin conjugated with horseradish peroxidase (SA—HRP) and monomeric avidin were purchased from Pierce. The fluorogenic substrate PyPG for measuring phospholipase activity was prepared from 1-hexadecanoyl-2-(1-pyrenedecanoyl)-*sn*-glycero-3-phosphoglycerol (Molecular Probes) as described [24]. Bovine α-chymotrypsin, Triton X-100, Tween 20, dithiothreitol (DTT), N-2-hydroxyethylpiperazine-N-2-ethanesulfonic acid (HEPES), glutathione (reduced and oxidized forms) and fatty acid-free bovine serum albumin (BSA) were from Sigma. Human group V and group X $sPLA_2$ (hGV and hGX $sPLA_2$) were produced as described [25]. Recombinant wild type yeast PDI (wt yPDI) and its domains were a gift from Dr. William J. Lennarz, Stony Brook University, New York, USA. These proteins were produced as described [26]. Recombinant human PDI-A1 (hPDI-A1) was from Biorbyt. Rabbit polyclonal anti-PDI IgGs were form Enzo Life Sciences. Mouse polyclonal anti-calmodulin (CaM) IgGs were from Abcam. Protein-A Sepharose was from Amersham Biosciences. BM Chemiluminescence and Lumi-Light^{PLUS} Western Blotting Substrate were from Roche Diagnostics. Other chemicals were obtained mainly from Sigma and Serva and were of at least analytical grade.

PC12 cell culture

PC12 is a cell line derived from a pheochromocytoma of the rat adrenal medulla [27]. PC12 cells ATCC CRL-1721 (American Type Culture Collection, USA) were grown at 37°C under 5% (v/v) CO_2 in 10-cm culture plates in F12K (Kaighn's modification of Ham's F-12) growth medium (Gibco, USA) containing 15% (v/v) horse serum, 2.5% (v/v) fetal bovine serum, 100 units/mL of penicillin and 100 μg/mL streptomycin (culture medium). To induce differentiation, nerve growth factor (NGF) was added to the growth medium (100 ng/mL). After 48 hours, the cells were washed with phosphate buffered saline (PBS), fresh NGF-containing growth medium was added, and the cells grown for a further 48 hours. For microscopy, cells were plated on poly-L-Lys coated coverslips and, for viability and mitochondrial membrane potential assays, the cells were plated on 96-well plates.

Testing the influence of Atx on PC12 cells

The influence of Atx on the morphological integrity of non-differentiated (ND) and NGF-differentiated (NGFD) cells was examined. These cells were grown for 120 min at 37°C in the presence of 100 nM AtxC, then inspected for their morphological integrity under a phase contrast microscope Axio Observer Z1 (Carl Zeiss, Germany) using a Plan-Apochromat 40x/0.95 Corr Ph3 M27 objective.

The effect of Atx on the mitochondrial potential of PC12 cells was evaluated. The cells (ND and NGFD), in 96-well plates (10^4 cells per well), were incubated in the dark with 2 μM JC-1 dye (Life Technologies, USA) in F12K growth medium for 20 min at 37°C under 5% (v/v) CO_2. After washing with the medium, the cells were incubated in the dark for a further 30 min at 37°C under 5% (v/v) CO_2 in the growth medium alone (control) or in the medium

supplemented with either 100 nM AtxA or 50 μM CCCP (mitochondrial uncoupler carbonyl cyanide m-chlorophenyl hydrazone). The green fluorescence of JC-1 at 529 nm and the red fluorescence at 590 nm of aggregated JC-1 were measured in triplicate samples on a SAFIRE microplate reader (Tecan, Austria), using the excitation wavelength 488 nm. The mitochondrial membrane potential was exhibited as the ratio of red to green signals of the cells in the presence of the substance investigated relative to the same ratio in the absence of this substance.

The influence of Atx on the metabolic activity of PC12 cells was measured as follows. PC12 cells (ND and NGFD) in 96-well plates (5×10^4 cells per well) were incubated without (control) or with either 100 nM AtxA or 1% (m/v) Triton X-100 in culture medium at 37°C and 5% (v/v) CO_2. After different incubation times, the cells were washed twice with F12K growth medium and incubated in the dark for a further 2 hours at 37°C under 5% (v/v) CO_2 with MTS (3-(4,5-dimethylthiazol-2-yl)-5-(3-carboxymethoxyphenyl)-2-(4-sulfophenyl)-2H-tetrazolium) (20 μL per 100 μL F12K growth medium) prepared according to the manufacturer's (Promega, USA) instructions. After 2 hours, the absorbance at 490 nm was measured on a SAFIRE microplate reader. The background absorbance was measured on wells containing MTS in F12K growth medium without cells. Viability of cells was calculated from A_{490} corrected for background absorbance and presented relative to the control cells. Measurements were performed in triplicate.

Testing internalization of Atx into PC12 cells

The internalization test used by Jenko Pražnikar et al. [14] was used. In brief, sulfo-SBED-Atx, synthesized as described [28,29], was incubated in the dark with ND and NGFD PC12 cells in culture. Following photo-activation of the Atx probe, cellular proteins in tight complexes with the probe were labelled with biotin. Cells were lysed, the biotinylated proteins selectively extracted using avidin beads and probed for anti-CaM IgG cross-reactivity by Western blotting.

Labelling PDI in PC12 cells with sulfo-SBED-Atx

Intact PC12 cells (both ND and NGFD), plated on 10 cm plates at 80–90% confluence, were treated with sulfo-SBED-Atx at a final concentration of 100 nM for 1, 2, 5, 15, 30 and 60 min in Hank's balanced salt solution supplemented with 1.26 mM Ca^{2+} (Ca^{2+}/HBSS) in the dark at 37°C and 5% (v/v) CO_2. Subsequently, cells were cooled on ice, exposed for 5 min to five 15 W 312 nm UV lamps from a distance of 5 cm, washed twice with Ca^{2+}/HBSS, 1.5% (w/v). Triton X-100/Ca^{2+}/HBSS extracts were then prepared. Experiments were performed in duplicate using cells of the same passage. The extracts were centrifuged for 45 min at 14.000 × *g* and 4°C. Supernatants were incubated with 375 μL monomeric avidin beads for 1 hour at 4°C. The beads were thoroughly washed with Ca^{2+}/HBSS containing 0.1% (w/v) Triton X-100 and biotin containing proteins then eluted with 2 mM *D*-biotin. The fractions were concentrated and the proteins recovered as described [30]. The resulting pellets were dissolved in SDS-PAGE loading buffer and analyzed as described below. To standardize the amount of samples applied the intensity of the band corresponding to a protein of 85 kDa (present in control and sulfo-SBED-Atx labelled samples analysed on SDS-PAGE with silver staining) was used as a measure. The position of biotinylated PDI on the gel was determined immunologically using 0.3 μg/mL rabbit polyclonal anti-PDI antibodies.

Immunofluorescence studies

AtxA was dissolved in DMSO (2 mg/mL final concentration) and Alexa Fluor 546 (Molecular Probes Alexa Fluor546 Protein Labelling Kit, Life Technologies, USA) was added to a final protein: dye molar ratio of 1: 1.5 in the presence of 100 mM triethylamine. After 1 h shaking in the

dark at room temperature, taurine was added (5 mM final concentration) and the mixture incubated for a further 30 min. The reaction products were separated on RP-HPLC using an Aquapore BU 300 column (30 mm × 4.6 mm) (PerkinElmer, USA) equilibrated with 5% (v/v) solvent B (90% (v/v) acetonitrile and 0.1% (v/v) trifluoroacetic acid (TFA) in water) in solvent A (0.1% (v/v) TFA in water). After application of the sample, the column was washed with 5 mL of solvent A at a flow rate of 1 mL/min and the bound proteins then eluted with a gradient of solvent B in solvent A from 5% to 20% for 3 min, then from 20% to 60% B for 20 min and finally to 100% B for 3 min. Their absorbance was monitored at 215 nm. As selected by mass spectrometry analysis, the Alexa mono-derivative of AtxA (^{546}Alexa-Atx) was further characterized to confirm that its enzymatic activity and ability to bind to CaM do not differ from those of the native toxin.

PC12 cells on poly-L-lysine coated coverslips were incubated at 37°C and 5% (v/v) CO_2 in the presence of 100 nM ^{546}Alexa-Atx for 1, 2, 5, 15, 30, and 60 min. The cells were first washed three times with Dulbecco's phosphate buffered saline (DPBS) at room temperature and then fixed for 10 min in 4% (w/v) paraformaldehyde in DPBS at room temperature. After fixing, the cells were washed for 5 min with ice-cold DPBS, permeabilized for 5 min with ice-cold 0.1% (w/v) Triton X-100 in DPBS and then incubated at room temperature in blocking solution, containing 0.5% (w/v) fish skin gelatine and 10% (w/v) fetal bovine serum in DPBS. Coverslips were then immersed into primary anti-PDI antibody solution (diluted 1: 300 in blocking solution). After 60 min incubation at room temperature, the cells were rinsed three times for 5 min each in DPBS and then incubated for 60 min at room temperature in secondary antibody solution (Alexa Fluor 488 Goat Anti-Rabbit, diluted 1: 2.000 in blocking solution) and, finally, washed three times 5 min each in DPBS. Excess fluid was removed and the slides mounted using ProLong Gold antifade reagent and left to cure. After 24 hours at room temperature in the dark, the edges of the coverslips were sealed with nail polish and analyzed on an inverted confocal laser scanning microscope (Axio Observer Z1 LSM 710, Carl Zeiss, Germany) with a Plan-Apochromat 63/1.40 oil objective. Fluorophores were excited sequentially using Ar (488 nm) and He-Ne (543 nm) lasers. The emitted light was collected through SP 545 and LP 545 filters. Stacks of fluorescent images were acquired and co-localization of the red and green signal calculated with ImageJ [31] and co-localization plugin JACoP [32]. The signal threshold was determined from autofluorescence of the control cells, and was set at 20% of the maximum signal for both red and green channels. Co-localization was represented by Manders' coefficient, *i.e.* the ratio of the summed intensities of pixels from the green channel, for which the intensity in the red channel is above zero, to the total intensity in the green channel.

Preparation of sulfo-SBED-Atx—yPDI conjugates and their analysis

Equimolar amounts of sulfo-SBED-Atx and wt yPDI or its domains in 75 mM HEPES/HCl, pH 8.2, 150 mM NaCl and 2 mM $CaCl_2$ (labelling buffer) were mixed to give 7 μM concentration of each in a final volume of 50 μL. In competition binding assays, 0.5 μM yPDI or 0.2 μM wt hPDI was incubated with sulfo-SBED-Atx (0.5 μM) in the dark, in the absence or the presence of the following competitors: AtxC (50 μM), GV $sPLA_2$ (18 μM) or GX $sPLA_2$ (13 μM). For mapping the Atx—yPDI interaction surface, the final volume of the reaction mixture was 1 mL. After 60 min incubation at room temperature in the dark, the mixtures were irradiated for 10 min on ice by five 15 W UV lamps at 312 nm from a distance of 5 cm.

Sulfo-SBED-Atx labelled samples were analyzed on SDS-PAGE under reducing conditions. Proteins were transferred from the gel to the PVDF or nitrocellulose membrane by Western blotting in a tank filled with Towbin buffer (25 mM Tris/HCl, 192 mM glycine, 0.1% (w/v) SDS and 20% (v/v) MeOH) for 90 min at 200 mA. On the membrane the biotinylated proteins

were detected by SA—HRP and Lumi—Light^{PLUS} Western Blotting Substrate or the BM Chemiluminescence Western blotting detection system according to the manufacturer's instructions. Kodak BioMax Light Film was used for light capturing (Sigma—Aldrich).

Isolation and identification of biotinylated peptides

The sulfo-SBED-Atx—yPDI conjugate in 1 mL was cleaved at 37°C with three consecutive additions of 1% (w/w) α-chymotrypsin in 30 min intervals. 10% of the digested reaction mixture was analyzed on a reversed-phase high-pressure liquid chromatography (RP-HPLC) system using a Chrompack C18 (100 × 3.0 mm) column equilibrated with 0.1% (v/v) TFA in water (solvent A). After application of the sample, the column was washed with 5 mL of solvent A at a flow rate of 1 mL/min and the bound peptides then eluted with a gradient of 0% to 60% solvent B (90% (v/v) acetonitrile and 0.1% (v/v) TFA in water) in solvent A in 30 min and then to 100% B in 12 min. Absorbance was monitored at 215 nm. To isolate the biotinylated peptides, 90% of the chymotrypsin-digested sulfo-SBED-Atx—yPDI was added to 150 μL monomeric-avidin beads equilibrated with labelling buffer. The beads were then thoroughly washed with the labelling buffer, followed by a short wash with water. The bound biotinylated peptides were stripped off the beads with 0.1% (v/v) TFA in water and separated on RP-HPLC, using the same protocol as described above for the separation of the 10% of the total digestion reaction mixture. 10% of the material not bound to avidin beads was also analyzed under identical conditions. Isolated biotinylated peptides were N-terminally sequenced by automated Edman degradation on an Applied Biosystems Procise 492A sequencing system.

Modelling the tridimensional structure of the Atx—yPDI complex

All water molecules were removed from the crystal structures of yPDI (PDB ID 2b5e and 3boa [26]) and AtxA (PDB ID 3g8g [33]). Models of the Atx—yPDI complex were generated using two protocols. The rigid-body docking protocol Hex 5.1 [34] (http://www.csd.abdn.ac.uk/hex) was carried out as described [29]. Steric clashes between side-chain atoms were removed by energy minimization (the root mean square gradient for energy conversion was set to 3.0 kcal/mol/Å) with the Tinker Molecular Modeling Package [35] (http://dasher.wustl.edu/tinker/), using CHARMM27 force field parameters [36]. The high ambiguity-driven docking (HADDOCK) protocol has been run as described [37–39]. For HADDOCK trials, the default parameters on the web server version of HADDOCK (http://haddock.science.uu.nl/services/HADDOCK/haddock.php) [39] were used with the setting of passive residues (*i.e.* residues not involved in the interaction) identified from the sequences of the surface exposed biotinylated peptides. Both approaches resulted in two models. In the first model Atx binds to the surface of yPDI at a site between its domains b and b' (bb'-binding site) while, in the second model, it binds between its domains a' and c (a'c-binding site). In this way, the interaction of several other $sPLA_2$s, structurally similar to Atx, with both yPDI and hPDI was modelled. Coordinates of porcine GIB (pGIB) $sPLA_2$ (ID 1pir), hGIIA $sPLA_2$ (ID 1pod), hGX $sPLA_2$ (ID 1le7) and hPDI (ID 4el1), were obtained from the Protein Data Bank, while the model of hGV $sPLA_2$ was constructed as described [29]. All water molecules and ions were removed from the three-dimensional (3D) structures. $sPLA_2$ structures were superimposed on the structure of Atx in the bb' and a'c models of the Atx—yPDI complex. In the same way, the hPDI structure was superimposed on the yPDI structure in the bb'-model of the Atx—yPDI complex. In the thus obtained initial structures, potential active residues (*i.e.* residues constituting the interaction area or being situated not more than 10 Å from it) were identified. Semi-flexible segments were manually defined (each PDI domain represented one segment) while passive residues were defined automatically. The HADDOCK procedure was then performed with other

parameters set to default values. Docking trials of the $sPLA_2$–yPDI interaction yielded models that differ only slightly in the relative positions of $sPLA_2$s and yPDI. The models with the lowest non-bonded interaction energy (*i.e.* energy of interactions between atoms that are more than three bonds apart) and similar interaction sites were chosen.

In the case of hPDI, no structural restraints were available. Choice of the best Atx—hPDI model was therefore made based on the similarity of the interaction site with that of the Atx—yPDI model and on lowest non-bonded energy criteria. Models of other $sPLA_2$–hPDI complexes were then evaluated by comparing them to the chosen Atx—hPDI model. The lowest energy $sPLA_2$–hPDI models that had interaction sites similar to that of Atx in the hPDI model were chosen. In all cases, excepting that of hGX $sPLA_2$, the process of choosing the best $sPLA_2$–hPDI model was very straightforward, since the models with the same interaction site as Atx had the lowest non-bonded energy. For hGX $sPLA_2$, the respective $sPLA_2$ in the majority of models was offset significantly relative to Atx. Models in which hGX $sPLA_2$ exhibited the same interaction site as Atx in the Atx—hPDI complex had significantly higher non-bonded energies; we therefore chose the lowest energy model.

Measurement of phospholipase activity using the fluorogenic substrate PyPG

The phospholipase activity of AtxC, in the presence or the absence of yPDI, was determined as described [40] in 50 mM Tris/HCl, pH 7.4, 50 mM KCl, 1 mM $CaCl_2$, 0.6% (w/v) fatty acid-free BSA.

Results and Discussion

Atx does not significantly affect the integrity of PC12 cells

Influence of Atx on ND and NGFD PC12 cells was evaluated by measuring its effect on the mitochondrial potential, the metabolic activity and the morphology of the cells. While the mitochondrial potential of the cells was about 40% lower in the presence of 100 nM Atx than in its absence, the MTS test showed increased viability of PC12 cells in the presence of Atx (S1 Fig.). These results are in line with previous findings [41]. As part of the complex influence of $sPLA_2$s on the cells, they can induce opposing effects, proliferation and apoptosis, in mammalian cells. The morphology of both ND and NGFD PC12 cells was examined, under phase contrast microscopy, following their incubation in the absence and presence of the neurotoxic $sPLA_2$. No visual changes were observed in either type of PC12 cells in the presence of 100 nM Atx, as compared with control cells grown in the absence of Atx (Fig. 1A). Under these experimental conditions therefore neither proliferation of the cells by Atx nor the negative effect of the $sPLA_2$ on their mitochondria was dominant enough to be reflected in the modified morphology of the cells.

Atx enters the cytosol of PC12 cells

PC12 cells exhibit properties similar to those of neurons, so they were examined as to whether they constitute an appropriate system for studying the mechanism of internalization of the neurotoxic $sPLA_2$. A photo-reactive derivative of Atx, sulfo-SBED-Atx, was employed. As was shown previously, this molecule is able to cross the plasma membrane and enter the cytosol of NSC-34 motoneuron cells, but not that of the non-neuronal HEK-293 [14] and Caco-2 cells (unpublished results). Using the same protocol, our results clearly show that sulfo-SBED-Atx is capable of entering very quickly the cytosol of both ND and NGFD PC12 cells when added to the culture medium. Thus, after about 1 min of incubation with NGFD PC12 cells and about 2

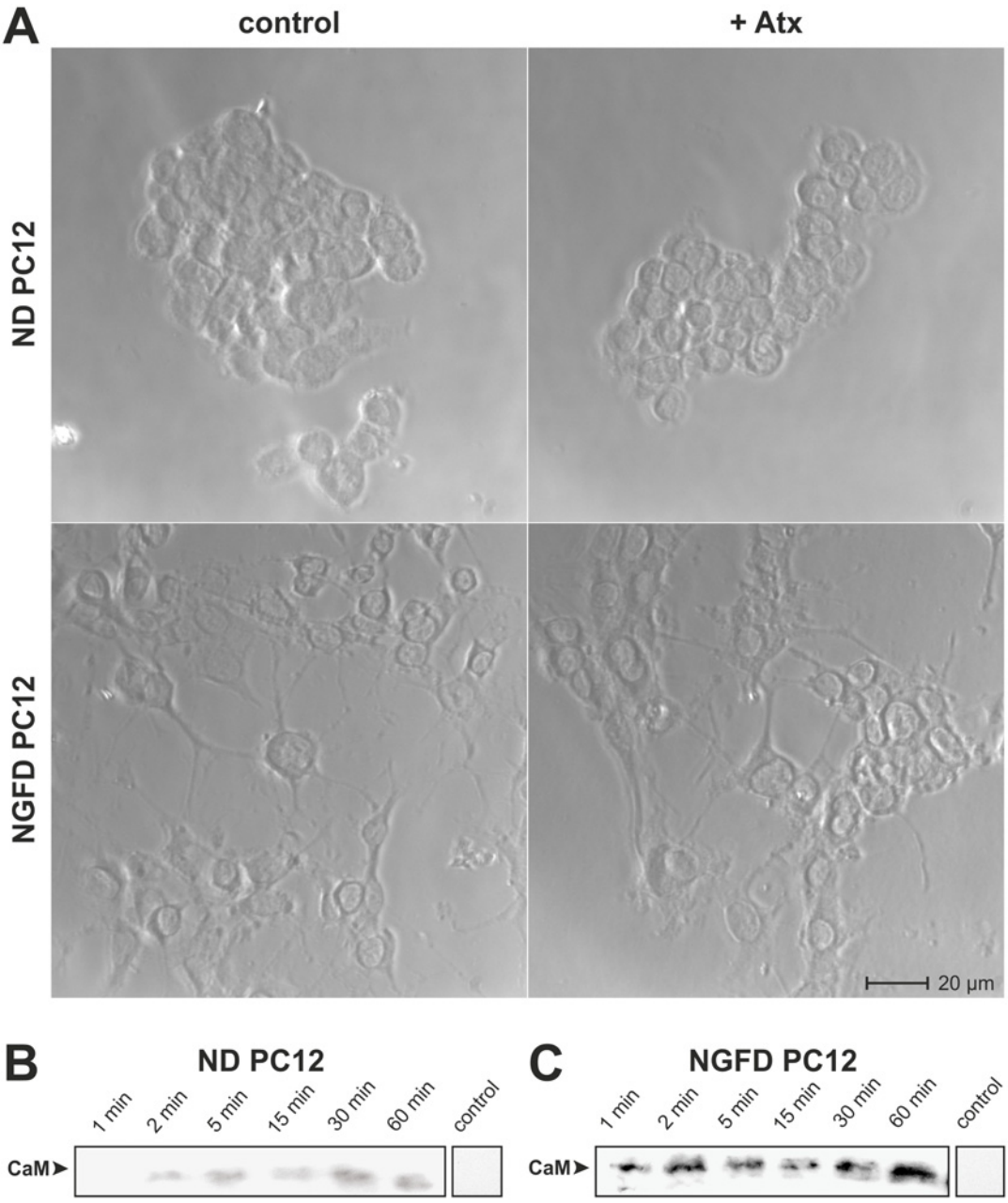

Fig 1. Atx translocates into the cytosol of PC12 cells but does not affect their morphology. (A) Non-differentiated (ND) and NGF-differentiated (NGFD) PC12 cells were incubated with 100 nM AtxC for 120 min at 37°C and then inspected for their morphology under the phase contrast microscope. In control experiments cells were incubated under identical conditions only in the absence of Atx. (B) ND and (C) NGFD PC12 cells were incubated for indicated periods of time with 100 nM sulfo-SBED-Atx in the dark before they were exposed to UV light to trigger photo-cross-linking of the biotin-carrying probe with proteins in close contact. Cells were extracted and biotinylated proteins isolated from extracts on avidin-beads. After reductive SDS-PAGE of biotinylated proteins, these were Western blotted from the gel to a PVDF membrane. The presence of CaM on the PVDF membrane was examined using anti-CaM antibodies and chemiluminescence detection system. Control experiments were performed in an identical way, only without sulfo-SBED-Atx during the 5 min incubation. Experiments were performed in duplicate. Experimental details are given in Materials and Methods.

doi:10.1371/journal.pone.0120692.g001

min with the non-differentiated cells, the photo-reactive probe, tagged its cytosolic high-affinity binding protein CaM with biotin (Figs. 1B and 1C). The degree of labelling of CaM by sulfo-SBED-Atx increased with time of incubation. Similarly rapid internalization of Atx in nerve cells has also been observed with rat hippocampal neurons [42] and with motoneuron-like NSC-34 cells [14]. The fact that Atx is able to enter the cytosol of PC12 cells, apparently without affecting them adversely, qualifies them as suitable for studying the pathway of the neurotoxic $sPLA_2$ from outside the plasma membrane into the cytosol.

Atx and PDI are significantly co-localized in PC12 cells

The affinity between Atx and PDI has been demonstrated *in vitro* [16]. PDI is a protein in the lumen of the endoplasmic reticulum (ER) known to assist cell invasion by some bacterial toxins such as cholera toxin [18–20]. By analogy, PDI has been proposed as being able to detain and concentrate $sPLA_2$ molecules in the ER of certain types of cells and to assist them to translocate across the ER membrane into the cytosol [16]. To examine this suggested role of PDI in the (patho)physiology of Atx we first compared the subcellular localization of Atx and PDI in PC12 cells. ND and NGFD cells were incubated in the presence of ^{546}Alexa-Atx (red) for different periods of time, fixed and labelled with anti-PDI antibodies (green) (Figs. 2A and 2B).The distribution of both the red and green signals in the cells was analyzed using confocal laser microscopy, acquiring several optical sections for each sample. Significant red ^{546}Alexa-Atx signal was detected after incubation times of 5 min and longer. It was located on the plasma membrane as well as inside the cells, but absent from the nuclei, at least after up to 120 min of incubation. In all cells, the signal appears discrete. This suggests the localization of Atx in vesicular structures, possibly endosomes. In differentiated PC12 cells, ^{546}Alexa-Atx was distributed in soma and neurites without evident preference, as reported also for the distribution of Atx and β-bungarotoxins, an $sPLA_2$ neurotoxin from the snake *Bungarus multicinctus*, in rat hippocampal neurons [42,43]. Stacks of images of each sample were quantified and the degree of co-localization of the red and the green signal calculated using ImageJ with co-localization plugin JACoP (Figs. 2C and 2D). To eliminate autofluorescence signals, control experiments without the addition of either ^{546}Alexa-Atx or ^{488}Alexa-conjugated secondary antibodies were used to determine the threshold signal for each channel using Zeiss ZEN Software. The results are represented as the ratio of the number of green pixels that co-localize with red pixels to the total number of green pixels above the threshold. While low co-localization of signals for ^{546}Alexa-Atx and PDI was observed at incubation times up to 5 min, co-localization became significant after 30 min. Based on these results we can conclude that PDI and the neurotoxic $sPLA_2$ on its way from the external space into the cytosol of the PC12 cell locate regularly at the same sites of the cell.

Atx encounters PDI in living PC12 cells

To further substantiate the suggested role of PDI in the (patho)physiology of some $sPLA_2$s we investigated the possible formation of the complex between PDI and Atx in living cells. Photoreactive sulfo-SBED-Atx was added to cultures of ND and NGFD PC12 cells and photocrosslinking initiated at the incubation times indicated in Figs. 2E and 2F. Cell proteins that were in close contact with Atx at these times remained biotinylated. The cells were then lysed, proteins extracted and loaded to an avidin-affinity column that specifically retained only the biotinylated ones. The avidin-binding proteins were then resolved on SDS-PAGE, electroblotted onto the PVDF membrane and inspected for the presence of PDI using specific anti-PDI IgGs. As evident from Figs. 2E and 2F, the photoreactive derivative of Atx encountered PDI in both types of PC12 cells. 1 min after the addition of the $sPLA_2$ to the cell culture

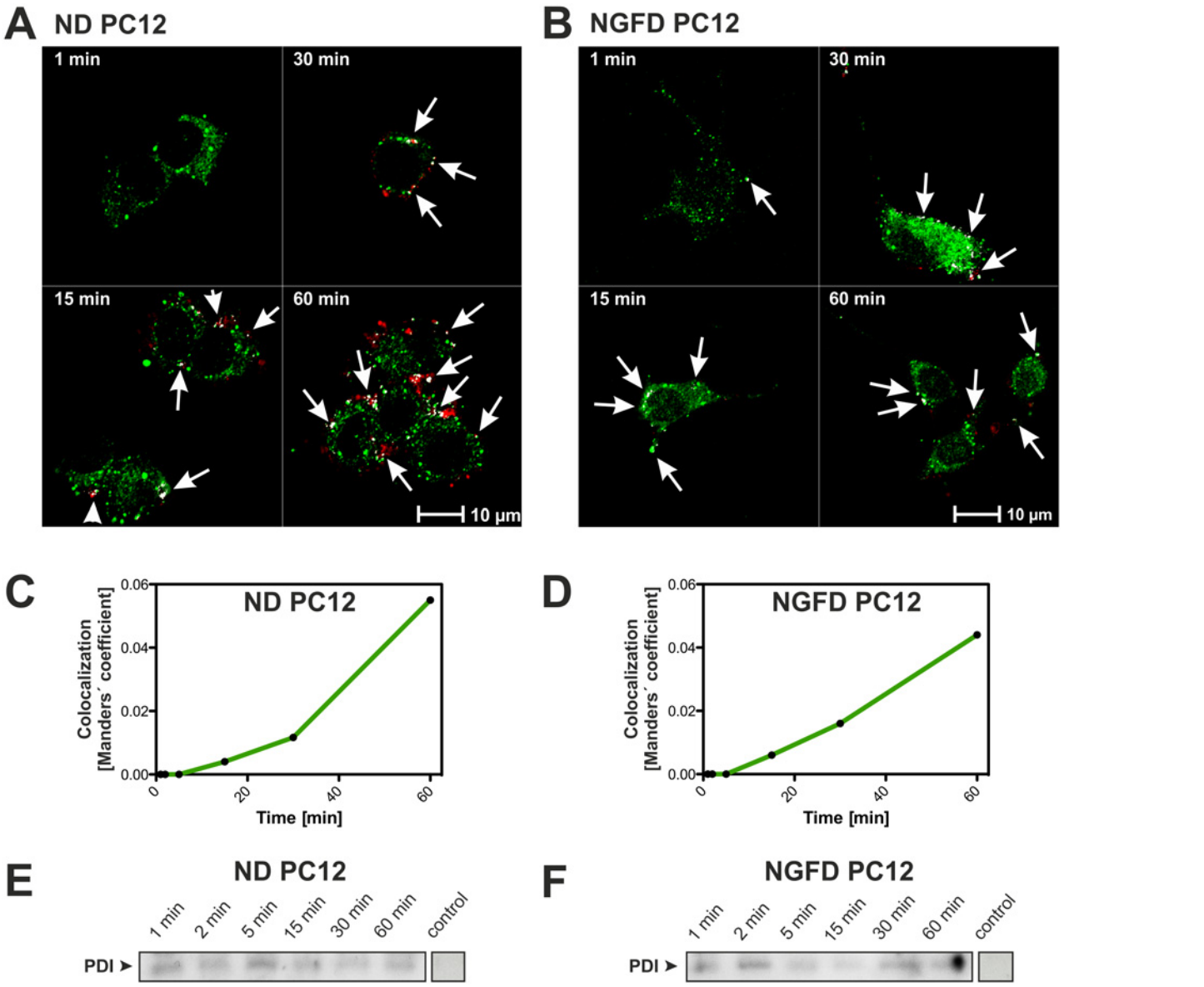

Fig 2. Atx and PDI co-localize and form a complex in living PC12 cells. (A) Non-differentiated (ND) and (B) NGF-differentiated (NGFD) PC12 cells were incubated in the presence of 100 nM ^{546}Alexa-Atx (red signal) for indicated times. Cells were fixed and PDI stained with anti-PDI antibodies (green signal). Co-localized green and red pixels are shown in white. Arrows point at most extensive areas of co-localization. Co-localization of Atx and PDI is expressed in terms of Manders' coefficient in time for ND (C) and NGFD (D) PC12 cells. (E) ND and (F) NGFD PC12 cells were incubated with biotin-containing sulfo-SBED-Atx photo-probe for the indicated time, when this was activated by UV light illumination. The photo-probe covalently links to proteins in close contact, thus biotinylating them. Biotinylated proteins were purified from cell extracts using avidin-affinity chromatography. After reductive SDS-PAGE of biotinylated proteins, these were Western blotted from the gel to a nitrocellulose membrane. The presence of PDI on the membrane was examined using anti-PDI antibodies and chemiluminescence detection system. Control experiments were performed in an identical way, only without sulfo-SBED-Atx during the 5 min incubation. All experiments were performed in duplicate. Experimental details are described in Materials and Methods.

doi:10.1371/journal.pone.0120692.g002

medium it reached the lumen of the ER of the PC12 cells, bound to and reacted with PDI, in agreement with the rapid downstream labelling of the cytosolic CaM (see above). Interestingly, unlike in the case of labelling CaM by sulfo-SBED-Atx (Figs. 1B and 1C), the extent of biotin tagged-PDI did not increase with time. This could indicate that the interaction between Atx and PDI is transient and that the equilibrium between Atx coming into the lumen of ER and

Atx leaving it through the ER membrane into the cytosol is rapidly established. In favour of transient nature of the interaction between Atx and PDI is the apparent dissociation constant of the interaction of 1.27 ± 0.05 μM as determined by surface plasmon resonance [16].

The apparent discrepancy between the results of labelling PDI with sulfo-SBED-Atx, where the product signal remained constant with time, and the result obtained in the co-localization study, where the extent of co-localization increased with time (Figs. 2C and 2D) can be explained by the different nature of the two experiments. In the affinity-labelling experiment only tightly associated molecules of Atx and PDI are observed while, in the co-localization experiment, molecules that are more distant from each other are also indicated. In addition, the methods use differently labelled Atx probes that may have different PDI-binding characteristics. The results, however, strongly support the involvement of PDI in the retrograde cell transport of Atx. A similar function to that of PDI, assistance at moving of $sPLA_2$ retrogradely from Golgi apparatus to ER, may be also envisaged in the case of two other ER-proteins, TCBP-49 and crocalbin, which bind, respectively, taipoxin and crotoxin, two snake venom neurotoxic $sPLA_2$s resembling Atx in their action [44,45]. Thus it is concluded that the retrograde cellular transport of $sPLA_2$s may rely on transient complexing between $sPLA_2$s and ER-proteins possessing the ER-retaining sequence at their C-termini.

Structural characterization of the interaction between Atx and PDI

In order to design mutants for further study of the role of PDI in cell trafficking of Atx, the interaction between Atx and PDI was characterized in terms of their structures. yPDI was used for three reasons. (1) As hPDI, it binds specifically to Atx (Fig. 3B). (2) It shares substantial homology to hPDI at the levels of the primary, secondary and ternary structure. For example, the orientation of domains b and b', important for enzymatic activity and substrate binding, is very similar in both PDIs. The main difference between the two proteins lies in their C-terminal part—the well-structured α-helix in yPDI (domain c) is absent from hPDI [26,46–48]. (3) In addition, separate recombinant domains of this protein and their fusions were available (Fig. 3A).

In order to locate the Atx-interacting site on yPDI, different parts of the protein—individual domains (a, b, a') and fusions of two or more yPDI domains (a'c, ab, abb', bb'a'c, b'a'c and abb'a') (Fig. 3A)—were reacted with the Atx photo-probe. As evident from Fig. 3C, sulfo-SBED-Atx specifically labelled the following yPDI elements: b, ab, a'c and structures containing these elements, but not domains a and b'. This suggests that two binding sites for $sPLA_2$ exist on yPDI.

To localize Atx binding sites on yPDI more precisely the interaction area between Atx and yPDI was mapped. To this end, the covalent complex between sulfo-SBED-Atx and yPDI was prepared and fragmented with α-chymotrypsin. The biotin-containing peptides were purified by avidin-affinity chromatography and RP-HPLC (Fig. 4A). The most abundant peptides (peaks 14, 16, 19, 22, 26, 28, 31 and 33 in Fig. 4A) were N-terminally sequenced, enabling their position in the primary structure of Atx or yPDI to be determined (Fig. 4B) and the structural elements in the two proteins that were cross-linked (colour coded in Fig. 4) to be defined. The biotinylated peptides were identified as elements of Atx β-sheet, αE-helix and the C-terminal unstructured area. In the case of yPDI such peptides originated from the bb`- and a`c-region. Identification of peptides clustered in two separate regions of PDI additionally supports the conclusion that yPDI contains two sites to which Atx can bind.

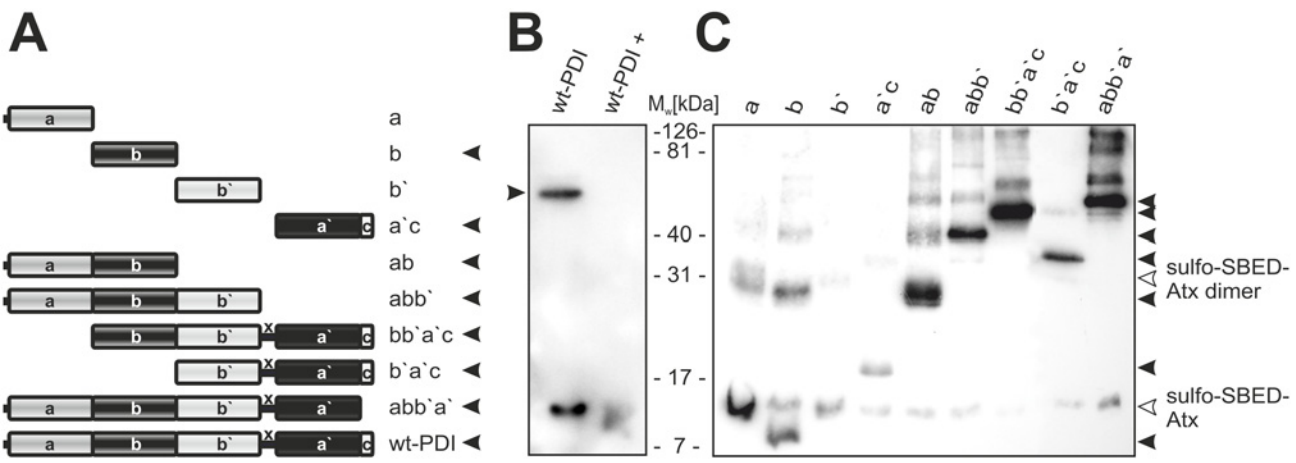

Fig 3. Atx interacts with several domains of yPDI. (A) yPDI is a multi-domain protein. It consists of domains a, a', b, b' and c. Domain b' is linked to domain a' by a linker sequence x. Separate domains and their fusions, as schematically presented, were employed in affinity-labelling experiments using photo-reactive sulfo-SBED-Atx. Atx photo-probe was incubated with the wt yPDI (wt-PDI) (B) or its various parts (C) for 30 min, followed by the UV light-initiated reaction of the photo-probe with proteins in close contact, which were thus biotinylated. Samples were analysed on SDS-PAGE under reducing conditions, electro-transferred to a PVDF membrane. Biotin-containing bands on the PVDF membrane were detected using streptavidin-HRP. Labelling specificity in (B) was verified with the addition of 100-fold unlabelled Atx over sulfo-SBED-Atx (wt-PDI+). Black arrowheads in (A) point at those elements of yPDI which bind and react with sulfo-SBED-Atx. In (B) and (C) black arrowheads are pointing at biotinylated yPDI-structures. Positions on the membrane with biotinylated monomer and dimer of Atx are pointed at by white arrowheads. Experimental details are described in section Materials and Methods. Experiment was performed in triplicate.

doi:10.1371/journal.pone.0120692.g003

Construction of a 3D model of the complex between Atx and yPDI

The structures of Atx and yPDI were docked as described in Materials and Methods, and by considering the structural constraints of the interaction revealed during the binding site mapping experiment. Two alternative docking procedures were employed. In the first, rigid-body docking protocol Hex 5.1 was used. Out of 89 solutions only 2 with the lowest calculated non-bonded energy suited also all of the established structural restraints. Both models were further refined by mild energy minimization allowing only smaller movements of side chain atoms to eliminate steric clashes produced by rigid-body docking. The definition of two final models was confirmed by the high ambiguity-driven docking (HADDOCK) method. Comparison of the two models resulted in only 1.1 Å average backbone Root Mean Square Deviation (RMSD) and, more importantly, in only 0.6 Å average backbone RMSD for the Atx—yPDI interaction surface. In the first model Atx binds to the hydrophobic and acidic surface between domains b and b' of the yPDI (bb'-model). In the second, it binds to the acidic surface at the edge of domain a' of the yPDI that extends to the neighbouring α-helix c (a'c-model) (Fig. 4C). Modelling thus confirmed the view stemming from affinity labelling and interaction area mapping experiments that Atx can bind at two diverse sites on yPDI.

The details of the interaction between Atx and yPDI at the two binding sites are shown in Fig. 5. The Atx-interacting surface on yPDI in the bb'-model is more extensive than that in the a'c-model. In the latter the electrostatic forces (ionic interactions and hydrogen bonds) between Atx and yPDI are predominant, while in the bb'-model the interaction between Atx and yPDI is supported also by hydrophobic interactions. For this reason it appears that the bb'-binding site is the primary binding site of $sPLA_2$ on yPDI. The basic R77 and R118 are important amino acid residues in Atx that are involved in binding to the two binding sites on yPDI. In the bb'-model Atx also contacts yPDI with hydrophobic residues, L3, L19 and F24, two polar residues, N17 and N119, and four basic residues, K69, R72, K74 and K86. In the a'c-model Atx interacts with yPDI by two hydrophobic residues, L110 and Y115, a polar N114 and

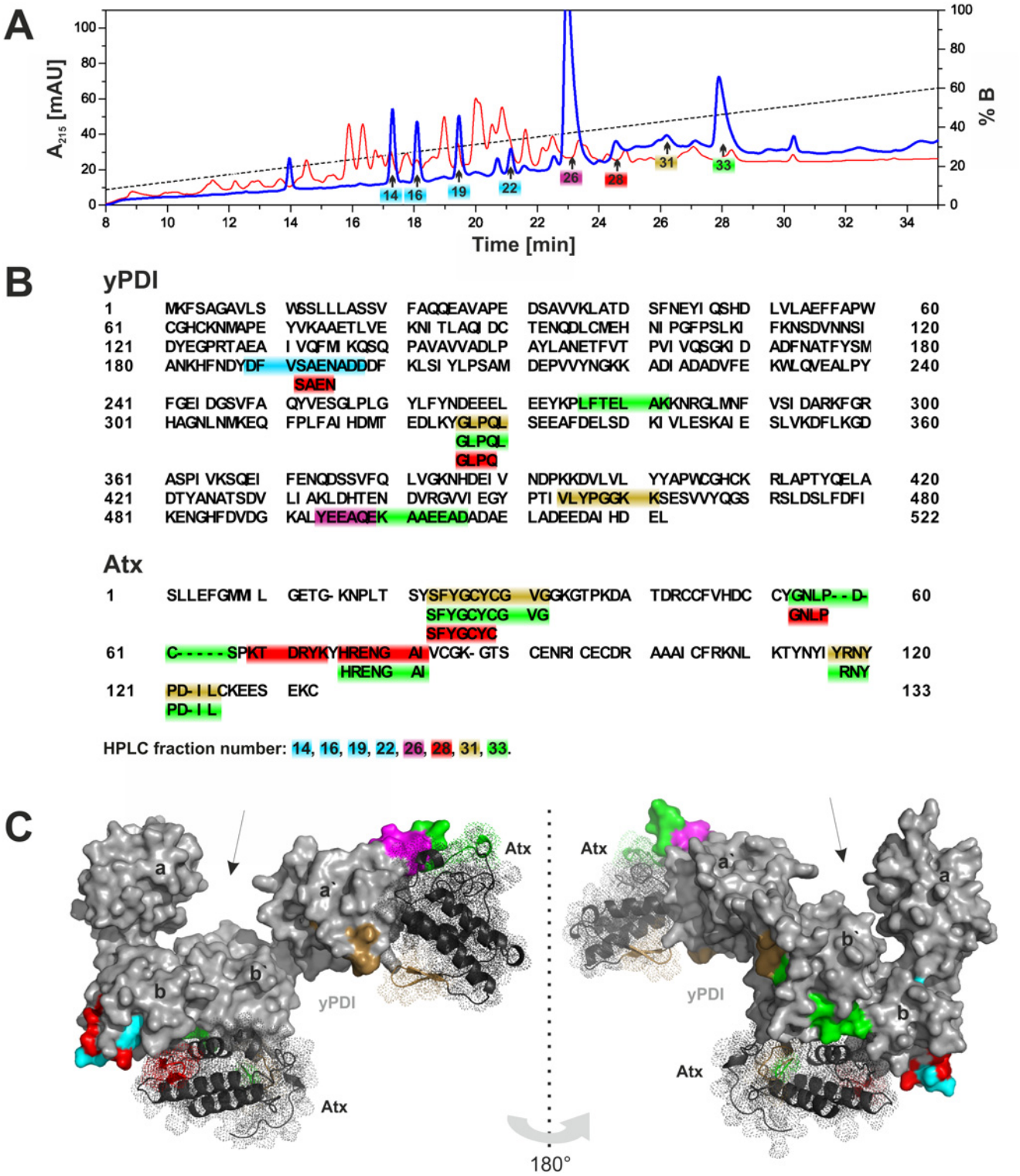

Fig 4. The 3D model of Atx—yPDI complex. (A) Covalent complex of sulfo-SBED-Atx and yPDI was digested with α-chymotrypsin and 10% of the reaction mixture (whole sample) was chromatographed on a Chrompack C18 (100 × 3.0 mm) HPLC column (red line) equilibrated in 0.1% (v/v) TFA and eluted with a gradient of 0.1% (v/v) TFA containing 90% (v/v) acetonitrile. From the rest of the whole sample biotin-containing peptides were isolated on avidin-beads and analysed on HPLC under identical conditions as the whole sample (blue line). Arrows point at fractions containing the major biotinylated peptides. (B) The major biotinylated peptides were identified by N-terminal sequencing. Their positions in primary structures of yPDI or Atx are marked by different colours. A colour designates yPDI and Atx peptides identified in the same fraction. Such peptides are covalently cross-linked and lie close together in the complex, at

the rim of the interaction area between yPDI and Atx. (C) Modelling using rigid-body docking protocol Hex 5.1, HADDOCK procedure and experimentally defined structural restraints resulted in two solutions for Atx binding to yPDI. According to the first, Atx binds to yPDI between domains b and b' (bb'-model or binding site), while according to the second, it binds at domains a' and c of yPDI (a'c-model or binding site). Both solutions are displayed on the same molecule of yPDI using the PyMOL program in two views rotated by 180°. Peptides cross-linked at Atx—yPDI interaction site mapping experiment are indicated by the same colours as in (B). Arrows point towards the active side of yPDI. Experimental details are in Materials and Methods.

doi:10.1371/journal.pone.0120692.g004

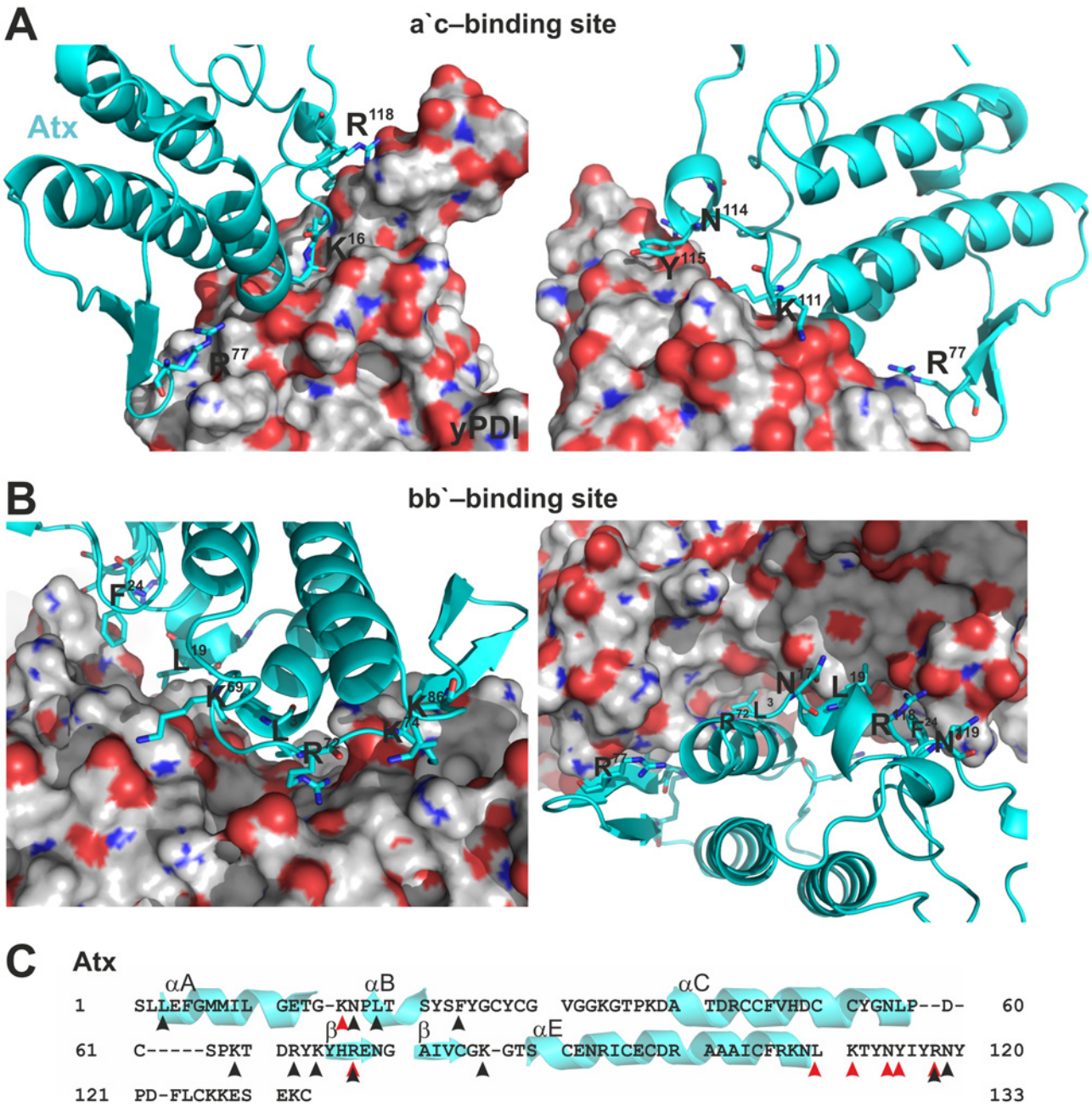

Fig 5. Detailed view of the Atx—yPDI interaction areas. (A) Details of the interaction between Atx and the a'c-binding site of yPDI. (B) Details of the interaction between Atx and the bb'-binding site of yPDI. Structures are prepared using the PyMOL program. yPDI is presented in space-filling mode while Atx in the ribbon mode, with side chains of the yPDI-interacting amino acids shown. (C) The yPDI-contacting amino acid residues of Atx are marked on its primary structure (arrowheads). Black arrowheads point at residues contacting yPDI at the bb'-binding site, while red at those contacting yPDI at the a'c-binding site. Elements of the secondary structure of Atx, α-helices and β-sheets, are shown behind corresponding parts of the primary structure.

doi:10.1371/journal.pone.0120692.g005

two positively charged residues, K16 and K111. Atx faces the bb'-binding site on yPDI with its interfacial binding surface (IBS). Atx binds, with a part of its IBS, to the a'c-binding site on yPDI [49]. Such a mode of binding to PDI should obstruct the binding of Atx to phospholipid membranes, inhibiting its phospholipase activity. However, no influence on the enzymatic activity of Atx has been detected in the presence of PDI. This apparent inconsistency can be explained by the almost 10.000-fold higher affinity of the $sPLA_2$ molecule for PG membranes than to yPDI [16,50].

Construction of a 3D model of the complex between Atx and hPDI

Human PDIs are heterogeneous with respect to their domain composition. While there are several hPDIs that contain the bb' domain combination, none of them possesses the combination of a'c regions [17]. Our assumption that the bb'-binding site on yPDI is the main $sPLA_2$-binding site is thus supported from the evolutionary point of view. The bb'-Atx interacting site on yPDI is highly homologous to corresponding regions in the bb'-hPDIs. Misfolded proteins, to be transported back to the cytosol, bind to this region in hPDI [26] as well as cholera toxin [51–53].

The first step in constructing the Atx-hPDI model was to superimpose the 3D structure of hPDI on the structure of yPDI in its bb'-model of the complex with Atx. The HADDOCK procedure was then implemented to obtain the energetically most favourable model of the complex (Fig. 6A). The docking resulted in a structure in which the position of the Atx molecule in the complex is substantially different from that in the complex with yPDI (Fig. 4C). Atx in the complex with hPDI is rotated by 180° and tilted by 5° with respect to its position in the complex with yPDI. Nevertheless, Atx interacts with hPDI *via* its IBS as in the case of yPDI. Interestingly, the same amino acid residues of the $sPLA_2$, except R77, are involved in ionic, hydrophobic and hydrogen bond interactions with hPDI as with yPDI.

Complexes between PDI and Atx-like mammalian $sPLA_2$s

Toxins often take advantage of their similarity with endogenous molecules to conquer cells. Several mammalian $sPLA_2$ molecules, for example GIB, GIIA, GV and GX $sPLA_2$, are structurally highly homologous to Atx. GIB, GIIA and GV $sPLA_2$ have been detected inside cells [9–11,54,55] while GX $sPLA_2$ was not. The pathway of the $sPLA_2$ cellular internalization has not yet been established. In order to consider the possible involvement of PDI in the cell trafficking of mammalian $sPLA_2$s, we inspected *in silico* whether the latter are able to form complexes with PDI or not. The 3D structure of each of these molecules was superimposed on the structure of Atx in its complex with PDI. HADDOCK was then used to generate the energetically most favourable models. Besides some differences in relative orientation between respective $sPLA_2$s in complexes, mammalian $sPLA_2$s and Atx form very similar complexes with yPDI and hPDI. This is reflected in the average backbone RMSD values calculated for Atx and for each of the replacing $sPLA_2$s in the complex with PDI. These values for GIB, GIIA, GV or GX $sPLA_2$ in the case of the yPDI a`c-complex are 4, 3, 3 and 6 Å, respectively. For the yPDI bb'-complex the average backbone RMSD values for GIB, GIIA, GV and GX $sPLA_2$ are much lower at 0.5, 2, 3 and 1 Å, exposing again the bb'-binding site on the yPDI as the main binding site for $sPLA_2$s. Average RMSD values for comparison of the backbone atoms of Atx with those of GIB, GIIA, GV and GX $sPLA_2$ in complex with hPDI are 3, 7, 4 and 12 Å. Consistent with the average RMSD values, GIB, GIIA and GV $sPLA_2$ form complexes with hPDI similar to the Atx—hPDI complex (Fig. 6B, upper picture), while the interaction area of GX $sPLA_2$ on hPDI is quite different (Fig. 6B, lower picture), only partially overlapping with those of Atx, GIB, GIIA or GV $sPLA_2$.

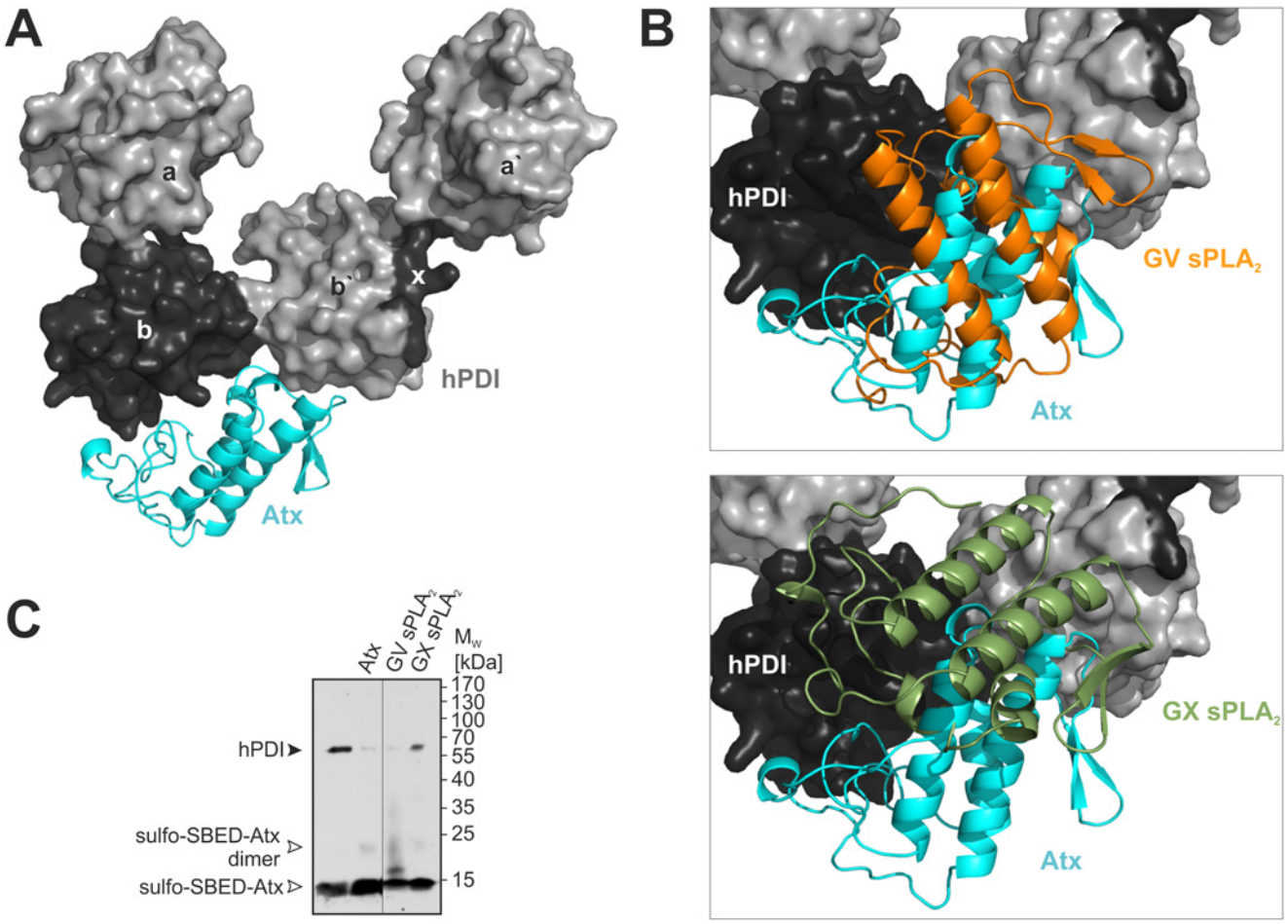

Fig 6. 3D models of complexes between sPLA2s and hPDI. (A) Structure of hPDI was superimposed on the structure of yPDI in the complex with Atx bound to the bb'-binding site and the 3D model optimised by HADDOCK. The model is presented using the PyMOL program with hPDI in space-filling style and Atx in the ribbon style. (B) By substitution of Atx in the Atx—hPDI model with GIB, GIIA, GV or GX sPLA$_2$, and HADDOCK molecular docking, the models of mammalian sPLA$_2$s bound to hPDI were generated. GV sPLA$_2$ (as also GIB and GIIA) occupies the same area on hPDI as Atx (upper picture), while GX sPLA$_2$ occupies only part of this area (lower picture). (C) Heterologous competition of sulfo-SBED-Atx binding to hPDI by GV and GX sPLA$_2$s confirms validity of the proposed sPLA$_2$–hPDI 3D model. Human PDI was incubated with sulfo-SBED-Atx in the dark in the presence of 26 to 100-fold molar excess of AtxC, hGV or hGX sPLA$_2$ over the sulfo-SBED-Atx. The photo cross-linking reaction was triggered by irradiation at 312 nm. SDS-PAGE analysis under reducing conditions was followed by Western blotting of the samples and biotin-specific detection on the nitrocellulose membranes. Black arrowhead is pointing at the biotinylated hPDI. White arrows are pointing at positions with biotinylated monomer and dimer of Atx. Experimental details are described in Materials and Methods section.

doi:10.1371/journal.pone.0120692.g006

To validate our strategy of modelling the complex between an sPLA$_2$ and hPDI, we tested experimentally the ability of GV sPLA$_2$, representative of mammalian sPLA$_2$s that bind hPDI in the same way as Atx, and GX sPLA$_2$, the mammalian sPLA$_2$s that does not bind hPDI in the same way as Atx, to inhibit the binding of sulfo-SBED-Atx on hPDI. From the model we expected that GV sPLA$_2$ should block biotin-tagging of hPDI more effectively than GX sPLA$_2$. The results of experimental heterologous competition of sulfo-SBED-Atx binding to hPDI by GV or GX sPLA$_2$ confirmed our prediction (Fig. 6C). GV sPLA$_2$ indeed inhibited biotinylation of the hPDI more efficiently than the GX sPLA$_2$. Our modelling approach thus gives relevant models of complexes between mammalian sPLA$_2$s and hPDI. Models of the complex between Atx and hPDI, and the Atx-related mammalian sPLA$_2$s and hPDI thus provide us with a

structural understanding of how these proteins associate. This offers the possibility of facilitating the study of the role of PDI in the $sPLA_2$ cell internalization process by targeted mutagenesis.

Conclusions

The rat PC12 cell line has been shown to be a suitable neuron-like cell model to study the mechanism of the internalization of Atx, the snake venom neurotoxic GIIA $sPLA_2$. Atx does not affect the morphology of these cells but is able to enter their cytosol. We showed that Atx and PDI substantially co-localize in PC12 cells, and, most importantly, are able to form a complex inside living PC12 cells. The results presented here strongly support the proposal that PDI, an oxido-reductase from the lumen of ER, is involved in the retrograde cell transport of Atx. Further study of the role of PDI in cell trafficking of Atx and structurally related mammalian $sPLA_2$s included construction of a 3D model of the complex between Atx and hPDI. Based on this model, the complexes between GIB, GIIA, GV or GX $sPLA_2$, and hPDI were described. These models predict that $sPLA_2$s interact with hPDI in the region including its domains b and b', the same region as that where unfolded proteins and cholera toxin bind on their retrograde pathway to the cytosol. The interaction area with hPDI is the same in the cases of Atx and the mammalian GIB, GIIA and GV $sPLA_2$s, which have been detected intracellularly, while that of GX $sPLA_2$, which has not so far been observed inside cells, is quite diverse in its location. In heterologous competition of Atx binding to hPDI, GV $sPLA_2$ proved to be a better inhibitor than GX $sPLA_2$. The validity of the $sPLA_2$–hPDI 3D model was thus verified experimentally. It qualifies as an important tool to accelerate further insight into the role of PDI in assisting the retrograde transport of certain snake venom and mammalian $sPLA_2$s from the cell surface and into (patho)physiological processes related to the intracellular action of these molecules.

Supporting Information

S1 Fig. The viability of PC12 cells is increased in the presence of Atx. (A) Non-differentiated (ND) and (B) NGF-differentiated (NGFD) PC12 cells were incubated with 100 nM AtxA, in its absence (control) or with 1% (w/v) Triton X-100 for the indicated periods of time. The viability of cells, determined using the MTS viability test, was calculated from A_{490} corrected for background absorbance and is presented relative to the control cells. Experimental details are described in Materials and Methods section.
(TIF)

Acknowledgments

We are grateful to Dr. William J. Lennarz, Stony Brook University, New York, USA, who kindly provided yeast PDI and its domains. We also thank Dr. Roger H. Pain for critical reading of the manuscript.

Author Contributions

Conceived and designed the experiments: LK JŠ IK. Performed the experiments: JO LK JŠ AL KD APJ. Analyzed the data: JO LK JŠ AL KD APJ IK. Contributed reagents/materials/analysis tools: LK IK. Wrote the paper: JO LK JŠ AL KD IK.

References

1. Berg OG, Gelb MH, Tsai MD, Jain MK. Interfacial enzymology: the secreted phospholipase A_2 paradigm. Chem Rev. 2001; 101: 2613–2654. PMID: 11749391

2. Murakami M, Taketomi Y, Miki Y, Sato H, Hirabayashi T, Yamamoto K. Recent progress in phospholipase A_2 research: from cells to animals to humans. Prog Lipid Res. 2011; 50: 152–192. doi: 10.1016/j.plipres.2010.12.001 PMID: 21185866
3. Eerola LI, Surrel F, Nevalainen TJ, Gelb MH, Lambeau G, Laine VJ. Analysis of expression of secreted phospholipases A_2 in mouse tissues at protein and mRNA levels. Biochim Biophys Acta. 2006; 1761: 745–756. PMID: 16757211
4. Šribar J, Križaj I. Secreted phospholipases A_2—not just enzymes. Acta Chim Slov. 2011; 58: 678–688. PMID: 24061115
5. Murakami M, Taketomi Y, Girard C, Yamamoto K, Lambeau G. Emerging roles of secreted phospholipase A_2 enzymes: lessons from transgenic and knockout mice. Biochimie. 2010; 92: 561–582. doi: 10.1016/j.biochi.2010.03.015 PMID: 20347923
6. Murakami M, Lambeau G. Emerging roles of secreted phospholipase A_2 enzymes: an update. Biochimie. 2013; 95: 43–50. doi: 10.1016/j.biochi.2012.09.007 PMID: 23022039
7. Brglez V, Lambeau G, Petan T. Secreted phospholipases A_2 in cancer: diverse mechanisms of action. Biochimie. 2014; 107: 114–23. doi: 10.1016/j.biochi.2014.09.023 PMID: 25286228
8. Križaj I. Roles of secreted phospholipases A_2 in the mammalian immune system. Protein Pept Lett. 2014; 21: 1201–1208. PMID: 25141938
9. Fayard JM, Tessier C, Pageaux JF, Lagarde M, Laugier C. Nuclear location of PLA_2-I in proliferative cells. J Cell Sci. 1998; 111: 985–994. PMID: 9490642
10. Macchioni L, Corazzi L, Nardicchi V, Mannucci R, Arcuri C, Porcellati S, et al. Rat brain cortex mitochondria release group II secretory phospholipase A_2 under reduced membrane potential. J Biol Chem. 2004; 279: 37860–37869. PMID: 15231825
11. Nardicchi V, Macchioni L, Ferrini M, Goracci G. The presence of a secretory phospholipase A_2 in the nuclei of neuronal and glial cells of rat brain cortex. Biochim Biophys Acta. 2007; 1771: 1345–1352. PMID: 17950028
12. Balboa MA, Shirai Y, Gaietta G, Ellisman MH, Balsinde J, Dennis EA. Localization of group V phospholipase A_2 in caveolin-enriched granules in activated P388D1 macrophage-like cells. J Biol Chem. 2003; 278: 48059–48065. PMID: 12963740
13. Križaj I. Ammodytoxin: a window into understanding presynaptic toxicity of secreted phospholipases A_2 and more. Toxicon. 2011; 58: 219–229. doi: 10.1016/j.toxicon.2011.06.009 PMID: 21726572
14. Jenko Pražnikar Z, Kovačič L, Rowan EG, Romih R, Rusmini P, Poletti A, et al. A presynaptically toxic secreted phospholipase A_2 is internalized into motoneuron-like cells where it is rapidly translocated into the cytosol. Biochim Biophys Acta. 2008; 1783: 1129–1139. doi: 10.1016/j.bbamcr.2008.01.011 PMID: 18261469
15. Logonder U, Jenko-Pražnikar Z, Scott-Davey T, Pungerčar J, Križaj I, Harris JB. Ultrastructural evidence for the uptake of a neurotoxic snake venom phospholipase A_2 into mammalian motor nerve terminals. Exp Neurol. 2009; 219: 591–594. doi: 10.1016/j.expneurol.2009.07.017 PMID: 19631643
16. Šribar J, Anderluh G, Fox JW, Križaj I. Protein disulphide isomerase binds ammodytoxin strongly: possible implications for toxin trafficking. Biochem Biophys Res Commun. 2005; 329: 733–737. PMID: 15737647
17. Appenzeller-Herzog C, Ellgaard L. The human PDI family: versatility packed into a single fold. Biochim Biophys Acta. 2008; 1783: 535–548. PMID: 18093543
18. Tsai B, Ye Y, Rapoport TA. Retro-translocation of proteins from the endoplasmic reticulum into the cytosol. Nat Rev Mol Cell Biol. 2002; 3: 246–255. PMID: 11994744
19. Lencer WI, Tsai B. The intracellular voyage of cholera toxin: going retro. Trends Biochem Sci. 2003; 28: 639–645. PMID: 14659695
20. Lord JM, Roberts LM, Lencer WI. Entry of protein toxins into mammalian cells by crossing the endoplasmic reticulum membrane: co-opting basic mechanisms of endoplasmic reticulum-associated degradation. Curr Top Microbiol Immunol. 2005; 300: 149–168. PMID: 16573240
21. Wernick NLB, Chinnapen DJ-F, Cho JA, Lencer WI. Cholera toxin: an intracellular journey into the cytosol by way of the endoplasmic reticulum. Toxins. 2010; 2: 310–325. doi: 10.3390/toxins2030310 PMID: 22069586
22. Sandvig K, Skotland T, van Deurs B, Klokk TI. Retrograde transport of protein toxins through the Golgi apparatus. Histochem Cell Biol. 2013; 140: 317–326. doi: 10.1007/s00418-013-1111-z PMID: 23765164
23. Gubenšek F, Ritonja A, Zupan J, Turk V. Basic proteins of *Vipera ammodytes* venom—studies of structure and function. Period Biol. 1980; 82: 443–447.

24. Leslie CC, Gelb MH. Assaying phospholipase A_2 activity. Methods Mol Biol. 2004; 284: 229–242. PMID: 15173620

25. Singer AG, Ghomashchi F, Le Calvez C, Bollinger J, Bezzine S, Rouault M, et al. Interfacial kinetic and binding properties of the complete set of human and mouse groups I, II, V, X, and XII secreted phospholipases A_2. J Biol Chem. 2002; 277: 48535–48549. PMID: 12359733

26. Tian G, Xiang S, Noiva R, Lennarz WJ, Schindelin H. The crystal structure of yeast protein disulfide isomerase suggests cooperativity between its active sites. Cell. 2006; 124: 61–73. PMID: 16413482

27. Greene LA, Tischler AS. Establishment of a noradrenergic clonal line of rat adrenal pheochromocytoma cells which respond to nerve growth factor. Proc Natl Acad Sci USA. 1976; 73: 2424–2428. PMID: 1065897

28. Kovačič L, Šribar J, Križaj I. A new photoprobe for studying biological activities of secreted phospholipases A_2. Bioorg Chem. 2007; 35: 295–305. PMID: 17303214

29. Kovačič L, Novinec M, Petan T, Križaj I. Structural basis of the significant calmodulin-induced increase in the enzymatic activity of secreted phospholipases A_2. Protein Eng Des Sel. 2010; 23: 479–487. doi: 10.1093/protein/gzq019 PMID: 20348188

30. Wessel D, Flügge UI. A method for the quantitative recovery of protein in dilute solution in the presence of detergents and lipids. Anal Biochem. 1984; 138: 141–143. PMID: 6731838

31. Schneider CA, Rasband WS, Eliceiri KW. NIH Image to ImageJ: 25 years of image analysis. Nat Methods. 2012; 9: 671–675. PMID: 22930834

32. Bolte S, Cordelières FP. A guided tour into subcellular colocalization analysis in light microscopy. J Microsc. 2006; 224: 213–232. PMID: 17210054

33. Saul FA, Prijatelj-Žnidaršič P, Vulliez-le Normand B, Villette B, Raynal B, Pungerčar J, et al. Comparative structural studies of two natural isoforms of ammodytoxin, phospholipases A_2 from *Vipera ammodytes ammodytes* which differ in neurotoxicity and anticoagulant activity. J Struct Biol. 2010; 169: 360–369. doi: 10.1016/j.jsb.2009.10.010 PMID: 19857576

34. Mustard D, Ritchie DW. Docking essential dynamics eigenstructures. Proteins. 2005; 60: 269–274. PMID: 15981272

35. Ren P, Ponder JW. Polarizable atomic multipole water model for molecular mechanics simulation. J Phys Chem B. 2003; 107: 5933–5947.

36. Foloppe N, MacKerell AD Jr.. All-atom empirical force field for nucleic acids: I. Parameter optimization based on small molecule and condensed phase macromolecular target data. J Comput Chem. 2000; 21: 86–104.

37. Dominguez C, Boelens R, Bonvin AMJJ. HADDOCK: A protein-protein docking approach based on biochemical or biophysical information. J Am Chem Soc. 2003; 125: 1731–1737. PMID: 12580598

38. De Vries SJ, van Dijk M, Bonvin AMJJ. The HADDOCK web server for data-driven biomolecular docking. Nat Protoc. 2010; 5: 883–897. doi: 10.1038/nprot.2010.32 PMID: 20431534

39. Karaca E, Melquiond ASJ, de Vries SJ, Kastritis PL, Bonvin AMJJ. Building macromolecular assemblies by information-driven docking: introducing the HADDOCK multibody docking server. Mol Cell Proteomics. 2010; 9: 1784–1794. doi: 10.1074/mcp.M000051-MCP201 PMID: 20305088

40. Radvanyi F, Jordan L, Russo-Marie F, Bon C. A sensitive and continuous fluorometric assay for phospholipase A_2 using pyrene-labeled phospholipids in the presence of serum albumin. Anal Biochem. 1989; 177: 103–109. PMID: 2742139

41. Petrovič U, Šribar J, Matis M, Anderluh G, Peter-Katalinić J, Križaj I, et al. Ammodytoxin, a secretory phospholipase A_2, inhibits G_2 cell cycle arrest in yeast *Saccharomyces cerevisiae*. Biochem J. 2005; 391: 383–388. PMID: 16008522

42. Petrovič U, Šribar J, Pariš A, Rupnik M, Kržan M, Vardjan N, et al. Ammodytoxin, a neurotoxic secreted phospholipase A_2, can act in the cytosol of the nerve cell. Biochem Biophys Res Commun. 2004; 324: 981–985. PMID: 15485650

43. Herkert M, Shakhman O, Schweins E, Becker CM. Beta-bungarotoxin is a potent inducer of apoptosis in cultured rat neurons by receptor-mediated internalization. Eur J Neurosci. 2001; 14: 821–828. PMID: 11576186

44. Dodds D, Schlimgen AK, Lu SY, Perin MS. Novel reticular calcium binding protein is purified on taipoxin columns. J Neurochem. 1995; 64: 2339–2344. PMID: 7722520

45. Hseu MJ, Yen CY, Tseng CC, Tzeng MC. Purification and partial amino acid sequence of a novel protein of the reticulocalbin family. Biochem Biophys Res Commun. 1997; 239: 18–22. PMID: 9345262

46. Darby NJ, Penka E, Vincentelli R. The multi-domain structure of protein disulfide isomerase is essential for high catalytic efficiency. J Mol Biol. 1998; 276: 239–247. PMID: 9514721

47. Koivunen P, Pirneskoski A, Karvonen P, Ljung J, Helaakoski T, Notbohm H, et al. The acidic C-terminal domain of protein disulfide isomerase is not critical for the enzyme subunit function or for the chaperone or disulfide isomerase activities of the polypeptide. EMBO J. 1999; 18: 65–74. PMID: 9878051

48. Kozlov G, Määttänen P, Thomas DY, Gehring K. A structural overview of the PDI family of proteins. FEBS J. 2010; 277: 3924–3936. doi: 10.1111/j.1742-4658.2010.07793.x PMID: 20796029

49. Petan T, Križaj I, Gelb MH, Pungerčar J. Ammodytoxins, potent presynaptic neurotoxins, are also highly efficient phospholipase A_2 enzymes. Biochemistry. 2005; 44: 12535–12545. PMID: 16156665

50. Šribar J, Čopič A, Pariš A, Sherman NE, Gubenšek F, Fox JW, et al. A high affinity acceptor for phospholipase A_2 with neurotoxic activity is a calmodulin. J Biol Chem. 2001; 276: 12493–12496. PMID: 11278260

51. Forster ML, Mahn JJ, Tsai B. Generating an unfoldase from thioredoxin-like domains. J Biol Chem. 2009; 284: 13045–13056. doi: 10.1074/jbc.M808352200 PMID: 19289469

52. Taylor M, Banerjee T, Navarro-Garcia F, Huerta J, Massey S, Burlingame M, et al. A therapeutic chemical chaperone inhibits cholera intoxication and unfolding/translocation of the cholera toxin A1 subunit. PLoS One. 2011; 6: e18825. doi: 10.1371/journal.pone.0018825 PMID: 21526142

53. Taylor M, Banerjee T, Ray S, Tatulian SA, Teter K. Protein-disulfide isomerase displaces the cholera toxin A1 subunit from the holotoxin without unfolding the A1 subunit. J Biol Chem. 2011; 286: 22090–22100. doi: 10.1074/jbc.M111.237966 PMID: 21543321

54. Kim YJ, Kim KP, Han SK, Munoz NM, Zhu X, Sano H, et al. Group V phospholipase A_2 induces leukotriene biosynthesis in human neutrophils through the activation of group IVA phospholipase A_2. J Biol Chem. 2002; 277: 36479–36488. PMID: 12124392

55. Birts CN, Barton CH, Wilton DC. A catalytically independent physiological function for human acute phase protein group IIA phospholipase A_2: cellular uptake facilitates cell debris removal. J Biol Chem. 2008; 283: 5034–5045. PMID: 18089561

Toxicon 89 (2014) 9–16

Contents lists available at ScienceDirect

Toxicon

journal homepage: www.elsevier.com/locate/toxicon

Review

Understanding the molecular mechanism underlying the presynaptic toxicity of secreted phospholipases A_2: An update

Jernej Šribar [a], Jernej Oberčkal [a], Igor Križaj [a, b, *]

[a] Department of Molecular and Biomedical Sciences, Jožef Stefan Institute, Jamova 39, 1000 Ljubljana, Slovenia
[b] Department of Chemistry and Biochemistry, Faculty of Chemistry and Chemical Technology, University of Ljubljana, Aškerčeva 5, SI-1000 Ljubljana, Slovenia

ARTICLE INFO

Article history:
Received 18 March 2014
Received in revised form 19 June 2014
Accepted 24 June 2014
Available online 5 July 2014

Keywords:
Snake venom
Phospholipase A_2
Presynaptic neurotoxicity
Mechanism of action

ABSTRACT

β-neurotoxins are enzymes, secreted phospholipases A_2, that inhibit neurotransmission in neuromuscular synapses by poisoning the motoneuron. They were reviewed extensively several years ago (Pungerčar and Križaj, 2007). Here we present and critically discuss the most important experimental facts reported since then. Evidence has been presented for specific internalization of β-neurotoxins into the nerve endings of motoneurons, their *in vivo* binding to some cytosolic proteins, direct action on mitochondria, disruption of Ca^{2+} homoeostasis and inhibition of amphiphysin function. New insights have led to a more confident interpretation of the action of these toxins at the molecular level. The most important questions that remain to be answered are listed.

© 2014 Elsevier Ltd. All rights reserved.

1. Introduction

Secreted phospholipases A_2 (sPLA$_2$s; EC 3.1.1.4) are the active factors in many animal venoms. Their role there is not only digesting phospholipids, as initially thought, but also participating in hunting and defending. Over decades of research a variety of pharmacological activities have been ascribed to these proteins. Some venom sPLA$_2$s have been found to be neurotoxic, myotoxic, anticoagulant, cardiotoxic or cytotoxic (Kini, 1997). Due to their important medical relevance, particular attention has been devoted to a group of sPLA$_2$s that paralyse the neuromuscular junctions (NMJ) in vertebrate skeletal muscles. A subgroup of neurotoxic sPLA$_2$s acting on the neuronal side of the NMJ, the so-called β-neurotoxic sPLA$_2$s (β-ntxs), were reviewed several years ago (Pungerčar and Križaj, 2007). Since then, important new insights into the mechanism of action of these toxins have been established. These are presented and critically discussed in this paper.

sPLA$_2$s have been classified according to their structural characteristics into twelve groups (Murakami et al., 2011) but only a few members of groups GI, GII and GIII are β-ntxs and thus able to block NM transmission. The most abundant source of β-ntxs are venoms of the Elapidae and Viperidae snakes. They are rather small molecules, with molecular masses ranging from 13 to 19 kDa, containing 5 to 8 disulphide bridges and requiring Ca^{2+} ions for enzymatic activity. While β-ntxs are generally highly homologous in their primary structures, their quaternary structures can differ considerably. They appear as monomers or non-covalent complexes of two, three or five subunits, at least one of which is an sPLA$_2$. β-ntxs isolated from venoms of the *Bungarus* family of snakes, the so-called β-bungarotoxins (β-Butxs), are exceptional in terms of their quaternary structure. They consist of two subunits, an sPLA$_2$ and a bovine pancreatic trypsin inhibitor-like protein, linked by a disulphide bridge. A fascinating fact is that, despite structural differences, the pathological effects elicited by β-ntxs on the vertebrate NMJ are very similar.

* Corresponding author. Department of Molecular and Biomedical Sciences, Jožef Stefan Institute, Jamova 39, 1000 Ljubljana, Slovenia.
E-mail address: igor.krizaj@ijs.si (I. Križaj).

http://dx.doi.org/10.1016/j.toxicon.2014.06.019
0041-0101/© 2014 Elsevier Ltd. All rights reserved.

Recently, crystal structures of β-ntxs with different quaternary structures have been reported: ammodytoxin (Atx) (monomer) from the venom of *Vipera ammodytes ammodytes* (Saul et al., 2010), crotoxin (non-covalent dimer) from the venom of *Crotalus durissus terrificus* (Faure et al., 2011) and taipoxin (trimer) from the venom of *Oxyuranus scutellatus scutellatus* (Cendron et al., 2012).

2. Cell aspects of β-neurotoxicity

The site of action of β-ntxs is the peripheral nervous system, so the most appropriate system to study the mechanism of their action is an isolated NMJ. Various neuronal cell lines are affected by these toxins, among them primary cell lines from the central nervous system (CNS), such as hippocampal, cerebellar granule and cortical neurons, and also immortalized cell lines, for example the rat pheochromocytoma cell line (PC12) and mouse neuroblastoma spinal cord hybrid cell line (NSC34). However, the effects of β-ntxs on these model systems may differ from those at the NMJ. In CNS neurons, for example, intoxication with β-ntxs results in expansion of the plasma membrane and formation of distinct bulges (Rigoni et al., 2004, 2005; Bonanomi et al., 2005), while these toxins apparently did not significantly influence the terminal area in motoneurons (Prasarnpun et al., 2004; Logonder et al., 2008). Although the difference in this case may be explained also as a consequence of anatomical compression of the NMJ by perisynaptic Schwann cells and muscle, caution is always due when interpreting results obtained in model systems.

2.1. Electrophysiological observations

In experimental animals, blocking the NM transmission by β-ntxs results in flaccid paralysis of skeletal muscles. In experimental set-ups, in which small changes in neurotransmitter acetylcholine (ACh) release can be monitored by recording the amplitude of the muscle twitch, isolated vertebrate NM preparations, indirectly stimulated and exposed to β-ntxs, exhibit a characteristic three-phase response. In phase 1, occurring shortly after the addition of a β-ntx to the NM preparation and lasting for several minutes, a transient inhibition of muscle twitching is observed. Phase 2, reaching its maximum in 10–20 min following the addition of a β-ntx, is characterized by increased amplitude of muscle twitching due to facilitated neurotransmitter release. In phase 3, the indirectly elicited muscle twitching progressively decreases. Depending on factors that influence the phospholipase activity of a β-ntx, it ceases completely in one to 2 h. The resting membrane potential of skeletal muscle cells remains unaffected, even after complete arrest of the NM communication, and the muscle retains its ability to respond to neurotransmitter stimulation.

Such experiments (extensively reviewed in Pungerčar and Križaj, 2007) have led to several important conclusions. (1) Since no significant change in the amplitude of the miniature end plate potential is observed, synaptic vesicles (SVs) do not undergo substantial fusion inside the nerve terminal, (2) The action of β-ntxs does not affect the ACh transporter, (3) If the experimental temperature in the above described experiment was lowered below a certain value, the phase 1 disappeared while phases 2 and 3 normally occurred (Fathi et al., 2013). This suggests that phase 1 is not simply a reflection of the binding of a β-ntx to its presynaptic receptor. (4) There is no requirement for electro-stimulation of the NM activity for β-ntxs to induce paralysis of the NM preparation (Prasarnpun et al., 2004; Logonder et al., 2008).

2.2. Electron and fluorescence microscopy observations

Electron microscopy studies have revealed characteristic changes in the mammalian NMJ that have been acutely poisoned with β-ntxs: (1) depletion of SVs inside the nerve terminal by up to 80%, (2) appearance of Ω-shaped invaginations in the presynaptic membrane, (3) formation of large vesicles in the nerve terminal, and (4) damaged mitochondria. (5) Schwann cell processes spread into the synaptic cleft, leading to detachment of synaptic boutons from the postsynaptic membrane and subsequently to their complete degeneration. Morphometric data of the motor nerve terminals of the β-ntx-poisoned (AtxA and β-Butx) and control NM preparations revealed insignificant differences (Prasarnpun et al., 2004; Logonder et al., 2008). The fate of the proteins involved in neuroexocytosis was investigated by immunocytochemistry. While the immunoreactivity of two SNAREs (soluble N-ethylmaleimide-sensitive factor attachment protein receptors), SNAP-25 and syntaxin, remained mostly unchanged in the rat phrenic nerve terminal boutons exposed to β-Butx, the fluorescence signal for the SV marker, synaptophysin, was markedly reduced, consistent with the observed depletion of SVs (Prasarnpun et al., 2004). Interestingly, some findings obtained in experiments on a mouse NM preparation paralysed with AtxA (Logonder et al., 2008) differed from those obtained on rat NM preparation with β-Butx (Prasarnpun et al., 2004). In the terminal boutons poisoned with AtxA, only a 13.6% reduction in the volume fraction occupied by SVs was observed and was not sufficient to cause a loss of synaptophysin immunolabeling. This is in accordance with another unique observation linked to AtxA poisoning, namely the absence of Ω-shaped invaginations in the nerve endings. Drastic depletion of SVs is the principal cause of paralysis in the case of GIA $sPLA_2$s, such as β-ntxs from elapid venoms (*e.g.*, notexin, β-Butx, taipoxin and textilotoxin). Obviously, loss of SVs cannot play a major role in the cessation of NM communication by AtxA, GIIA $sPLA_2$ from the viperid venom. The major reason for NM blockade in this case may lie in the energy depletion at the nerve ending due to degeneration of mitochondria, resulting in the disruption of the coupling between the nerve terminal depolarization and consequent neurotransmitter release. This is consistent also with the observed clustering of SVs in the cytosol and at release sites in nerve endings. SV clustering has not been observed in nerve terminals exposed to GIA β-ntxs (Logonder et al., 2008).

Another hallmark of β-ntx action on nerve cells is fragmentation of the neuronal cytoskeleton (reviewed in Pungerčar and Križaj, 2007). This appears to be due to the activation of calpains, cytosolic proteases, following the β-ntxs-induced increase in Ca^{2+} concentration (Tedesco et al., 2009). Calpains thus act in the final stage of

intoxication of the NMJ by β-ntxs and partake in the complete degeneration of the nerve terminals (Duregotti et al., 2013). β-ntxs appear to disrupt Ca^{2+} homoeostasis in the nerve endings in two steps. First, by influencing the conductance of certain Ca^{2+} channels they induce an influx of Ca^{2+} ions (Prasarnpun et al., 2004; Yagami et al., 2013). Later on, the phospholipid hydrolysis products accumulated due to their enzymatic activity lead to increased ion permeability of the plasma membrane and of the membranes of intracellular Ca^{2+} stores, mitochondria and endoplasmic reticulum (ER) (Rigoni et al., 2007, 2008).

3. β-neurotoxicity from the molecular point of view

Present experimental methods do not allow for detailed studies of the complex NMJ at the molecular level. Hence, appropriate model systems are crucial for elucidation of the molecular basis of β-neurotoxicity. Biochemical experiments are often carried out on brain preparations and, furthermore, a large number of important findings have resulted from work with cell lines, either primary from the CNS or immortalized. For studying the toxic effects and certain cell processes of β-ntxs, the simplest eukaryotic cell, *Saccharomyces cerevisiae*, has proved to be a valuable experimental model. Common to most model cell lines is their susceptibility to β-ntxs. Not all of them, however, are cholinergic.

3.1. Enzyme function of sPLA$_2$s and β-neurotoxicity

A common feature of all known β-ntxs is catalysis of hydrolysis of the ester bond at the *sn*-2 position of 1,2-diacyl-*sn*-3-phosphoglycerides. Their preferred substrates are membranes containing anionic phospholipids: phosphatidylserine, phosphatidic acid or phosphorylated phosphatidylinositols that are, in eukaryotic cells, most abundantly present in the cytosolic leaflets of subcellular organelles and plasma membrane. β-ntxs bind to these membranes with much higher affinity than to the membranes composed exclusively of zwitterionic phospholipids (Petan et al., 2005). These are found predominantly in the extracellular leaflet of the plasma membrane. It is important to note that, upon high-affinity association of sPLA$_2$s with membranes, their requirement for Ca^{2+} for effective phospholipid hydrolysis is very much reduced, comparable to that of the cytosolic PLA$_2$s (reviewed in Pungerčar and Križaj, 2007). Protein engineering has provided additional confirmation that the phospholipase activity of β-ntxs is fundamental in the process of β-neurotoxicity. Myotoxic ammodytin L (AtnL), an enzymatically inactive paralogue of the β-neurotoxic AtxA, was converted into a β-ntx by replacing three key amino acid residues, His28, Asn33 and Ser49, by Tyr28, Gly33 and Asp49, endowing it with enzymatic activity (Petan et al., 2007; Vardjan et al., 2013). To date, no definite conclusion has been reached as to the relation between the rate of hydrolysis and the β-neurotoxic potential of sPLA$_2$s. Judging from *in vitro* phospholipase activity assays, the hydrolytic power and β-neurotoxicity of sPLA$_2$s do not correlate. On biologically relevant substrates, however, β-ntxs with different lethalities did not differ substantially in their phospholipase activities (Paoli et al., 2009). Moreover, the enzyme activities measured on live cultured neurons proved to be much lower than those measured *in vitro* on synthetic substrates.

The physicochemical properties of lysophospholipids and fatty acids, the products of enzymatic action of β-ntxs on biological membranes, differ from those of phospholipids, from which they are derived. Differences in charge, geometry and diffusion rate between lysophospholipids, fatty acids and phospholipids are responsible for changes in curvature, fluidity, fusogenity and permeability characteristics of the membranes that they constitute. Changed membrane characteristics are eventually reflected in functional perturbations of membrane proteins involved in neurotransmission. In addition, free fatty acids and their metabolites can influence the functionality of various ion channels and receptors (Davletov and Montecucco, 2010). NM preparations, when incubated in the presence of mixtures of fatty acids and lysophospholipids, exhibit some features similar to those caused by β-ntxs (Rigoni et al., 2005, 2007; Megighian et al., 2007; Caccin et al., 2009). Explanations of β-neurotoxicity however cannot be as simple and straightforward. This was underlined in a study of the action of β-Butx on botulinum toxin C (BoNT/C) pretreated motor nerves, so the SV cycling and apparently also the internalization of the toxin were blocked. In this work, enzymatically active β-Butx, with unimpeded access to the external leaflet of the axolemma, was shown to elicit only very limited β-neurotoxic effects (Prasarnpun et al., 2004). Quantitative analysis of hydrolytic products released by β-ntxs from cultured neurons suggested that they act predominantly on the outer surface of cells (Paoli et al., 2009). We can therefore conclude that, although minor in extent, the intracellular phospholipase activity of β-ntxs is an important determinant of β-neurotoxicity.

3.2. Binding of sPLA$_2$s on nerve cells and β-neurotoxicity

Many sPLA$_2$s are highly active enzymes but not all are β-neurotoxic. It is clear that the phospholipase activity of β-ntxs is not the only factor determining their β-neurotoxicity. Numerous studies have demonstrated specific high-affinity binding sites for β-ntxs on the presynaptic membrane (Table 1) (Šribar and Križaj, 2011). So far, a presynaptic β-ntx-binding receptor associated with β-neurotoxicity has not been identified. In the axolemma, existence of a heterogeneous population of β-neurotoxicity-related receptors is expected, due to the fact that β-neurotoxicities of certain pairs of β-ntxs are summated, while β-neurotoxicities of other pairs are not. Currently, the best candidate for the β-neurotoxicity-related receptor is the neuronal or N-type sPLA$_2$ receptor (N-type sPLA$_2$R) that was first detected in rat brain synaptic membrane preparation using OS$_2$, the β-ntx from the venom of *Oxyuranus s. scutellatus*. Binding affinities of different sPLA$_2$s for the N-type sPLA$_2$R correlate strongly with the lethalities of these sPLA$_2$s. At present, the identities of only two β-ntx-binding presynaptic membrane proteins are known. The first is a voltage-dependent K^+ channel, from a group of α-dendrotoxin-sensitive K^+ channels, that binds only β-Butx. There is, however, no evidence so far for the relevance of the binding of β-Butx to the K^+ channel at the NMJ for its

Table 1
$sPLA_2$-binding proteins and β-neurotoxicity. β-neurotoxicity is a receptor-mediated process, however a β-neurotoxicity-related receptor(s) has not been identified. All known $sPLA_2$-interacting proteins are here presented. The most frequently represented tridimensional structures of modules/domains/motifs that bind $sPLA_2$s in $sPLA_2$-binding proteins (also) binding β-neurotoxic $sPLA_2$s are shown in circles. The receptor-binding region on an $sPLA_2$ molecule can be located either on its interfacial binding site (IBS) or outside this area, as reflected in the inhibition, or not, of the enzymatic activity when the $sPLA_2$ molecule is bound to receptor. CRD: carbohydrate recognition domain; DM64: *Didelphis marsupialis* (Southern opossum) protein of 64 kDa; FXa: activated blood coagulation factor X; HSPG: heparan sulphate proteoglycan; n.a., not applicable; n.d., not determined; NP: neuronal pentraxin; PDI: protein disulphide isomerase; PLI: $sPLA_2$ inhibitor; R25: mitochondrial protein of 25 kDa; SP-A: surfactant protein A; $sPLA_2R$: $sPLA_2$ receptor; TCBP-49: taipoxin-associated Ca^{2+}-binding protein of 49 kDa; VEGFR: vascular endothelial growth factor receptor. *Lidija Kovačič, personal communication.

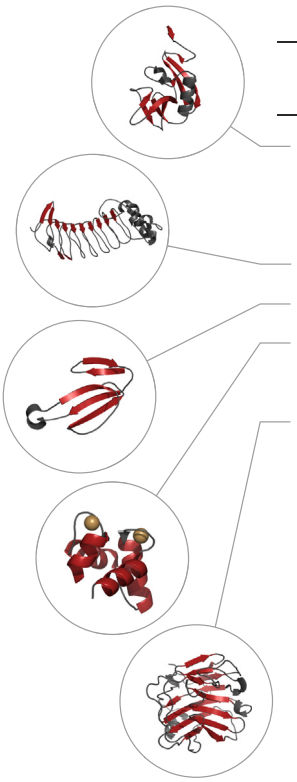

Table. $sPLA_2$-binding proteins and β-neurotoxicity.

$sPLA_2$-binding structure	$sPLA_2$-binding molecule	Effect on PLA_2 activity	Ca^{2+}-dep. of $sPLA_2$ binding	Binding of β-neurotoxic $sPLA_2$s	References
CRD-like domain	M-type $sPLA_2R$	inhibition	no	yes	1
	SP-A	inhibition	yes	yes	2
	α-PLI	inhibition	no	yes	3, 4, 5
Leucine-rich repeat	β-PLI	inhibition	n.d.	yes	6
Three-finger fold	γ-PLI	inhibition	no	yes	7, 8
EF-hand Ca^{2+}-binding motif	CaM	augmentation	yes	yes	9
	crocalbin	n.d.	yes	yes	10
	TCBP-49	n.d.	yes	yes	11
Pentraxin fold	NP1, NP2/Narp	n.d.	yes	yes	12, 13
Ig-like domain	VEGFR-1/Flt-1	no inhibition	n.d.	n.d.	14
	VEGFR-2/KDR	no inhibition	n.d.	n.d.	14
	DM64	no inhibition	n.d.	n.d.	15
Negatively charged carbohydrates	HSPG	no inhibition	n.d.	n.d.	16
Other	PDI	no inhibition*	no*	yes	17
	K^+-channel	n.d.	n.a.	yes	18
	N-type $sPLA_2R$	n.d.	yes	yes	19
	R25	n.d.	yes	yes	20
	14-3-3 proteins	no inhibition*	n.d.	yes	21
	FXa	no inhibition	yes	yes	22
	vimentin	no inhibition	no	n.d.	23
	integrins	n.d.	n.d.	n.d.	24

1: Lambeau et al., 1990, 2: Arbibe et al., 1998, 3: Kogaki et al., 1989, 4: Nobuhisa et al., 1998, 5: Inoue et al., 1997, 6: Ohkura et al., 1997, 7: Ohkura et al., 1994, 8: Fortes-Dias et al., 1994, 9: Šribar et al., 2001, 10: Hseu et al., 1997, 1999, 11: Dodds et al., 1995, 12: Schlimgen et al., 1995, 13: Kirkpatrick et al., 2000, 14: Yamazaki et al., 2005, 15: Rocha et al., 2002, 16: Murakami et al., 1999, 17: Šribar et al., 2005, 18: Scott et al., 1990, 19: Lambeau et al., 1989, 20: Vučemilo et al., 1998, 21: Šribar et al., 2003, 22: Mounier et al., 1998, 23: Boilard et al., 2003, 24: Saegusa et al., 2008

β-neurotoxicity. The second protein is the neuronal M-type $sPLA_2R$, a member of the mannose receptor family (the C-type lectin superfamily). The implication of this $sPLA_2R$ in the presynaptic neurotoxicity of AtxA has been excluded (reviewed in Pungerčar and Križaj, 2007).

3.3. *Intraneuronal localization of β-neurotoxic $sPLA_2$s*

β-neurotoxic $sPLA_2$s do not only bind specifically to the nerve cells they poison but, as experimentally demonstrated, they also internalize into such cells. Moreover, specific internalization of β-ntxs into nerve cells appears to be important for β-neurotoxicity to be fully expressed. Following the first descriptions of subcellular localization of β-ntxs in rat hippocampal neurons (reviewed in Pungerčar and Križaj, 2007), new demonstrations of internalization of β-ntxs into various neuronal cells have appeared. Using a photo-reactive derivative of AtxA, immunocytochemistry and nanogold labelling, Atx was shown to be internalized and rapidly translocated into the cytosol of motoneuron-like NSC34 cells. Furthermore, it was localized to certain intracellular organelles, including SVs and mitochondria (Jenko Pražnikar et al., 2008). Alexa-labelled notexin, β-Butx and taipoxin were shown to bind specifically to mitochondria of rat cerebellar granular neurons and spinal cord motor neurons (Rigoni et al., 2008). The first evidence of a β-ntx internalization into the terminal of a mammalian motoneuron came from the work of Logonder et al. (2009). Following inoculation with nanogold-decorated AtxA(N79C), mouse soleus muscles were isolated and analysed using transmission electron microscopy. Electron micrographs showed selective accumulation of electron-dense particles in the peri-synaptic regions at the NMJ and toxin internalization into the terminal boutons. The internalized toxin has been commonly observed within cytoplasmic vesicular structures and closely associated with mitochondria, many of which were morphologically damaged.

It is still unclear how β-ntxs are translocated across the plasma membrane of nerve cells. Hints have been provided as to which pathway(s) they may use and one possibility is by exploiting the SV recycling machinery, similarly to the way clostridial neurotoxins do. Support for this hypothesis comes from the fact that blocking SV exocytosis with BoNT/C (this prevents the SNARE-complex formation necessary for SV exocytosis by cleaving two SNARE proteins, syntaxin and SNAP-25) effectively reduced the toxic effect of β-Butx on motoneurons. It is unlikely though that β-ntxs use the same mechanism of SV membrane translocation as clostridial neurotoxins, which requires acidification of the SV. Thus, inhibition of the V-type ATP-ase, which acidifies the lumen of the SV, did not protect poisoning of the motoneuron by the β-ntx (reviewed in Pungerčar and Križaj, 2007). One of the characteristic features of β-ntx poisoning is the extensive depletion of SVs in the nerve terminal, so it is possible that a β-ntx finds its way out of the SV into the cytosol simply by hydrolysing the SV. A further, and original, idea, also including phospholipolysis, appeared recently. The authors suggested that, by progressive hydrolysis of the plasma membrane, β-ntxs create high local concentrations of lysophospholipids, together with fatty acids that are able to mediate their passage directly across the lipid bilayer (Montecucco et al., 2009).

3.4. Intracellular activities of $sPLA_2$s and β-neurotoxicity

As already stated, internalization of β-ntxs into nerve cells appears to be important for full manifestation of β-neurotoxicity. In the following lines, the intracellular binding proteins of β-ntxs are surveyed. Their roles in the process of β-neurotoxicity are only speculative at present.

Several intracellular proteins from different cellular compartments have been shown to bind $sPLA_2$s specifically and with high affinity. They are cytosolic proteins and include calmodulin (CaM), 14-3-3γ and 14-3-3ε proteins (14-3-3p); proteins from the lumen of the ER including crocalbin, a taipoxin-associated Ca^{2+}-binding protein of 49 kDa (TCBP-49) and protein disulphide isomerase (PDI); and a mitochondrial protein of 25 kDa (R25) whose identity remains to be determined (Šribar and Križaj, 2011). Interaction of β-ntxs with the intracellular proteins has been demonstrated *in vitro*, some of them also *in vivo*, raising the possibility of physiological relevance. AtxA co-localizes with PDI and R25 in PC12 cells (manuscript in preparation). Binding to the latter may be responsible for the specific association of β-ntxs with mitochondria, leading to opening of permeability transition pores (Rigoni et al., 2008), the release of mitochondrial alarmins (Zornetta et al., 2012) and other characteristic features of mitochondrial pathology induced by these β-ntxs. The *in vivo* complexing of AtxA with CaM and 14-3-3p has been demonstrated in NSC34 cells in culture (Jenko Pražnikar et al., 2008). CaM stabilized certain $sPLA_2$s and substantially increased their enzymatic activity under both non-reducing and cytosol-like conditions (Kovačič et al., 2009, 2010). This may allow β-ntxs to retain substantial phospholipase activity in the reducing environment of the nerve cell cytosol. Intracellular enzymatic action of β-ntxs is further supported by the influx of external Ca^{2+} into the nerve terminal (Tedesco et al., 2009). Some authors demonstrated that the initial influx of Ca^{2+} occurs through certain voltage gated Ca^{2+} channels activated by these toxins (Prasarnpun et al., 2004; Yagami et al., 2013). Rigoni et al., however, presented opposite results (2007). 14-3-3p, on the other hand, may play an important role in positioning β-ntxs to their specific site(s) of action within the nerve cell, for example, to the site of SV formation during endocytosis. In a study of the molecular basis of the inhibition of vesicle endocytosis by AtxA in *S. cerevisiae*, the importance of the interaction of the toxin with Bmh2, the yeast 14-3-3p homologue, for effective blocking of the process of SV formation, was demonstrated (Mattiazzi et al., 2012). The inhibition was phospholipase activity-dependent. Due to hydrolysis of phospholipids in the inner leaflet of the plasma membrane the latter's curvature changes. As the authors proposed, this interferes with the activity of amphiphysin, a membrane curvature–sensing protein, a function in vesicle endocytosis that is very important. Amphiphysin stabilizes the neck of the emerging vesicle when its curvature is appropriate to enable a tight association. Once bound, amphiphysin recruits dynamin to pinch the vesicle off the membrane (Fig. 1).

4. β-neurotoxicity on the molecular level as currently perceived

Despite extensive research, the molecular mechanism of action of β-ntxs is still not completely clear. Consistent with most experimental facts, we can presently interpret the action of β-ntxs as follows (Fig. 1):

β-ntxs specifically localize at NMJ. β-neurotoxicity-related receptors, that bind different sets of β-ntxs, appear to exist in the presynaptic membrane. In association with the presynaptic membrane β-ntxs hydrolyse phospholipids in its external leaflet, leading to formation of an excess of lysophospholipids and fatty acids. Products of phospholipolysis promote exocytosis of SVs. The conductivity of particular Ca^{2+}-channels is also increased, further promoting release of SNARE-mediated neurotransmitter. Nevertheless, the extracellular phospholipase activity of β-ntxs does not appear to be the only reason for intoxication of the motoneuron. β-ntx translocates into the nerve ending, localizing to the cytosol and mitochondria. Internalization is rapid and apparently depends on SNARE assembly but clearly not on the activity of the V-type ATP-ase. The recycling SVs are thus candidate translocation vehicles (Montecucco and Rossetto, 2000). β-ntxs bind to CaM and 14-3-3p in the cytosol of the nerve ending. These interactions could contribute to β-neurotoxicity. It has been proved that complexing of β-ntx with CaM stabilizes β-ntx and increases its enzyme activity in cytosol-like conditions. Complexing β-ntx with 14-3-3p may however assist localizing the former inside the nerve ending, for example to sites on the plasma membrane where SV are endocytosed. Amplified phospholipase activity in the right place inside the neuron is a crucial determinant of β-neurotoxicity. Targeted phospholipolysis of the inner leaflet of the plasma membrane results in the inhibition of endocytosis of SVs due to impairment of amphiphysin function, which is

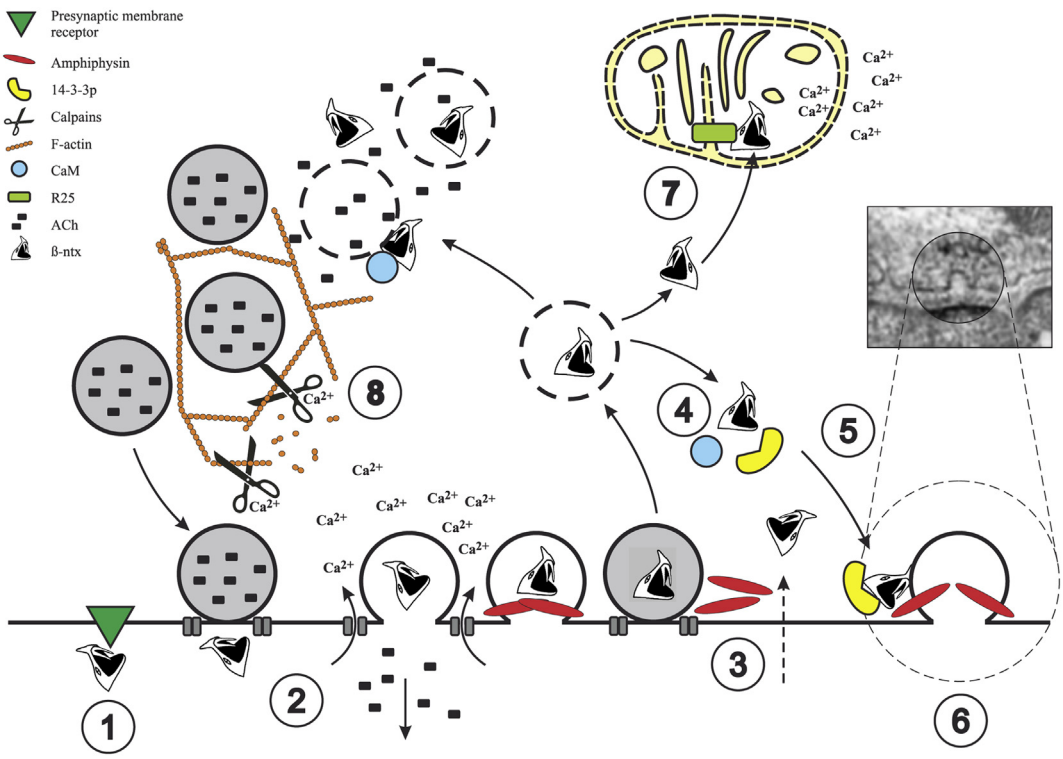

Fig. 1. Possible steps in poisoning of the NMJ by the β-neurotoxic sPLA$_2$. (1) At the NMJ, β-ntx binds specifically to β-neurotoxicity-related receptors in the presynaptic membrane. (2) Tightly associated with the axolemma, β-ntx hydrolyses phospholipids in its external leaflet thus promoting exocytosis of the SVs filled with acetylcholine (ACh) and conductance of certain Ca^{2+} channels. (3) β-ntx rapidly internalizes into the nerve ending in a process probably dependent on SNARE assembly but not on the activity of the V-type ATP-ase. Internalization pathways are probably multiple, one of which may include the recycling of SVs. (4) β-ntx is translocated to the cytosol and to mitochondria. (5) β-ntx interacts with calmodulin (CaM), 14-3-3p and, possibly, some other proteins in the cytosol. CaM stabilizes the sPLA$_2$, increasing its enzyme activity. 14-3-3p targets β-ntx to sites on the plasma membrane where SVs endocytose. (6) By hydrolysing the plasma membrane from the cytosolic side, β-ntx changes membrane curvature and thus prevents the function of amphiphysin in the process of SV endocytosis. Electron micrograph is showing the result: impaired endocytosis of SVs reflected in appearance of Ω-shaped invaginations in the presynaptic membrane. (7) β-ntx binds to mitochondria (R25 is a β-ntx receptor of 25 kDa in the mitochondria) and induces opening of permeability transition pores. Mitochondria uncouple and production of ATP terminates. Subsequently, the morphology of the mitochondria becomes degenerated. (8) Ca^{2+} homeostasis is lost due to extended phospholipolysis and consequent increased permeability of cellular membranes. The high cytosolic concentration of Ca^{2+} triggers additional intracellular phospholipase and proteinase (calpains) activities. This is reflected in dissipation of the F-actin cytoskeleton and extensive degeneration of the nerve ending.

crucial for this process. The next major pathological effect of β-ntxs is associated with mitochondria. Binding of β-ntxs to specific binding sites in these organelles, coupled with their phospholipase activity induce the opening of transition pores and uncoupling of mitochondria (Rigoni et al., 2008; Logonder et al., 2009; de Carvalho et al., 2014), resulting in cessation of ATP production and, ultimately, their complete degeneration. Progressive phospholipolysis of cell membranes by β-ntxs dissipates Ca^{2+} homoeostasis in the nerve ending. The increased cytosolic concentration of Ca^{2+} upregulates the activity of Ca^{2+}- controlled hydrolases in this compartment, including cytosolic PLA$_2$s and certain proteinases (calpains), leading to extensive degeneration of the nerve ending.

5. Perspectives

A detailed understanding of β-neurotoxicity at the molecular level will provide insight into possible ways of preventing intoxication with β-ntxs or how to accelerate regeneration of the affected tissue. Importantly, the knowledge gained from these toxins will contribute significantly to our understanding of the functioning and dysfunctioning of their mammalian counterparts, especially in the nervous system (Goracci et al., 2010; Yagami et al., 2014). To this end, some of the most important questions to be resolved in the future are the following: (1) What is the molecular identity of β-neurotoxicity-related receptors in the presynaptic membrane? (2) How do β-ntxs cross the presynaptic membrane and the outer membrane of mitochondria? (3) Why is the mature form of the mammalian GIIA sPLA$_2$, a homologue of β-ntxs located in mitochondria, not toxic to this organelle while β-ntxs are? (4) How do the cytosolic sPLA$_2$-binding proteins influence the rate, specificity and location of the phospholipase activity of β-ntxs?

Acknowledgements

This work was supported by a grant P1-0207 from the Slovenian Ministry of Higher Education, Science and Technology. We sincerely thank Dr. Roger H. Pain for critical reading of the manuscript.

Conflict of interest

The authors declare that there are no conflicts of interest.

Transparency document

Transparency document related to this article can be found online at http://dx.doi.org/10.1016/j.toxicon.2014.06.019.

References

Arbibe, L., Koumanov, K., Vial, D., Rougeot, C., Faure, G., Havet, N., Longacre, S., Vargaftig, B.B., Béréziat, G., Voelker, D.R., Wolf, C., Touqui, L., 1998. Generation of lyso-phospholipids from surfactant in acute lung injury is mediated by type-II phospholipase A_2 and inhibited by a direct surfactant protein A-phospholipase A_2 protein interaction. J. Clin. Invest. 102, 1152–1160.

Boilard, E., Bourgoin, S.G., Bernatchez, C., Surette, M.E., 2003. Identification of an autoantigen on the surface of apoptotic human T cells as a new protein interacting with inflammatory group IIA phospholipase A_2. Blood 102, 2901–2909.

Bonanomi, D., Pennuto, M., Rigoni, M., Rossetto, O., Montecucco, C., Valtorta, F., 2005. Taipoxin induces synaptic vesicle exocytosis and disrupts the interaction of synaptophysin I with VAMP2. Mol. Pharmacol. 67, 1901–1908.

Caccin, P., Rossetto, O., Montecucco, C., 2009. Neurotoxicity of inverted-cone shaped lipids. Neurotoxicology 30, 174–181.

Cendron, L., Mičetić, I., Polverino de Laureto, P., Paoli, M., 2012. Structural analysis of trimeric phospholipase A_2 neurotoxin from the Australian taipan snake venom. FEBS J. 279, 3121–3135.

Davletov, B., Montecucco, C., 2010. Lipid function at synapses. Curr. Opin. Neurobiol. 20, 543–549.

De Carvalho, N.D., Garcia, R.C., Kleber Ferreira, A., Rodrigo Batista, D., Carlos Cassola, A., Maria, D., Lebrun, I., Mendes Carneiro, S., Castro Afeche, S., Marcourakis, T., Sandoval, M.R.L., 2014. Neurotoxicity of coral snake phospholipases A_2 in cultured rat hippocampal neurons. Brain Res., 1–16.

Dodds, D., Schlimgen, A.K., Lu, S.Y., Perin, M.S., 1995. Novel reticular calcium binding protein is purified on taipoxin columns. J. Neurochem. 64, 2339–2344.

Duregotti, E., Tedesco, E., Montecucco, C., Rigoni, M., 2013. Calpains participate in nerve terminal degeneration induced by spider and snake presynaptic neurotoxins. Toxicon 64, 20–28.

Fathi, B., Harvey, A.L., Rowan, E.G., 2013. The effect of temperature on the effects of the phospholipase A_2 neurotoxins β-bungarotoxin and taipoxin at the neuromuscular junction. Toxicon 70, 86–89.

Faure, G., Xu, H., Saul, F.A., 2011. Crystal structure of crotoxin reveals key residues involved in the stability and toxicity of this potent heterodimeric β-neurotoxin. J. Mol. Biol. 412, 176–191.

Fortes-Dias, C.L., Lin, Y., Ewell, L., Diniz, C.R., Liu, T.Y., 1994. A phospholipase A_2 inhibitor from the plasma of the South American rattlesnake (*Crotalus durissus terrificus*). Protein structure, genomic structure, and mechanism of action. J. Biol. Chem. 269, 15646–15651.

Goracci, G., Ferrini, M., Nardicchi, V., 2010. Low molecular weight phospholipases A_2 in mammalian brain and neural cells: roles in functions and dysfunctions. Mol. Neurobiol. 41, 274–289.

Hseu, M.J., Yen, C.Y., Tseng, C.C., Tzeng, M.C., 1997. Purification and partial amino acid sequence of a novel protein of the reticulocalbin family. Biochem. Biophys. Res. Commun. 239, 18–22.

Hseu, M.J., Yen, C.Y., Tzeng, M.C., 1999. Crocalbin: a new calcium-binding protein that is also a binding protein for crotoxin, a neurotoxic phospholipase A_2. FEBS Lett. 445, 440–444.

Inoue, S., Shimada, A., Ohkura, N., Ikeda, K., Samejima, Y., Omori-Satoh, T., Hayashi, K., 1997. Specificity of two types of phospholipase A_2 inhibitors from the plasma of venomous snakes. Biochem. Mol. Biol. Int. 1997 (41), 529–537.

Jenko Pražnikar, Z., Kovačič, L., Rowan, E.G., Romih, R., Rusmini, P., Poletti, A., Križaj, I., Pungerčar, J., 2008. A presynaptically toxic secreted phospholipase A_2 is internalized into motoneuron-like cells where it is rapidly translocated into the cytosol. Biochim. Biophys. Acta 1783, 1129–1139.

Kini, R.M. (Ed.), 1997. Venom Phospholipase A_2 Enzymes: Structure, Function and Mechanism. John Wiley & Sons, Chichester.

Kirkpatrick, L.L., Matzuk, M.M., Dodds, D.C., Perin, M.S., 2000. Biochemical interactions of the neuronal pentraxins. Neuronal pentraxin (NP) receptor binds to taipoxin and taipoxin-associated calcium-binding protein 49 via NP1 and NP2. J. Biol. Chem. 275, 17786–17792.

Kogaki, H., Inoue, S., Ikeda, K., Samejima, Y., Omori-Satoh, T., Hamaguchi, K., 1989. Isolation and fundamental properties of a phospholipase A_2 inhibitor from the blood plasma of *Trimeresurus flavoviridis*. J. Biochem 106, 966–971.

Kovačič, L., Novinec, M., Petan, T., Baici, A., Križaj, I., 2009. Calmodulin is a nonessential activator of secretory phospholipase A_2. Biochemistry 48, 11319–11328.

Kovačič, L., Novinec, M., Petan, T., Križaj, I., 2010. Structural basis of the significant calmodulin-induced increase in the enzymatic activity of secreted phospholipases A_2. Protein Eng. Des. Sel. 23, 479–487.

Lambeau, G., Barhanin, J., Schweitz, H., Qar, J., Lazdunski, M., 1989. Identification and properties of very high affinity brain membrane-binding sites for a neurotoxic phospholipase from the taipan venom. J. Biol. Chem. 264, 11503–11510.

Lambeau, G., Schmid-Alliana, A., Lazdunski, M., Barhanin, J., 1990. Identification and purification of a very high affinity binding protein for toxic phospholipases A_2 in skeletal muscle. J. Biol. Chem. 265, 9526–9532.

Logonder, U., Križaj, I., Rowan, E.G., Harris, J.B., 2008. Neurotoxicity of ammodytoxin a in the envenoming bites of *Vipera ammodytes ammodytes*. J. Neuropathol. Exp. Neurol. 67, 1011–1019.

Logonder, U., Jenko-Pražnikar, Z., Scott-Davey, T., Pungerčar, J., Križaj, I., Harris, J.B., 2009. Ultrastructural evidence for the uptake of a neurotoxic snake venom phospholipase A_2 into mammalian motor nerve terminals. Exp. Neurol. 219, 591–594.

Mattiazzi, M., Sun, Y., Wolinski, H., Bavdek, A., Petan, T., Anderluh, G., Kohlwein, S.D., Drubin, D.G., Križaj, I., Petrovič, U., 2012. A neurotoxic phospholipase A_2 impairs yeast amphiphysin activity and reduces endocytosis. PLoS One 7, e40931.

Megighian, A., Rigoni, M., Caccin, P., Zordan, M. a, Montecucco, C., 2007. A lysolecithin/fatty acid mixture promotes and then blocks neurotransmitter release at the *Drosophila melanogaster* larval neuromuscular junction. Neurosci. Lett. 416, 6–11.

Montecucco, C., Rossetto, O., 2000. How do presynaptic PLA2 neurotoxins block nerve terminals? Trends Biochem. Sci. 25, 266–270.

Montecucco, C., Rossetto, O., Caccin, P., Rigoni, M., Carli, L., Morbiato, L., Muraro, L., Paoli, M., 2009. Different mechanisms of inhibition of nerve terminals by botulinum and snake presynaptic neurotoxins. Toxicon 54, 561–564.

Mounier, C.M., Hackeng, T.M., Schaeffer, F., Faure, G., Bon, C., Griffin, J.H., 1998. Inhibition of prothrombinase by human secretory phospholipase A_2 involves binding to factor Xa. J. Biol. Chem. 273, 23764–23772.

Murakami, M., Kambe, T., Shimbara, S., Yamamoto, S., Kuwata, H., Kudo, I., 1999. Functional association of type IIA secretory phospholipase A_2 with the glycosylphosphatidylinositol-anchored heparan sulfate proteoglycan in the cyclooxygenase-2-mediated delayed prostanoid-biosynthetic pathway. J. Biol. Chem. 274, 29927–29936.

Murakami, M., Taketomi, Y., Miki, Y., Sato, H., Hirabayashi, T., Yamamoto, K., 2011. Recent progress in phospholipase A_2 research: from cells to animals to humans. Prog. Lipid Res. 50, 152–192.

Nobuhisa, I., Chiwata, T., Fukumaki, Y., Hattori, S., Shimohigashi, Y., Ohno, M., 1998. Structural elements of *Trimeresurus flavoviridis* serum inhibitors for recognition of its venom phospholipase A_2 isozymes. FEBS Lett. 429, 385–389.

Ohkura, N., Inoue, S., Ikeda, K., Hayashi, K., 1994. Isolation and characterization of a phospholipase A_2 inhibitor from the blood plasma of the Thailand cobra *Naja naja kaouthia*. Biochem. Biophys. Res. Commun. 200, 784–788.

Ohkura, N., Okuhara, H., Inoue, S., Ikeda, K., Hayashi, K., 1997. Purification and characterization of three distinct types of phospholipase A_2 inhibitors from the blood plasma of the Chinese mamushi, *Agkistrodon blomhoffii siniticus*. Biochem. J. 325, 527–531.

Paoli, M., Rigoni, M., Koster, G., Rossetto, O., Montecucco, C., Postle, A.D., 2009. Mass spectrometry analysis of the phospholipase A_2 activity of snake pre-synaptic neurotoxins in cultured neurons. J. Neurochem. 111, 737–744.

Petan, T., Križaj, I., Gelb, M.H., Pungerčar, J., 2005. Ammodytoxins, potent presynaptic neurotoxins, are also highly efficient phospholipase A_2 enzymes. Biochemistry 44, 12535–12545.

Petan, T., Križaj, I., Pungerčar, J., 2007. Restoration of enzymatic activity in a Ser-49 phospholipase A_2 homologue decreases its Ca^{2+}-independent membrane-damaging activity and increases its toxicity. Biochemistry 46, 12795–12809.

Prasarnpun, S., Walsh, J., Harris, J.B., 2004. β-bungarotoxin-induced depletion of synaptic vesicles at the mammalian neuromuscular junction. Neuropharmacology 47, 304–314.

Pungerčar, J., Križaj, I., 2007. Understanding the molecular mechanism underlying the presynaptic toxicity of secreted phospholipases A_2. Toxicon 50, 871–892.

Rigoni, M., Schiavo, G., Weston, A.E., Caccin, P., Allegrini, F., Pennuto, M., Valtorta, F., Montecucco, C., Rossetto, O., 2004. Snake presynaptic neurotoxins with phospholipase A_2 activity induce punctate swellings of neurites and exocytosis of synaptic vesicles. J. Cell. Sci. 117, 3561–3570.

Rigoni, M., Caccin, P., Gschmeissner, S., Koster, G., Postle, A.D., Rossetto, O., Schiavo, G., Montecucco, C., 2005. Equivalent effects of snake PLA_2 neurotoxins and lysophospholipid-fatty acid mixtures. Science 310, 1678–1680.

Rigoni, M., Pizzo, P., Schiavo, G., Weston, A.E., Zatti, G., Caccin, P., Rossetto, O., Pozzan, T., Montecucco, C., 2007. Calcium influx and mitochondrial alterations at synapses exposed to snake neurotoxins or their phospholipid hydrolysis products. J. Biol. Chem. 282, 11238–11245.

Rigoni, M., Paoli, M., Milanesi, E., Caccin, P., Rasola, A., Bernardi, P., Montecucco, C., 2008. Snake phospholipase A_2 neurotoxins enter neurons, bind specifically to mitochondria, and open their transition pores. J. Biol. Chem. 283, 34013–34020.

Rocha, S.L., Lomonte, B., Neves-Ferreira, A.G., Trugilho, M.R., Junqueirade-Azevedo Ide, L., Ho, P.L., Domont, G.B., Gutierrez, J.M., Perales, J., 2002. Functional analysis of DM64, an antimyotoxic protein with immunoglobulin-like structure from *Didelphis marsupialis* serum. Eur. J. Biochem. 269, 6052–6062.

Saegusa, J., Akakura, N., Wu, C.Y., Hoogland, C., Ma, Z., Lam, K.S., Liu, F.T., Takada, Y.K., Takada, Y., 2008. Pro-inflammatory secretory phospholipase A_2 type IIA binds to integrins αvβ3 and α4β1 and induces proliferation of monocytic cells in an integrin-dependent manner. J. Biol. Chem. 283, 26107–26115.

Saul, F.A., Prijatelj-Žnidaršič, P., Vulliez-le Normand, B., Villette, B., Raynal, B., Pungerčar, J., Križaj, I., Faure, G., 2010. Comparative structural studies of two natural isoforms of ammodytoxin, phospholipases A_2 from *Vipera ammodytes ammodytes* which differ in neurotoxicity and anticoagulant activity. J. Struct. Biol. 169, 360–369.

Schlimgen, A.K., Helms, J.A., Vogel, H., Perin, M.S., 1995. Neuronal pentraxin, a secreted protein with homology to acute phase proteins of the immune system. Neuron 14, 519–526.

Scott, V.E.S., Parcej, D.N., Keen, J.N., Findlay, J.B.C., Dolly, J.O., 1990. α-dendrotoxin acceptor from bovine brain is a K^+ channel protein. Evidence from the N-terminal sequence of its larger subunit. J. Biol. Chem. 265, 20094–20097.

Šribar, J., Čopič, A., Pariš, A., Sherman, N.E., Gubenšek, F., Fox, J.W., Križaj, I., 2001. A high affinity acceptor for phospholipase A_2 with neurotoxic activity is a calmodulin. J. Biol. Chem. 276, 12493–12496.

Šribar, J., Sherman, N.E., Prijatelj, P., Faure, G., Gubenšek, F., Fox, J.W., Aitken, A., Pungerčar, J., Križaj, I., 2003. The neurotoxic phospholipase A_2 associates, through a non-phosphorylated binding motif, with 14-3-3 protein gamma and epsilon isoforms. Biochem. Biophys. Res. Commun. 302, 691–696.

Šribar, J., Anderluh, G., Fox, J.W., Križaj, I., 2005. Protein disulphide isomerase binds ammodytoxin strongly: possible implications for toxin trafficking. Biochem. Biophys. Res. Commun. 329, 733–737.

Šribar, J., Križaj, I., 2011. Secreted phospholipases A_2 – not just enzymes. Acta Chim. Slov. 58, 678–688.

Tedesco, E., Rigoni, M., Caccin, P., Grishin, E., Rossetto, O., Montecucco, C., 2009. Calcium overload in nerve terminals of cultured neurons intoxicated by alpha-latrotoxin and snake PLA_2 neurotoxins. Toxicon 54, 138–144.

Vardjan, N., Mattiazzi, M., Rowan, E.G., Križaj, I., Petrovič, U., Petan, T., 2013. Neurotoxic phospholipase A_2 toxicity model: an insight from mammalian cells. Commun. Integr. Biol. 6, e23600.

Vučemilo, N., Čopič, A., Gubenšek, F., Križaj, I., 1998. Identification of a new high-affinity binding protein for neurotoxic phospholipases A_2. Biochem. Biophys. Res. Commun. 251, 209–212.

Yagami, T., Yamamoto, Y., Kohma, H., Nakamura, T., Takasu, N., Okamura, N., 2013. L-type voltage-dependent calcium channel is involved in the snake venom group IA secretory phospholipase A_2-induced neuronal apoptosis. Neurotoxicology 35, 146–153.

Yagami, T., Yamamoto, Y., Koma, H., 2014. The role of secretory phospholipase A_2 in the central nervous system and neurological diseases. Mol. Neurobiol. 49, 863–876.

Yamazaki, Y., Matsunaga, Y., Nakano, Y., Morita, T., 2005. Identification of vascular endothelial growth factor receptor-binding protein in the venom of eastern cottonmouth. A new role of snake venom myotoxic Lys49-phospholipase A_2. J. Biol. Chem. 280, 29989–29992.

Zornetta, I., Caccin, P., Fernandez, J., Lomonte, B., Gutierrez, J.M., Montecucco, C., 2012. Envenomations by *Bothrops* and *Crotalus* snakes induce the release of mitochondrial alarmins. PLoS Negl. Trop. Dis. 6, e1526.